



Annual Report 2010

A
N
N
U
A
L

R
E
P
O
R
T

2
0
1
0

Laboratori Nazionali del Gran Sasso



Codice ISBN
ISBN-978-88-907304-7-4

Annual Report 2010

LNGS Director

Dr. Lucia Votano

Editor

Dr. Roberta Antolini

Technical Assistants

Dr. Adriano Di Giovanni
Mr. Marco Galeota

INFN

*Laboratori Nazionali
del Gran Sasso*

Annual Report 2010

Contents

BOREXINO	pag. 1
COBRA	pag. 11
CRESST	pag. 29
CUORE	pag. 41
DAMA	pag. 65
GERDA	pag. 91
ICARUS	pag. 107
LUNA	pag. 123
LVD	pag. 141
OPERA	pag. 149
THEORY	pag. 161
WARP	pag. 175
XENON	pag. 185
ERMES	pag. 195
GIGS	pag. 199
TELLUS	pag. 211
AUGER	pag. 215
LASEX	pag. 229
XILOPHON	pag. 235

THE BOREXINO EXPERIMENT

Borexino collaboration

G. Bellini^a, J. Benziger^c, S. Bonetti^a, M. Buizza Avanzini^a, B. Caccianiga^a, L. Cadonati^t,
F.P. Calaprice^d, C. Carraroⁱ, A. Chavarria^d, A. Chepurinov^z, D. D'Angelo^h, S. Daviniⁱ,
A. Derbin^u, A. Etenko^s, K. Fomenko^m, D. Franco^a, C. Galbiati^d, S. Gazzana^b, C. Ghiano^b,
M.G. Giammarchi^a, M. Goeger-Neff^h, A. Goretti^d, E. Guardincerriⁱ, C. Griebⁿ, S. Hardyⁿ,
A. Ianni^b, A.M. Ianni^d, M. Joyceⁿ, V. Kobychiev^v, D. Korablev^m, Y. Koshio^b, G. Korga^b,
D. Kryn^o, M. Laubenstein^b, M. Leung^d, T. Lewke^h, E. Litvinovich^s, B. Loer^d, P. Lombardi^a,
L. Ludhova^a, I. Machulin^s, S. Manecki^m, W. Maneschg^j, G. Manuzioⁱ, Q. Meindl^h,
E. Meroni^a, L. Miramonti^a, M. Misiaszek^q, D. Montanari^b, V. Muratova^u, L. Oberauer^h,
M. Obolensky^o, F. Ortica^g, M. Pallaviciniⁱ, L. Papp^b, L. Perasso^a, S. Perassoⁱ, A. Pocar^d,
R.S. Raghavanⁿ, G. Ranucci^a, A. Razeto^b, A. Re^a, P. Rissoⁱ, A. Romani^g, D. Rountreeⁿ,
A. Sabelnikov^s, R. Saldanha^d, C. Salvoⁱ, S. Schönert^j, H. Simgen^j, M. Skorokhvatov^s,
O. Smirnov^m, A. Sotnikov^m, S. Sukhotin^s, Y. Suvorov^s, R. Tartaglia^b, G. Testeraⁱ,
D. Vignaud^o, B. Vogelaarⁿ, F. von Feilitzsch^h, J. Winter^h, M. Wojcik^q, M. Wurm^h, J. Xu^d,
O. Zaimidoroga^m, S. Zavatarelliⁱ, G. Zuzel^j

^aDip. di Fisica dell'Università and Infn Milano - Italy

^bLaboratori Nazionali del Gran Sasso, Assergi (Aq) - Italy

^cDept. of Chemical Engineering, Princeton University - NJ USA

^dDept. of Physics, Princeton University - NJ USA

^gDip. di Chimica dell'Università and Infn Perugia - Italy

^hDept. of Physics, Technische Universität München - Germany

ⁱDip. di Fisica dell'Università and Infn Genova - Italy

^jMax Planck Inst. für Kernphysik, Heidelberg - Germany

^mJoint Institute for Nuclear Research Dubna - Russia

ⁿDept. of Physics, Virginia Polytechnic Institute - VA USA

^oLaboratoire de AstroParticule et Cosmologie, Paris - France

^qInstitute of Physics, Jagellonian University, Krakow - Poland

^sRRC Kurchatov Institute, Moscow - Russia

^tDept. of Physics, University of Massachusetts, Amherst - MA USA

^uSt. Petersburg Nuclear Physics Institute, Gatchina, Russia

^vKiev Institute for Nuclear Research, Kiev, Ukraine

^zInstitute of Nuclear Physics, Lomonosov State University, Moscow, Russia

Abstract

Borexino is a detector located in the Hall C of LNGS to study solar neutrino physics and other rare phenomena. The data taking started in May 2007 and led - among other things - to the first real time measurement of ^7Be solar neutrinos, the first experimental evidence of the matter/vacuum transition in solar neutrino oscillations and the observation of geo-neutrinos. We summarize here the status of the project and outline the perspectives for future measurements.

1 Introduction

Solar neutrino physics is a topic that originally started from the perspective of studying the basic working principle of the core of the Sun, nuclear fusion reactions producing energy and emitting neutrinos. The pioneer Davis experiment [1] was the first one to measure (with radiochemical methods) solar neutrinos as predicted by theoretical models and to detect a significant deficit with respect to the predicted flux. Additional experiments were performed starting from the end of the 80's, both in radiochemical mode [2, 3, 4] and in real-time mode [5, 6] while the most widely accepted model of the Sun evolved into what is now known as the Standard Solar Model [7] [8].

As a general statement, real-time experiments have been performed with large water Cerenkov detectors with an energy threshold of about 5 MeV, mainly due to natural radioactivity. This implies that only $\sim 0.001\%$ of the total neutrino flux has been observed in real time prior to 2007.

The issue of directly measuring low energy solar neutrinos has been the subject of an intensive research study carried out in the frame of the Borexino development and starting from the very beginning of the 90's. Borexino [9] is a real time experiment to study sub-MeV solar neutrinos having as the main experimental goal the detection of the 0.862 MeV ${}^7\text{Be}$ solar neutrino line through the neutrino-electron elastic scattering reaction $\nu e \rightarrow \nu e$. The maximum energy of the recoiling electron is 664 KeV and the experimental design threshold is of 50 keV while the analysis threshold is 200 keV. The detection reaction is observed in a large mass (100 tons fiducial volume) of well shielded liquid scintillator.

The prediction of the ${}^7\text{Be}$ solar flux depends both on the Standard Solar Model and the value of the parameters of the LMA solution of neutrino oscillations [10] [11]. The Borexino experimental program makes it possible to specifically test this prediction in a direct way as well as opening up the unexplored territory of real time sub-MeV solar neutrino spectroscopy.

The main problem of an experiment with such a low energy threshold is the background coming from natural sources such as cosmic rays or radioactivity. This problem has been addressed by means of an intense R&D program focused on low radioactivity materials and purification techniques. This effort was complemented by a comparably thorough research in the field of detection and measurement of very low radioactivity levels [12]. As a part of this program, a prototype of the Borexino detector, called Counting Test Facility [13], was built and operated at LNGS to demonstrate very low radioactive contamination levels (10^{-16} g/g of U-238 equivalent or less [14]) in a ton scale scintillator detector. The CTF is currently now being used as a low background facility for quality tests of the Borexino scintillator and possible future physics programs.

This research and development culminated into the construction, filling and operation of the full-scale Borexino detector. The experimental data taking in the final configuration began in May 2007.

2 The Borexino Detector

Borexino [15] is an unsegmented scintillation detector featuring 300 tonnes of well shielded liquid ultrapure scintillator viewed by 2200 photomultipliers (fig. 1). The detector core is a transparent spherical vessel (Nylon Sphere, $100\mu\text{m}$ thick), 8.5 m of diameter, filled with 300 tonnes of liquid scintillator and surrounded by 1000 tonnes of high-purity buffer liquid. The scintillator mixture is pseudocumene (PC) and PPO (1.5 g/l) as a fluor, while the buffer liquid consists of PC alone (with the addition of DMP as light quencher). The photomultipliers are supported by a Stainless Steel Sphere, which also separates the inner part of the detector from the external shielding, provided by 2400 tonnes of pure water (water buffer). An additional containment vessel (Nylon film Radon barrier) is interposed between the Scintillator Nylon Sphere and the photomultipliers, with the goal of reducing Radon diffusion towards the internal part of the detector.

The outer water shield is instrumented with 200 outward-pointing photomultipliers serving as a veto for penetrating muons, the only significant remaining cosmic ray background at the Gran Sasso depth (about 3500 meters of water equivalent). The innermost 2200 photomultipliers are divided into a set of 1800 photomultipliers equipped with light cones (so that they see light only from the Nylon Sphere region) and a set of 400 PMT's without light cones, sensitive to light originated in the whole Stainless Steel Sphere volume. This design greatly increases the capability of the system to identify muons crossing the PC buffer (and not the scintillator).

The Borexino design is based on the concept of a graded shield of progressively lower intrinsic radioactivity as one approaches the sensitive volume of the detector; this culminates in the use of 200 tonnes of the low background scintillator to shield the 100 tonnes innermost Fiducial Volume. In these conditions, the ultimate background will be dominated by the intrinsic contamination of the scintillator, while all backgrounds from the construction materials and external shieldings will be negligible.

Borexino also features several external systems conceived to purify the experimental fluids (water, nitrogen and scintillator) used by the experiment (see e.g. [16]).

3 Status of the project

The Borexino filling started in January 2007, with scintillator displacing the purified water from inside the detector volumes. The detector was completed and the data taking started in May 2007.

The radiopurity of the detector has been found in general to be better than the specifications. In particular, among the best radioactivity levels found during the data taking:

1. C-14 contamination of the scintillator was found to be at $\sim 2 \times 10^{-18}$ $^{14}\text{C}/^{12}\text{C}$.
2. The general level of Th-232 contamination - as measured by means of $^{212}\text{Bi}/^{212}\text{Po}$ delayed coincidences was found to be at $\sim 4.6 \times 10^{-18}$ g/g.
3. The U-238 family contamination - assessed by studying the $^{214}\text{Bi}/^{214}\text{Po}$ delayed coincidence rate, was measured to be $\sim 1.7 \times 10^{-17}$ g/g.

4. Kr-85 contamination, of considerable importance due to the spectral shape similar to the one of the signal searched for was found (by means of the ^{85m}Rb decay and the related β/γ tagging) to be at the level of 30 counts/day in the 100 tons fiducial volume.

This level of radiopurity, together with the use of mild cuts and the α/β discrimination technique has allowed - among other things - the first real-time detection of the Be-7 solar signal, the first observation of the B-8 spectrum below 5 MeV and the observation of geoneutrinos.

While we refer the interested reader to the published papers for the detailed description of the analysis [17] [18], fig. 2 shows a spectrum of the singles rate obtained after typical cuts (veto of external muons, Radon-related activity, Po-210 subtraction) in the Borexino fiducial volume. Neutrinos from Be-7 are visible in the electron recoil spectrum by means of the Compton-like shoulder generated by $\nu e^- \rightarrow \nu e^-$ scattering. The Be-7 solar flux was determined by fitting the observed distribution to the light yield, to the Be-7 interaction rate and to the other contributions shown in the figure. The measured value of $49 \pm 3 \pm 4$ counts/day in 100 tonnes is in agreement with the LMA-MSW oscillation scenario.

The high radiopurity of the scintillator was exploited to extend the observational range of the B-8 solar spectrum component [20]. While previous water Cerenkov experiments provided robust measurements down to a threshold of 5 MeV for the scattered electrons (with only a very recent SNO analysis down to 3.5 MeV), Borexino was able to suppress all the relevant backgrounds above the 2.614 MeV gamma line of the Tl-208. Muons and neutrons were also identified and subtracted. Short lived cosmogenic background was vetoed away with a livetime cut, while long-lived nuclides (Be-11 and C-10) were suitably accounted for. The final measured spectrum (fig. 3) is in agreement with the solar models and the LMA-MSW scenario for neutrino oscillation.

The combination of the Be-7 and B-8 measurements constitutes the first evidence of matter/vacuum transition of neutrino oscillations obtained within the same experiment.

Geoneutrinos, anti-neutrinos produced in β decays of naturally occurring radioactive isotopes in the Earth, are a unique probe of our planet's interior. Antineutrino interactions were studied for the first time at KamLAND (with a 2.5σ C.L. evidence [21] [22]) and can be detected in Borexino by using the inverse β decay reaction $\bar{\nu} p \rightarrow e^+ n$ [19]. The analysis was carried out using a fiducial exposure of 252.6 ton year and made use of the e^+ /neutron delayed coincidence as a powerful tool to reject backgrounds. The final energy spectrum of positrons was dominated by the geoneutrino signal and the european power plant reactor signal, see fig. 4, thereby establishing the observation of geoneutrinos at the 4.2σ C.L.

Additional physics topics that have been investigate during 2010 include a new experimental limit on Pauli-forbidden transitions of C-12 [23], a new limit on antineutrinos emitted by the Sun [24] and a study of the seasonal muon flux at Gran Sasso [25]. The detailed characteristics of the muon veto system and neutron detection have also been published [26].

During 2010 Borexino has benefitted from the calibration campaign carried over in 2009 Sources such as Co-57, Ce-139, Hg-203, Sr-85, Mn-54, Zn-65, Co-60 and K-40 were used for gamma calibration, while C-14, Bi-214 and Po214 activities were used to un-

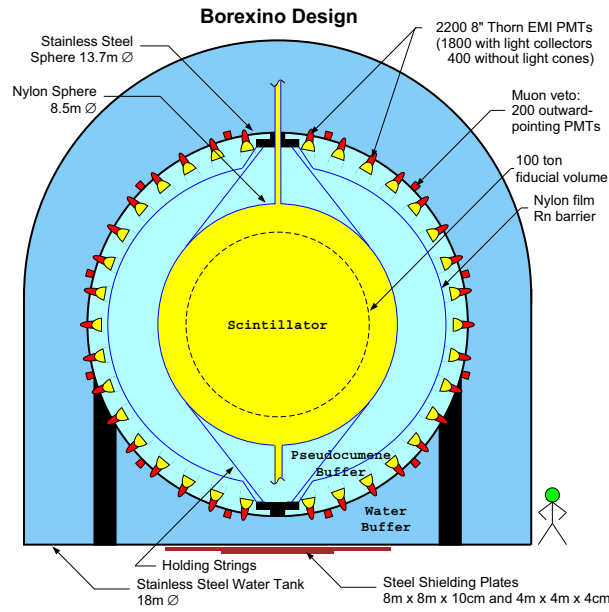


Figure 1: Schematic view of the Borexino detector.

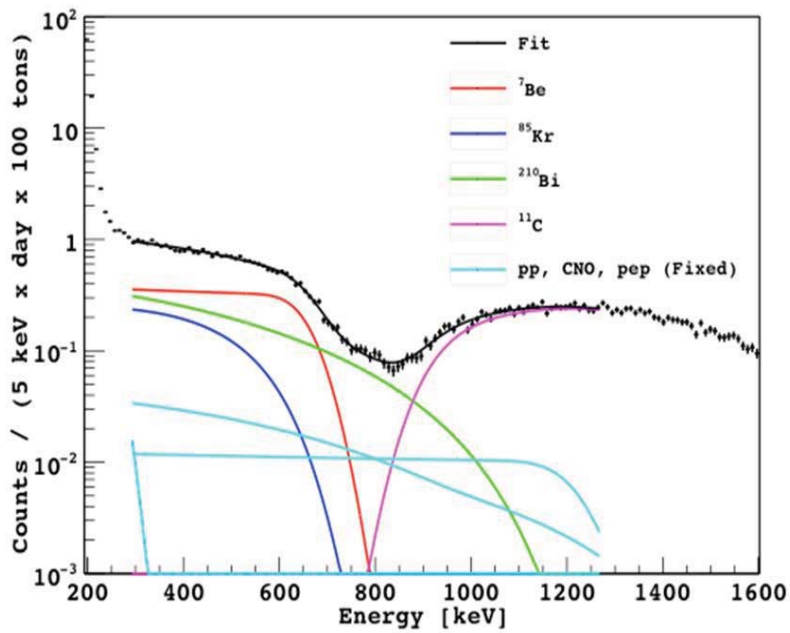


Figure 2: The observed Borexino spectrum after cuts, showing the shoulder due to solar Be-7 neutrino events (red line). The other main fit components in this energy region are also shown.

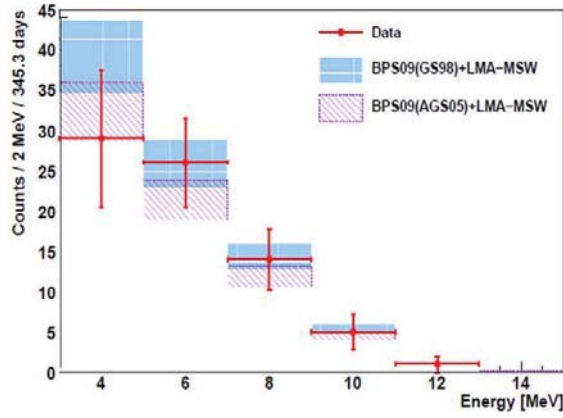


Figure 3: Comparison of the observed B-8 spectrum and the high-metallicity (GS98) and low-metallicity (AGS05) solar models, with LMA-MSW oscillations included.

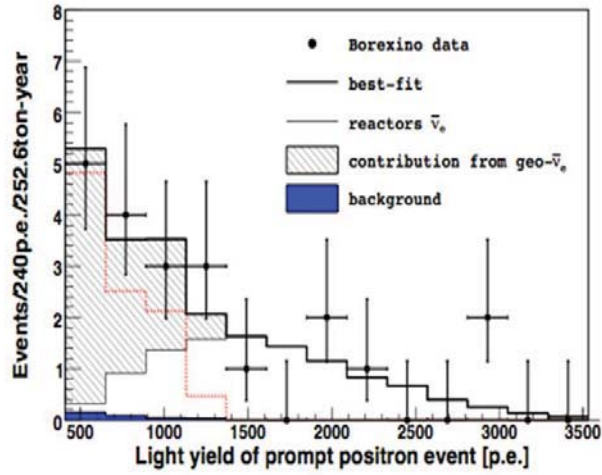


Figure 4: Light yield spectrum for positron events as a sum of geoneutrinos and nuclear reactor antineutrinos. The shaded area is the contribution of geoneutrinos alone.

derstand the response of the detector to β 's and α 's. Finally, an AmBe source was used for neutrons. These studies allowed a significant reduction of the systematic error on the determination of the Fiducial Mass and on the determination of the energy scale and made it possible to tune several parameters of the Monte Carlo simulation codes, such as the light yield and the quenching factor. The external sources were deployed in several positions inside the detector.

At the same time, purification campaigns have been conducted (water extraction and nitrogen stripping) that have significantly reduced two of the most important backgrounds, Kr-85 and Bi-210. The construction of a new purification plant for the distillation of the concentrated solution of PPO in pseudocumene has started; the plant will be completed, commissioned and tested within 2011.

4 Future perspectives

Further studies are being made on solar neutrino physics with the existing data that take advantage of the better understood performance of the detector. The Be-7 rate is being measured with an improved accuracy (less than 5%) with the potential of discriminating different metallicities in the Solar Models. This measurement together with the ongoing Day/Night asymmetry study and the B-8 measurement will be able to confirm the MSW-LMA scenario with Borexino data alone.

Additional physics topics are under study or being considered for future investigation, depending on the background conditions and on the refinement of the ongoing analysis:

1. Measuring (or putting upper limits) on CNO and possibly pep and pp solar ν 's.
2. Watch for neutrino bursts from Supernovae events.
3. Short baseline oscillation tests with Cr-51 and Sr-90 neutrino and antineutrino sources. This topic is of particular interest in view of the present controversial experimental scenario, encompassing the recently highlighted reactor and Gallium anomalies, the long standing LSND puzzle confirmed by the newest Miniboone antineutrino data, and the intriguing hints of CPT violating effects coming from MINOS. The emerging picture of an oscillation paradigm comprising 3 active plus 2 sterile neutrinos, the latter with masses at eV scale, could be nicely and effectively verified with a source test in Borexino for a significant portion of the parameter space, through the search of the oscillation pattern that at the considered L/E values should develop clearly throughout the detector. Furthermore, the compared neutrino-antineutrino measurements should help clarify the significance of the CPT indications from MINOS.

5 List of articles published in year 2010

1. G. Bellini et al., *New experimental limits on the Pauli forbidden transitions in ^{12}C nuclei obtained with 485 days Borexino data.* Phys. Rev. C, 81 (2010) 034317.
2. G. Bellini et al., *Observation of geo-neutrinos.* Phys. Lett. B, 687 (2010) 299.
3. G. Bellini et al., *Measurement of the solar ^8B neutrino rate with a liquid scintillator target and 3 MeV energy threshold in the Borexino detector.* Phys. Rev. D 82 (2010) 033006.

References

- [1] R. Davis, Nobel Prize Lecture 2002.
- [2] W. Hampel et al., Phys. Lett. B 447 (1999) 127.
- [3] J.N. Abdurashitov et al., Phys. Rev. Lett. 83 (1999) 4686.
- [4] M. Altmann et al., Phys. Lett. B 616 (2005) 174.
- [5] S. Fukuda et al., Phys. Rev. Lett. 86 (2001) 5651; Phys. Lett. B 539 (2002) 179.
- [6] Q.R. Ahmad et al., Phys. Rev. Lett. 87 (2001) 071301.
- [7] J.N. Bahcall and M.H. Pinsonneault, Phys. Rev. Lett. 92 (2004) 121301.
- [8] A. Serenelli et al., Astr. J. Lett., 705 (2009) L123.
- [9] G. Alimonti et al., Astroparticle Physics 16 (2002) 205.
- [10] J.N. Bahcall et al., JHEP 0408 (2004) 016.
- [11] G.L. Fogli et al., Progr. Nucl. Phys., 57 (2006) 742.
- [12] C. Arpesella et al., Astroparticle Physics 18 (2002) 1.
- [13] G. Alimonti et al., Nucl. Instr. & Methods A406 (1998) 411.
- [14] G. Alimonti et al., Astroparticle Physics 8 (1998) 141.
- [15] G. Alimonti et al., Nucl. Instr. & Methods, A600 (2009) 568.
- [16] G. Alimonti et al., Nucl. Instr. & Methods, A609 (2009) 58.
- [17] C. Arpesella et al., Phys. Lett. B 658 (2008) 101.
- [18] C. Arpesella et al., Phys. Rev. Lett. 101 (2008) 091302.

- [19] G. Bellini et al., Phys. Lett. B, 687 (2010) 299.
- [20] G. Bellini et al., Phys. Rev. D, 82 (2010) 033006.
- [21] T. Araki et al., Nature 436 (2005) 499.
- [22] S. Abe et al., Phys. Rev. Lett., 100 (2008) 221803.
- [23] G. Bellini et al., Phys. Rev. C, 81 (2010) 034317.
- [24] G. Bellini et al., Phys Lett B, 696 (2011) 191.
- [25] D. D'Angelo, talk given at BEYOND 2010, Fifth International Conference on Beyond the Standard Models of Particle Physics, Cosmology and Astrophysics, Cape Town (S. Africa) February 2010.
- [26] G. Bellini et al., in publication by J. of Instrumentation.

COBRA

G. Anton^a, V. Bocarov^b, M. Bellicke^e, P. Cermak^b, O. Civitarese^c, J. Durst^a, J. Ebert^h, A. Fauler^d, M. Filipenko^a, M. Fiederle^d, A. Garson^e, D. Gehre^f, T. Gleixner^a, C. Gößling^g, Q. Guo^e, C. Hagner^h, N. Heidrich^h, M. Heine^f, B. Janutta^f, M. Junkerⁱ, J. M. Jose^b, S. Kietzmann^h, T. Köttig^g, H. Krawczynski^e, V.K. Lee^e, Q. Li^e, J. Martin^e, T. Michel^a, D. Münstermann^g, T. Neddermann^g, C. Oldorf^h, S. Rajek^g, O. Reinecke^f, W. Schmidt-Parzefall^h, O. Schulz^g, M. Schwenke^f, F. Simkovic^j, A. Sörensen^f, I. Stekl^b, J. Suhonen^k, J. Timm^h, W. Thurow^f, B. Wonsak^h, K. Zuber^{f,*}

^a *Universität Erlangen–Nürnberg – Germany*

^b *Technical University of Prague – Czech Republic*

^c *University of La Plata – Argentina*

^d *Freiburg Materials Research Center – Germany*

^e *Washington University in St. Louis – USA*

^f *Technische Universität Dresden – Germany*

^g *Technische Universität Dortmund – Germany*

^h *Universität Hamburg – Germany*

ⁱ *Laboratori Nazionali del Gran Sasso – Italy*

^j *University of Bratislava – Slovakia*

^k *University of Jyväskylä – Finland*

(* Spokesperson)

Abstract

COBRA is an experiment searching for the $0\nu\beta\beta$ -decay using Cadmium Zinc Telluride (CdZnTe) semiconductor detectors arranged in a large array. Out of the several candidate isotopes in CdZnTe, COBRA is focusing on ^{116}Cd , because of its high Q-value of 2.8 MeV. Beside coplanar grid (CPG) detectors COBRA also uses pixelised CdZnTe detectors. The latter are unique within this field of physics and have the potential to reduce the expected background of the experiment by several orders of magnitude, using their tracking capability. Beside the current status of the COBRA setup at the Laboratori Nazionali del Gran Sasso (LNGS), analysis aspects of recent data are described. In addition, background studies are shown and different pixelised detector types tested within the COBRA setup are presented.

1 Introduction

The COBRA experiment, proposed in [1], uses CdZnTe crystals as its detectors. Within this material, 9 isotopes are double-beta-decay candidates, the most promising being ^{130}Te and ^{116}Cd . The main virtue of ^{130}Te is its very high natural abundance of 33.8 %. Whereas ^{116}Cd is superior due to its high Q-value of 2809 keV, which lies above the ^{208}Tl peak at 2614 keV, the most intense gamma line from natural radioactivity. This advantage is quite crucial: Not only does a higher Q-value increase the phase space – and thus the probability – for the sought-after decay, but it also reduces the gamma background from natural radioactivity by more than one order of magnitude with respect to isotopes with Q-values below the ^{208}Tl peak. In contrast to other semiconductor or bolometric detectors, CdZnTe crystals have the convenience that they can be operated at room temperature, still providing an excellent energy resolution of a few percent. Also, they are commercially available, making them comparatively inexpensive. Furthermore, they have proven to be very radiopure, which is crucial for avoiding intrinsic background.

To reach competitive sensitivities, future $0\nu\beta\beta$ -experiments need to reduce their background rates to less than 10^{-3} counts/kg/keV/year. To achieve this, the COBRA experiment considers to use a large array of several thousand CPG detectors. Background could then be discriminated by restricting the analysis to events in a single detector unit. Another option is the usage of pixelised detectors. Even relatively large pixels have a high capability to increase the signal to background ratio, as described in chapter 5. Finer grains would even make it possible to resolve the decay topology, dramatically reducing the background.

COBRA is currently in the R&D phase. Beside the aforementioned detector-related subjects, other experimental topics like the shielding and pulse shape-analysis are studied to further lessen the background. At the LNGS, a prototype setup is maintained to prove the feasibility of the large-scale experiment and study the power of the design in terms of background reduction. Recent work on the prototype setup is summarised in chapter 2. Chapter 3 presents studies regarding the background from natural radioactivity and external sources, while chapter 4 reports on R&D dealing with CPG. Various types of pixelised detectors tested in the COBRA setup at the LNGS are then introduced in chapter 5. Chapter 6 gives a report on the progress of crystal growing and detector assembly within the collaboration. Finally, after a view on the treatment of previous data in chapter 7, a summary is given in chapter 8.

2 LNGS Setup and Upgrade

In 2010, a prototype COBRA setup, capable of handling a total of sixty-four 1 cm^3 CdZnTe crystals has been in operation at the LNGS. It consists of four layers, each capable of holding 4×4 detector crystals in a Delrin support. This array is surrounded by 10 cm of pure copper shielding and 20 cm of low-radioactivity lead. Supply of bias voltages and signal readout occurs via low-diameter coaxial cables and copper traces on Kapton foils, being fed through the shielding. The whole apparatus, including the electronics, is placed inside a copper Faraday cage, surrounded by 7 cm of borated polyethylene,

shielding against neutrons. In addition, the inner volume is flushed with nitrogen gas, to reduce the background from radon.

Lately 8 CPG detectors and several pixelised detectors have been taking data. It is planned to move the setup to a new position inside the LNGS and then put in operation a complete array of 64 CPG by the end of 2011. This chapter describes the latest improvements in electronics and data acquisition (DAQ), as well as the design of a new shielding, planned for the revised setup.

2.1 New COBRA DAQ Chain

Parts of the FADC¹ system previously used by the AMANDA experiment[2] were granted to the COBRA Collaboration in 2010. As a first test, a prototype pulse-shape based DAQ system was installed at LNGS at the end of August 2010 to instrument the 8 CPG detectors currently underground. The system uses two AMANDA FADCs of the same type that were reassigned to COBRA, a modified COBRA preamplifier and two fast linear amplifiers newly developed at the TU Dortmund for signal conditioning. For the readout also a completely new DAQ software had to be developed. After a testing phase the new DAQ electronics and software were operated in normal run conditions at the LNGS. In the 1 kg days of data collected so far only four events occurred in the region of interest (ROI) between 2.7 MeV and 2.9 MeV. The pulse shapes of these four events are shown in Figure 1. One of these four events can be identified as disturbance not coming from energie deposition within the crystals. Even though the number of electromagnetic interferences will significantly decrease with the new COBRA electronics and setup, this example shows the potential for reducing backgrounds with pulse shape analysis (see also [3]).

2.2 Electronics Upgrade for Pulse Shape Readout

For the pulse shape readout new electronics are required. For the first tests at LNGS the newly developed 8 channel fast linear amplifier proofed to be reliable and tests in the lab showed a good performance. With the linear amplifier and digital processing of the pulse shapes an energy resolution of 2.3% FWHM² was achieved, the best energy resolution ever measured by COBRA with CPG detectors. The obtained energy resolution was even better than the resolution information provided by the manufacturer of 2.6% FWHM.

To enhance the quality of the signals and minimize electromagnetic interferences, differential signal transmission from the preamplifiers to the FADCs as well as for the device control will be applied. A prototype for the conversion of single-ended to differential signals and back was designed and tested. The application of differential signal transmission, even over a long distance of several meters, did not result in a degradation of energy resolution.

¹Flash-ADC

²Full Width Half Maximum

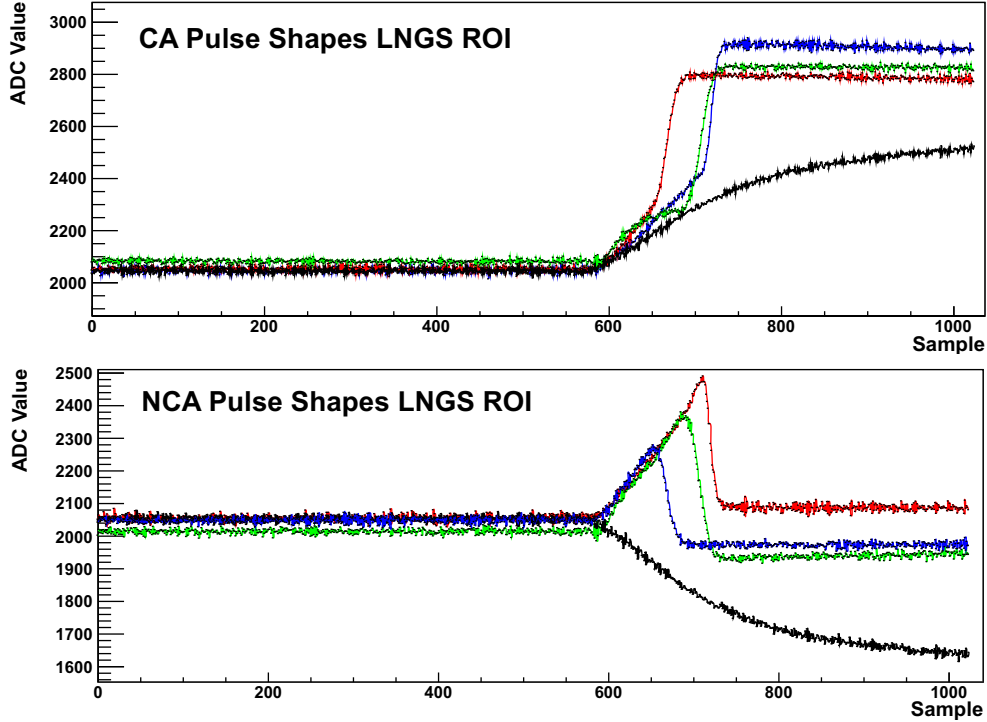


Figure 1: Pulse shapes of the four events in the ROI. The black event can clearly be rejected as non physical due to its shape. The upper part shows the signals at the collecting anode (CA) and the lower part at the non-collecting anode (NCA).

2.3 New COBRA Hut and Shielding Upgrade

Due to the progressing research activities the COBRA collaboration requested a larger lab space in the LNGS Underground Facilities. This request was kindly fulfilled with the reassignment of a part of the former Heidelberg-Moscow hut to the COBRA collaboration.

The relocation of the COBRA setup to this new position offers the opportunity to redesign and improve the shielding. Therefore the neutron shielding, which houses an electromagnetic shielding and the shield against environmental radioactivity, is currently rebuilt to allow a better utilization of the space inside and to give better access. Also, an extensive MC study was undertaken, to optimize the performance of the shield. Since the current electromagnetic shielding made of copper does not shield sufficiently against disturbances like radiocommunication, a new one made of galvanized steel sheets with special seals is currently designed and manufactured.

To suppress the background induced by the radioactive noble gas radon, the setup is currently flushed with nitrogen gas. In the new hut the setup will additionally be sealed with a special barrier foil to prevent radon diffusion into the setup.

3 Background Studies

Among several experimental parameters relevant for the sensitivity of an $0\nu\beta\beta$ -experiment only the background rate can easily be modified by several orders of magnitude. For this reason, it is essential to not only minimise the background as best as possible, but also to understand the remaining background, thus allowing estimations of the sensitivity. In this chapter, a background analysis of the 2009 data using timing coincidence and results of material test for the crystal passivation are presented. In addition, simulation for the shielding, especially of neutrons, are presented.

3.1 Timing Coincidence Analysis

One major background source in the COBRA experiment arises from the natural decay chains ^{232}Th , ^{238}U and ^{235}U , with ^{238}U being the dominant one. This background may be reduced and estimated by coincidence analysis: Some of the nuclides occurring within the decay chains have a very short half-life and thus a unique decay signature that is unlikely to be mimicked by other events. Therefore a timing coincidence analysis was done to deduce the internal contamination of the CdZnTe detectors. It has been performed for the datasets of 2008 and 2009 taken with four colourless passivated detectors at LNGS that were constantly flushed with nitrogen in order to reduce background arising from ^{222}Rn . Furthermore energy cuts were applied to consider only internal decays.

The most important timing coincidence is the decay of ^{214}Bi occurring within the ^{238}U -chain: ^{214}Bi decays via β -decay into ^{214}Po with a Q-value of 3.272 MeV. ^{214}Po has a half-life of only 164.3 μs and decays via α -decay into ^{210}Pb with an α -energy of 7.687 MeV: This decay sequence accounts for 70 % of all background events arising from the ^{238}U -chain in the 2-3 MeV energy region. The applied analysis determines the intrinsic contamination to be $(8.1^{+9.1}_{-5.1}) \frac{\mu\text{Bq}}{\text{kg}}$.

Another important decay sequence to investigate is the decay of ^{212}Bi occurring in the ^{232}Th -chain, which decays via α -decay into ^{208}Tl with a branching ratio of 35.94 % and α -energies of 6.051 MeV and 6.090 MeV. ^{208}Tl has a half-life of 3.083 min and decays via β -decay into ^{208}Pb with β -energies up to 1.796 MeV:

^{208}Tl has a much larger half-life compared to ^{214}Po . This causes random events other than the $^{212}\text{Bi} \xrightarrow{\alpha} ^{208}\text{Tl} \xrightarrow{\beta} ^{208}\text{Pb}$ decay sequence to occur within the observation period. It is therefore essential to choose selective energy cuts. Applying them a detector contamination of $(30^{+20}_{-12.1}) \frac{\mu\text{Bq}}{\text{kg}}$ was found. However, due to the large half-life used in this coincidence, the calculated contamination can only function as an upper limit on the true intrinsic contamination of the detectors.

3.2 Material Assaying of Passivation Parylene C

CdZnTe detectors have to be passivated in order to prevent the detector material from degrading. During the last years the COBRA collaboration investigated several detector passivations to replace a red passivation lacquer applied by the detector manufacturer eV Microelectronics. This passivation is known to have a comparatively large radioactive

contamination. As a promising alternative passivation, the polymer Parylene C was examined regarding its radiopurity.

A first measurement was done with the ultra-low-background Germanium detector at the Dortmund Low Background facility (DLB). Because the impurity level of Parylene C turned out to be too low to be measured with the DLB, 500 g of Parylene C were measured by spectroscopy by Matthias Laubenstein at LNGS and a small sample was investigated via Inductively Coupled Plasma-Mass Spectrometry analysis (ICP-MS) by the Chemistry and Chemical Plant Service at LNGS. The activities determined in the Parylene C sample are about two orders of magnitude smaller than the activities obtained from the red passivation sample and have approximately the same amount of contamination as the colourless passivation of eV Microelectronics. Furthermore, Parylene is used as an extremely thin coating with a coat thickness of a few μm , much less than the other passivation lacquers.

Simulations show, that for a coating of $4\ \mu\text{m}$ with the measured contamination, the contribution of a passivation with Parylene C to the background would be less than 5% compared to the aim of 1 counts/keV/kg/yr for the 64 crystal array. Regarding a large-scale setup the obtained background level achievable with Parylene C still seems to be comparatively high. However, the scenario simulated is a worst case scenario and much lower contributions seem to be realistic.

3.3 MC-Studies for Neutron Shielding

Based upon earlier studies[5] several alternative variants of a neutron shielding for a 64.000 crystal COBRA array have been tested. The usual COBRA simulation framework has been used, utilising Geant4 with the low energy expansion for dark matter experiments. The aim was to find a passive shielding of similar effectiveness with a less complicated composition (to minimise the construction cost and effort) and to determine the resulting background. Types of shieldings considered are: shieldings consisting of a single material layer, multilayer shieldings, large water or liquid scintillator tanks and composite like shieldings with many thin layers of different materials. In total more than 250 different setups have been under investigation (see [6]).

The spectrum of muon induced neutrons at the Gran Sasso laboratory as described in [7] has been used to see how many signals are generated in the detector array. Some of the results can be seen in Figure 2. The best passive shielding in this study performs a factor four better than the best variant of the previous study with the same total thickness. The effect of the active shielding components however has not yet been taken into account.

The analysis also showed, that using the array to reject multiside events, this rate could be reduced by at least another order of magnitude. Low-energy neutrons produced by natural radioactivity lead to an even lower background, in spite of their abundance at the LNGS being about three orders of magnitude higher than that for muon induced neutrons.

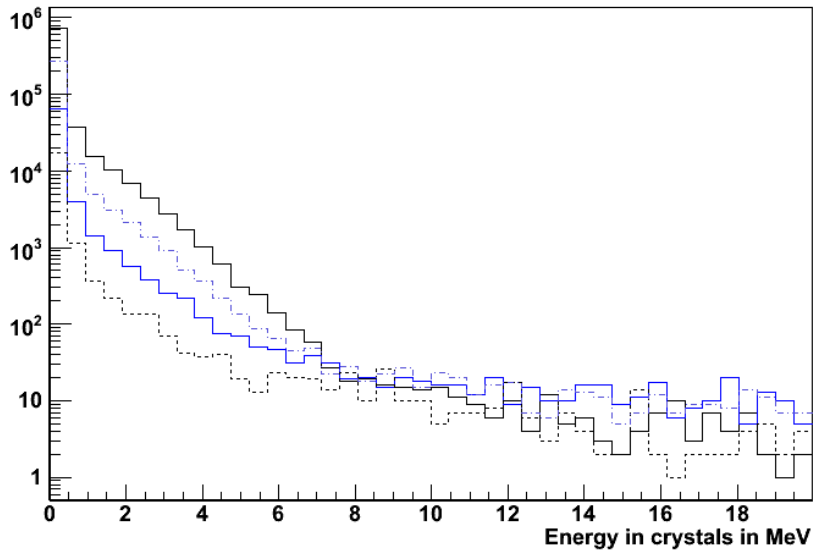


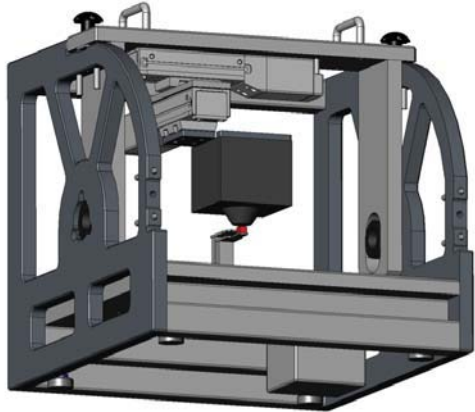
Figure 2: Simulated spectrum of the neutron induced energy deposition in a COBRA-detector made up of 64.000 crystals for different shieldings with the same total thickness. The black full line indicates a pure lead shielding, the blue dotted line a standard multilayer shielding, the full blue line a composite like shielding and the dashed grey line an optimised multilayer shielding of the ongoing study.

4 CPG Activities

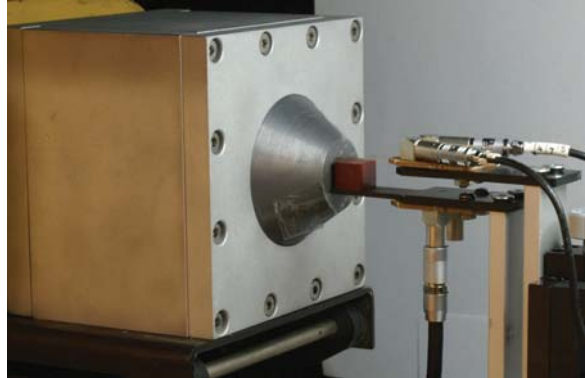
The basic idea of the COBRA experiment is to use a large array of CPG detectors. In comparison to fine grained pixelised detectors, CPGs are available with large active volumes and need few readout-channels. The latter point minimises the amount of other material in the direct surroundings and thus the risk of possible contamination. In the near future, the COBRA prototype setup at the LNGS will be upgraded to a complete array of 64 CPG detectors. To optimise this setup and to be able to understand its performance it is necessary to ascertain the quality of each crystals. A dedicated apparatus, currently installed at the TU Dresden, is described below. Additional studies concerning the operation of CPG detectors when immersed in liquid scintillator are also presented.

4.1 Detector Characterization

Beside the energy resolution, the charge collection efficiency (CCE) ϵ is the second major contributor in terms of detector performance. As the supplied detectors are from different batches and of different quality grades the performance of each detector has to be examined before the installation. Since all detectors are of the same geometry and grid layout, the performance is strictly related to the quality of the material. To gain information about the spatial distribution of the CCE a scanning device and a highly collimated γ -ray source is needed. For this purpose a special test rig has been designed that allows the irradiation of the detector from all three directions in a well controlled way (Figure 3a).



(a) Scheme of the detector test rig, the detector can be scanned from three sides with a minimum distance of about 1 mm between the collimator and the detector surface.



(b) Closeup view of the collimator and detector mounting in operational position. The detector is contacted with Cu-Be-lamellas for quick exchange of the device under test.

Figure 3: Detector test rig and collimator setup

In this setup a collimator is moved along the sides and the top of the detector (anode-side), scanning each side completely. This allows to calculate the CCE as a function of the 3-dimensional position within the crystal volume. In combination with a pulse shape analysis it is possible to correct the charge loss in dependence on the interaction depth (z-direction). The main drawback of this approach is, that a possible inhomogeneous CCE distribution in the x-y-plane cannot be corrected since the CPG detectors are not able to resolve the point of origin in this plane. First one dimensional test have successfully been performed with a high intensity (100 MBq) ^{137}Cs source.

The setup of the test rig is ongoing and will be finalized in spring 2011. As soon as this device is fully operational, the 2-dimensional mapping and the 3-dimensional back projection of the CCE for the 64 detectors will start. Beside the CCE investigations of the detectors further experiments are carried out to test the influence of a lowered operational temperatures of the detectors to the charge collection efficiency and energy resolution. Therefore a test box has been build and equipped as well. All the investigations will be performed with pulse shape analysis and digital post processing of the data.

4.2 Operation of CdZnTe Detectors in Liquid Scintillator

One possibility to generate a low-background environment, proposed by Heusser [4], is to use a passive and ultra-clean environment like liquid nitrogen to cool and shield HPG 3 detectors. The COBRA collaboration adopted this idea and investigates liquid scintillators as an ultra-low-background environment for CdZnTe detectors. Experiments like BOREXINO or KamLAND have shown that the production of liquid scintillators with high radiopurity is possible.

3 high purity Germanium

The design of the test setup built and operated at the University of Hamburg is shown in Figure 4. The unpassivated CdZnTe crystals are dumped in liquid scintillator, which acts as an active veto and shield. First measurements demonstrate the power of this veto system: In the main ROI for the COBRA experiment between 2.7 MeV and 2.9 MeV, the background counts are reduced by about 90% compared to the operation in nitrogen or liquid scintillator without active veto.

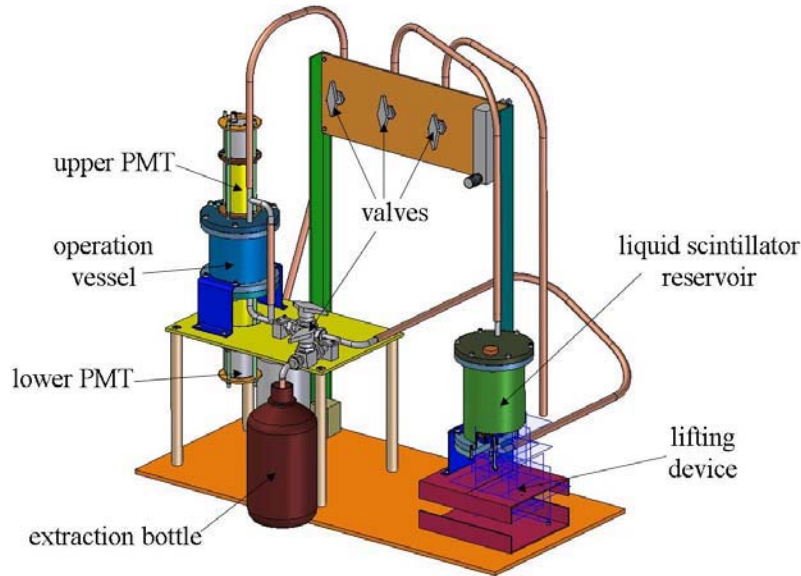


Figure 4: Schematics of the test setup constructed and built at the University of Hamburg. The CdZnTe detectors are suspended in liquid scintillator within the operation vessel.

The setup is currently revised to be operated with eight CdZnTe detectors. This will allow for coincidence analysis, more statistics and certainty on long term stability. The setup is also implemented into the COBRA Monte Carlo framework to optimize the veto efficiency and study the shielding prospects of the liquid scintillator.

5 Pixel Detectors

Pixelised detectors have a very high potential to reduce background, by using topological information. However, they require a large amount of readout electronics, increasing the danger of contamination and leading to other technical challenges. Thus, it is essential to understand both the possible win in background reduction as well as the possible limitations of this technology. Therefore, three different systems are being studied in the COBRA test setup. The test results are presented below.

5.1 WUSTL Pixel System

A prototype pixel experiment was tested underground at Gran Sasso from mid-January to mid-April 2010. The detector system was developed at Washington University in Saint

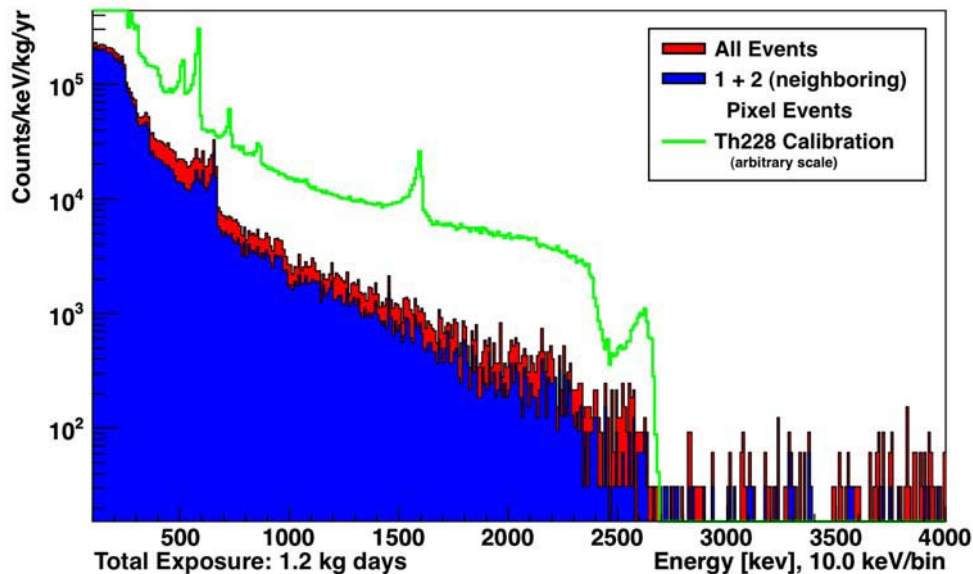


Figure 5: Energy spectra for the $10 \times 20 \times 20 \text{ mm}^3$ detector from the Washington University group which ran for three months in early 2010. The red spectrum includes all events from the 1.2 kg-days of data, while the blue spectrum is composed of only events which trigger either a single pixel or two neighboring-pixels. The green line shows the ^{228}Th calibration spectrum for reference.

Louis under the direction of Henric Krawczynski. The system uses a $10 \times 20 \times 20 \text{ mm}^3$ CdZnTe sensor contacted with an 8×8 array of pixels at a pitch of 2.5 mm. The pixels are read out using a low-noise ASIC⁴ system based on the Brookhaven NCI-ASIC with a low-gain dynamic range from 10 to approximately 5000 keV per channel. With a sensor mass of more than 23 grams, the experiment produced about 1.2 kg-days of data.

The pixel prototype was operated in the same low-background enclosure used for COBRA's coplanar grid detectors. The prototype system itself was not optimized for low-background operation. However, a second prototype is being designed which would make use of special materials and components such as Kapton foil and Teflon boards.

The system was calibrated and characterized with ^{22}Na and ^{228}Th sources upon installation at LNGS. The prototype showed an energy resolution of 9.2 keV FWHM at 583 keV (1.6%) while the best detector of this design produced at Washington University showed a resolution of 5.6 keV FWHM at 662 keV (0.85%).

One of the primary benefits of a pixelated detector is additional background reduction. For example, an event where two non-neighboring pixels are triggered is most likely a gamma-ray interaction, rather than a double-beta event. Therefore, at this stage of data analysis only events which trigger a single pixel or two neighboring pixels are counted (see Figure 5). In the signal region, the background level for the full 1.2 kg-day dataset then drops from 29.2 to 12.3 counts/keV/kg/yr.

⁴Application Specific Integrated Circuit

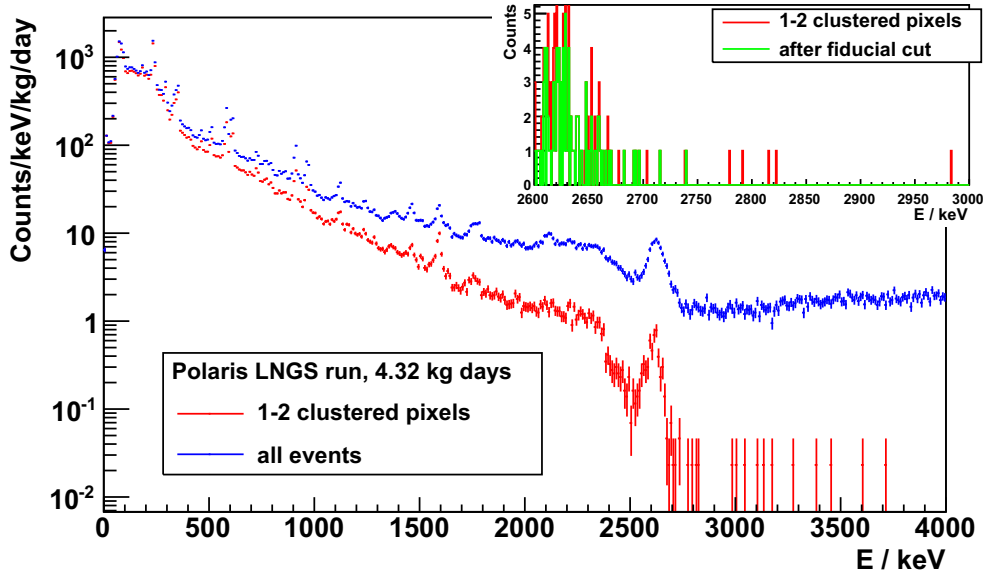


Figure 6: Low-background data taken with the Polaris CdZnTe pixel detector at LNGS. After cuts, zero events remain in the region of between 2.75 and 2.85 MeV for the $0\nu\beta\beta$ decay of ^{116}Cd .

5.2 The Polaris CdZnTe Pixel System

In September 2009, the collaboration installed a large-volume CdZnTe pixel detector at LNGS, in cooperation with Prof. Zhong He (University of Michigan). The detector, measuring $2\times 2\times 1.5\text{ cm}^3$, was successfully run underground from September 2009 to January 2010, collecting 4.32 kg days of data.

To achieve an optimal signal to background ratio for the applied cuts, $0\nu\beta\beta$ decays of ^{116}Cd were simulated in the 11×11 pixel detector. The distribution of the number of pixels hit and the distance between these pixels in a $0\nu\beta\beta$ event was examined.

As the investigation of the measured spectrum showed, the restriction to two hit pixels results in a high background rejection. The simulations showed that less than 72% of all $0\nu\beta\beta$ events and 67% of all double beta events with full energy deposition have less than three hit pixels. Further restriction to neighbouring pixels marginally decreases this efficiency because the electrons lose their full energy after a few mm. With this cut the background level can be reduced to 6.3 counts/keV/kg/yr in the ROI. The choice of this cut therefore significantly increases the signal to background ratio.

Since the detector was coated with a red passivation paint, known to be a significant background source, a fiducial cut was applied to the data, removing all event affecting pixels at the detector boundary. This fiducial cut reduces the detector volume and therefore the efficiency by an additional factor of 70% but further increases the signal to background ratio. The number of events in the ROI reduces to two counts what is equivalent to 0.9 counts/keV/kg/yr. With the chosen cut of two or less clustered pixels and the fiducial cut, the efficiency for a full energy deposition of a $0\nu\beta\beta$ event of ^{116}Cd was calculated to be 29%. The impact of the cuts to the background spectra is shown in Figure 6.

5.3 Simulations for the Timepix Detector

The Timepix detector has been developed by the international Medipix collaboration. It can be used in time-projection-chambers or as an X-ray imaging detector. The Timepix ASIC comprises 256×256 electronic cells at a pitch of $55 \mu\text{m}$ with preamplifier, discriminator and counter which can be bump-bonded to a pixelated semiconductor sensor layer. The active area of the sensor layer is $14 \times 14 \text{mm}^2$. The energy deposition is measured in each pixel by the time-over-threshold (TOT).

In order to assess the feasibility and performance of CdTe pixel detectors in a search for the neutrinoless double beta decay in ^{116}Cd , simulations have been performed to find the optimal parameters and possible sensitivity of a setup with Timepix-like detectors. In the simulation we take into account the electronic analog noise, the energy-to-TOT conversion, digital TOT-noise, electric field map in the sensor, diffusion and drift of charge carriers and the weighting potential.

It turned out that the resolution of the TOT-measurement of the Timepix detector leads to an energy resolution of about 1.3% for the sum energy of the two decay electrons occurring in double beta decay events if we assume that the energy-TOT-calibration curve of all pixels is known with negligible errors. Without calibration we would be able to achieve a sum energy resolution of about 3%. This sum energy resolution is approximately 5 times better than the energy resolution in each pixel - a result of summing energy depositions in a lot of pixels.

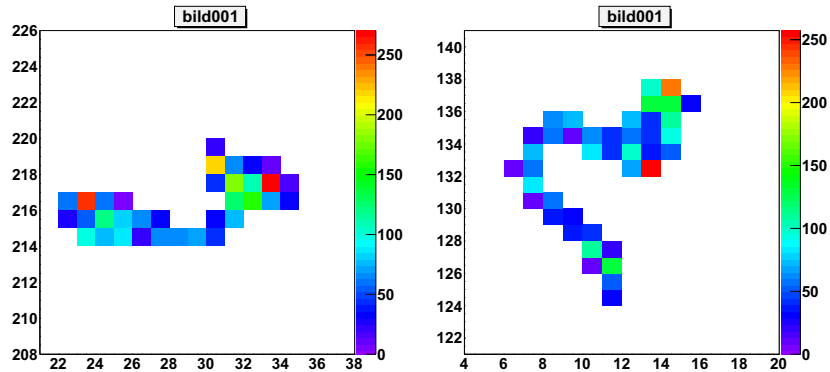


Figure 7: Comparison of a $0\nu\beta\beta$ event (left) with a total energy of 2768 keV and the track of a single electron (right) with an energy of 2761 keV deposited in the sensor. The colorbar represents deposited energy in keV

5.3.1 Background Suppression by Track Analysis

The main advantage of the fine pixel pitch detector is, that it is possible to identify particles, by their track structure in the sensor. While it is easy to distinguish between an α particle and a double beta event, the difference between one electron and a double beta event is not always obvious. An example of the corresponding tracks is shown in Figure 7. Both tracks were simulated with the same sensor with a pixel pitch of $110 \mu\text{m}$.

Currently we are investigating the background suppression by analyzing different criteria of a track with a neural network.

5.4 Data Taking with the Timepix Detector at the LNGS

In 2010, a 1 mm thick CdTe detector with 128×128 pixels of $110 \mu\text{m}$ pitch has been installed at the LNGS. The Timepix ASIC, bump-bonded to it, was connected to the computer using a USB readout system developed at IEAP CTU Prague and controlled using the Pixelman software developed at the same place. The pixel detector was enclosed in an aluminium casing to mechanically protect it and allow for nitrogen gas flushing. This assembly was located on top of the COBRA setup and surrounded by 10 cm of lead shielding.

An analysis of the event topology has been performed, aiming at the differentiation of the various types of events (alpha, electron, muon etc.). For this, the Pixelman software was used, exploiting properties like roundness, linearity and cluster size. The spectrum of the background measurement is shown in Figure 8. In addition, the spectrum of events with a linearity of larger than 0.9 and a cluster size of 5 or more is shown. The remaining signals are mainly from electrons and only one signal remains above 2.5 MeV. This clearly shows the great potential for background reduction. However, while it is easy to identify alpha particles by the high roundness of their clusters, electrons do not feature a signature being that clear. Studies for finding optimal electron selection criteria are currently being conducted.

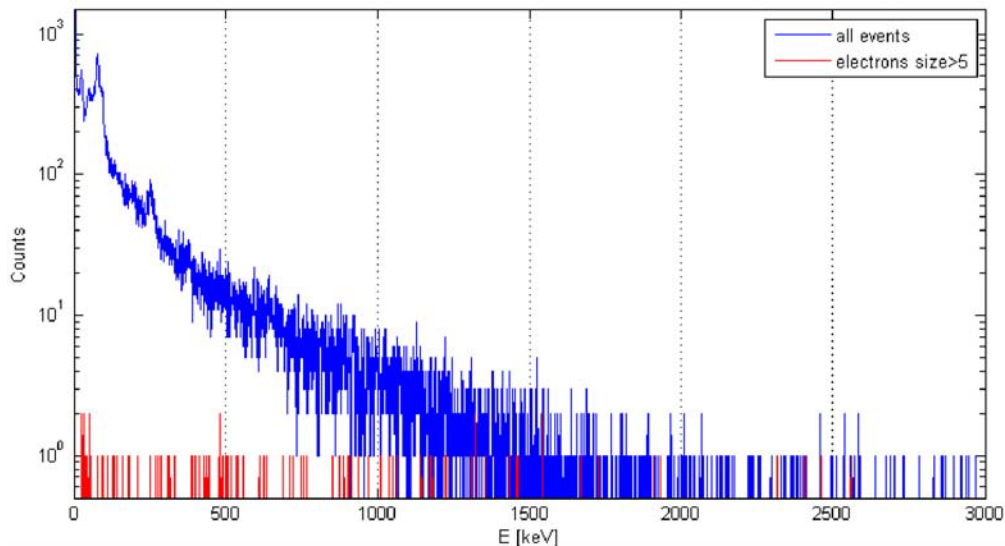


Figure 8: Comparison of spectrum of all events (after 5 weeks of measurement) with spectrum of electron (linearity 0.9, cluster size five and above) events.

6 Crystal Growing and Detector Preparation

6.1 Crystal Growing of Detectorgrade CdZnTe

Two facilities are available for the production of CdZnTe crystals from high purity source material at the Freiburger Materialforschungszentrum (FMF). The Bridgman⁵ furnace allows the growth of 75 and 100 mm diameter CdZnTe crystals. Recent improvements have been made including a new patent for the improvement of the quality of the detector grade crystals. The use of this patent reduces the number and the average size of tellurium inclusions. The tellurium inclusions are the main limiting factor of the detector performance of CdZnTe crystals. The average size of the inclusions was reduced below 15 μm .

6.2 Detector Preparation

The FMF has the experience and the facilities for preparation of CdZnTe and CdTe detectors. The crystals were cut by wire saw and polished for further processing in the clean room facility. The production of CPG detectors as well as pixel detectors for the Medipix2 and Timepix readout electronics is done in the FMF. The FMF has developed the complete process chain for radiation detectors using CdZnTe and CdTe 75 mm diameter wafers. The preparation of CPG detectors was improved by the introduction of a new permanent passivation based on Parylene. The Parylene is protecting the detector with a thin film which capsules the surface and the contact of the detector from pollution and oxidation. Measurements have been performed which show a positive effect on the detector performance with Parylene. This protection layer will be applied to the production of pixel detectors as well.

Latest development of the Medipix based pixel detectors was the successful processing of 2 mm CdTe crystals for a pixel detector with 110 μm pixel pitch. This configuration offers the possibility of high spatial resolution and high efficiency. The wafer thickness with 2 mm is a challenge for the processing of 110 μm pixel pitch. The complete production chain was modified and adapted to the thick and heavy detectors. The stability of the interconnecting bumps was improved and comparable to the 1 mm assemblies.

The investigation of the homogeneity of the Medipix assemblies is the most important task of the further development of the pixel detectors. The correlation between material properties and the detector performance has to be evaluated. The features are the homogeneity, the efficiency and the stability of the processing. Different tests with x-ray tubes, radiation sources and a Synchrotron have been performed to characterize the Medipix assemblies. It was possible to identify dislocation planes in the crystal wafers causing a reduced detector signal in the related pixels. The size of such a spot is around 10×10 pixels. This spots can be avoided by intensive material characterization before processing and selection of the right CdTe wafers.

⁵The Bridgman-Stockbarger-Methode ist a crystal growth method for production of single crystals like silicon, GaAs and CdZnTe.

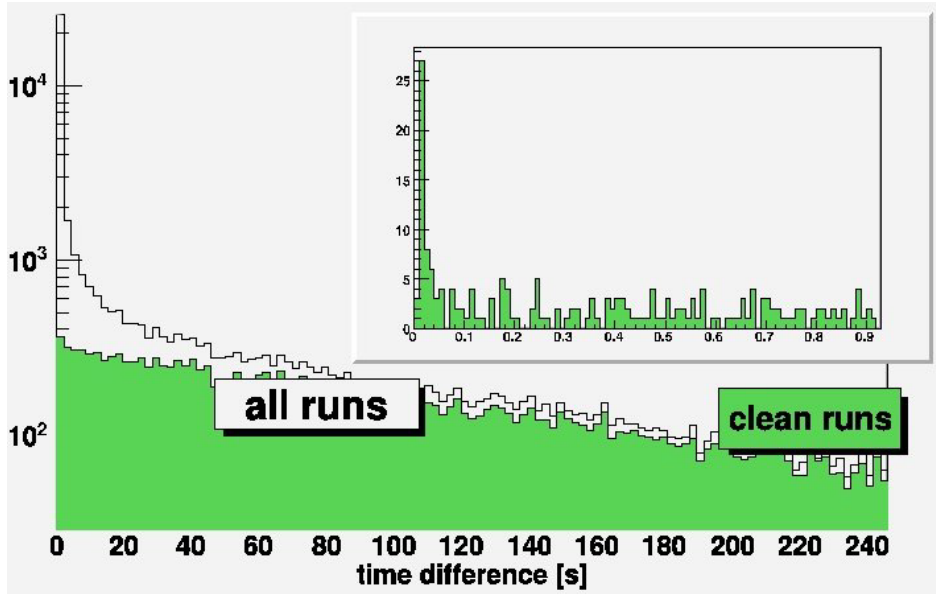


Figure 9: Example for the spectrum of time differences before and after the removal of unclean runs. The smaller plot shows, that residual pairs of noise events could be removed using a new smaller time limit of 0.1 s.

7 Data Cleaning of the 2009 Gran Sasso Data

In 2009, the COBRA setup at the LNGS has been running for about 850 h with 8 CPG detectors. The corresponding data is divided into runs of one hour operational time. Before and after each run, the crystals have been calibrated. As result, the built-in hardware energy threshold for each crystal has been reset from time to time. So, for each crystal, there are several threshold energies, which have to be taken into account if comparing different runs.

If the threshold energy is left unchanged, the detector setup should report a constant rate of events per run. However, due to a defective high voltage supply, some periods of data taking show increased noise. In this case, a set of two or more events with arbitrary energies are written into the data. In contrast to ordinary signals, these events are correlated and occur within a short timespan. For uncorrelated events an exponential spectrum of time differences is expected. However, as can be seen in Figure 9, the spectrum for a given group of runs with constant run conditions differs significantly from this exponential behaviour for small time differences. Therefore, a lower time limit t_{cut} has been introduced to enclose the non-exponential part. Using Poisson statistics and the results of exponential fits, the minimum number N_{cut} of events pairs below this time threshold was calculated, for which the probability of finding more than N_{cut} random pairs below t_{cut} is smaller than 1%. Runs with more entries below t_{cut} as calculated in this way have then been discarded. As Figure 9 suggests, t_{cut} may be reevaluated using thus cleaned spectrum. Usually, the time limit was much smaller than before and the probability, to have a zero random pairs of uncorrelated signals below this time threshold, grew to more than 99%. Thus removing the event pairs below the new t_{cut} completed the cleaning.

It turned out that two of the crystals have been affected by this kind of noise all the time. For the rest of the crystals 25% of the runs had to be removed.

8 Summary

The COBRA experiment aims to search for the $0\nu\beta\beta$ -decay of ^{116}Cd with CdZnTe semiconductors. It is currently in the R&D phase. The collaboration is maintaining a test setup at the LNGS. Beside CPG detectors with different passivations, several pixelised detectors have been in operation at the setup during 2010. Newly installed electronics have allowed to reach the best energy resolution for CPG detectors in COBRA so far. In addition, pulse shape information are also available now, considerably reducing the electronic background. Furthermore, the shielding is being redesigned, as the setup will soon be moved to a new position at the LNGS.

The MC studies, as well as the analysis of recent data presented here, show the large progress made so far by the collaboration in the understanding of the background and methods reducing it. In particular, the operation of pixelised detectors demonstrates their high potential in terms of background reduction. Presently, various pixelised systems are investigated, also regarding their suitability for a large-scale setup of several hundred kilograms of detector material.

It is planned to establish an array of 64 CPG in 2011, demonstrating the feasibility of a larger setup. The data of this array will further improve the understanding of the expected background for the full-scale experiment. Systematic characterisations of the CPG detectors in a dedicated apparatus at the TU Dresden and a material survey with the DLB will help to improve the performance in terms of sensitivity. Finally, a scientific proposal, based on all the above research activities, is foreseen by the end of 2012.

9 List of Publications

1. *Detecting multi-hit events in a CdZnTe coplanar grid detector using pulse shape analysis: A method for improving background rejection in the COBRA $0\nu\beta\beta$ experiment*, J. McGrath, B. R. Fulton, P. Joshi *et al.*, Nucl. Instrum. Meth. **A615** (2010) 57-61.
2. *Background capabilities of pixel detectors for double beta decay measurements*, P. Cermak, I. Stekl, V. Bocarov *et al.*, Nucl. Instrum. Meth. A (2010)
3. *The status of the COBRA double-beta-decay experiment*, K. Zuber, Prog. Part. Nucl. Phys. **64** (2010) 267-269
4. *Status of the COBRA double beta decay experiment*, K. Zuber, J. Phys. Conf. Ser. **203** (2010) 012070
5. *Long term prospects for double beta deca*, K. Zuber, [arXiv:1002.4313 [nucl-ex]] (2010)

References

- [1] K. Zuber, *Physics Letters B* **519** (2001) 1.
- [2] E. Andres *et al.*, *Astropart. Phys.* **13** (2000) 1-20.
- [3] J. McGrath *et al.*, *Nucl. Instrum. Meth.* **A615** (2010) 57-61.
- [4] G. Heusser, *Ann. Rev. Nucl. Part. Sci.* **45** (1995) 543.
- [5] D. Y. Stewart, P. F. Harrison, B. Morgan and Y. Ramachers, *Nucl. Instrum. Meth. A* **571** (2007) 651.
- [6] N. Heidrich, diploma thesis, <http://neutrino.desy.de/publikationen/diplomarbeiten/>
- [7] D. Mei and A. Hime, *Phys. Rev. D* **73** (2006) 053004.

The CRESST Dark Matter Search

G. Angloher ^a, M. Bauer ^e, I. Bavykina ^a, C. Bucci ^d, A. Brown ^b, C. Ciemniak ^c,
R. Falkenstein ^e, F. von Feilitzsch ^c, D. Hauff ^a, P. Huff ^a, S. Henry ^b, S. Ingleby ^b, C. Isaila
^c, J. Jochum ^e, M. Kiefer ^a, M. Kimmerle ^e, R. Kleindienst ^a, H. Kraus ^b, Q. Kronseder ^a,
J.C. Lanfranchi ^c, F. Petricca ^a, S. Pfister ^c, W. Potzel ^c, F. Pröbst ^a, S. Roth ^c, K. Rottler
^e, S. Scholl ^e, J. Schmalzer ^a, W. Seidel ^{a, +}, C. Strandhagen ^e, L. Stodolsky ^a, A. J.
B. Tolhurst ^b,

^a *MPI für Physik, Föhringer Ring 6, 80805 Munich, Germany*

^b *University of Oxford, Department of Physics, Oxford OX1 3RH, U.K.*

^c *Technische Universität München, Physik Department, D-85747 Garching, Germany*

^d *Laboratori Nazionali del Gran Sasso, I-67010 Assergi, Italy*

^e *Eberhard-Karls-Universität Tübingen, D-72076 Tübingen, Germany*

⁺ *Spokesperson E-mail address: seidel@mppmu.mpg.de*

^{*} *present address: University of Warwick, Coventry CV4 7AL, U.K.*

Abstract

The aim of CRESST (**C**ryogenic **R**are **E**vent **S**earch with **S**uperconducting **T**hermometers) is to search for particle Dark Matter and to contribute to the elucidation of its nature. The experiment is located at the ‘Laboratori Nazionali del Gran Sasso’ (LNGS), Italy, and it uses low background cryogenic detectors with superconducting phase transition thermometers for the direct detection of WIMP-nucleus scattering events.

1 Dark Matter

There is strong evidence for the existence of dark matter on all astronomical scales, ranging from dwarf galaxies, through spiral galaxies like our own, to large-scale structures. The history of the universe is difficult to reconstruct without dark matter, be it Big Bang Nucleosynthesis or structure formation.

Despite this persuasive indirect evidence for its existence, the direct detection of dark matter remains one of the outstanding experimental challenges of present-day physics and cosmology.

A plausible candidate for the dark matter is the Weakly Interacting Massive Particle (WIMP) and it is possible that it can be detected by laboratory experiments, particularly using cryogenic methods, which are well adapted to the small energy deposit anticipated. Supersymmetry provides a well-motivated WIMP candidate in the form of the Lightest Supersymmetric Particle. WIMPs are expected to be gravitationally bound in a roughly isothermal halo around the visible part of our galaxy with a density of about $0.3 \text{ GeV}/\text{cm}^3$ at the position of the Earth.

Interaction with ordinary matter is expected via elastic scattering on nuclei. This elastic scattering can occur via coherent (“spin-independent”) and spin-dependent interactions. For the coherent case, a factor A^2 is expected in the cross-section, favouring heavy nuclei.

Conventional methods for direct detection rely on the ionisation or scintillation caused by the recoiling nucleus. This leads to certain limitations connected with the low ionisation or scintillation efficiency of the slow recoil nuclei. The cryogenic detectors developed for CRESST measure the deposited energy calorimetrically, independent of the type of interaction, and allow for the detection of much smaller recoil energies. When such a calorimetric measurement of the deposited energy is combined with a measurement of scintillation light, an extremely efficient discrimination of the nuclear recoil signals from radioactive background signals can be obtained. These type of detectors are being used in the present phase CRESST-II.

2 Detection Principle

The low-temperature calorimeters consist of a target crystal with an extremely sensitive superconducting phase transition thermometer on its surface. A weak thermal coupling to a heat bath restores again the equilibrium temperature after an interaction. The thermometer is made of a tungsten film evaporated onto the target crystal. Its temperature is stabilised within the transition from the superconducting to the normal conducting state, which occurs at temperatures of about 10 mK. A typical width of the transition is about 1 mK. A small temperature rise e.g. from a WIMP–nucleus scattering event (typically some μK), leads to an increase of resistance, which is measured with a SQUID (**S**uperconducting **Q**uantum **I**nterference **D**evice). For the first phase of CRESST, which ended in 2001, 262 g sapphire detectors had been developed at MPI. These detectors pro-

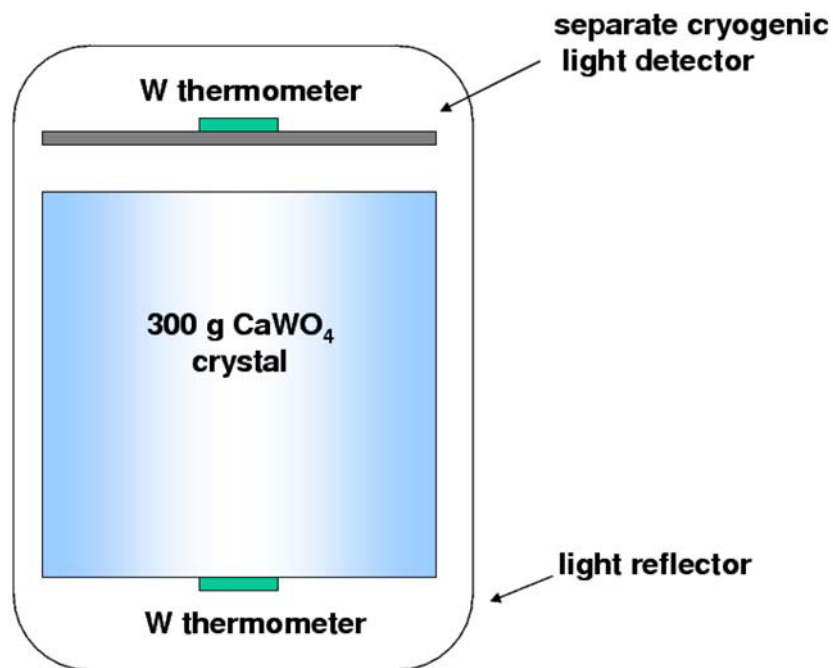


Figure 1: Schematic representation of the detector for simultaneous phonon and light measurement. It consists of two separate cryogenic detectors enclosed in a highly reflective housing, read out by tungsten superconducting phase-transition thermometers. This concept, developed by scientists of the institute, is used in CRESST-II. It allows a very efficient discrimination of the searched nuclear recoil signals from the dominant radioactive β - and γ -backgrounds.

vided an excellent energy resolution of 133 eV at 6 keV and a very low energy threshold of 600 eV.

In the second phase, CRESST-II, we are using 300 g scintillating CaWO_4 target crystals. The scintillating crystal is equipped with a superconducting tungsten phase-transition thermometer for the detection of the phonons created by a particle interaction in the scintillating crystal. A small fraction of $\sim 1\%$ of the deposited energy is emitted as scintillation light, which is measured with a separate cryogenic detector, optimised for light detection. Fig. 1 shows a scheme of this composite detector.

Starting with a proof-of-principle experiment in 1998, the technique of simultaneous measurement of phonons and scintillation light has been developed at the Max-Planck-Institute. The important advantage of this technique is that it offers an extremely efficient suppression of the radioactive background down to very low recoil energies of about 10 keV. While the phonon signal measures the deposited energy, the amplitude of the corresponding light signal depends on the type of interaction. Nuclear recoils, such as WIMP or neutron scattering events, emit substantially less scintillation light than fully ionising interactions, e.g. γ or β interactions, do. As the overwhelming part of the background consists of β and γ interactions, this phonon/light technique provides a very effective method of background suppression. Fig. 2 illustrates this detection method.

Compared with the alternative approach of simultaneous measurement of phonons and charge in a semiconductor crystal, which is applied in the experiments CDMS-II and Edelweiss-II, the method developed for CRESST-II has the important advantage that it does not suffer from dead layers at the surface. A reduced charge collection for ionising events occurring close to the surface in semiconducting crystals may lead to a false identification of low energetic γ 's and β 's as nuclear recoils. The result in Fig. 2, which was obtained with a gamma and beta source, confirms that the suppression also works for low-energy electrons impinging onto the crystal surface.

3 The CRESST Setup in Gran Sasso

The central part of the CRESST installation at Gran Sasso is the cryostat. The low temperature which is generated in the mixing chamber of the dilution refrigerator is transferred into the radio-pure cold box, via a 1.5 m long cold finger. The cold finger is protected by thermal radiation shields, all fabricated of low-background copper. The detectors are mounted inside the cold box at the end of the cold finger. Two internal cold shields consisting of low-level lead are attached to the mixing chamber and to a thermal radiation shield at liquid N_2 temperature, respectively, in order to block any line-of-sight from the non-radio-pure parts of the dilution refrigerator to the detectors inside the cold box. The design completely avoids potentially contaminated cryogenic liquids inside the cold box.

An extensive passive shielding of low-background copper and lead surrounds the cold box and serves to shield radioactivity from the surrounding rock. The entire shielding is enclosed inside a gas-tight radon box that is flushed with boil of N_2 gas and maintained

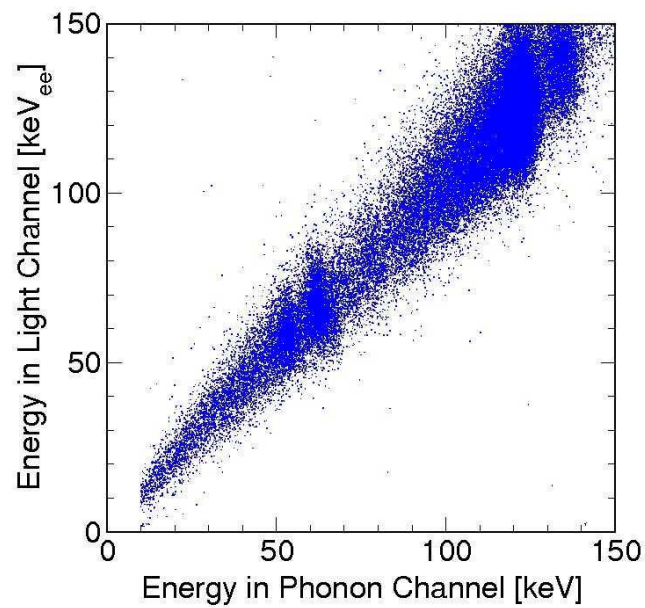
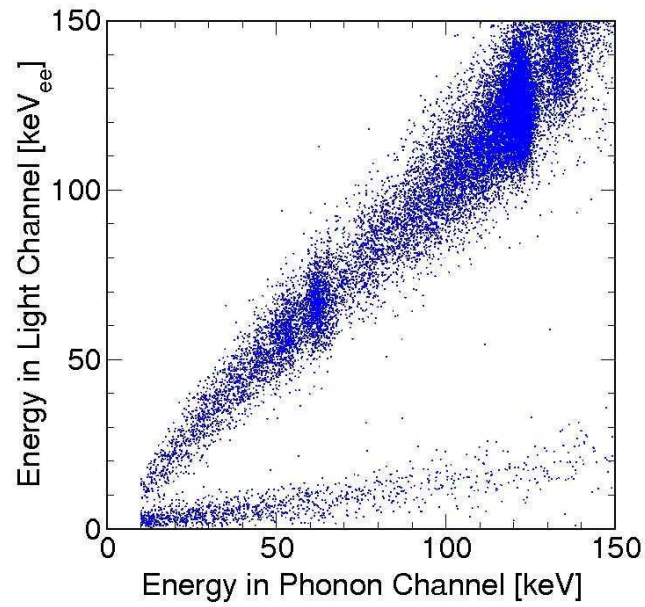


Figure 2: Coincident detection of phonons and scintillation light with a CaWO_4 detector. Left: The upper band of events is due to irradiation of the CaWO_4 crystal with electrons and gammas, whereas the lower band with lower light yield, is from nuclear recoils caused by a neutron source. Right: Removing the neutron source confirms that there is no leakage of ionising events into the nuclear recoil region.

at a small overpressure. Special care was taken to minimise above-ground exposure of the construction materials of the cold box and the shielding to cosmic rays, in order to avoid activation.

This setup has been upgraded for the experimental program of CRESST-II, to allow the operation of 33 phonon/light detector modules. The upgrade included the installation of a 66-channel SQUID readout in the existing cryostat, a system for the integration of the 33 detectors in the cold box, the installation of a passive neutron shield, a muon veto, and a new multichannel electronics and DAQ. The cryostat with the upgraded shielding is shown schematically in Fig. 3. In this upgrade the institute was responsible for the neutron shield, the wiring of the cryostat from the mixing chamber down to the detectors, the detector integration system and the DAQ. The upgrade began in 2004 after a 52-day run with two 300 g prototype phonon/light detector modules in the old setup. With this short run a competitive sensitivity of 1.6×10^{-6} pb for the WIMP nucleon scattering cross section was reached despite the absence of any neutron shield.

4 Situation After Previous Runs

4.1 Commissioning Run

CRESST has shown the success of the combined phonon-light technique for the first time in a commissioning run in the year 2007. Although this was mainly for optimization purposes, two detector modules could be reliably operated and collected data with a total exposure of about 48 kg days. In this data, a total of three candidate events were found in the acceptance region of the tungsten recoils (between 10 and 40 keV of recoil energy). From this, using standard assumptions for the dark matter distribution in our galaxy, we derived an upper limit on the coherent WIMP-nucleon scattering cross section which is as low as 4.8×10^{-7} pb for an assumed WIMP mass of 50 GeV/c² [1].

While the above analysis is based on the conventionally made assumption of an elastic WIMP scattering, also other theories have been proposed. In particular, Smith and Wiener suggested a model named *inelastic Dark Matter*, which assumes that the WIMP undergoes a transition to an excited state (order of 100 keV above the ground state) during the scattering process [2]. The different kinematics of such an interaction changes the sensitivities of experiments such that the DAMA annual modulation signal can be reconciled with the absence of a positive signal in the other experiments, rendering this model particularly interesting. Due to its heavy target nucleus (tungsten), CRESST is able to give the tightest limits of the current experiments on this inelastic Dark Matter, and already from the data of the commissioning run large areas of the parameter space could be excluded [3].

4.2 2008 Data Taking

In order to improve on the limit obtained from the commissioning run, a subsequent run was performed between August and December 2008, with the goal to get a better

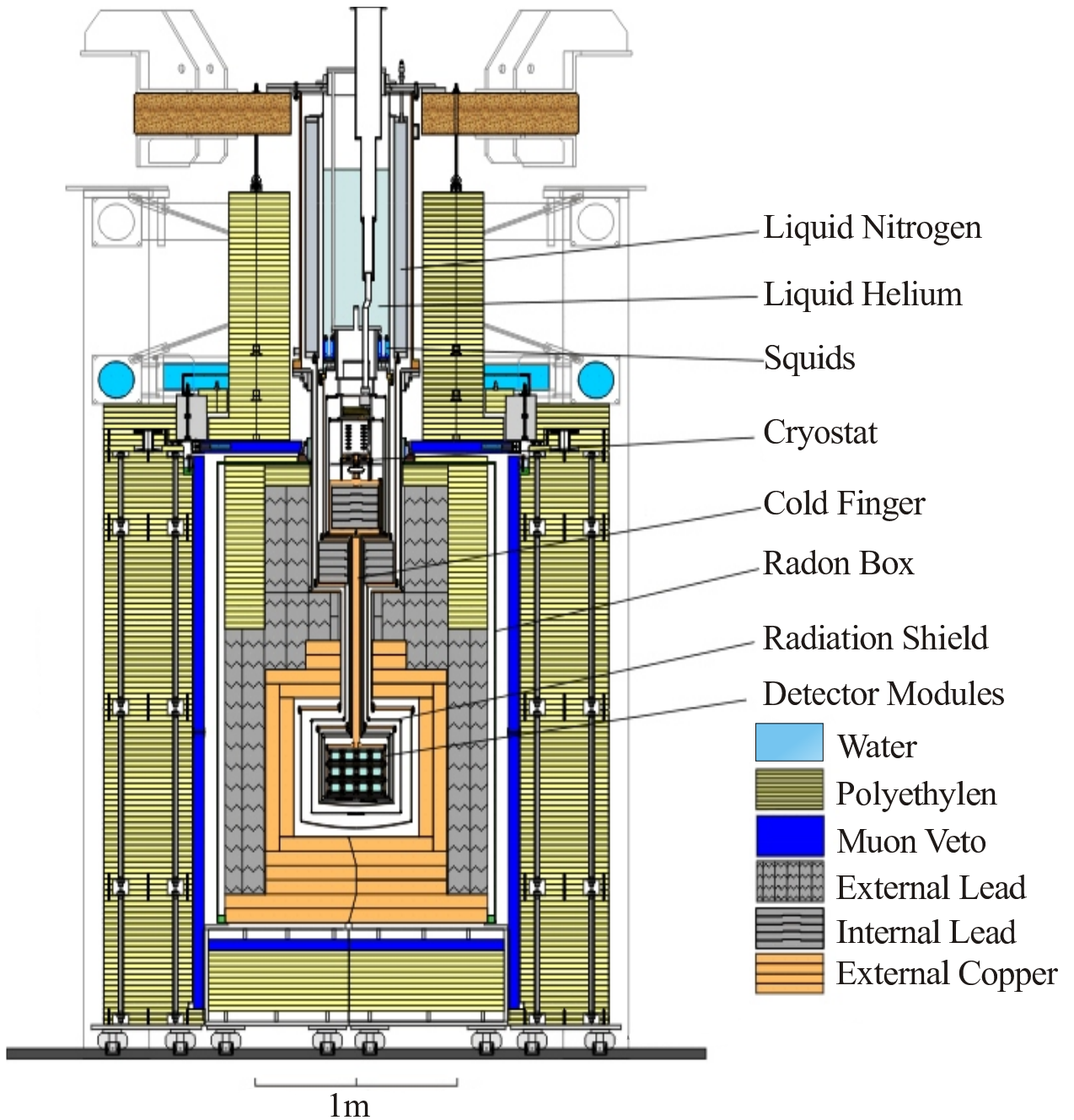


Figure 3: Dilution refrigerator and low-background cold box with its shielding upgraded for CRESST-II. The gas-tight radon box enclosing the Cu (shown in gray) and Pb (blue) shielding is completely covered by a plastic scintillator μ -veto (pink) and 40 cm of polyethylene (red).

understanding and suppression of the remaining events in the signal acceptance region. The target mass was increased to 9 operational detector modules. Apart from that, the

main changes with respect to the commissioning run were the following:

1. New phonon detectors with a higher light output were developed. This was realized by not directly evaporating the tungsten film onto the large crystal but on a separate smaller crystal which was then glued to the actual target crystal. This avoids a degradation of the light output of the target crystal during the evaporation process. The higher amount of scintillation light then allows for a considerably better discrimination of nuclear recoils. In the 2008 run, one such crystal was operational.
2. New holding clamps for the crystals were manufactured which were completely covered with scintillating epoxy. This abolished the last non-scintillating areas in the vicinity of our detectors. Such a scintillating surrounding is important as a veto for surface α -decays. If an α -decay happens on a surface near one of the crystals, it can happen that the α -particle escapes detection but the recoiling daughter nucleus hits the crystal and mimics a WIMP event. However, if the α -particle hits a scintillating surface, this creates additional light in coincidence with the recoil event, moving the event out of the signal acceptance region.

During analysis, it turned out that almost all detector modules in this run had seen events where no scintillation light could be detected (and which therefore lie within the signal acceptance region), with the rate of such events varying considerably between the different detectors. Part of these events showed a slightly different pulse shape (longer decay time) from normal particle pulses and could thus be rejected by pulse shape cuts, but several events with particle-like pulses still remained. We attribute these no-light events to stress-relaxation processes which can happen at the contact surface between the crystals and their holding clamps due to the rather tight clamping. While one would expect a particle-like pulse shape if such a relaxation happens in the crystal (in the form of a microscopic crack), similar relaxations in the clamps might explain the no-light events with longer pulses. In particular, it seems that the epoxy layer on the clamps can be a major source of such events, since one module which had been mounted with pure metal clamps for comparison was almost background free (one event only).

As a consequence of the 2008 run, the holding clamps of all crystals were exchanged by redesigned, new ones. They are made from thinner bronze material to be as soft as possible (in order not to lead to cracks in the crystals) and any kind of scintillating coverage is avoided. This requires even more cleanliness during detector mounting and handling in order to avoid contamination of the surfaces.

5 2009/2010 Data Taking

The 2009 run finally started in May after it had been delayed for several weeks by the earth quake in the L'Aquila region. 10 complete detector modules are operational and have been taking data since then. Included are three crystals with a glued thermometer as described above, one crystal made from the alternative material ZnWO_4 (which, compared to CaWO_4 , has a considerably higher light output at low temperatures), as well as one

detector module which is equipped with two light detectors (one on each side of the crystal) in order to collect as much scintillation light as possible. A gamma calibration of all modules was performed before starting the background run.

Generally, the detectors are running stably, with occasional disturbances due to the continuing seismic activity. The new, softer clamps have lead to an even higher sensitivity to external vibrations, even the ones coming from the cryostat itself (e.g. bubbling in the nitrogen or helium tank). In order to eliminate the influence of the nitrogen level in the tank, a cooling system has been installed which uses a continuous flow of cold nitrogen gas and thus avoids liquid in the tank.

In Mai 2010 a neutron calibration was performed. Until the end of 2010 more than 600 kg days of data were collected.

A preliminary (but already blind) analysis of several modules has shown that the new clamps have lead to an improvement of the background situation. No-light events with different pulse shape are not observed anymore, which supports the hypothesis that the scintillating layer on the clamps was the source of these events.

With respect to the inelastic Dark Matter scenario preliminary new limits could be obtained. The limits obtained for different mass splittings δ in the relevant range are shown in Fig. 4.

Final results of this measurement run will be reported in 2011 after performing another neutron calibration.

6 R&D-Cryostat

Due to strong pile up effects CRESST detector modules cannot be operated in an overground or a shallow underground laboratory. Up to now, these modules could thus only be tested in the CRESST cryostat at the LNGS. In the past, this situation forced us to use "untested modules" (except for the transition temperature of the thermometers) in CRESST and to mix R&D and physics measurements in the Dark Matter experiment.

In order to decouple these two issues, we have set up in 2009 a small, simple, moderately shielded cryostat in the LNGS underground lab. This cryostat is be dedicated to R&D work and enables us to test and develop detector modules before we use them in the CRESST low background cryostat. In 2010 several detector modules were tested proofing the extreme usefulness of this cryostat.

References

- [1] Godehard Angloher et al. Commissioning run of the CRESST-II dark matter search. *Astropart. Phys.*, 31(4):270 – 276, 2009.
- [2] David Smith and Neal Weiner. Inelastic dark matter. *Phys.Rev.D*, 64:043502, 2001.

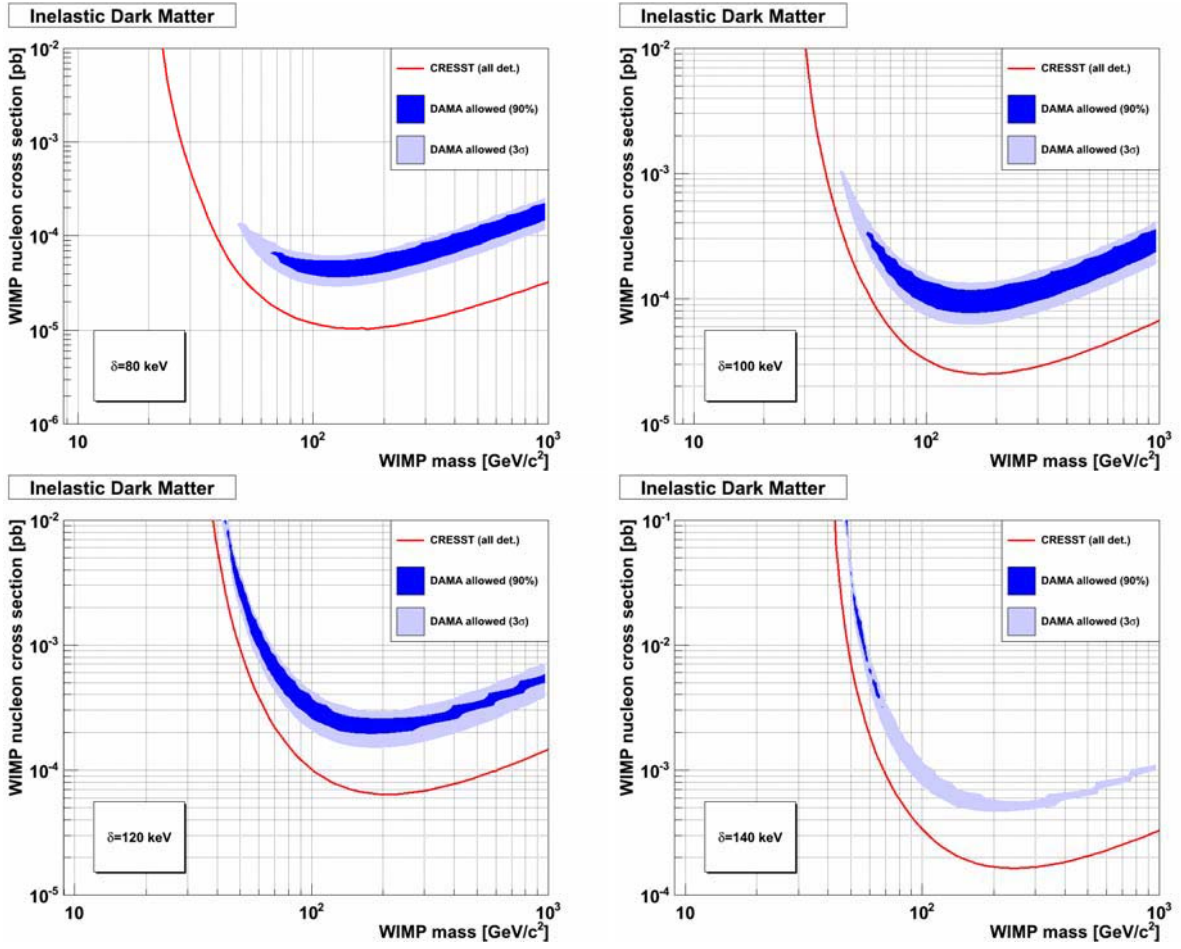


Figure 4: Inelastic dark matter limits for mass splittings δ of 80, 100, 120 and 140 keV.

- [3] John March-Russell, Christopher McCabe, and Matthew McCullough. Inelastic dark matter, non-standard halos and the DAMA/LIBRA results. arxiv:0812.1931, December 2008.

CUORE

2010 LNGS Report

May 3, 2011

F. Alessandria^h, M. Ameri^d, E. Andreotti^{f,j}, R. Ardito^k, C. Arnaboldiⁱ, F. T. Avignone III^{ae},
M. Balata^e, I. Bandac^{ae}, T. Banks^{v,e}, G. Bari^o, M. Barucci^{a,b}, J. Beeman^u, F. Bellini^{l,m},
M. Biassoni^{i,j}, C. Brofferio^{i,j}, A. Bryant^{v,y}, A. Buccheri^m, C. Bucci^e, C. Bulfon^m, X. Z. Cai^{ag},
L. Canonica^{c,d}, S. Capelli^{i,j}, M. Capodiferro^m, L. Carbone^j, L. Cardani^{l,m}, M. Cariello^d,
M. Carrettoni^{i,j}, R. Cereseto^d, G. Ceruti^j, N. Chott^{ae}, M. Clemenza^{i,j}, C. Cosmelli^{l,m}, O. Cremonesi^j,
C. Crescentini^o, R. J. Creswick^{ae}, I. Dafinei^m, A. Dally^{af}, A. De Biasi^g, M. P. Decowski^{v,y},
M. M. Deninno^o, A. de Waard^s, S. Di Domizio^{c,d}, L. Ejzak^{af}, R. Faccini^{l,m}, D. Q. Fang^{ag},
H. A. Farach^{ae}, E. Ferri^{i,j}, F. Ferroni^{l,m}, S. Finelli^o, E. Fiorini^j, L. Foggetta^{f,j}, M. A. Franceschi^q,
S.J. Freedman^{v,y}, G. Frossati^s, B. Fujikawa^v, C. Gargiulo^m, R. Geigher^j, A. Giachero^j, L. Gironi^{i,j},
A. Giuliani^{f,j}, P. Gorla^e, C. Gotti^{i,j}, E. Guardincerri^e, C. Guendalini^o, M. Guerzoni^o,
T. D. Gutierrez^{ad}, E. E. Haller^{u,z}, K. Han^v, K. M. Heeger^{af}, H. Z. Huang^{ac}, M. Iannone^m,
R. Kadel^w, K. Kazkaz^{aa}, S. Kraft^{i,j}, G. Keppel^g, L. Kogler^{v,y}, Yu. G. Kolomensky^{w,y}, D. Lenz^{af},
Y. L. Li^{ag}, C. Ligi^q, X. Liu^{ac}, E. Longo^{l,m}, Y. G. Ma^{ag}, C. Maiano^{i,j}, G. Maier^k, R. H. Maruyama^{af},
C. Martinez^{ae}, M. Martinez^{j,r}, R. Mazza^j, R. Michinelli^o, L. Mizouni^{ae}, N. Moggi^o, S. Morganti^m,
T. Napolitano^q, S. Newman^{ae,e}, S. Nisi^e, C. Nones^{f,j}, E. B. Norman^{aa,ab}, A. Nucciotti^{i,j}, M. Olcese^d,
F. Orio^{l,m}, D. Orlandi^e, P. Ottonello^{c,d}, J. Oullet^v, M. Pallavicini^{c,d}, V. Palmieri^g, G. Pancaldi^o,
M. Pavan^{i,j}, L. Pattavina^j, M. Pedretti^{aa}, A. Pelosi^m, M. Perego^j, G. Pessina^j, V. Pettinacci^m,
S. Pirro^j, E. Previtali^j, V. Rampazzo^g, F. Rimondi^{n,o}, C. Rosenfeld^{ae}, C. Rusconi^{f,j}, C. Salvioni^{f,j},
S. Sangiorgio^{aa}, A. Saputi^q, D. Schaeffer^{i,j}, N. D. Scielzo^{aa}, M. Sisti^{i,j}, A. R. Smith^x, F. Stivanello^g,
L. Taffarello^p, L. Tatananni^e, G. Terenziani^g, W. D. Tian^{ag}, A. Tiburzi^q, C. Tomei^m,
S. Trentalange^{ac}, G. Ventura^{a,b}, M. Vignati^{l,m}, B. Wang^{aa,ab}, H. W. Wang^{ag}, C. A. Whitten Jr.^{ac},
T. Wise^{af}, A. Woodcraft^t, N. Xu^v, L. Zanutti^{i,j}, C. Zarra^e, B. X. Zhu^{ac}, and S. Zucchelli^{n,o}

- ^a Dipartimento di Fisica, Università di Firenze, Firenze I-50125 - Italy
- ^b INFN - Sezione di Firenze, Firenze I-50125 - Italy
- ^c Dipartimento di Fisica, Università di Genova, Genova I-16146 - Italy
- ^d INFN - Sezione di Genova, Genova I-16146 - Italy
- ^e INFN - Laboratori Nazionali del Gran Sasso, Assergi (L'Aquila) I-67010 - Italy
- ^f Dipartimento di Fisica e Matematica, Università dell'Insubria, Como I-22100 - Italy
- ^g INFN - Laboratori Nazionali di Legnaro, Legnaro (Padova) I-35020 - Italy
- ^h INFN - Sezione di Milano, Milano I-20133 - Italy
- ⁱ Dipartimento di Fisica, Università di Milano-Bicocca, Milano I-20126 - Italy
- ^j INFN - Sezione di Milano Bicocca, Milano I-20126 - Italy
- ^k Dipartimento di Ingegneria Strutturale, Politecnico di Milano, Milano I-20133 - Italy
- ^l Dipartimento di Fisica, Università di Roma La Sapienza, Roma I-00185 - Italy
- ^m INFN - Sezione di Roma, Roma I-00185 - Italy
- ⁿ Dipartimento di Fisica, Università di Bologna, Bologna I-40126 - Italy
- ^o INFN - Sezione di Bologna, Bologna I-40126 - Italy
- ^p INFN - Sezione di Padova, Padova I-35131 - Italy
- ^q INFN - Laboratori Nazionali di Frascati, Frascati I-00044 - Italy
- ^r Lab. de Fisica Nuclear y Altas Energias, Univ. de Zaragoza, 50009 Zaragoza - Spain
- ^s Kamerling Onnes Laboratory, Leiden University, 23000 RAQ, Leiden - The Netherlands
- ^t SUPA, Institute for Astronomy, University of Edinburgh, Blackford Hill, Edinburgh EH9 3HJ - UK
- ^u Materials Science Division, Lawrence Berkeley National Laboratory, Berkeley, CA 94720 - USA
- ^v Nuclear Science Division, Lawrence Berkeley National Laboratory, Berkeley, CA 94720 - USA
- ^w Physics Division, Lawrence Berkeley National Laboratory, Berkeley, CA 94720 - USA
- ^x EH&S Division, Lawrence Berkeley National Laboratory, Berkeley, CA 94720 - USA
- ^y Department of Physics, University of California, Berkeley, CA 94720 - USA
- ^z Department of Materials Science and Engineering, University of California, Berkeley, CA 94720 - USA
- ^{aa} Lawrence Livermore National Laboratory, Livermore, CA 94550 - USA
- ^{ab} Department of Nuclear Engineering, University of California, Berkeley, CA 94720 - USA
- ^{ac} Department of Physics and Astronomy, University of California, Los Angeles, CA 90095 - USA
- ^{ad} Physics Department, California Polytechnic State University, San Luis Obispo, CA 93407 - USA
- ^{ae} Department of Physics and Astronomy, University of South Carolina, Columbia, SC 29208 - USA
- ^{af} Department of Physics, University of Wisconsin, Madison, WI 53706 - USA
- ^{ag} Shanghai Institute of Applied Physics (Chinese Academy of Sciences), Shanghai 201800 - China

Abstract

We report on activities carried out in 2010 for the CUORE neutrinoless double beta decay experiment.

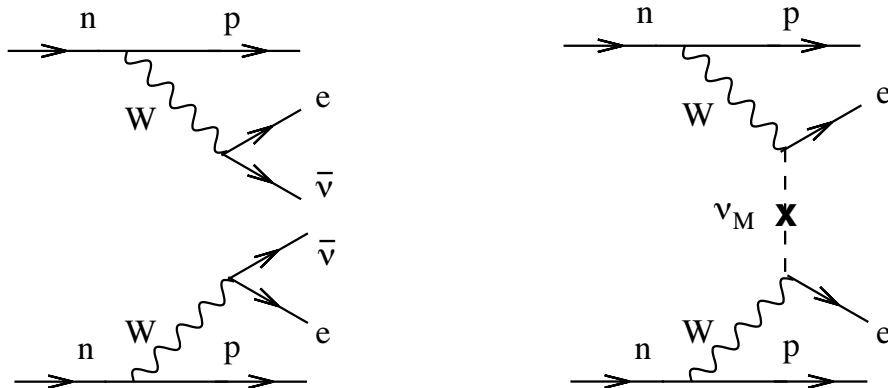


Figure 1: Feynman diagrams of the second-order weak-interaction processes of 2-neutrino and neutrinoless double beta ($\beta\beta$) decay.

1 Introduction

Neutrinoless double beta decay ($\beta\beta(0\nu)$) is an extremely rare process, if it occurs at all, in which a nucleus spontaneously undergoes two simultaneous beta decays without emitting any neutrinos (Figure 1). This can occur only if neutrinos have nonzero mass and are their own anti-particles, or so-called “Majorana” particles. In the past decade, neutrino oscillation experiments conclusively established that neutrinos are indeed massive particles, but those experiments could only measure the differences between neutrino mass eigenstates; the absolute neutrino masses, though known to be small, have yet to be determined.

The search for $\beta\beta(0\nu)$ is therefore important for two reasons: (1) it is the only feasible way to discover if the neutrino is a Majorana particle—and thus unique among the known constituents of matter—and (2) if the process is observed it can help to establish the absolute mass scale of neutrinos. To date there has been only one published claim of observation of $\beta\beta(0\nu)$ [1], and the result is somewhat controversial. There are currently numerous experimental programs underway employing a variety of techniques to search for $\beta\beta(0\nu)$ in a number of different isotopes, and it is expected that confirmation or refutation of the existing claim will appear within the next few years.

The Cryogenic Underground Observatory for Rare Events (CUORE) [2] is an upcoming cryogenic bolometer experiment designed to search for $\beta\beta(0\nu)$ in the isotope ^{130}Te . The CUORE detector will consist of a close-packed array of 988 TeO_2 crystals containing ~ 200 kg of ^{130}Te and cooled inside a large cryostat to 10 mK (Figure 2). At this low temperature the crystals function as highly sensitive calorimeters, converting the relatively small energies deposited inside them by particles into measurable rises in temperature. TeO_2 bolometers have long been used to search for $\beta\beta(0\nu)$ in ^{130}Te because their properties are well-matched to the experimental requirements for such searches [4, 5, 6, 3]. Namely, the bolometers exhibit excellent energy resolution, they serve simultaneously as both the source of $\beta\beta(0\nu)$ and the detector, they possess low intrinsic background, and they can be operated stably for several years.

The expected signature of $\beta\beta(0\nu)$ in ^{130}Te is a peak in the measured energy spectrum

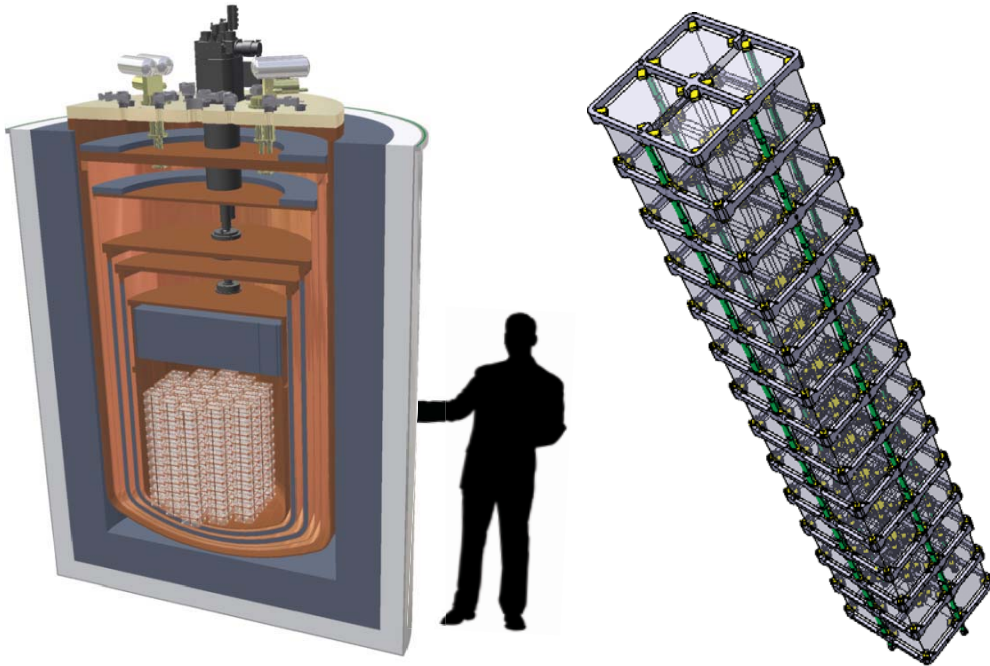


Figure 2: (Left) A drawing of the CUORE cryostat in cross-section, revealing the shielding layers and array of 19 detector towers. (Right) A tower of crystal detectors.

at 2527 keV, the Q-value for the transition $^{130}\text{Te} \rightarrow ^{130}\text{Xe} + 2\beta^-$. The goal of CUORE is to reduce the background level below 10^{-2} counts/keV/kg/y in this region of interest (ROI) and to make a high-precision measurement of the spectrum in a narrow energy window around the Q-value of the decay. If successful, the experiment will be sensitive to an effective Majorana neutrino mass of the order of 50 meV, better than any previous experiment. While the primary focus of the experiment is to search for $\beta\beta(0\nu)$, other rare-event studies will also be possible, such as searches for dark matter particles and axions.

The current best limit on $\beta\beta(0\nu)$ in ^{130}Te , $\tau_{1/2}^{\beta\beta(0\nu)} > 2.8 \times 10^{24}$ y (90% C.L.), comes from CUORE's predecessor, the Cuoricino experiment [3]. The Cuoricino detector was comprised of a tower of 62 TeO_2 crystal bolometers containing 11 kg of ^{130}Te and operated in a cryostat at the underground Laboratori Nazionali del Gran Sasso (LNGS), Italy, from 2003–2008. CUORE is essentially a scaled-up version of Cuoricino that exploits the experience and results gained from its predecessor while aiming at an improvement in sensitivity by roughly two orders of magnitude. The CUORE bolometers will be arranged in a cylindrical matrix of 19 towers, each tower containing 13 planes of four crystals supported inside a copper frame. The array will be surrounded by a 6-cm-thick shield of ancient Roman lead and operated at ~ 10 mK inside a cryostat cooled by a He^3/He^4 dilution refrigerator. An additional 30-cm thickness of low-activity lead will shield the array from the refrigerator's dilution unit and environmental radioactivity. A borated polyethylene shield and an airtight cage will surround the exterior of the cryostat. Construction of most CUORE components is now underway.

The location, design, and construction of CUORE have been optimized to ensure

the experiment attains the lowest backgrounds possible. The rock overburden provides 3650 m.w.e. of shielding against cosmic rays, while the cryostat has numerous internal and external lead shields to block natural environmental radiation. The apparatus will also be constructed from select materials which will undergo special cleaning treatments and be stored underground to minimize cosmic-ray activation. In addition to these methods of passive background suppression, the compact structure of the crystal array will render the detector more effective at active rejection of background events. Minimizing the amount of material and dead space between the crystals increases the likelihood that unwanted cosmics and radioactive decays will produce simultaneous hits in multiple crystals, unlike $\beta\beta(0\nu)$ decays which should usually be confined to a single crystal. The configuration of crystals thus allows for more efficient identification and rejection of background events.

2 Detector components

A bolometric detector is an exquisitely sensitive low-temperature calorimeter whose temperature changes in response to the amount of energy it absorbs. A bolometer consists of three main components: an energy absorber, a temperature sensor, and a thermal link to a heat sink (Figure 3).

The absorber is the object in which particles deposit their energy; it can range in mass from few micrograms to almost 1 kg. The primary constraints on the absorber material are that it must have a low heat capacity and it must be able to withstand cryogenic cooling in vacuum. CUORE uses TeO_2 crystals for its bolometric absorbers. The crystals are dielectric and diamagnetic, and because they contain $\sim 30\%$ ^{130}Te by mass they simultaneously serve as both the source and detector of $\beta\beta(0\nu)$ decay.

According to the Debye law, the heat capacity of a crystal at temperature T varies as $(T/\Theta_D)^3$, where Θ_D is its Debye temperature. As a result, at low temperatures the relatively small energies released by the interactions of single particles inside the crystal can produce measurable rises in its temperature: the heat capacity of a TeO_2 crystal at 10 mK is roughly $2.3 \text{ nJ/K} = 1 \text{ MeV}/0.1 \text{ mK}$. The small variations in a crystal's temperature are measured by a thermal sensor. Among the wide variety of sensors available, CUORE elected to use neutron-transmutation-doped (NTD) Ge thermistors, which are robust, easy to use, and can be produced in large quantities.

The crystals are secured inside a copper frame by PTFE (Teflon) supports. The PTFE reduces the amount of mechanical stress placed on the crystals when cooled to cryogenic temperatures, and they also serve as a weak thermal link to the copper frame which functions as the heat sink. The combined heat conductance of these elements strongly affects the time response of the bolometers.

2.1 Procurement of TeO_2 crystals

CUORE requires 988 $5 \times 5 \times 5 \text{ cm}^3$ TeO_2 crystals with extremely precise dimensional tolerances and exceptionally low levels of radioactive impurities. After an extensive worldwide search, the Shanghai Institute of Ceramics, Chinese Academy of Sciences (SICCAS) was selected as the crystal vendor. In 2007–2008, two contracts were negotiated and signed

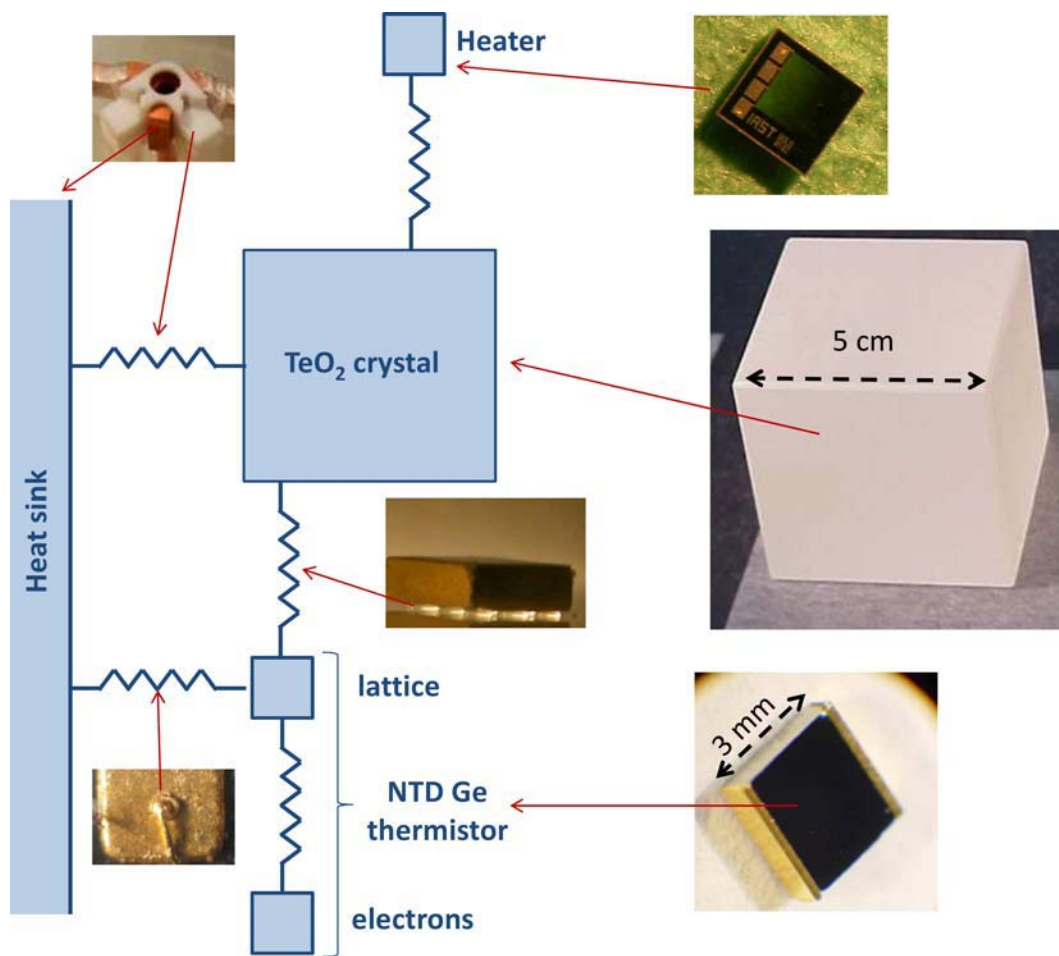


Figure 3: Schematic diagram of a CUORE bolometer, with a photo of each component.

for the production of CUORE crystals: INFN agreed to purchase 560 crystals and the US DOE agreed to purchase 500 crystals. The crystals were to be grown, etched, and polished at the SICCAS facility in Jiading, China, and then delivered to LNGS.

In the last 2.5 years, a total of 651 crystals have been produced by SICCAS and delivered to LNGS, where they are stored underground in the Parts Storage Area (PSA) of the CUORE experiment. During this time, both US and Italian members of the CUORE collaboration have spent substantial amounts of time at SICCAS performing quality assurance and control checks. Approximately 4% of the delivered crystals have been instrumented as bolometers and tested in the R&D cryostat in Hall C at LNGS as part of a joint US/Italian effort. All of the tested crystals have met or exceeded the contract specifications for bulk radioactivity and dimensional tolerances.

2010 marked the completion of production of the INFN-purchased crystals and the transition to production of the US-purchased crystals; crystal production and shipment will continue under the same conditions as before. In the coming year the remaining crystals required for CUORE will be produced and delivered to LNGS, and we plan to continue testing $\sim 4\%$ of them as bolometers. Based on our experience thus far, we expect that all of the crystals produced for CUORE will perform as well or better than specified in the SICCAS contracts.

2.2 Production of Ge thermistors

Neutron-transmutation-doped (NTD) Ge thermistors are used to convert small temperature changes in the TeO_2 crystals into voltage signals which can be read out by the room-temperature front-end electronics. The thermistors are small Ge single crystals (volume $\sim 3 \times 3 \times 1 \text{ mm}^3$) doped through exposure to thermal neutrons in a nuclear reactor at the Massachusetts Institute of Technology. The design of the devices is critical because they play a crucial role in determining the bolometers' signal-to-noise ratio and therefore their energy resolution and threshold. The thermistor design is based on experience gathered in both Cuoricino and R&D tests performed for CUORE. The desired operating resistance, which is well-matched features of the front-end electronics, is in the range 40–1000 M Ω . The resistance-temperature behaviour follows the Shklovskii–Efros law, $R(T) = R_0 \exp \left[(T_0/T)^{1/2} \right]$, where T_0 is determined by the doping level (i.e., the neutron dose) and R_0 is determined by both the doping level and the geometry. The target for the CUORE thermistors is $T_0 \sim 4.0 \text{ K}$ and $R_0 \sim 1.3 \Omega$, which correspond to the desired resistance range when operated in the temperature range 10–15 mK.

A thermistor will be glued to each crystal before it is inserted into a CUORE tower. After a tower has been assembled, a custom wire-bonding machine will attach gold readout wires to each thermistor. Ideally, the two electrical contacts on a thermistor should be attached to opposite sides of the device, as this geometry yields the most uniform electric field inside it. The contacts were indeed done this way in Cuoricino, but the technique presents a serious drawback: the wire bonding must be performed *before* the thermistor is bonded to the crystal, because it is extremely difficult to access the sides of the NTD after gluing. Fixing a broken wire bond in this case required disassembling the tower to remove the affected crystal, removing the thermistor from the crystal, repairing the bonds on the thermistor, regluing it to the crystal, and rebuilding the tower.

The new CUORE scheme allows each wire bond to be made in situ, and therefore repairs can be performed without any disassembly. To make this possible, the gold bonding pads on opposing sides of the NTD have been extended around the edges to create two narrow strips on its face, opposite the glued surface (the so-called “wrap-around” configuration). This provides two outward-facing gold regions for wire bonding while preserving the same current path as in the side-bonded thermistors.

After a careful tuning of the doping process, which entailed producing and testing many samples, we have doped two 60-mm-diameter, 3-mm-thick Ge wafers which should yield ~ 1200 thermistors in total. In a static characterization, samples from these wafers exhibited T_0 and R_0 parameters very close to the target. A dynamic characterization, in which these samples are used as sensors on real detectors, is ongoing as a final validation of the CUORE thermistor production. Other underdoped backup wafers are available and can be further irradiated for a final tuning to the requested doping level if necessary.

2.3 Production of Si heaters

Low-temperature detectors are sensitive to slow drifts in temperature which can spoil their intrinsically excellent energy resolution. This problem is solved in CUORE by periodically injecting a fixed amount of energy into each crystal via a silicon heater glued to its surface. The pulses of energy from the heaters emulate particle interactions, and the crystal response to these controlled events is used in the offline analysis to correct for the effects of temperature drifts.

The heaters are specially made, individually characterized silicon chips on which a heavily doped meander is realized through the standard processes of silicon planar technology. The meander has a low-mobility metallic behaviour at low temperatures, providing a constant resistance of $\sim 300 \text{ K}\Omega$. More than 1000 heaters have been manufactured and characterized at 77 K, 4.2 K and 1.5 K. The CUORE heater production is nearly complete and only a small back-up batch remains to be tested at low temperatures.

2.4 Thermistor-crystal gluing

A thermistor is mechanically and thermally coupled to each TeO_2 crystal by a matrix of small glue spots. A matrix of nine dots is used for the thermistors, while five dots are used for the smaller heaters. Distributing the glue into separate dots prevents fractures or detachments at low temperatures from the the differential thermal contractions of the TeO_2 crystal and the semiconductor chips.

The glue coupling is a critical component of bolometric detectors which influences the quality of their performance. In Cuoricino, the sensor-to-absorber coupling was accomplished through a labor-intensive, manual procedure, and the resulting variability in quality led to a lack of reproducibility in the signal shape and detector performance. For CUORE-0 and CUORE we have developed a partially automated system to obtain far more reproducible sensor-to-absorber couplings. The new system uses a dedicated glue dispenser and a robotic arm to handle and precisely position the crystals and the chips. The system has been designed to be fast and reliable despite limitations arising from the glue’s short curing time—indeed, the precise timing of the robot is useful in managing

the short time window for curing the glue. The use of the robotic system also ensures that when the crystals are handled they come into contact with cleaner materials and for a shorter amount of time than would occur with a manual system.

As of February 2011, testing of the gluing system is complete and it has been disassembled for cleaning prior to its reassembly and installation in the clean room inside the underground CUORE hut. The final commissioning of the gluing system as part of the assembly line will occur before Summer 2011.

3 Detector array

The tower is the minimal single entity of the CUORE detector. There will be 19 identical towers in all, packed closely together in a cylindrical configuration (Figure 2). The tower design was guided by several requirements, such as limitations on allowable materials (primarily Cu and PTFE, due to radiopurity cryogenic restrictions), the shape and size of the crystal modules (limiting as much as possible the Cu mass, number of pieces, and dimensions) and assembly requirements (simple, fast, reproducible and recontamination-free). Constructing a tower requires selecting nonradioactive materials, machining and cleaning the components, assembling the detector modules, storing all components (before and after assembly) in a Rn-free environment, and finally assembling the tower and installing it inside the cryostat.

3.1 Copper machining and cleaning

We have established a protocol for machining and cleaning the Cu which better satisfies the radioactivity requirements, and this protocol is now in regular use in the preparation of all Cu pieces for the tower structures (see Section 9.3). In addition, significant effort has gone into establishing a logistics infrastructure for preventing cosmic activation of the Cu (see Section 9.4). The Cu parts for CUORE-0, the first tower from the CUORE assembly line, were machined in 2010 and their cleaning should be completed in Spring 2011. Work is now in progress on preparing Cu parts for CUORE, and this is expected to continue for approximately two years.

3.2 PTFE machining and cleaning

The PTFE blocks supporting the crystals inside the Cu structure play an important role. The pieces must be made to precise dimensions to ensure that the correct pressure is placed on the crystals when cooled inside the cryostat. Half of the total number of PTFE pieces required for CUORE were manufactured in 2010, and examination of samples confirmed that the pieces have been made within tight tolerances. Since the PTFE blocks will touch the crystals, they must be made from specially selected PTFE and their surfaces must be perfectly decontaminated before use. A cleaning protocol was implemented in 2010, and the blocks which have been received have been cleaned and placed into storage under nitrogen.

3.3 Wiring

More than 2000 readout links are needed to instrument the thermistors, heaters, and thermometers on the detector's 988 crystals. A study was conducted in recent years to determine the best materials for the wiring in terms of radiopurity, simplicity, and modularity.

A cryogenic test of the CUORE-type wiring for the upper portion of the cryostat was prepared in the former Cuoricino cryostat in late 2010 and carried out in early 2011. This test was intended to check not only the noise and reliability of the wiring, but also its heat load and thermalization.

The wiring on the detector towers is on the contrary realized through the FFC special tape approach, with gold ball bonding performed in situ from thermistor to tape pads. This procedure was selected in order to reduce soldering and the resulting particulates near the bolometers, but the difficulties of bonding very small pads with 25 μm gold wires while the tower and bonding machine are inside a nitrogen-flushed glove box are immense. Many tests have been performed to investigate the feasibility of such an approach, and in 2010 tests were conducted on the final wire tapes and trays with the motorized tower elevator. The glove box was designed and manufactured by a specialized company, and is now available for the final tests before CUORE-0 in 2011. The FFC tapes have been carefully designed and manufactured for CUORE-0 by a company in 2010. The tapes for CUORE will be produced only after the wiring tests are done with CUORE-0. As with all materials located near the crystals, it will be essential to study how to clean them of any radioactive residuals without removing the 17 μm thick Cu layer from which the readout strips are realized. Studies on the quality check procedures for each tape prior to assembly commenced in 2010 and will continue in 2011, prior to the assembly of CUORE-0.

3.4 Tower assembly line

Due to the extraordinary radiopurity requirements for a successful $\beta\beta(0\nu)$ experiment, the CUORE towers must be assembled following strict protocols under extremely clean conditions. This not only requires that all the assembly be performed inside glove-boxes flushed with nitrogen gas (to avoid exposing any detector parts to air and hence possible radon contamination), but also that strict controls are implemented on all materials which come into contact with the tower components during assembly. Contact with tools is also kept to a minimum.

The time required to assemble and mount the detectors inside the cryostat is estimated to be several months, so the assembly line operators will not necessarily always be the same. It is therefore essential that the eventual assembly procedure be simple, fast, and have reproducible results—i.e., produce clean, functioning detectors—when applied by different persons. The functions of the different glove boxes and their ergonomics were carefully studied during the past few years, and in 2010 the details were essentially finalized. Technical drawings of the glove boxes, tools and ancillaries were sent to specialized companies at the end of the year and orders were placed. The assembly line will consist of five separate glove boxes for specialized operations on the detector components, and a main table containing an elevator platform to facilitate tower assembly. (More details

on the assembly line can be found in the previous CUORE LNGS reports.) We expect to finish constructing the assembly line in Spring 2011, and to assemble CUORE-0 in Summer 2011.

4 Cryogenics

The technical specifications for the CUORE experiment—namely, the total detector mass, the working temperature, and the background level—place very stringent requirements on the refrigerator, suspension system, the radiopurity of materials, and the reliability of the cryogenic system. The CUORE cryogenic apparatus (Figure 2) is separated into different sections having specific goals:

- Cooling system: A $^3\text{He}/^4\text{He}$ dilution refrigerator (including its control system), the ^3He circulation system, and the pumping and compressor system.
- Cryostat: A system of 6 vacuum chambers at decreasing temperatures: 300 K, 40 K, 4 K, 600 mK, 50 mK, and 10 mK.
- Cold lead shield: 4π solid-angle lead shielding of the detector.
- Detector suspension system: Mechanically decoupled to minimize vibrations.
- Calibration system: A system allowing insertion of gamma-calibration sources in between the detector towers.

4.1 Cryostat

The CUORE cryostat is described in detail in the 2007 LNGS Annual Report, so here we merely summarize its present status.

The cryostat's design and construction drawings underwent significant revision following the comprehensive seismic analysis of the CUORE setup in 2009. Consultants from Milano Polytechnic reviewed the project and proposed actions to improve the safety of the structure. For the cryostat this involved redesigning the internal tie rods and introducing stoppers between the vessels. The construction schedule has been updated accordingly, restarting at the beginning of 2010.

Much progress was made on the cryostat hardware in 2010. Simic, the cryostat vendor, machined and welded all components for the 300 K, 40 K and 4 K flanges and vessels. The flanges are currently being gold plated. The vessels and the flanges were recently e-beam welded at Pro-Beam in Burg, Germany, and will be shipped back soon, after the required X-ray analysis. Finalization operations will then start, consisting of mechanical optimizing, cleaning, validating, and testing the items. After these first three chambers are delivered to LNGS, the second phase of the production will begin, this time for the 4 K, 50 mK and 10 mK vessels.

The Milano-Bicocca group has worked on preparing for the commissioning 300 K, 40 K and 4 K cryostat vessels at LNGS. A preliminary liquid-nitrogen-temperature vacuum test of the 300 K and 4 K vessels is planned at Simic a couple of months after the three external

chambers have been completed. All tools necessary for the test are being prepared—in particular, a high-vacuum system and a computer system for controlling the cooldown process have been developed and successfully tested in the Milano-Bicocca laboratory. At the same time, the design of the cryostat’s stainless steel tie rods and access ports has been completed, and production has commenced. Special care has been devoted to the design of pivoting CuBe supports for the tie rods, which will allow the cryostat structure to safely displace in case of a seismic event. Progress has also been made on the copper thermal links for the tie rods and the pulse tubes. High-thermal-conductance copper has been procured and characterized in the Milano-Bicocca laboratory, and assembly procedures have been developed. The design of multilayer insulation for the cryostat has been completed and the blankets have been procured. Laboratory tests have been made on the 4 K indium-sealed flanges and the low-pressure safety valves.

The progress on production of the cryostat’s vacuum chambers and their connecting systems suggests a likely start of the integration process in Spring 2011. The first step will be to assemble the 300 K, 40 K and 4 K vessels with one detector calibration box, the upper suspension components, one upper wire insert, and two pulse tubes. The system will be cooled to 4 K and the functionality of the various subsystems will be tested. Integration of the dilution unit will follow shortly.

4.2 Detector and shield suspension system

The detector suspension has been designed to minimize the transmission of mechanical vibrations due to both seismic noise and the operation of cryocoolers and pumps. The suspension is a two-stage low-frequency isolator in the vertical direction, while in the horizontal direction the structure is a pendulum with a natural frequency of about 0.4 Hz. A second suspension system, designed in a similar way as the one for the detector, is foreseen for the top lead disk. Both the suspensions have been designed and the detector suspension parts have been built and are ready to be pre-assembled before summer.

4.3 Detector calibration system

The CUORE bolometer array’s energy response will be calibrated by regular exposure to γ sources. To overcome the detector self-shielding, the sources will be placed in between the detector towers. The detector calibration system (DCS) will consist of 12 radioactive source strings that will be lowered under their own weight through a set of guide tubes running from the cryostat’s uppermost 300 K flange down to the detectors.

In 2010 the CUORE group at the University of Wisconsin completed the design of the motion and deployment boxes and started fabricating the first deployment system. Prototype components have been tested over hundreds of deployment and calibration cycles at room temperature in the laboratory.

A critical element in the design of the DCS is the thermalization of the radioactive source string to 4 K inside the cryostat. A solenoid-based, mechanical system has been developed that establishes contact between the copper calibration source capsules on the string and the cryostat itself. A prototype has undergone mechanical testing down to 77 K; cold tests with liquid helium and a pulse tube are being prepared to verify the

thermal functionality of the system at lower temperatures. We expect to complete the thermal tests in Spring 2011. The first full-scale test of the detector calibration system in the CUORE cryostat is planned for Summer 2011.

5 Electronics

TeO₂ bolometers are operated by biasing their attached NTD thermistors in a constant current regime. In this way temperature changes in the TeO₂ crystal are converted into voltage pulses. The optimal biasing of the thermistor is obtained by measuring its voltage-to-current relationship, or load curve. While constructing the load curve, the pulse amplitude produced by a monochromatic pulse (the reference pulse produced by the Si heater) is also measured. A simplified diagram of the amplifying chain for a single detector is shown in Figure Fig. 4. The detector, represented by the thermistor impedance R_B , is inside a refrigerator at ~ 10 mK, while the front-end is at room temperature. A pair of very close lines connects the thermistor to the preamplifier (PR) through the configuration block (CB). The thermistor floats from ground and is biased in a differential way, with a pair of load resistances connected to each of its legs, which greatly attenuates electromagnetic interferences. Moreover, crosstalk from nearby channels is avoided.

The PR is a differential, voltage-sensitive preamplifier designed according to very stringent characteristics [10]. It has low noise, a programmable gain, DC coupling (since the DC level of the detector provides information on its temperature), offset adjustment (provided by the Offset Corrector block) and finally a few-Hz bandwidth matching that typical of bolometers.

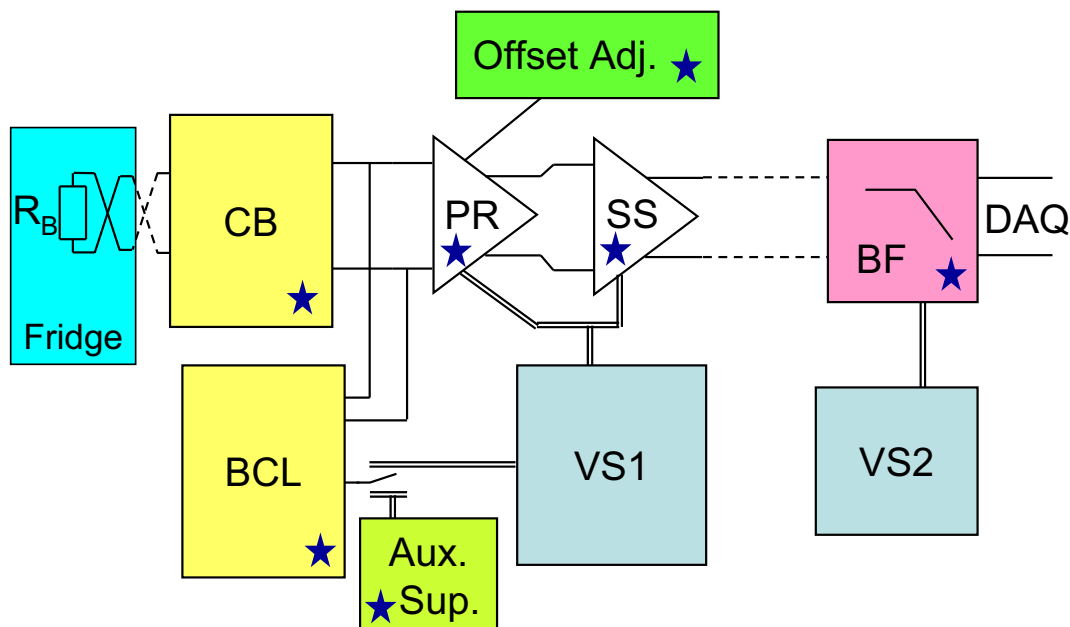


Figure 4: Schematic diagram of the analog amplification chain. Stars on the blocks individuates the presence of remote programmability options.

The very small bandwidth of the detector signal requires that series and parallel noises must be reduced especially at low frequencies. A quantitative contribution of the amplifying chain on the energy resolution is difficult to estimate due to the typically large spread of the energy conversion gains of the detectors, but is anyways smaller than 10%.

The Biasing Circuit (BC) block represented in Figure Fig. 4 includes the $30G\Omega + 30G\Omega$ resistances mentioned above and a pair of $6G\Omega + 6G\Omega$ that can be connected in parallel to the former pair (for use in the DC characterization phase). Finally, the Second Stage amplifier (SS) buffers the output of the PR with a programmable gain. The output of the SS is connected to the DAQ system after the antialiasing Bessel Filter (BF), which consists of a 6-pole-roll-off Thompson or Bessel filter. The BF has 4 programmable front-end bandwidths to match the speed of the detector signal.

Two Voltage Supply (VS) blocks are depicted in Figure Fig. 4. VS1 is used to bias the detectors, the PR, and the SS, and also provides a reference for the Offset Adjustment system. Therefore it needs to be very stable and to show low noise. VS2 is the voltage supply used for the BF.

In addition to the setup in Figure Fig. 4, two other apparatuses have been designed: an accurate temperature stabilization of the detector's copper frame, and a very stable programmable pulser. The latter is used to produce a reference pulse on the bolometer, as discussed in Section 2.3. The design of most of the described elements that compose the CUORE Electronic System was based on the experience of the CUORICINO experiment and is now completed.

The present status of the front-end and the next progress of the development are given.

- the preamplifier PF has been designed and prototyped at Milano-Bicocca [13]. The pre-production and the final production have been made at the University of South Carolina. The differential JFETs at its input has been selected based on a semi-custom process fully supported by INFN funds. The final production is now available and is under test at UCLA. The calibration of the preamplifiers will be done in Milano-Bicocca during 2011.
- the front-end board will consist of 6 channels each including the preamplifier PF and the amplifier SS, and the detector biasing network, the detector load resistors, a number of secondary features, the glue logic and the remotely-programmable interface, ARM-microcontroller based. It has been fully designed in Milano-Bicocca during 2009. In late 2010 it was laid out, to be prototyped at USC and qualified at Milano-Bicocca during 2011. The production and testing will be done during 2012 at USC and UCLA respectively.
- the antialiasing filter BF was prototyped in Genova, following the design done in Milano-Bicocca. This board has been validated during 2009. The prototype Bessel filter will be available for qualification in Milano-Bicocca at the beginning of 2011. The final production (USC) is foreseen at the end of 2011 and the test (UCLA) at the beginning of the next year.
- the two voltage supplies VS1 and VS2 for the remote (48 V) supply voltage of the Electronic System are already available, supported by INFN. The second pair needed for CUORE has been provided by USC in 2009.

- the power supplies PF are in the prototype phase in Milano-Bicocca to be produced (USC) and tested (UCLA) during 2012.
- the programmable pulser is in the prototype phase [14] in Milano-Bicocca to be produced (USC) and tested (UCLA) during 2012.

6 Data acquisition

The CUORE data acquisition (DAQ) system, *Apollo*, will be responsible for reading signals from nearly 1000 bolometers. It will digitize the analog waveforms, run trigger algorithms, and store data for offline analysis. *Apollo* will also provide a graphical user interface for run control and monitoring, and a slow control system for interacting with the front-end electronics. It will contain tools for automated characterization and optimization of the detectors in the commissioning phase of the experiment.

The core DAQ system, both in hardware and software, is already designed. The digitizing boards, NI-628x from National Instruments, have been selected and tested. This 18-bit ADC is capable of sampling differential signals at rates as high as 2 kHz and is adequate for digitizing the bolometer waveforms. The software for data acquisition, slow control, and several graphical user interfaces has been written and tested on data from actual bolometers. All detector parameters and run configurations are stored in a database which is accessible for offline analysis. Data are saved in two formats: triggered pulses are saved in ROOT files, while the continuous bolometer waveforms are saved in compressed ASCII files for offline reprocessing.

Two *Apollo* prototypes have been installed at LNGS: one is in the CUORE R&D cryostat in Hall C, and the other is in the former Cuoricino cryostat in Hall A. The Hall C DAQ prototype, installed in 2007, has 48 channels, while the Hall A DAQ prototype, installed in 2008, has 80 channels. After a testing phase the two systems have been officially adopted by the collaboration for the acquisition of all the measurements performed at these two facilities.

The Hall A DAQ prototype is ready for use in the CUORE-0 experiment without further major modifications. The only improvement will be the introduction of automated procedures for determining the optimal electronics configuration parameters for each bolometer. These procedures are being developed and some have already been successfully tested in bolometric measurements.

The major difference between the aforementioned prototypes and the final CUORE DAQ will be the large increase in the number of channels. Scaling up will require distributing the digitizer boards over \sim ten synchronized DAQ crates, each handling roughly 100 channels and controlled by a separate computer. The data streams from each crate controller computer will be collected by a main computer that performs event building. Resources for the storage and transmission of acquired data are not especially demanding, as the CUORE data production rate is expected to be \sim 10 TB per year.

7 Hut and LNGS infrastructure

The CUORE cryostat will be housed inside a dedicated three-floor hut in the underground Hall A facility at LNGS. The relatively noisy refrigeration equipment will be located on the ground floor, the cryostat vessels and surrounding lead and neutron shields will be movable between the ground and first floors, the clean room where the detectors are assembled will be located on the first floor, and the electronics counting room will be located on the second floor.

Much of the hut's infrastructure was constructed in the last two years. The building is complete and its basic utilities are functional. Construction of the clean room is in progress and nearly complete. The main detector support, a suspension frame atop four concrete columns which is mechanically separated from the hut itself, has been installed. A set of three hoists for lifting the cryostat vessels and shielding will be installed in mid-March 2011.

The support have been tested to characterize any unwanted resonances. We found that most of its resonances are comfortably high in frequency (> 20 Hz) and do not pose a problem for the detector. A worrisome low-frequency (~ 3 Hz) resonance was also observed, but it was determined that this vibration is in the hut itself and does not arise from the (mechanically decoupled) suspension system.

As a result of the 2009 L'Aquila earthquake, seismic codes have been rigorously adhered to. Of critical importance was the elucidation of life and health safety requirements for occupation of the building, in addition to the standard safety requirements for mechanical systems. The critical issues were identified and remedied by Milano Polytechnic. Their study resulted in the addition of earthquake straps between the support columns and the 120-ton external lead shield, as well as an anti-sway frame attached to the concrete frame on the ground floor of the hut. Other recommendations were made regarding the detector support inside the cryostat; their resolutions are described in Section 4.

A class 1000 clean room of total surface area of 92 m² is now under construction on the first floor of the hut. It will provide space for the assembly of the detector towers (avoiding ²²²Rn and dust) as well as their installation inside the cryostat. The clean room is organized into five areas: a changing room, a gluing room, two assembly rooms, and a cryostat room. All that remains is to perform a final cleaning of the room and to certify the oxygen and fire safety alarms; both will be completed by mid-March 2011.

A radon abatement system has been ordered (US contribution) for use during the installation of the detector towers inside the cryostat, and preparations for its utility plant have commenced. The system will be installed atop the CUORE hut and its clean-air output will be piped down to the clean room.

All components for the Parts Storage Area (PSA) building adjacent to the CUORE hut have been delivered and installed—including electrical systems, storage lockers and network connections—and all that remains is to approve the emergency procedures. Crystals and copper components are already in storage in the PSA.

We have experienced good progress, though several tasks still remain. The design of the external 120-ton lead shield was recently completed and a company has been selected for its fabrication; we expect the shield to be installed on its support by Summer 2011. A draft proposal is being circulated for the cranes occupying the ground floor level, the

cranes on the upper floor above the cryostat's 300 K flange, and the screw jacks that operate through openings in the floor of the clean room to allow vertical passage of the cryostat and external shielding; these are expected to be installed before August 2011. A conceptual design for the water cooling systems for the refrigeration equipment is under internal review. The layout of the compressors and vacuum systems is under development.

The most significant missing hut component is the Faraday cage that will occupy the top floor. When coupled with the metal container for the 120-ton lead shield, the cage will protect the detector electronics from outside electrical interference. The most critical design feature of the Faraday cage will be the manner in which various subsystems are permitted to penetrate its walls. An inventory of subsystem feedthroughs was prepared some time ago and is being updated in anticipation of fabrication of the cage in 2012.

8 Internal and external shields

The CUORE apparatus will employ two different γ ray shields to protect the detector from radioactivity emanating from within the cryogenic set-up—a need identified in previous experiments [4, 5, 6]. First, a uniform, 6-cm-thick layer of ancient Roman lead will be used inside the cryostat, close to the detectors, to shield the detector's sides and underside from contaminations in the multilayer insulation (see Section 4) and the surfaces of the cryostat's outer vessels. This lead, which comes from a Roman-era shipwreck discovered off the coast of Sardinia in the 1980s, was provided to through an agreement between INFN, the Soprintendenza ai Beni Culturali of Sardinia, and the Ministero per i Beni e le Attivita` Culturali. Ancient lead is appealing because ^{210}Pb contamination in modern lead can spoil the detector's sensitivity to rare events, especially in the low-energy region.

A second lead shield of modern low-activity lead will surround the apparatus to protect the detectors from environmental radioactivity in the underground laboratories. This second shield will consist of two main parts: a 25-cm-thick lead layer located outside the outer vacuum chamber (to shield the sides and bottom of the detector), and a 30-cm-thick disk located above the detectors, inside the cryostat, with an additional ring placed near the still plate. A 20-cm-thick layer of polyethylene will surround the outer lead shield to thermalise environmental neutrons, which will then be absorbed by the 3-cm-thick layer of H_3BO_3 powder in the space between the lead and the polyethylene. More details on the shields and their efficiencies can be found in Ref. [9].

9 Radiopurity of materials

The design of the experiment and its construction have been strongly constrained by stringent background requirements. This has imposed a number of limitations on allowable materials, and necessitated the development of special treatments for surface cleaning and dedicated protocols for machining and handling. Background requirements have been established with the help of a dedicated GEANT4-based Monte Carlo simulation. The simulation models the entire apparatus and enables us to define the maximum contamination allowed for each element based of the desired final counting rate in the $\beta\beta(0\nu)$ region. The design of the internal (to the cryostat) and external shields have also been optimized

with the same simulation by considering the environmental background sources present in the LNGS underground laboratories—in particular, the residual muon flux, the neutron flux, and the gamma radioactivity [9]. Experience from MiDBD [6, 8] and Cuoricino [3] has indicated what might be responsible for the more pernicious backgrounds—namely, contamination or re-contamination of the surfaces of the detector components (crystals and copper structure) [2, 7]. The collaboration has expended considerable effort in studying the best surface treatments for the detector parts. In the following subsections we summarize recent activities in this area.

9.1 Material selection and treatment

All materials used in the construction of the experiment, from the external lead and polyethylene shields to the detector, are selected according to their radioactive content. The materials used for the inner parts of the cryostat and detector have to fulfill even more stringent criteria, since they must also meet cryogenic requirements. A large-scale campaign was started some years ago to assess the radiopurity of different materials and identify which could be used for the detector and cryogenic apparatus, as well as for the machining, cleaning, and storage of the various components. Particular care was dedicated to the materials used for the detector construction—namely, TeO_2 , copper, and lead. A specific supplier was identified for each of the acceptable materials. HPGe and Si surface barrier spectroscopy (at the Milano-Bicocca and LNGS laboratories), ICPMS analysis in (at LNGS and Milano-Bicocca facilities) and neutron activation analysis (a collaboration between the INFN Milano-Bicocca and the LENA reactor in Pavia) are the main tools used in this activity. In most cases, preliminary work on optimizing the measurement techniques was necessary to improve their sensitivity to the best results achievable today.

In some cases the techniques which are usually employed to check the radioactive level of a material are not sensitive enough and only bolometric measurements can be used. This is certainly the case of the measurements of crystal bulk (with a required sensitivity of 10^{-13} g/g) or crystal and copper surface contaminations (with a required sensitivity of nBq/cm²). The cost, manpower and time required to organize bolometric runs limit their use to only what is absolutely essential.

9.2 TeO_2 crystals

The contracts with SICCAS specify very stringent requirements on the geometry and radiopurity of the crystals. The contracts also specify that most of the ancillary materials (lapping pads and powders, chemical reagents, etc.) are provided to SICCAS by the collaboration. The suppliers for these products were selected using the radioassay techniques described above.

The materials and protocols for producing, packaging, and delivering crystals were defined in detail by the Rome and Milano-Bicocca groups. US and Italian members of CUORE spent considerable time in China training the SICCAS staff on the procedures for handling, etching, polishing, and packaging the crystals in order to ensure that the requirements would be met. In addition, the raw materials used for crystal production have been periodically assayed for K, U, and Th content using inductively coupled mass

spectroscopy (ICPMS) at laboratories in the US, Italy, and China prior to their use, and the materials have always been found to be within contract specifications.

The SICCAS facility employs a combination of chemical etching and abrasive lapping to bring the crystal dimensions as close as possible to the specified tolerances, as well as to remove crystal surface layers and thereby reduce surface contamination by up to a factor of 5. This procedure was studied and optimized some years ago as a joint effort of Milano-Bicocca and LNGS groups and proved to be able to efficiently reduce the crystal surface contaminations observed in Cuoricino crystals [7].

CUORE crystal production is checked by randomly selecting four crystals from the batches received at LNGS, instrumenting them as bolometers, and operating them in the Hall C cryostat at LNGS. The purpose of the measurements is primarily to assess that the bulk contamination levels of the crystal are within the contract limits for ^{238}U and ^{232}Th . The cryogenic runs typically last for about 2–3 months. Six such measurements have been performed (involving 22 crystals in total), and each run indicated that the bulk radiopurity requirements were met. The data collected on individual crystal runs is statistically too small to check crystal surface contamination levels, but a preliminary analysis based on the summed statistics indicates that they are within CUORE requirements.

9.3 Copper

Copper is one of the larger materials by mass present in CUORE. Most of the copper is an Oxygen Free Electrolytic (OFE) alloy produced by Norddeutsche Affinerie (NA); the base-temperature components will be machined from Electronic Tough Pitch (ETP1) alloy, a.k.a. NOSV. The NOSV copper has been chosen for its low hydrogen content, and it exhibits low contamination levels (already verified several years ago by the Heidelberg group) with upper limits of $2.4 \cdot 10^{-12}$ g/g for ^{232}Th and $1.3 \cdot 10^{-12}$ g/g for ^{238}U .

In Cuoricino a large fraction of the background in the ROI is ascribed to a deep (> 5 microns) surface contamination in the copper of the mounting structure. This contamination, due to ^{238}U or ^{232}Th or ^{210}Pb and their daughters, does not have a strong signature. Its most evident effect is the presence of a flat background in the energy spectrum extending from above the 2615 keV ^{208}Tl line up to 4 MeV, where the spectrum starts being dominated by alpha peaks. For this reason an intense R&D activity study of different copper surface-treatment strategies has been pursued for the last two years. A final test to fix the cleaning procedure for CUORE copper was performed in 2009–2010 with the Three Tower Detector (TTD). The detector consisted of three stacked 12-crystal towers separated from one another by copper shields. The surfaces of the copper parts in each tower were cleaned using a different procedures. The TTD was installed in the former Cuoricino cryostat and collected data from September 2009 through January 2010. The copper for the uppermost tower (T1) was treated following the procedure that produced the best result in previous R&D tests: the copper pieces were cleaned with soap, treated with $\text{H}_2\text{O}_2 + \text{H}_2\text{O} + \text{citric acid}$ and wrapped with seven layers of polyethylene. The middle tower (T2) was cleaned at LNGS by a new chemical process, starting with simple soap and water, followed by electroerosion with 85% phosphoric acid, 5% butanol, and 10% water, followed by chemical etching with nitric acid, and finally passivation with $\text{H}_2\text{O}_2 + \text{H}_2\text{O} + \text{citric acid}$. The copper for the lowermost tower (T3) was

cleaned with a sophisticated so-called “TECM” procedure at the Laboratori Nazionali di Legnaro, consisting of tumbling, electropolishing, chemical etching, and a magnetron plasma-cleaning technique. The result of the TTD measurement was that the copper treatment adopted for T1 and T3 gave similar results, the measured rate in the 2.7–3.9 MeV region being compatible within 1σ . The counting rate measured in T2, on the other hand, was much higher, indicating that this technique is less effective in reducing the contamination responsible for the flat background between 2.6 and 4 MeV.

As a result, the copper cleaning procedure for the CUORE detector components has been defined as follows: frames, columns, and wire trays will be treated in Legnaro using the TECM technique, while copper screens delimiting the detector volume will be cleaned at LNGS using the same process as for T1—namely, a soft chemical cleaning and polyethylene wrapping—due to the screen dimensions and schedule constraints.

9.4 Parts storage and handling

Underground storage areas have been organized at LNGS in order to avoid dangerous cosmogenic activation of some detector components, primarily copper and tellurium. A storage protocol was defined for each detector part, with special care devoted to the TeO_2 crystals which are transported from China to Italy. Polyethylene bags for vacuum storage were radioassayed in order to avoid contamination of the enclosed components. The TeO_2 crystals and copper are stored in three successive layers of polyethylene vacuum bags which were selected for their negligible radon diffusion. A specifically dedicated vacuum pump was realized for evacuating the plastic bags in order to prevent oil or grease from diffusing back into the bags.

The logistics of transporting and storing the copper was organized with particular care in order to avoid cosmogenic activation. Cosmic rays interacting with Cu readily produce the isotope ^{60}Co which beta decays with an endpoint only slightly lower than the ^{130}Te transition energy. Activated Cu could therefore induce a dangerous, unwanted background in the experiment, and only four months of exposure are needed before Cu activation becomes nonnegligible,

The Cu sheets and rods are stored underground in LNGS shortly after production in Germany, and the Cu is taken aboveground only briefly for transportation to the Milano-Bicocca and Legnaro workshops for machining. A temporary shallow-depth storage area was also organized in Baradello, Como, for use during transportation of the Cu between LNGS and the workshops. The location history of the Cu is recorded in the collaboration’s parts database. The final copper parts are vacuum-packaged and stored inside nitrogen-flux cabinets in CUORE’s underground PSA building at LNGS.

The materials must to be handled in a Rn-free environment to avoid recontamination after surface treatments. For this purpose a class 1000 clean room has been constructed in the CUORE hut (Section 7) and the detector will be assembled in specially designed glove boxes (Section 3) inside the clean room. All of the tools used for detector assembly will be rigorously cleaned and checked for radioactivity.

10 CUORE-0

The first step of the CUORE experiment will be CUORE-0, the bolometric operation of the first tower of TeO₂ crystals produced by the CUORE detector assembly line. The CUORE-0 tower will be operated inside the former Cuoricino refrigerator in Hall A at LNGS. CUORE-0 has three main goals: (1) to test the new CUORE assembly line; (2) to check with high statistics the improvements in reducing radioactive backgrounds; and (3) to optimize the bolometric behavior of the detectors. Its anticipated sensitivity will improve the limit set by Cuoricino in just a few months, making CUORE-0 one of the most sensitive $\beta\beta(0\nu)$ experiments worldwide.

The CUORE-0 tower will be assembled according to the CUORE procedures, which differ substantially from those used in Cuoricino. The detector will be constructed using the CUORE assembly line equipment (see Sections 2.4 and 3.4) inside the CUORE hut's newly constructed clean room (see Section 7). Most of the components for the detector are ready. 60 packaged crystals from the CUORE production line have been stored underground in nitrogen-fluxed cupboards since February 2009. The thermistors, heaters, and PTFE parts have been prepared and are also currently stored in the underground Parts Storage Area (PSA) between the Cuoricino and CUORE huts. The tower's copper pieces (frames, columns, and thermal shields) have been produced, and their cleaning will be completed at the beginning of April by the Legnaro Laboratory in Italy.

The former Cuoricino refrigerator has been instrumented for CUORE-0 using the same type of wiring that will be used in CUORE. A test of the wires at low temperature was recently completed using a 12-detector tower leftover from the former Three Towers Test.

The semi-automatic gluing system will be installed in the CUORE clean room in March 2011, and its operating parameters will be tuned shortly after. Thermistors will be glued to the CUORE-0 crystals in May 2011. Meanwhile, the system for assembling the CUORE-0 tower will be installed, and assembly is anticipated to commence early in the summer. The installation of the tower inside the Cuoricino cryostat, its cooldown, and optimization of the measurement parameters will be performed in late summer, and CUORE-0 will start taking data in earnest in Fall 2011.

11 Publications in 2010

1. M. Vignati, J. of Appl. Phys. **108** (2010) 084903.
2. A. Nucciotti, "CUORICINO and CUORE: present and future of 130-Te neutrinoless double beta decay searches", presented at 35th International Conference of High Energy Physics (ICHEP 2010), July 22-28, 2010, Paris, France. Published on-line: PoS(ICHEP 2010)312.
3. C. Arnaboldi *et al.*, Nucl. Instr. Meth. A **617** (2010) 327-328.
4. C. Arnaboldi *et al.*, J. of Crystal Growth **312** (2010) 2999-3008
5. C. Arnaboldi *et al.*, Astrop. Phys. **34** (2010) 18-24.

6. F. Bellini *et al.*, *Astrop. Phys.* **33** (2010) 169-174.
7. E. Andreotti *et al.*, *Astroparticle Physics* **34** (2010) 18-24
8. G. Ventura, V. Martelli, N. Toccifondi, *Physica B* **405** (2010) 4247-4249.
9. A. L. Woodcraft, G. Ventura, V. Martelli and W. S. Holland, *Cryogenics* **50** (2010) 465-468.
10. C. Nones, *Astroparticle, Particle, Space Physics, Radiation Interaction, Detectors and Medical Physics Applications* **5** (2010) 298.

References

- [1] H. V. Klapdor-Kleingrothaus *et al.*, *Phys. Lett. B* **586** (2004) 198.
H. V. Klapdor-Kleingrothaus *et al.*, *Nucl. Instrum. Meth. A* **522** (2004) 371.
H. V. Klapdor-Kleingrothaus and I. V. Krivosheina, *Mod. Phys. Lett. A* **21** (2006) 1547.
- [2] C. Arnaboldi *et al.*, *Astropart. Phys.* **20** (2003) 91.
C. Arnaboldi *et al.*, *Nucl. Instr. Meth. A* **518**(2004) 775.
R. Ardito *et al.*, CUORE: A cryogenic underground observatory for rare events, arXiv hep-ex/0501010 (2005).
- [3] C. Arnaboldi *et al.*, *Phys. Rev. Lett.* **95** (2005) 14501.
E. Andreotti, et al., ^{130}Te Neutrinoless Double-Beta Decay with CUORICINO, 2010. Accepted by *Astroparticle Physics*, doi:10.1016/j.astropartphys.2011.02.002, arXiv:1012.3266.
- [4] A. Alessandrello *et al.*, *Phys. Lett. B* **285** (1992) 176.
A. Alessandrello *et al.*, *Phys. Lett. B* **335** (1994) 519-525.
- [5] A. Alessandrello *et al.*, *Nucl. Instr. Meth. A* **360** (1995) 363.
A. Alessandrello *et al.*, *Nucl. Instr. Meth. A* **370** (1996) 241.
- [6] A. Alessandrello *et al.*, *Phys. Lett. B* **433** (1998) 156.
- [7] M. Pavan *et al.*, *Eur. Phys. J A* **36** (2008) 159.
- [8] C. Bucci *et al.*, *Eur. Phys. J A* **41** (2009) 155.
- [9] F. Bellini *et al.*, *Astroparticle Physics* **33** (2010) 169-174.
- [10] A. Alessandrello *et al.*, *IEEE Tran. on Nucl. Sc.* **44**, 416-423 (1997).
- [11] A. Alessandrello *et al.*, *Nucl. Instr. Meth. A* **444** (2000) 111-114.
- [12] G. Pessina, *Nucl. Instr. Meth. A* **44** (2000) 132-135.

- [13] C.Arnaboldi, X.Liu, G.Pessina, 2009 IEEE NSS Conf Rec, 25 - 31 Ottobre 2009, N13-042 pp 389 395, Orlando.
- [14] C. Arnaboldi, A. Giachero, C. Gotti and G. Pessina, Accepted by Nucl. Instr. and Meth. A (2010), doi:10.1016/j.nima.2010.09.151.

DAMA

Collaboration:

P. Belli^a, R. Bernabei^{a,@}, A. Bussolotti^{a,*}, F. Montecchia^a, F. Nozzoli^a, A. d'Angelo^b, F. Cappella^b, A. Incicchitti^b, A. Mattei^{b,*}, D. Prosperi^{b,+}, R. Cerulli^c, V. Caracciolo^c, C.J. Dai^d, H.L. He^d, H.H. Kuang^d, X.H. Ma^d, X.D. Sheng^d, Z.P. Ye^{d,e}, R.G. Wang^d, Y.J. Zhang^d

in some detector developments, by-product results and small scale experiments: R.S. Boiko^g, V.B. Brudanin^h, N. Bukilicⁱ, D.M. Chernyak^g, F.A. Danevich^g, S. d'Angelo^a, V.Ya. Degoda^j, J.R. de Laeterⁱ, A.E. Dossovitskiy^k, E.N. Galashov^l, Yu.A. Hyzhnyj^j, S.V. Ildyakov^l, V.V. Kobychiev^g, O.S. Kolesnyk^j, G.P. Kovtun^m, V.M. Kudovbenko-Mokina^g, B.N. Kropivynsky^g, M. Laubenstein^c, A.L. Mikhlin^k, L.L. Nagornayaⁿ, P.G. Nagornyj^j, S.S. Nagorny^g, S.G. Nedilko^j, A.S. Nikolaiko^g, S. Nisi^c, D.V. Poda^{c,g}, R.B. Podvujanyuk^g, O.G. Polischuk-Shkulkova^g, A.P. Shcherban^m, V.P. Shcherbatskiy^j, V.N. Shlegel^l, D.A. Solopikhin^m, Yu.G. Stenin^l, J. Suhonen^o, V.I. Tretyak^g, Ya.V. Vasiliev^l, V.D. Virich^m, S.S. Yurchenko^g, I.M. Vyshnevskiy^g

in some studies on $\beta^+\beta^+$, EC/β^+ , EC/EC decay modes (under the joint Indo-Italian DST-MAE project and inter-universities agreement): P.K. Raina^p, A.K. Singh^p, P.K. Rath^p, S. Ghorui^p

^aDip. Fisica, Univ. Roma "Tor Vergata" and INFN-Roma Tor Vergata, Roma, Italy.

^bDip. Fisica, Univ. Roma "La Sapienza" and INFN-Roma, 00185 Roma, Italy.

^cLaboratorio Nazionale del Gran Sasso, INFN, 67010 Assergi (Aq), Italy.

^dIHEP, Chinese Academy, P.O. Box 918/3, Beijing 100039, China.

^ePhysics Dept, Jing Gangshan University 343009, Jiangxi, China.

^fRussian Chemistry-Technological University of D.I.Mendeleev, Moscow, Russia.

^gInstitute for Nuclear Research, MSP 03680, Kiev, Ukraine.

^hJoint Institute for Nuclear Research, 141980 Dubna, Russia.

ⁱDepartment of Applied Physics, Curtin University, GPO, Box U1987 Perth, Australia.

^jKiev National Taras Shevchenko University, MSP 01033 Kiev, Ukraine.

^kJoint stock company NeoChem, 117647 Moscow, Russia.

^lNikolaev Institute of Inorganic Chemistry, 630090 Novosibirsk, Russia.

^mNational Science Center Kharkiv Institute of Physics and Technology, Kharkiv, Ukraine.

ⁿInstitute for Scintillation Materials, 61001 Kharkiv, Ukraine.

^oDep. of Physics, University of Jyvaskyla, P.O. Box 35, FIN-40351, Jyvaskyla, Finland

^pIndian Institute of Technology, Kharagpur, India.

[@] Spokesperson; * technical staff; + deceased

Abstract

DAMA is an observatory for rare processes located deep underground at the Gran Sasso National Laboratory of the I.N.F.N. (LNGS). It develops and uses low background scintillators. At present the main low background experimental set-ups in operation are: i) the second generation DAMA/LIBRA set-up (sensitive mass: $\simeq 250$ kg highly radiopure NaI(Tl)), which has been further upgraded during 2010; ii) the DAMA/LXe set-up (sensitive mass: $\simeq 6.5$ kg liquid Kr-free Xenon enriched either in ^{129}Xe or in ^{136}Xe); iii) the DAMA/R&D set-up (a facility dedicated to test prototypes and to perform small scale experiments, mainly investigating double beta decay modes in various isotopes); iv) the DAMA/Ge set-up (mainly dedicated to sample measurements and to specific measurements on rare processes). Efforts on various aspects are also carried out towards a possible multipurpose 1 ton highly radiopure NaI(Tl) set-up, DAMA proposed in 1996. In the following main arguments on the activity developed during 2010 are summarized.

1 DAMA/LIBRA

A large particle zoology is available in literature for the Dark Matter (DM) candidate particles, their interaction types and overall phenomenologies; on the other hand even a particle not yet foreseen by theory can be the solution. Considering the richness in particles of the visible matter which is less than 1% of the Universe density, one could also expect that the particle part of the Dark Matter in the Universe may be multicomponent. Moreover, at present level of knowledge very large uncertainties exist on general aspects and on the parameters values in the related astrophysical, nuclear and particle Physics arguments. Thus, a model independent approach for the DM detection with a widely sensitive detector in fully controlled conditions is mandatory.

This is the main aim of the second generation experiment DAMA/LIBRA ($\simeq 250$ kg highly radiopure NaI(Tl) see [1, 2, 3] and in the 2010 publication list, after the pioneer DAMA/NaI ($\simeq 100$ kg of highly radiopure NaI(Tl))) [4, 5, 6, 7, 8, 9, 10, 11, 12, 13, 14, 15, 16, 17, 18, 19, 20, 21, 22, 23, 24, 25], which took data at LNGS over seven annual cycles up to July 2002.

Both DAMA/NaI and DAMA/LIBRA have the main aim to perform a direct detection of DM particles in the galactic halo by exploiting the model independent DM annual modulation signature, originally suggested by [26, 27] in the mid-80's. In fact, as a consequence of its annual revolution around the Sun, which is moving in the Galaxy travelling with respect to the Local Standard of Rest towards the star Vega near the constellation of Hercules, the Earth should be crossed by a larger flux of Dark Matter particles around ~ 2 June (when the Earth orbital velocity is summed to the one of the solar system with respect to the Galaxy) and by a smaller one around ~ 2 December (when the two velocities are subtracted). Thus, this signature has a different origin and peculiarities than the seasons on the Earth and than those effects correlated with seasons (consider e.g. the expected value of the phase as well as the other requirements listed below).

Thus, the contribution of the signal to the counting rate in the k -th energy interval can be written as: $S_k = S_{0,k} + S_{m,k} \cos \omega(t - t_0)$, where: i) $S_{0,k}$ is the constant part of the

signal; ii) $S_{m,k}$ is the modulation amplitude; iii) $\omega = \frac{2\pi}{T}$ with period T ; iv) t_0 is the phase.

The DM annual modulation signature is very distinctive since it requires the simultaneous satisfaction of all the following peculiarities: the rate must contain a component modulated according to a cosine function (1) with one year period (2) and a phase that peaks roughly around $\simeq 2^{nd}$ June (3); this modulation must only be found in a well-defined low energy range, where DM particle induced events can be present (4); it must apply only to those events in which just one detector of many actually “fires” (*single-hit events*), since the DM particle multi-interaction probability is negligible (5); the modulation amplitude in the region of maximal sensitivity must be $\lesssim 7\%$ for usually adopted halo distributions (6), but it can be larger in case of some possible scenarios such as e.g. those in Ref. [28, 29, 30]. Only systematic effects or side reactions able to fulfil these requirements and to account for the whole observed modulation amplitude could mimic this signature; thus, no other effect investigated so far in the field of rare processes offers a so stringent and unambiguous signature.

At present status of technology the DM annual modulation is the only model independent signature available in direct dark matter investigation that can be effectively exploited.

It is worth noting that approaches based on many selections and handling procedures to “reject” the electromagnetic component of the counting rate are insensitive to various DM scenarios and cannot offer any signature also for the particular candidates, they would look for. In fact, even under the assumption of an “ideal” electromagnetic component rejection, e.g. the neutrons and the internal end-range α 's induce signals indistinguishable from recoils which cannot be estimated and subtracted in any reliable manner at the needed (and sometime claimed) precision. In addition, part or all the signal can have electromagnetic nature; see in literature. Moreover, in a safe investigation of the DM annual modulation signature those data handlings cannot be applied e.g. because of their – always – statistical nature which would affect the reliability of an annual modulation analysis and restrict the sensitivity to many kinds of candidates. On the other hand, as pointed out already in the 80's, the exploitation of the DM annual modulation signature acts itself as an effective background rejection.

After the first upgrading occurred on October 2008, DAMA/LIBRA has continued its data taking uninterruptedly up to end of October 2010, when a new upgrade has been carried out (see later).

1.1 The model-independent experimental result on DM

As already reported in the LNGS Annual report 2008 (see also [1, 2] and references therein), several analyses investigating the model-independent DM annual modulation signature have been performed on the DAMA/LIBRA data collected over the first four annual cycles (exposure: $0.53 \text{ ton} \times \text{yr}$). They have further confirmed the peculiar annual modulation of the *single-hit* events in the (2–6) keV¹ energy region satisfying all the many requests of the DM annual modulation signature.

In 2010 the results obtained with the data collected in the period 2007-2009 (exposure: $0.34 \text{ ton} \times \text{yr}$), corresponding to two additional annual cycles, have been released (now the

¹Here and after, keV means keV electron equivalent.

total DAMA/LIBRA exposure over six annual cycles is: $0.87 \text{ ton} \times \text{yr}$). The cumulative exposure with the former DAMA/NaI is $1.17 \text{ ton} \times \text{yr}$ – corresponding to 13 annual cycles in total – which is orders of magnitude larger than the exposures typically considered in the field. The DM model independent evidence is now at about 9σ C.L.. For details

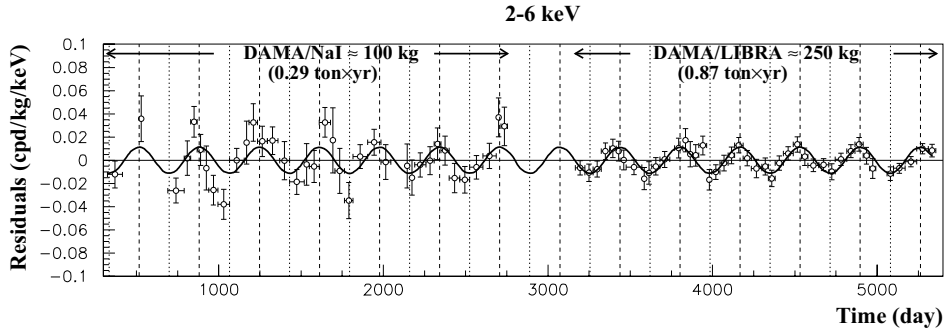


Figure 1: Experimental model-independent residual rate of the *single-hit* scintillation events, measured by DAMA/NaI over seven and by DAMA/LIBRA over six annual cycles in the (2 – 6) keV energy interval as a function of the time [8, 9, 2] and 2010 publication list. The zero of the time scale is January 1st of the first year of data taking of the former DAMA/NaI experiment. The experimental points present the errors as vertical bars and the associated time bin width as horizontal bars. The superimposed curve is the cosinusoidal function behavior $A \cos \omega(t - t_0)$ with a period $T = \frac{2\pi}{\omega} = 1 \text{ yr}$, with a phase $t_0 = 152.5 \text{ day}$ (June 2nd) and with modulation amplitude, A , equal to the central value obtained by best fit over the whole data: cumulative exposure is $1.17 \text{ ton} \times \text{yr}$. The dashed vertical lines correspond to the maximum expected for the DM signal (June 2nd), while the dotted vertical lines correspond to the minimum. When all the three parameters are kept free, one gets from the data: $A = (0.0116 \pm 0.0013) \text{ cpd/kg/keV}$, $T = (0.999 \pm 0.002) \text{ yr}$ and $t_0 = (146 \pm 7) \text{ day}$, values well in agreement with expectations for DM signal.

see in the 2010 publication list. Here just few arguments are mentioned. In particular, Fig. 1 shows the time behaviour of the experimental residual rates of the *single-hit* events collected by DAMA/NaI and by DAMA/LIBRA in the (2–6) keV energy interval. The superimposed curve is the cosinusoidal function: $A \cos \omega(t - t_0)$ with a period $T = \frac{2\pi}{\omega} = 1 \text{ yr}$, with a phase $t_0 = 152.5 \text{ day}$ (June 2nd), and modulation amplitude, A , obtained by best fit over the 13 cycles of DAMA/NaI [8, 9] and DAMA/LIBRA (see e.g. Ref. [2] and 2010 publication list). The hypothesis of absence of modulation in the data can be discarded. Moreover, when the period and the phase parameters are also released in the fit, values well compatible with those expected for a DM particle induced effect are obtained for the cumulative exposure; for example, the fitting procedure gives in the cumulative (2–6) keV energy interval: $A = (0.0116 \pm 0.0013) \text{ cpd/kg/keV}$, $T = (0.999 \pm 0.002) \text{ yr}$ and $t_0 = (146 \pm 7) \text{ day}$. Summarizing, the analysis of the *single-hit* residual rate favours the presence of a modulated cosine-like behaviour with proper features at 8.9σ C.L..

The same data of Fig. 1 have also been investigated by a Fourier analysis, obtaining a clear peak corresponding to a period of 1 year as expected for a DM signal (see in 2010 publication list); this analysis in other energy region shows instead only aliasing peaks. Moreover, while in the (2–6) keV *single-hit* residuals a clear modulation is present, it is

absent at energies just above. The measured energy distribution has been investigated in other energy regions not of interest for Dark Matter, also verifying the absence of any significant background modulation. In fact, the background in the lowest energy region is essentially due to “Compton” electrons, X-rays and/or Auger electrons, muon induced events, etc., which are strictly correlated with the events in the higher energy part of the spectrum; thus, if a modulation detected in the lowest energy region would be due to a modulation of the background (rather than to a signal), an equal or larger modulation in the higher energy regions should be present. The data analyses have allowed to exclude the presence of a background modulation in the whole energy spectrum at a level much lower than the effect found in the lowest energy region for the *single-hit* events (see in 2010 publication list).

A further relevant investigation has been done by applying the same hardware and software procedures, used to acquire and to analyse the *single-hit* residual rate, to the *multiple-hits* one. In fact, since the probability that a DM particle interacts in more than one detector is negligible, a DM signal can be present just in the *single-hit* residual rate. Thus, this allows the test of the background behaviour in the same energy interval of the observed positive effect. A clear modulation is present in the *single-hit* events, while the fitted modulation amplitude of the *multiple-hits* residual rate is well compatible with zero (see in 2010 publication list). Similar results were previously obtained also for the

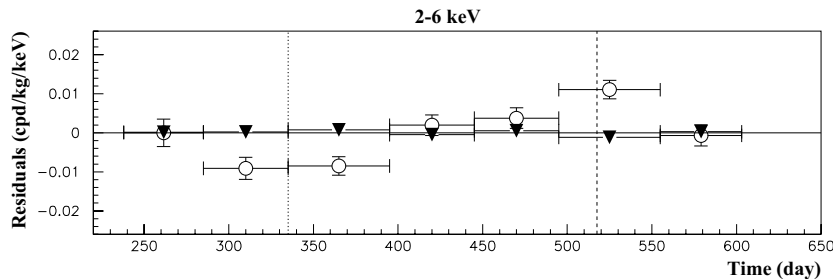


Figure 2: Experimental residual rates over the six DAMA/LIBRA annual cycles for *single-hit* events (open circles) (class of events to which DM events belong) and for *multiple-hit* events (filled triangles) (class of events to which DM events do not belong). They have been obtained by considering for each class of events the data as collected in a single annual cycle and by using in both cases the same identical hardware and the same identical software procedures. The initial time of the figure is taken on August 7th. The experimental points present the errors as vertical bars and the associated time bin width as horizontal bars. Analogous results were obtained for the DAMA/NaI data [9].

DAMA/NaI case [9]. Thus, again evidence of annual modulation with proper features, as required by the DM annual modulation signature, is present in the *single-hit* residuals (events class to which the DM particle induced events belong), while it is absent in the *multiple-hits* residual rate (event class to which only background events belong). Since the same identical hardware and the same identical software procedures have been used to analyse the two classes of events, the obtained result offers an additional strong support for the presence of DM particles in the galactic halo further excluding any side effect either from hardware or from software procedures or from background.

The annual modulation present at low energy has also been analyzed by depicting the

differential modulation amplitudes, $S_{m,k}$, as a function of the energy (the k index identifies the energy interval); the $S_{m,k}$ is the modulation amplitude of the modulated part of the signal obtained by maximum likelihood (see in 2010 publication list). The $S_{m,k}$ values are reported as function of the energy in Fig. 3 (for simplicity the k index is omitted in the following). It has been also verified that the measured modulation amplitudes

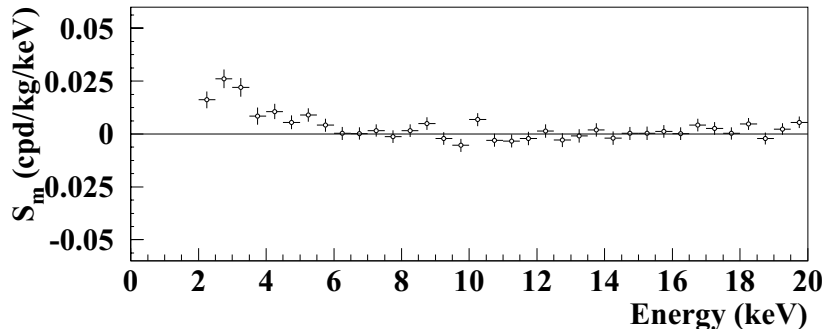


Figure 3: Energy distribution of the S_m variable for the total cumulative exposure 1.17 ton \times yr. The energy bin is 0.5 keV. A clear modulation is present in the lowest energy region, while S_m values compatible with zero are present just above. In fact, the S_m values in the (6–20) keV energy interval have random fluctuations around zero with χ^2 equal to 27.5 for 28 degrees of freedom.

are statistically well distributed in all the crystals, in all the annual cycles and energy bins; several other kinds of analyses are presented in the dedicated paper in the 2010 publication list and Ref. therein.

These results confirm those achieved by other kinds of analyses. In fact, as required by the DM annual modulation signature: 1) the *single-hit* events show a clear cosine-like modulation as expected for the DM signal; 2) the measured period is equal to (0.999 ± 0.002) yr well compatible with the 1 yr period as expected for the DM signal; 3) the measured phase (146 ± 7) days is well compatible with the roughly $\simeq 152.5$ days expected for the DM signal; 4) the modulation is present only in the low energy (2–6) keV interval and not in other higher energy regions, consistently with expectation for the DM signal; 5) the modulation is present only in the *single-hit* events, while it is absent in the *multiple-hit* ones as expected for the DM signal; 6) the measured modulation amplitude in NaI(Tl) of the *single-hit* events in the (2–6) keV energy interval is: (0.0116 ± 0.0013) cpd/kg/keV (8.9σ C.L.).

As previously done for DAMA/NaI, careful investigations on absence of any significant systematics or side reaction in DAMA/LIBRA have been quantitatively carried out and reported in details in Ref. [2, 31], Refs. therein and in the 2010 publication list. No effect able to account for the measured modulation amplitude and simultaneously satisfy all the requirements of the signature has been found or suggested by anyone over more than a decade.

In conclusion, DAMA/LIBRA has confirmed the presence of an annual modulation satisfying all the requirements of the DM annual modulation signature, as previously pointed out by DAMA/NaI; in particular, the evidence for the presence of DM particles in the galactic halo is cumulatively supported by the exposure of 1.17 ton \times yr collected

over 13 annual cycles at 8.9σ C.L..

The obtained model-independent evidence is compatible with a wide set of scenarios regarding the nature of the DM candidate and related astrophysical, nuclear and particle Physics (see e.g. Ref. [8, 9, 10, 11, 12, 13, 14, 15], Appendix A of Ref. [2] and in literature, for example see [28, 32, 33, 30, 34, 35, 36, 37, 38, 39, 40, 41]); and many other possibilities are open. Further future works are also foreseen.

It is worth noting that no other experiment exists, whose result can be directly compared in a model-independent way with those by DAMA/NaI and DAMA/LIBRA. In particular, let us also point out that results obtained with different target materials and/or different approaches cannot intrinsically be directly compared among them even when considering the same kind of candidate and of coupling, although apparently all the presentations generally refer to cross sections on nucleon. Therefore, claims for contradictions made by experiments insensitive to the DM annual modulation signature, using different target materials and approaches, having well different sensitivities to various DM candidate and interactions, etc. have by the fact no impact even in the single arbitrary scenario they usually consider without – in addition – accounting for the existing experimental and theoretical uncertainties, using often crude approximation in the calculation, and optimistic estimates for their experimental/theoretical parameters and the worst/arbitrary for the others, etc. Moreover, (see for example [8, 42, 43, 44]), some critical points exist in those activities, claiming for exclusion, on important experimental aspects (energy threshold, energy scale, UV light lost/absorption, disuniformity of detector’s response, multiple selection procedures, related efficiencies, stabilities, etc.. A relevant argument is also the methodological robustness [45]. Finally, they generally quote some of the implications of the DAMA model independent result in incorrect, partial and unupdated way, as done elsewhere also in this book of activities reports. Thus, claims for contradiction have no scientific basis.

On the other hand, whatever possible positive hint (just as examples we mention e.g. Ref. [46, 47, 38]) has to be interpreted and a large room of compatibility with DAMA annual modulation evidence is present, and even more when properly considering the existence of large uncertainties in the adopted experimental and theoretical parameters and a right evaluation of the DAMA allowed volumes for each scenario.

For completeness we mention that, as regards the model-dependent indirect detection searches, it does not exist a biunivocal correspondence between the observables in the direct and indirect experiments. However, if possible excesses in the positron to electron flux ratio and in the γ rays flux with respect to some modeling of the background contribution, might be interpreted – under some specific assumptions – in terms of Dark Matter, this would also be not in conflict with the effect observed by DAMA experiments; as also discussed in literature at some extent. It is worth noting that the idea that a possible DM candidate able to account both for the absence of excess in the antiproton flux and for the possible model dependent excess in the positron one should have coupling in the lepton sector, excludes that direct search experiments looking just for recoils might see it, while DAMA can. However, different possibilities either considering different background modeling or accounting for other kinds of astrophysical sources can also explain the indirect observations.

1.2 The upgrade 2010

The data of another annual cycle collected before the 2010 DAMA/LIBRA upgrade are already at hand. In fact, considering the relevance to lower the software energy threshold of the experiment, in order to improve the performance and the sensitivity of the experiment and to allow also deeper corollary information on the nature of the DM candidate particle(s) and on the various related astrophysical, nuclear and particle Physics scenarios, the replacement of all the PMTs with new ones having higher quantum efficiency has been planned. A special dedicated development has been realized by HAMAMATSU co. Thus, at end of October 2010 the DAMA/LIBRA set-up has stopped the data taking and the shield has been opened in high purity Nitrogen atmosphere to replace all the low background PMTs with new ones having higher quantum efficiency. After the replacement and the electronics optimization, long data taking periods are foreseen in the new running condition to achieve all the physical goals of the experiment. Further upgrade of some parts of the electronics are already in preparation for future.

1.3 Conclusions and perspectives

The data of the former DAMA/NaI and those of the first 6 annual cycles of DAMA/LIBRA (cumulative exposure exposure 1.17 ton \times yr) have given positive model independent evidence for the presence of DM particles in the galactic halo with high confidence level on the basis of the DM annual modulation signature. Another year exposure has already been collected. Moreover, the upgrade occurred in November 2010 with the substitution of all the low background PMTs with new ones having higher quantum efficiency will be important in the new data takings.

A larger exposure collected by DAMA/LIBRA (or by a possible future DAMA/1ton) in the improved configuration will increase: i) the experimental sensitivity; ii) the corollary information on the nature of the DM candidate particle(s) and on the various related astrophysical, nuclear and particle physics scenarios. Moreover, it will also allow the investigation – with high sensitivity – of other DM features, of second order effects and of several rare processes other than DM. In particular, some of the many topics – not yet well known at present and which can affect whatever model dependent result and comparison – are: i) the velocity and spatial distribution of the Dark Matter particles in the galactic halo; ii) the effects induced on the Dark Matter particles distribution in the galactic halo by contributions from satellite galaxies tidal streams; iii) the effects induced on the Dark Matter particles distribution in the galactic halo by the possible existence of caustics; iv) the detection of possible "solar wakes" (the gravitational focusing effect of the Sun on the Dark Matter particle of a stream); v) the investigation of possible diurnal effects; vi) the study of possible structures as clumpiness with small scale size; vii) the coupling(s) of the Dark Matter particle with the ^{23}Na and ^{127}I and its nature; viii) the scaling laws and cross sections; etc.

In addition, it is worth noting that ultra low background NaI(Tl) scintillators can also offer the possibility to achieve significant results on several other rare processes as already done with the former DAMA/NaI and just started with DAMA/LIBRA.

In conclusion, it is worth noting that DAMA/LIBRA is still in the DM field the set-

up having the highest intrinsic radiopurity, the largest exposed sensitive mass, the largest collected exposure, the deepest controlled running condition and stability, and the only one with highly sensitive ULB NaI(Tl).

2 Towards the possible DAMA/1ton

A third generation R&D effort towards a possible highly radiopure NaI(Tl) “general purpose” experiment having full sensitive mass of 1 ton (we already proposed in 1996 as general purpose set-up) was funded by I.N.F.N.. The original main design of the set-up was to realize three replica of the present DAMA/LIBRA set-up; then, after that a possible location for the set-up was given by the former director, a dedicated different mechanical design was realized in the framework of a POR-Abruzzo fellowship. At present due to different space allocation, the project design is back to the original form. Thus, all executive project is by the fact available, being the operative DAMA/LIBRA one of the four modules of DAMA/1ton.

Activities have been continued in the light of overcoming the present problems regarding the supplying and purifications of high quality NaI and, mainly, TlI powders and the creation of new improved protocols, as necessary also because the changes in expertise, in materials suppliers and organization have made difficult to develop ULB NaI(Tl) in Saint Gobain.

3 DAMA/LXe

As mentioned in previous reports, we pointed out many years ago (see e.g. Ref. [48]) the possible interest in using the liquid Xenon as target-detector material for particle dark matter investigations. Since the end of 80’s (former Xelidon experiment of the INFN) we have realized several liquid Xenon (LXe) prototype detectors and, then, we have preliminarily put in measurement the set-up used in the data taking of Ref. [49] at LNGS in the framework of the DAMA project. This set-up (having a Cu inner vessel filled by $\simeq 6.5$ kg - i.e. $\simeq 2$ l - of liquid Xenon) was firstly upgraded at fall 1995 [50]. At that time it used Kr-free Xenon enriched in ^{129}Xe at 99.5%. Then, in 2000 the set-up was deeply modified reaching the configuration of Ref. [51] in order to alternatively handle also Kr-free Xenon enriched in ^{136}Xe at 68.8%. The main features of the set-up, the details on the data acquisition, on the cryogenic and vacuum systems and on the running parameters control can be found in Ref. [50, 51, 52]. Some other upgrades have been carried out in recent years.

Investigations on several rare processes have been carried out with time passing in the various configurations, as well as measurements at low energies both with neutron source and with neutron beams [49, 50, 51, 53, 52, 54]. In particular, first and/or competing results have been obtained on some approaches for Dark Matter investigations (including pulse shape analysis), on double beta decay modes in ^{136}Xe and ^{134}Xe , on possible charge non-conserving processes, on nucleon, di-nucleon and tri-nucleon decay into invisible channels both in ^{129}Xe and in ^{136}Xe .

It is worth noting that the mass exposed when using the Xenon enriched in ^{129}Xe correspond for spin-dependent coupled particles to expose 24.5 kg of natural Xenon, while the exposed mass when using the Xenon enriched in ^{136}Xe correspond for spin-independent coupled particles to an exposed mass of 50.4 kg of natural Xenon.

On the contrary of the NaI(Tl) case, plans for enlarging the exposed mass have never been considered because of the technical reasons (specific of liquid noble gas detectors and, in particular, of liquid xenon detectors), pointed out several times in the past (see e.g. [43, 44]); moreover, the extremely expensive cost of the needed Kr-free (and possibly enriched) Xenon is an additional constraint.

After the forbiddenness of using cryogenic liquids in the LNGS underground laboratories, the set-up took data just few months until December 2004; then, it has been put in standby waiting for the restarting of the LNGS cooling water plant and of the local water refrigeration system. We profited from this period to perform several upgrades of the apparatus. Finally, thanks to a new chiller system and to the restoring of the use of water plants deep underground, the DAMA/LXe set-up restarted the data taking in December 2007, continuously during 2008 up to January 2009. Then, the Leybold periodical maintenance has occurred as well as an improvement of the remote computer control and setting of the cryogenic parameters. The data taking has been restarted at fall 2009 and data taking periods have been carried out during 2010. In all these last periods DAMA/LXe was filled with Xenon enriched in ^{136}Xe and has taken data focusing mainly the high energy region. Maintenance will occur at beginning of 2011. Data analyses are in progress.

4 DAMA/R&D

DAMA/R&D is a low-background set-up dedicated to measurements on low background prototype scintillators and PMTs realized in various R&D developments. Moreover, it is also regularly used to perform relatively small scale experiments (often in collaboration with INR-Kiev as foreseen in the agreements). This set-up has been upgraded several times. The measurements mainly investigate 2β decay modes in various isotopes; both the active and the passive source techniques have been exploited as well as – sometimes – the coincidence technique [55, 56, 57].

Some of the 2010 results and works are shortly summarized in the following. Here we just add that the analysis of the data collected with a commercial BaF_2 crystal to obtain accurate determinations of the decay times of some Po and Rn isotopes (in U/Th chain) is in progress; moreover, studies on rare α processes and on R&D for radiopure BaF_2 crystal scintillators to search for 2β decay of ^{130}Ba and ^{132}Ba on the level of sensitivity $\sim 10^{21} - 10^{22}$ yr with aim to confirm or disprove the result of a geochemical experiment are also considered. In addition the data taking with a CeCl_3 scintillator to search for 2β decay of cerium with the source=detector approach has been completed and a paper has been prepared. Other information can be derived from the 2010 publication list. Finally, investigations on various kinds of new scintillators and preliminary works for the future measurements are also in progress.

4.1 Radiopurity of ZnWO_4 crystal scintillators

In recent years we have made measurements with ZnWO_4 crystal scintillators to investigate double beta decay of Zn and W isotopes [56]. In order to perform new improved measurements in future the radioactive contamination of various ZnWO_4 crystal scintillators has been investigated deep underground in the low background DAMA/R&D set-up with a total exposure of $3197 \text{ kg} \times \text{h}$. Four clear, slightly colored ZnWO_4 crystal scintillators have been used in the study (see Fig. 4); they have been produced by different companies with different procedures. The time-amplitude analysis, the pulse-shape discrimination

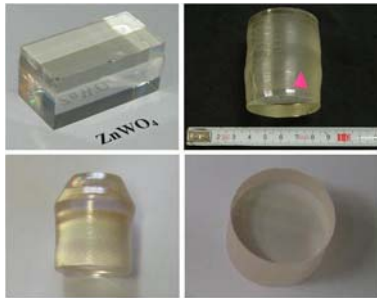


Figure 4: The ZnWO_4 crystal scintillators developed and used in the investigation of the radiopurity of ZnWO_4 crystals.

between $\gamma(\beta)$ and α particles, and the Monte Carlo simulation of the measured energy distributions have been applied to estimate the radioactive contamination of the ZnWO_4 crystals. In addition, one of ZnWO_4 crystal has been tested by ultra-low background γ spectrometry. For all details and results see the dedicated publication given in the 2010 publication list, where the measured contaminations levels are also compared with results for other tungstates and for specially developed low background $\text{NaI}(\text{Tl})$. A peculiarity has also been observed in the α spectrum of the ZnWO_4 detectors at the energy of $325(11)$ keV in γ scale, which corresponds to the α particle energy of $2358(80)$ keV. These alpha events can be ascribed to the α decay of ^{180}W (expected energy of alphas is $2460(5)$ keV, isotopic abundance of ^{180}W is 0.12%) with derived half-life $T_{1/2} = (1.3^{+0.5}_{-0.6}) \times 10^{18}$ yr; this result is in agreement with previous determination. Finally, from the obtained results we have concluded that the re-crystallization does not improve the radiopurity level of the ZnWO_4 , while the creation of more radiopure ZnWO_4 crystals could be expected by applying vacuum distillation and filtering to obtain high purity zinc, and by zone melting for additional purification of the tungsten. Obviously all the more accurate techniques for the screening, purification and protection from environment of all the materials in every stage should be improved and applied to increase the sensitivities – we reached in previous measurements [56] – to various double β decay modes of Zn and W isotopes.

4.2 Development of enriched $^{106}\text{CdWO}_4$ crystal scintillator to search for 2β processes in ^{106}Cd .

The ^{106}Cd isotope is one of the best candidates for the $2\beta^+$ decay. An advantage of experiments using detectors containing cadmium is the higher detection efficiency of the ^{106}Cd

double β decay effects, especially in the case of the double electron capture. Therefore, the development of CdWO_4 crystal scintillators enriched in the ^{106}Cd is an important step to go towards the level of the theoretical predictions for the two neutrino mode of 2ϵ and $\epsilon\beta^+$ processes: $T_{1/2} \simeq 10^{21} - 10^{22}$ yr. Thus, a cadmium tungstate crystal scintillator (see Fig. 5) was produced from cadmium enriched in ^{106}Cd ($^{106}\text{CdWO}_4$) for an experiment to search for double beta processes in ^{106}Cd , as described in details in the 2010 publication list. Samples of cadmium with natural isotopic composition and enriched in ^{106}Cd were purified by vacuum distillation. Cadmium tungstate compounds were synthesized from solutions. The absolute isotopic composition of the enriched cadmium was accurately determined as 66.4% by thermal ionisation mass-spectrometry. A $^{106}\text{CdWO}_4$ crystal boule was grown by the low-thermal-gradient Czochralski technique. The total irrecoverable loss of the enriched cadmium in all the stages of the crystal scintillator production does not exceed 2.3%. The produced $^{106}\text{CdWO}_4$ crystal scintillator with mass of 216 g exhibits good optical and scintillation properties. All the main stages of the $^{106}\text{CdWO}_4$ crystal development and the detector performances have been discussed in details in the dedicated paper (see 2010 publication list). During 2010 data have been collected with



Figure 5: Boule of $^{106}\text{CdWO}_4$ single crystal grown by the low-thermal-gradient Czochralski process (left; the scale is in centimeters and inches). Scintillation element $^{106}\text{CdWO}_4$ with mass of 215.8 g produced from the boule (right; the scale is in centimeters). The side surface of the scintillation element was made diffuse with the help of fine-grain polishing paper to improve the uniformity of the scintillation light collection.

this enriched detector to search for 2β decay of ^{106}Cd in the DAMA/R&D set-up; a new detectors set-up is also in preparation for future improved measurements (see later).

4.3 Investigation of double beta decay processes in ^{106}Cd

As mentioned above the isotope ^{106}Cd is one of the most promising objects for $2\beta^+$ decay because of: 1) its natural isotopic abundance $\delta = (1.25 \pm 0.06)\%$ and of the possibility to achieve samples enriched up to 100% with the present technology; 2) its rather large $Q_{2\beta} = (2770 \pm 7)$ keV and of the possibility to study the various $2\beta^+$, $\epsilon\beta^+$ e 2ϵ decay modes; 3) the favorable theoretical estimates of the half-lives. The experiments up to now only give $T_{1/2}$ limits on 2β processes in ^{106}Cd on the level of $10^{18} - 10^{20}$ yr [57, 58, 59]. Taking into account theoretical calculations [60, 61], double beta decay of ^{106}Cd could be detected at the level of sensitivity of $10^{21} - 10^{22}$ yr. The CdWO_4 crystal scintillator enriched in ^{106}Cd at 66%, mentioned above, was developed to realize a high sensitivity experiment to search for 2β processes in ^{106}Cd (see in the 2010 publication list). The detector was

installed in the low-background DAMA/R&D set-up and took data there up to February 2011. Preliminary results with partial exposure have been presented at conference. In

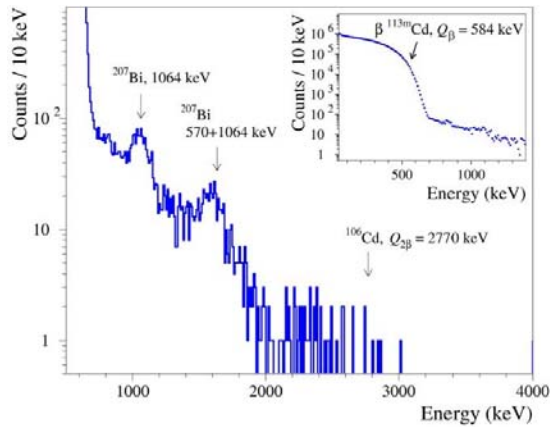


Figure 6: Preliminary energy spectrum of $\gamma(\beta)$ events measured with $^{106}\text{CdWO}_4$ scintillator over the first 1320 h in the low-background DAMA/R&D set-up. (Inset) β decay of ^{113m}Cd dominates at low energy (the data obtained over 268 h).

fact, the energy spectrum of the $\gamma(\beta)$ events accumulated with the $^{106}\text{CdWO}_4$ detector over the first 1320 h is presented in Fig. 6. The counting rate ~ 24 counts/s below the energy of ~ 0.6 MeV is mainly due to the β decay of ^{113m}Cd ($Q_\beta = 584$ keV, $T_{1/2} = 14.1$ yr [61]) with the activity (112 ± 5) Bq/kg. Contributions to the background above the energy 0.6 MeV were analyzed by the time-amplitude and the pulse-shape discrimination techniques, as well by fit of the energy spectrum by models of background simulated with the help of the EGS4 code. The details of the contributions to the background are reported in the dedicated paper in the 2010 publication list. Preliminarily only lower limits on the half-life of 2β processes in ^{106}Cd can be set on the basis of these initial 1320 h of running time; already with this preliminary statistics limits similar or higher than those previously available in literature have been set, while the limit for the channel resonant $0\nu 2K$ decay has been set for the first time (see for details in the 2010 publication list).

A sensitivity of the experiment to different 2β decay modes in ^{106}Cd after ~ 3 yr of measurements is expected to be on the level of $\sim 10^{21}$ yr. However, to allow the installation in DAMA/R&D of the ^{116}Cd detectors system, this first stage of data taking is concluded in February 2011. New data taking will start in near future when the $^{106}\text{CdWO}_4$ scintillator will be equipped with a light guide – which is already under construction – made of PbWO_4 from purified archaeological lead, and installed in a four HPGe detectors system working in coincidence. Such a set-up configuration will be effective to investigate 2ν mode of $\epsilon\beta^+$ and $2\beta^+$ decays, and also 2ϵ transitions of ^{106}Cd to excited states of ^{106}Pd , at the level of sensitivity of the theoretical predictions: $T_{1/2} \sim 10^{20} - 10^{22}$ yr. Moreover, the development of a $^{106}\text{CdWO}_4$ crystal scintillator depleted in $^{113}/^{113m}\text{Cd}$ isotopes is also foreseen.

4.4 Search for neutrinoless double β decay of ^{116}Cd

The ^{116}Cd isotope is one of the best candidates for the neutrinoless $2\beta^-$ decay because of: 1) its natural isotopic abundance is comparatively high (7.49%) and of the possibility to achieve samples enriched up to 100% with the present technology; 2) its rather large $Q_{\beta\beta}$ value (2805 keV); 3) the favorable theoretical estimates of the half-lives and nuclear matrix elements. To enhance the experimental sensitivity with respect to the previous

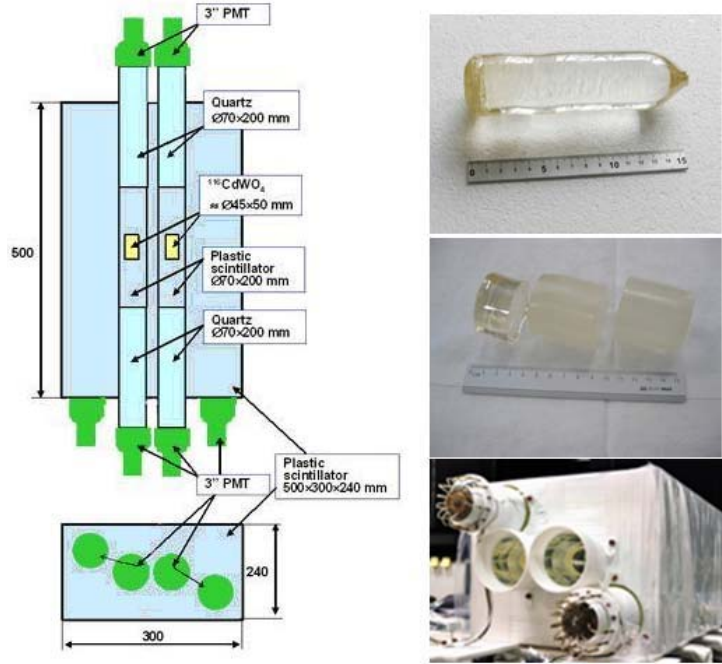


Figure 7: Left: The scheme of the detector system. Right top: Boule of enriched $^{116}\text{CdWO}_4$ crystal with 1868 g mass. The conic part of the boule (right) is the beginning of the crystal growth. Right middle: Crystal scintillators produced from the boule, the smaller crystal (whose surface has not been treated) at present will be used for some corollary investigations on the crystal properties and radiopurity by ultra-low background γ spectrometry at LNGS. Right bottom: The detectors system during assembling; the anti-coincidence is wrapped in Tetratec and equipped with its PMTs; the light guides having in the middle the $^{116}\text{CdWO}_4$ crystals are shown before mounting PMTs.

Soltvina experiment [62] one has to increase the measuring time and the mass of the enriched $^{116}\text{CdWO}_4$, to improve the energy resolution and to reduce the background of the detector. With this purpose several chemical methods have been adopted to built a cadmium tungstate crystal from the enriched ^{116}Cd by the low-thermal-gradient Czochralski technique in platinum crucible (a detailed technical paper is in preparation). A crystal boule of 1868 g (see Fig. 7-right top) has been grown from the 2139 g of the initial $^{116}\text{CdWO}_4$ charge; three near cylindrical shape crystal scintillators (see Fig. 7-right middle) have been cut from the crystal boule. The two main $^{116}\text{CdWO}_4$ are installed in the detectors system shown in Fig. 7-left and right bottom.

The isotopic composition of the sample of enriched $^{116}\text{CdWO}_4$ crystal was measured. The transmittance of the scintillation elements was also measured in the spectral range

330-700 nm using a PERKIN ELMER UV/VIS spectrometer Lambda 18. From the data we have derived the attenuation length of the material as 34 cm at the wavelength of the emission maximum 490 nm; at 400 nm the attenuation lengths of the samples are 6 cm. The scintillation properties of the crystals have been also tested; an energy resolution 11.1% and 10.1% (FWHM) was preliminarily obtained for the 662 keV line of ^{137}Cs with the two main detectors, respectively, by coupling them to Philips XP2412 Photomultipliers. We expect some improvement of the energy resolution in the running conditions thanks to the application of the high quantum efficiency green-enhanced PMTs. The detectors system is in installation in DAMA/R&D on February 2011 and will take data during 3 years to achieve the sensitivity of the project. The $^{116}\text{CdWO}_4$ crystal scintillator will also be used to investigate $2\nu 2\beta$ transitions of ^{116}Cd to the excited states of ^{116}Sn (the detection technique is the same described above the low-background HP Ge detectors facility with $^{106}\text{CdWO}_4$ crystal) at the level of sensitivity $T_{1/2} \approx 10^{22}$ yr of theoretical predictions. An annealing of the $^{116}\text{CdWO}_4$ detectors is foreseen in 2011 after a preliminary data taking to further improve their energy resolution.

5 Measurements with DAMA/Ge and LNGS Ge facility

Various R&D developments to improve low background set-ups and scintillators are carried out. Thus, measurements on samples are performed by means of the DAMA low background Ge detector, specially realized with a low Z window; it is operative deep underground in the low background facility of the LNGS. Some selected materials are in addition measured with high sensitivity ICP-MS and mass spectrometers.

In particular, the main data takings/results during year 2010 are summarized in the following.

- Some measurements on samples have been carried out.
- The analysis of the data collected with a $\simeq 1$ kg Molybdenum sample enriched in ^{100}Mo at 99.5% inside the 4π low-background HPGe detectors facility (measurements named ARMONIA) has been completed. A new observation of the $2\nu 2\beta$ decay of ^{100}Mo to the first excited 0_1^+ level of ^{100}Ru has been obtained; the scientific paper has been published. See later.
- The chemical/physical procedures to purify $\simeq 1$ kg of Ru in order to further investigate the 2β processes of ^{96}Ru and ^{104}Ru with higher sensitivity have been developed and tested. The purified $\simeq 1$ kg of Ru sample will be again at LNGS in spring 2011.
- The measurements with a preliminary 42.5 g of natural Pt have been completed; the analyses on rare processes in Pt isotopes have been completed. In particular, the α decay of ^{190}Pt to the first excited level ($E_{exc} = 137.2$ keV) of ^{186}Os has been observed for the first time. New limits on double beta decay of ^{190}Pt and ^{198}Pt have also been set. Two scientific papers have been in preparation during 2010 and completed in 2011 (see for details in the next LNGS report 2011). New measurements will be performed with a larger Pt sample in future.

- A first search for 2ϵ (including the resonant process) and $\epsilon\beta^+$ decay of ^{190}Pt by using $\simeq 0.1$ kg sample of platinum installed in an ultra-low background HP Ge γ spectrometer of the LNGS is in preparation.
- The measurements with about 200 g of Dy have been completed and analyses have been in progress in 2010. Investigations on future measurements with increased sensitivity are in progress.
- The feasibility investigations to test a previous report on observation of $2\nu 2\beta$ decay of ^{150}Nd to the first excited 0_1^+ level of ^{150}Sm by using neodymium sample of a few kg mass installed in an ultra-low background HP Ge γ spectrometers at LNGS have been progressed.
- A first search for 2ϵ (including the resonant process) and $\epsilon\beta^+$ decay of ^{184}Os by using $\simeq 0.1 - 0.3$ kg sample of ultra-pure osmium installed in an ultra-low background HPGe γ spectrometer at LNGS is in preparation.
- The future measurements on all other topics for incoming years are in preparation.

Subsequent improvements of all these measurements are foreseen depending on the achieved results.

In the following just the results of the ARMONIA measurements published in 2010 are summarized.

5.1 ARMONIA experiment

5.1.1 New observation of $2\beta 2\nu$ decay of ^{100}Mo to the 0_1^+ level of ^{100}Ru

The ^{100}Mo is one of the most interesting isotopes for $2\beta 0\nu$ searches among all the 35 naturally occurring $2\beta^-$ candidates due to: i) its rather high natural abundance: $\delta = 9.824(50)\%$; ii) the possibility to obtain isotopically enriched material using the comparatively inexpensive ultra-speed centrifuge technology; iii) the high energy release of $Q_{2\beta} = 3034.40(17)$ keV which defines a large phase space integral of the decay and, thus, a relatively high probability of 2β processes. Thus, the ^{100}Mo is one of the most investigated 2β isotopes. Its half life was measured in a geochemical experiment as $T_{1/2}^{geo} = (2.1 \pm 0.3) \times 10^{18}$ yr [63]; the allowed $2\beta 2\nu$ decay to the ground state of ^{100}Ru was observed in several direct experiments, with $T_{1/2}^{2\nu}$ values in the range of $(3.3 - 11.5) \times 10^{18}$ yr. The most accurate value comes from the recent experiment NEMO-3 with 7 kg of ^{100}Mo : $T_{1/2}^{2\nu} = (7.1 \pm 0.5) \times 10^{18}$ yr.

In addition to the transition to the ground state, the $2\beta 2\nu$ decay of ^{100}Mo was also registered for the transition to the first excited 0_1^+ level of ^{100}Ru . The half lives for $^{100}\text{Mo} \rightarrow ^{100}\text{Ru}(0_1^+)$ decay were measured in several experiments in the range: $(5.5 - 9.3) \times 10^{20}$ yr (recommended value is $5.9_{-0.6}^{+0.8} \times 10^{20}$ yr) [64]. However, these positive evidences were in contradiction with an earlier paper [65], where only the limit $T_{1/2} > 1.2 \times 10^{21}$ yr was obtained at 90% C.L.

The aim of the ARMONIA² measurements was a re-measurement of the $\simeq 1$ kg of Mo enriched in ^{100}Mo to 99.5%, used before in [65], with higher statistics and higher sensitivity than those reached there, in order to confirm the reported observations or to set an even more severe $T_{1/2}$ restriction. Preliminary results of the work were already reported at Conferences.

If the 0_1^+ excited level of ^{100}Ru with $E_{exc} = 1130.3$ keV is populated, two γ quanta with energies of 590.8 keV and 539.5 keV will be emitted in cascade in the following deexcitation process. To search for these γ quanta, we use the set-up with four low-background HP Ge detectors mounted in one cryostat with a well in the center at the LNGS low background Ge facility. The typical energy resolution (FWHM) of the detectors is 2.0 keV at the 1332 keV line of ^{60}Co .

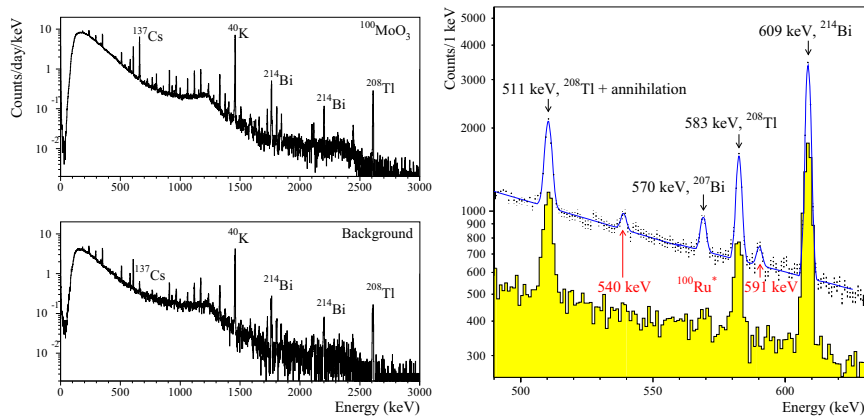


Figure 8: *Left* - The energy spectrum collected for 18120 h with the 1199 g $^{100}\text{MoO}_3$ sample (top) and the background spectrum collected for 7711 h (bottom). *Right* - Energy spectrum of the $^{100}\text{MoO}_3$ sample (points with error bars) in the 490 – 630 keV energy interval together with its fit (continuous curve). The background spectrum (normalized here to 18120 h) is also shown (filled histogram). Both peaks at 540 keV and 591 keV of the $2\beta 2\nu$ decay $^{100}\text{Mo} \rightarrow ^{100}\text{Ru}(0_1^+)$ are clearly visible in the $^{100}\text{MoO}_3$ spectrum.

At the first stage of the experiment, a sample of metallic ^{100}Mo powder with mass of 1009 g and 99.5% enrichment was measured. The data collected during 1927 h already gave indication on the observation of $^{100}\text{Mo} \rightarrow ^{100}\text{Ru}(0_1^+)$ decay, but the counting rate with the ^{100}Mo sample was near 3 times higher than the background rate of the set-up without the sample in the region of interest 500 – 600 keV; thus, a further purification of the sample from radioactive pollutions by U/Th chains, ^{40}K , ^{137}Cs has been performed. As a result we have obtained 1199 g of purified molybdenum oxide ($^{100}\text{MoO}_3$).

The obtained purified sample of $^{100}\text{MoO}_3$ was measured for 18120 h. For details see the dedicated paper in the 2010 publication list. Here we just show the 1-dimensional (1-d) spectrum (sum of all 4 HP Ge detectors) with the $^{100}\text{MoO}_3$ accumulated for 18120 h up to 3 MeV in Fig. 8-Left together with the background spectrum for comparison. The 1-dimensional energy spectra of the $^{100}\text{MoO}_3$ sample and of the background in the 490 – 630 keV energy interval are given in more detail in Fig. 8-Right. Both peaks at 540 keV and 591

²ARMONIA: meAsuReMent of twO NeutrIno 2β decAy of ^{100}Mo to the first excited 0_1^+ level of ^{100}Ru .

keV expected for $^{100}\text{Mo} \rightarrow ^{100}\text{Ru}(0_1^+) 2\beta 2\nu$ decay are observed in the experimental data collected with the $^{100}\text{MoO}_3$ sample; in the background spectrum these peaks are absent. The determined half-life of the process is: $T_{1/2} = 6.9_{-0.8}^{+1.0}(\text{stat.}) \pm 0.7(\text{syst.}) \times 10^{20}$ yr. An analysis of the background has been carried out as well.

Fixing the energy of one of the detectors to the expected energy of the γ quanta emitted in the $2\beta 2\nu$ decay of ^{100}Mo to $^{100}\text{Ru}(0_1^+)$ (540 or 591 keV; width of the window, ± 2 keV), we observe the coincidence peak at the corresponding supplemental energy (591 or 540 keV). Such coincidence spectra are shown in Fig. 9. The bottom part of the figure shows the background events, when the energy window is shifted to the neighboring value of (545 ± 2) keV. The derived half life is: $T_{1/2} = 6.8_{-1.8}^{+3.7}(\text{stat.}) \times 10^{20}$ yr for the $2\beta 2\nu$ decay of $^{100}\text{Mo} \rightarrow ^{100}\text{Ru}(0_1^+)$. This value is in agreement with the half life derived previously from the 1-dimensional spectrum, although it has a much larger statistical uncertainty because of the low statistics (only 8 events).

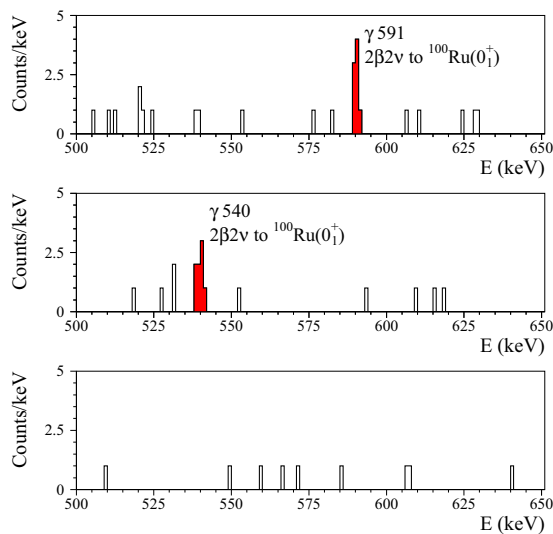


Figure 9: The coincidence energy spectra accumulated during 17807 h with the $^{100}\text{MoO}_3$ sample in the 4 HP Ge set-up, when the energy of one detector is fixed at the value expected for the $^{100}\text{Mo} \rightarrow ^{100}\text{Ru}(0_1^+) 2\beta 2\nu$ decay: (540 ± 2) keV (top) and (591 ± 2) keV (middle). The bottom figure gives the background obtained by shifting the energy of one detector to (545 ± 2) keV.

In conclusion the present observation does not confirm the negative result of Ref. [65] where a limit of $T_{1/2} > 1.2 \times 10^{21}$ yr (90% C.L.) was set by using the same but unpurified sample of ^{100}Mo , and the measured half life value: $6.9_{-1.1}^{+1.2} \times 10^{20}$ yr is in agreement both with other experimental results [64] and with the recent theoretical calculations [66].

5.1.2 Limit on charge non-conserving β decay of ^{100}Mo

The measurements have also given the possibility to set, for the first time, a limit on the charge non-conserving (CNC) β decay of ^{100}Mo . The search for this hypothetical process was firstly proposed in [67] in order to test the law of conservation of the electric charge. It was supposed that, if the weak interactions contain a small CNC admixture, the nuclear

transformation $(A, Z) \rightarrow (A, Z + 1)$ sometimes could be not accompanied by the emission of an electron, but – instead of the emission of an e^- – some massless particle would be emitted (e.g. a ν_e or a γ quantum): $(A, Z) \rightarrow (A, Z + 1) + (\nu_e \text{ or } \gamma) + \bar{\nu}_e$. In this case the energy available in the (A, Z) decay would be increased by 511 keV, that are normally spent for the electron rest mass. This would allow some transitions to the ground or to the excited states of the daughter $(A, Z + 1)$ nucleus which are energetically forbidden for the normal charge conserving (CC) β decay. To-date the CNC β decays were searched for with few nuclides: ^{71}Ga , ^{73}Ge , ^{87}Rb , ^{113}Cd , ^{115}In , ^{136}Xe , and ^{139}La . The effect was not observed, and only lower limits on corresponding life times τ_{CNC} were set in the range of $10^{18} - 10^{26}$ yr.

In case of ^{100}Mo , the additional 511 keV in the CNC β decay allow the population of the ground state (1^+) of ^{100}Tc . The excited states of ^{100}Tc with energies up to $E_{exc} = 343$ keV could also be populated, however these CNC transitions would be suppressed by the higher changes in spin between the parent and the daughter states and by the lower Q_β values; anyway, after the deexcitation processes, the ^{100}Tc in the ground state will be formed. It is unstable with a quite short half life of $T_{1/2} = 15.46$ s. In its β^- decay, the excited levels of ^{100}Ru with $E_{exc} = 539.5$ keV and 1130.3 keV are populated with probabilities of 0.75% and 5.36%, respectively; this leads to subsequent emission of the same γ quanta of 539.5 keV and 590.8 keV as in 2β decay $^{100}\text{Mo} \rightarrow ^{100}\text{Ru}(0_1^+)$. In fact, in an experimental configuration like the used one, where only energies of γ quanta are measured with HP Ge detectors, it is impossible to distinguish the CNC β decay of ^{100}Mo from the 2β process $^{100}\text{Mo} \rightarrow ^{100}\text{Ru}(0_1^+)$. This concerns also almost all previous experiments; the only exception is the NEMO-3 measurement, in which tracks of both electrons from 2β decay were also registered in addition to the γ quanta.

We consider the γ quanta of 539.5 keV and of 590.8 keV, observed in the present experiment, as a result of the 2β decay of the $^{100}\text{Mo} \rightarrow ^{100}\text{Ru}(0_1^+)$ instead of ascribing them to exotic CNC β decay of ^{100}Mo , and we use the number of events in the corresponding peaks in the 1-dimensional spectrum just to set a limit on the life time of the CNC process, obtaining (see in the 2010 publication list for the details): $\tau_{CNC} > 5.1 \times 10^{19}$ yr for the 539.5 keV peak and $\tau_{CNC} > 4.5 \times 10^{19}$ yr for the 590.8 keV peak. We accept the more conservative value as the final result. This value is comparatively low, however it is determined for the first time for ^{100}Mo .

From the obtained τ_{CNC} limit we can derive constraints on the CNC admixture in the weak interactions deriving the value of the ϵ_ν^2 parameter, which is in the present case: $\epsilon_\nu^2 < 2.9 \times 10^{-21}$. This derived ϵ_ν^2 is lower than the most restrictive value reached with ^{71}Ga [68]; nevertheless, comparing with other values, one can see that it is better than the limits obtained with ^{87}Rb , ^{113}Cd , ^{73}Ge , ^{115}In , ^{136}Xe and ^{139}La in the recent experiments. It should also be noted that the ϵ_ν^2 parameter is related only to emission of neutrino; at the same time the obtained τ_{CNC} limit has more general implication being valid also for emission of any massless particle (γ , ν , Majoron, axion, etc.) or for non-emission of any particle at all.

6 Conclusions

In conclusion, the main activities during year 2010 can be summarized as in the following:

I. The DAMA/LIBRA results of other two annual cycles (exposure: $0.34 \text{ ton} \times \text{yr}$) have been published in 2010. The cumulative exposure with those previously released by the former DAMA/NaI and by DAMA/LIBRA is now $1.17 \text{ ton} \times \text{yr}$, corresponding to 13 annual cycles. The data further confirm the previous positive results obtained investigating the presence of Dark Matter (DM) particles in the galactic halo by means of the model independent Dark Matter annual modulation signature; the confidence level is now 8.9σ for the cumulative exposure. The modulation amplitude of the *single-hit* events in the $(2 - 6) \text{ keV}$ (electron equivalent) energy interval measured in NaI(Tl) target is $(0.0116 \pm 0.0013) \text{ cpd/kg/keV}$; the measured phase is $(146 \pm 7) \text{ days}$ and the measured period is $(0.999 \pm 0.002) \text{ yr}$, values well in agreement with those expected for the DM particles. The DAMA/LIBRA set-up has regularly taken data up to November 2010 when the upgrade to substitute all the PMTs with new ones having higher quantum efficiency has been realized. Various kinds of analyses are in progress.

II. The RD-III towards the possible DAMA/1ton has been carried out on various aspects.

III. The DAMA/LXe set-up has been in data taking with Kr-free Xenon enriched in ^{136}Xe .

IV. The DAMA/R&D set-up has been used to perform various kinds of measurements; several data analyses have been completed and other ones are in progress. In particular: i) the investigation on the radiopurity of the ZnWO_4 crystal scintillators has been published; ii) the technical paper on the creation of the CdWO_4 detector with Cd enriched in ^{106}Cd has been completed; iii) the data taking with the $^{106}\text{CdWO}_4$ detector in DAMA/R&D has been carried out; iv) a CdWO_4 detector with Cd enriched in ^{116}Cd has been built and a related technical paper is in preparation; v) the new detectors system to investigate 2β decay in ^{116}Cd has been realized and tested. vi) various other relatively small scale experiments are in preparation.

V. The DAMA/Ge has been regularly in operation and various small scale experiments have been performed, are in progress and in preparation as listed above. Several competing results have been achieved with various isotopes in the search of rare processes.

7 List of Publications during 2010

1. R. Bernabei, P.Belli, F.Cappella, R.Cerulli, C.J.Dai, A. d'Angelo, H.L.He, A. Incicchitti, H.H.Kuang, X.H.Ma, F.Montecchia, F.Nozzoli, D.Prosperti, X.D. Sheng, R.G.Wang, Z.P.Ye, DAMA/LIBRA results, in the volume "Particle Physics in the Year of Astronomy", ed. by A.Studenikin (14th Lomonosov Conf. Moscow, August 2009), World Scientific pub. (2010) 207.
2. R. Bernabei, P. Belli, F. Cappella, R. Cerulli, F.A. Danevich, B.V. Grinyov, A. Incicchitti, V.V. Kobychhev, V.M. Mokina, S.S. Nagorny, L.L. Nagornaya, S. Nisi, F.

- Nozzoli, D.V. Poda, D. Prosperi, V.I. Tretyak, S.S. Yurchenko, Search for 2β decay of zinc and tungsten with low background ZnWO_4 crystal scintillators, *J. Phys.: Conf. Ser.* 202 (2010), 012038.
3. R. Bernabei, P. Belli, F. Cappella, R. Cerulli, C.J. Dai, A. d'Angelo, H.L. He, A. Incicchitti, H.H. Kuang, J.M. Ma, F. Montecchia, F. Nozzoli, D. Prosperi, X.D. Sheng, Z.P. Ye, Particle Dark Matter in the galactic halo: results from DAMA/LIBRA", *AIP Conf. Proc.* 1200 (2010), 993.
 4. R. Bernabei, P. Belli, F. Cappella, R. Cerulli, C. J. Dai, A. d'Angelo, H. L. He, A. Incicchitti, H.H. Kuang, X. H. Ma, F. Montecchia, F. Nozzoli, D. Prosperi, X. D. Sheng, R. G. Wang, Z.P. Ye, Results from the DAMA/LIBRA experiment, *J. Phys.: Conf. Ser.* 203 (2010), 012003.
 5. R. Bernabei, P. Belli, F. Cappella, R. Cerulli, C. J. Dai, A. d'Angelo, H. L. He, A. Incicchitti, X.H. Ma, F. Montecchia, F. Nozzoli, D. Prosperi, X. D. Sheng, R. G. Wang, Z. P. Ye, Technical aspects and dark matter searches, *J. Phys.: Conf. Ser.* 203 (2010) 012040.
 6. R. Bernabei, P. Belli, F. Cappella, R. Cerulli, C. J. Dai, A. d'Angelo, H. L. He, A. Incicchitti, H. H. Kuang, X. M. Ma, F. Montecchia, F. Nozzoli, D. Prosperi, X. D. Sheng, Z. P. Ye, Non-paulian nuclear processes in highly radiopure NaI(Tl): status and perspectives, *Found. Phys.* 40 (2010) 807.
 7. R. Bernabei, P. Belli, F. Cappella, R. Cerulli, C.J. Dai, A. d'Angelo, H.L. He, A. Incicchitti, H.H. Kuang, X.M. Ma, F. Montecchia, F. Nozzoli, D. Prosperi, X.D. Sheng, Z.P. Ye, Results from DAMA/LIBRA at Gran Sasso, *Found. Phys.* 40 (2010) 900.
 8. P. Belli, R. Bernabei, F. Cappella, R. Cerulli, F.A. Danevich, A.M. Dubovik, S. d'Angelo, E.N. Galashov, B.V. Grinyov, A. Incicchitti, V.V. Kobychyev, L.L. Nagornaya, S. Nisi, F. Nozzoli, D.V. Poda, R.B. Podviyanyuk, D. Prosperi, V.N. Shlegel, V.I. Tretyak, Ya.V. Vasiliev, Yu.Ya. Vostretsov, Radiopurity of ZnWO_4 crystal scintillators, *Acta Physica Polonica* 117 (2010) 139.
 9. R. Bernabei, P. Belli, F. Cappella, R. Cerulli, C.J. Dai, A. d'Angelo, H.L. He, A. Incicchitti, H.H. Kuang, X.H. Ma, F. Montecchia, F. Nozzoli, D. Prosperi, X.D. Sheng, R.G. Wang, Z.P. Ye, Signals from the dark Universe: new results from DAMA/LIBRA, to appear in the *Proceed. of the Int. Conf. Beyond 2010*, Cape Town, South Africa (2010)
 10. R. Bernabei, P. Belli, F. Montecchia, F. Nozzoli, F. Cappella, A. d'Angelo, A. Incicchitti, D. Prosperi, R. Cerulli, C. J. Dai, H. L. He, X. H. Ma, X. D. Sheng, R.G. Wang, Z. P. Ye, Signals from Dark Universe: DAMA/LIBRA at LNGS, *PRAMANA-Journal of Physics* 72 (2010) 293.
 11. P. Belli, R. Bernabei, R.S. Boiko, V.B. Brudanin, N. Bukilic, R. Cerulli, D.M. Chernyak, F.A. Danevich, S. d'Angelo, V.Ya. Degoda, A.E. Dossovitskiy, E.N.

- Galashov, Yu.A.Hyzhnyi, S.V. Ildyakov, A. Incicchitti, V.V. Kobychhev, O.S. Kolesnyk, G.P. Kovtun, V.M. Kudovbenko, J.R. de Laeter, A.L. Mikhlin, S.S. Nagorny, S.G. Nedilko, A.S. Nikolaiko, S. Nisi, D.V. Poda, R.B. Podviyanyuk, O.G. Polischuk, D. Prospero, A.P. Shcherban, V.P. Shcherbatskyi, V.N. Shlegel, D.A. Solopikhin, Yu.G. Stenin, V.I. Tretyak, Ya.V. Vasiliev, V.D. Virich, Development of enriched $^{106}\text{CdWO}_4$ crystal scintillators to search for double beta decay processes in ^{106}Cd , Nucl. Instr. & Meth. A 615 (2010) 301.
12. R. Bernabei, P.Belli, F.Cappella, R.Cerulli, C.J.Dai, A. d'Angelo, H.L.He, A. Incicchitti, H.H.Kuang, X.H.Ma, F.Montecchia, F.Nozzoli, D.Prosperi, X.D. Sheng, R.G.Wang, Z.P.Ye, New results from DAMA/LIBRA, (arXiv:1002.1028) Eur. Phys. J. C 67 (2010) 39.
 13. P. Belli, R. Bernabei, R.S. Boiko, F. Cappella, R. Cerulli, F.A. Danevich, S. d'Angelo, A. Incicchitti, V.V. Kobychhev, B.N. Kropivnyansky, M. Laubenstein, P.G. Nagorny, S.S. Nagorny, S. Nisi, F. Nozzoli, D.V. Poda, D. Prospero, O.G. Polischuk, V.I. Tretyak, I.M. Vyshnevskyi, S.S. Yurchenko, New observation of $2\beta 2\nu$ decay of ^{100}Mo to the 0_1^+ level of ^{100}Ru in the ARMONIA experiment, Nucl. Phys. A 846 (2010) 143.
 14. P. Belli, R. Bernabei, F. Cappella, R. Cerulli, F.A. Danevich, S. d'Angelo, A. Incicchitti, M. Laubenstein, O.G. Polischuk, D. Prospero and V.I. Tretyak, Search for double beta decays of ^{96}Ru and ^{104}Ru by ultra-low background gamma spectrometry, Nucl. Phys. and Atomic Energy 11 (2010) 362
 15. P. Belli, R. Bernabei, R. Cerulli, F.A. Danevich, S. d'Angelo, A. Incicchitti, V.V. Kobychhev, M. Laubenstein, S. Nisi, O.G. Polischuk, D. Prospero and V.I. Tretyak, Search for ^7Li solar axions, to appear in the Proceed. of the 3rd Int. Conf. on Current Problems in Nuclear Physics and Atomic Energy June 2010, Kyiv (UKRAINE)
 16. P. Belli, R. Bernabei, R.S. Boiko, V.B. Brudanin, N. Bukilic, R. Cerulli, D.M. Chernyak, F.A. Danevich, S. d'Angelo, V.Ya. Degoda, A.E. Dossovitskiy, E.N. Galashov, Yu.A. Hyzhnyi, S.V. Ildyakov, A. Incicchitti, V.V. Kobychhev, O.S. Kolesnyk, G.P. Kovtun, V.M. Kudovbenko, J.R. de Laeter, A.L. Mikhlin, S.S. Nagorny, S.G. Nedilko, A.S. Nikolaiko, S. Nisi, D.V. Poda, R.B. Podviyanuk, O.G. Polischuk, D. Prospero, A.P. Shcherban, V.P. Shcherbatskyi, V.N. Shlegel, D.A. Solopikhin, Yu.G. Stenin, V.I. Tretyak, Ya.V. Vasiliev, V.D. Virich, Development of enriched $^{106}\text{CdWO}_4$ crystal scintillators to search for double beta decay processes in ^{106}Cd , to appear in the Proceed. of the 3rd Int. Conf. on Current Problems in Nuclear Physics and Atomic Energy, June 2010, Kyiv (UKRAINE)
 17. R. Bernabei, P.Belli, F.Cappella, R.Cerulli, C.J.Dai, A. d'Angelo, H.L.He, A. Incicchitti, H.H.Kuang, X.H.Ma, F.Montecchia, F.Nozzoli, D.Prosperi, X.D. Sheng, R.G.Wang, Z.P.Ye, Results on Dark Matter by DAMA/LIBRA at Gran Sasso, in the Proceed. of the 3rd Int. Conf. on Current Problems in Nuclear Physics and Atomic Energy, Kyiv (2010) 85.

18. R. Bernabei, P. Belli, F. Montecchia, F. Nozzoli, F. Cappella, A. Incicchitti, D. Prosperi, R. Cerulli, C.J. Dai, V.I. Tretyak, The DAMA/LXe experiment at Gran Sasso: recent performances and results, in the Proceed. of the 3rd Int. Conf. on Current Problems in Nuclear Physics and Atomic Energy, Kyiv (2010) 409.
19. R. Bernabei, P. Belli, F. Cappella, R. Cerulli, C.J. Dai, A. d'Angelo, H.L. He, A. Incicchitti, X.H. Ma, F. Montecchia, F. Nozzoli, D. Prosperi, X.D. Sheng, R.G. Wang, Z.P. Ye, Particle Dark Matter in DAMA/LIBRA, arXiv:1007.0595, and to appear in the Proceed. of the Int. Conf. Frontier Objects in Astrophysics and Particle Physics (Vulcano 2010), May 2010, Vulcano (Italy)
20. P. Belli, R. Bernabei, R. S. Boiko, V. B. Brudanin, F. Cappella, V. Caracciolo, R. Cerulli, D. M. Chernyak, F. A. Danevich, S. d'Angelo, A. E. Dossovitskiy, E. N. Galashov, A. Incicchitti, V. V. Kobychyev, S. S. Nagorny, F. Nozzoli, B. N. Kropivnyansky, V. M. Kudovbenko, A. L. Mikhlin, A. S. Nikolaiko, D. V. Poda, R. B. Podviyanuk, O. G. Polischuk, D. Prosperi, V. N. Shlegel, Yu. G. Stenin, J. Suhonen, V. I. Tretyak, Ya. V. Vasiliev, First results of the experiment to search for 2β decay of ^{106}Cd with the help of $^{106}\text{CdWO}_4$ crystal scintillators, AIP Conf. Proc. 1304 (2010) 354.
21. R. Bernabei, P. Belli, F. Cappella, R. Cerulli, C.J. Dai, A. d'Angelo, H.L. He, A. Incicchitti, X.H. Ma, F. Montecchia, F. Nozzoli, D. Prosperi, X.D. Sheng, R.G. Wang, Z.P. Ye Particle Dark Matter in the galactic halo, to appear in Progress in Particle and Nuclear Physics (2011), DOI: 10.1016/j.pnpnp.2011.01.002

References

- [1] R. Bernabei et al., Nucl. Instr. & Meth. A 592 (2008) 297.
- [2] R. Bernabei et al., Eur. Phys. J. C 56 (2008) 333.
- [3] R. Bernabei et al., Eur. Phys. J. C 62 (2009) 327.
- [4] P. Belli, R. Bernabei, C. Bacci, A. Incicchitti, R. Marcovaldi, D. Prosperi, DAMA proposal to INFN Scientific Committee II, April 24th 1990.
- [5] R. Bernabei et al., Phys. Lett. B 389 (1996) 757; R. Bernabei et al., Phys. Lett. B 424 (1998) 195; R. Bernabei et al., Phys. Lett. B 450 (1999) 448; P. Belli et al., Phys. Rev. D 61 (2000) 023512; R. Bernabei et al., Phys. Lett. B 480 (2000) 23; R. Bernabei et al., Phys. Lett. B 509 (2001) 197; R. Bernabei et al., Eur. Phys. J. C 23 (2002) 61; P. Belli et al., Phys. Rev. D 66 (2002) 043503.
- [6] R. Bernabei et al., Il Nuovo Cim. A 112 (1999) 545.
- [7] R. Bernabei et al., Eur. Phys. J. C18 (2000) 283.
- [8] R. Bernabei et al., La Rivista del Nuovo Cimento 26 n.1 (2003) 1-73.
- [9] R. Bernabei et al., Int. J. Mod. Phys. D 13 (2004) 2127.
- [10] R. Bernabei et al., Int. J. Mod. Phys. A 21 (2006) 1445.
- [11] R. Bernabei et al., Eur. Phys. J. C. 47 (2006) 263.

- [12] R. Bernabei et al., *Int. J. Mod. Phys. A* 22 (2007) 3155.
- [13] R. Bernabei et al., *Eur. Phys. J. C* 53 (2008) 205.
- [14] R. Bernabei et al., *Phys. Rev. D* 77 (2008) 023506.
- [15] R. Bernabei et al., *Mod. Phys. Lett. A* 23 (2008) 2125.
- [16] R. Bernabei et al., *Phys. Lett. B* 408 (1997) 439; P. Belli et al., *Phys. Lett. B* 460 (1999) 236; R. Bernabei et al., *Phys. Rev. Lett.* 83 (1999) 4918; P. Belli et al., *Phys. Rev. C* 60 (1999) 065501; R. Bernabei et al., *Il Nuovo Cimento A* 112 (1999) 1541; R. Bernabei et al., *Phys. Lett. B* 515 (2001) 6; F. Cappella et al., *Eur. Phys. J.-direct C* 14 (2002) 1; R. Bernabei et al., *Eur. Phys. J. A* 23 (2005) 7; R. Bernabei et al., *Eur. Phys. J. A* 24 (2005) 51; R. Bernabei et al., *Astrop. Phys.* 4 (1995) 45;
- [17] R. Bernabei, in the volume *The identification of Dark Matter*, World Sc. Pub. (1997) 574.
- [18] R. Bernabei et al., *Phys. Lett. B* 424 (1998) 195.
- [19] R. Bernabei et al., *Phys. Lett. B* 450 (1999) 448.
- [20] P. Belli et al., *Phys. Rev. D* 61 (2000) 023512.
- [21] R. Bernabei et al., *Eur. Phys. J. C* 18 (2000) 283.
- [22] R. Bernabei et al., *Phys. Lett. B* 509 (2001) 197.
- [23] R. Bernabei et al., *Eur. Phys. J. C* 23 (2002) 61.
- [24] P. Belli et al., *Phys. Rev. D* 66 (2002) 043503.
- [25] R. Bernabei et al., *Int. J. Mod. Phys. A* 22 (2007) 3155-3168.
- [26] K.A. Drukier et al., *Phys. Rev. D* 33 (1986) 3495.
- [27] K. Freese et al., *Phys. Rev. D* 37 (1988) 3388.
- [28] D. Smith and N. Weiner, *Phys. Rev. D* 64 (2001) 043502.
- [29] K. Freese et al., *Phys. Rev. D* 71 (2005) 043516–15; *Phys. Rev. Lett.* 92 (2004) 111301–4.
- [30] Y. Bai and P.J. Fox, arXiv:0909.2900
- [31] R. Bernabei et al., *AIP Conf. Proceed.* 1223 (2010) 50 (arXiv:0912.0660); arXiv:1007.0595 to appear on *Proceed. of the Int. Conf. Frontier Objects in Astrophysics and Particle Physics*, May 2010, Vulcano, Italy.
- [32] A. Bottino, N. Fornengo, and S. Scopel, *Phys. Rev. D* 67 (2003) 063519; A. Bottino, F. Donato, N. Fornengo, and S. Scopel, *Phys. Rev. D* 69 (2003) 037302; *Phys. Rev. D* 78 (2008) 083520; A. Bottino, F. Donato, N. Fornengo, S. Scopel, arXiv:0912.4025.
- [33] R. Foot, *Phys. Rev. D* 78 (2008) 043529.
- [34] K. Belotsky, D. Fargion, M. Khlopov and R.V. Konoplich, *Phys. Atom. Nucl.* 71 (2008) 147.
- [35] E.M. Drobyshevski et al., *Astrophys. & Astronom. Trans.* 26:4 (2007) 289; *Mod. Phys. Lett. A* 23 (2008) 3077.
- [36] Nima Arkani-Hamed et al., *Phys. Rev. D* 79 (2009) 015014.
- [37] Daniele S.M. Alves et al., arXiv:0903.3945.
- [38] D. Hooper, L. Goodenough, arXiv:1010.2752; D. Hooper et al., arXiv:1007.1005.

- [39] S. Chang, R. F. Lang, N. Weiner, [arXiv:1007.2688](#).
- [40] S. Chang, N. Weiner, I. Yavin, [arXiv:1007.4200](#).
- [41] S. Andreas, A. Ringwald, [arXiv:1008.4519](#).
- [42] A. Benoit et al., *Phys. Lett. B* 637 (2006) 156.
- [43] R. Bernabei et al., in the volume “Cosmology and particle Physics”, AIP ed. (2001) 189; *J. Phys.: Conf. Ser.* 203 (2010) 012040 ([arXiv:0912.4200](#)); <http://taup2009.lngs.infn.it/slides/jul3/nozzoli.pdf>, talk given by F. Nozzoli; ISBN 978-88-95688-12-1, pages 1-53 (2009) Exorma Ed. ([arXiv:0806.0011v2](#)).
- [44] J.I. Collar and D.N. McKinsey, [arXiv:1005.0838](#); [arXiv:1005.3723](#); J.I. Collar, [arXiv:1006.2031](#); [arXiv:1010.5187](#).
- [45] R. Hudson, *Found. Phys.* 39 (2009) 174-193.
- [46] C.E. Aalseth et al., [arXiv:1002.4703](#).
- [47] W. Seidel (CRESST collaboration), presented at the 8th Intl. Workshop on Identification of Dark Matter, Montpellier, July 2010, available from <http://indico.in2p3.fr/conferenceDisplay.py?confId=156>
- [48] P. Belli et al., *Il Nuovo Cim.* 103A (1990) 767.
- [49] P. Belli et al., *Il Nuovo Cim.* C 19 (1996) 537; *Astrop. Phys.* 5 (1996) 217.
- [50] P. Belli et al., *Phys. Lett. B* 387 (1996) 222 and *Phys. Lett. B* 389 (1996) 783 (erratum); R. Bernabei et al., *New J. Phys.* 2 (2000) 15.1; *Eur. Phys. J.-direct C11* (2001) 1. *Phys. Lett. B* 436 (1998) 379. R. Bernabei et al., in the volume “Beyond the Desert 2003”, Springer (2003) 365.
- [51] R. Bernabei et al., *Nucl. Instr. & Meth.* A482 (2002) 728.
- [52] R. Bernabei et al., *Phys. Lett. B* 546 (2002) 23; F. Cappella, PhD Thesis, Università di Roma “Tor Vergata”, 2005.
- [53] R. Bernabei et al., *Phys. Lett. B* 527 (2002) 182.
- [54] P. Belli et al., *Phys. Rev. D* 61 (2000) 117301; *Phys. Lett. B* 465 (1999) 315; R. Bernabei et al., *Phys. Lett. B* 493 (2000) 12; *Eur. Phys. J. A* 27 s01 (2006) 35;
- [55] R. Bernabei et al., *Astropart. Phys.* 7 (1997) 73; R. Bernabei et al., *Il Nuovo Cim.* A 110 (1997) 189; P. Belli et al., *Nucl. Phys. B* 563 (1999) 97; R. Bernabei et al., *Nucl. Phys. A* 705 (2002) 29; P. Belli et al., *Nucl. Instr. Meth. A* 498 (2003) 352; R. Cerulli et al., *Nucl. Instr. Meth. A* 525 (2004) 535; R. Bernabei et al., *Nucl. Instr. Meth. A* 555 (2005) 270; R. Bernabei et al., *Ukr. J. Phys.* 51 (2006) 1037; P. Belli et al., *Nucl. Phys. A* 789 (2007) 15; P. Belli et al., *Phys. Rev. C* 76 (2007) 064603; P. Belli et al., *Eur. Phys. J. A* 36 (2008) 167; P. Belli et al., *J. Phys. G* 38 (2011) 015103; P. Belli et al., *Nucl. Instr. Meth. A* 626 (2011) 31.
- [56] P. Belli et al., *Nucl. Phys. A* 826 (2009) 256; P. Belli et al., *Phys. Lett. B* 658 (2008) 193.
- [57] P. Belli et al., *Astropart. Phys.* 10 (1999) 115.
- [58] F.A. Danevich et al., *Phys. Rev.* C68 (2003) 035501.
- [59] F.A. Danevich et al., *Z. Phys. A* 355 (1996) 433; A.S. Barabash et al., *Nucl. Phys. A* 604 (1996) 115; J. Suhonen and O. Civitarese, *Phys. Lett. B* 497 (2001) 221; N.I. Rukhadze et al., *J. Phys. Conf. Ser.* 203 (2010) 012072.

- [60] M. Hirsch et al., *Z. Phys. A* 347 (1994) 151; A. Staudt, K. Muto, H.V. Klapdor-Kleingrothaus, *Phys. Lett. B* 268 (1991) 312; J. Toivanen and J. Suhonen, *Phys. Rev. C* 55 (1997) 2314; S. Stoica, H.V. Klapdor-Kleingrothaus, *Eur. Phys. J. A* 17 (2003) 529; A. Shukla et al., *Eur. Phys. J. A* 23 (2005) 235.
- [61] P. Domin, S. Kovalenko, F. Simkovic, S.V. Semenov, *Nucl. Phys. A* 753 (2005) 337.
- [62] M. Hirsch et al., *Z. Phys. A* 347 (1994) 151.
- [63] H. Hidaka, C.V. Ly, K. Suzuki, *Phys. Rev. C* 70 (2004) 025501.
- [64] A.S. Barabash et al., *Phys. Lett. B* 345 (1995) 408; A.S. Barabash et al., *Phys. At. Nucl.* 62 (1999) 2039; R. Arnold et al., *Nucl. Phys. A* 781 (2007) 209; M.F. Kidd et al., *Nucl. Phys. A* 821 (2009) 251.
- [65] D. Blum et al., *Phys. Lett. B* 275 (1992) 506.
- [66] J. Kotila, J. Suhonen, D.S. Delion, *J. Phys. G* 37 (2010) 015101; S.K.L. Sjue et al., *Phys. Rev. C* 78 (2008) 064317; P. Domin et al., *Nucl. Phys. A* 753 (2005) 337; J. Suhonen, *Nucl. Phys. A* 700 (2002) 649; F. Simkovic, P. Domin, S.V. Semenov, *J. Phys. G* 27 (2001) 2233.
- [67] G. Feinberg, M. Goldhaber, *Proc. Nat. Ac. Sci.* 45 (1959) 1301.
- [68] E.B. Norman, J.N. Bahcall, M. Goldhaber, *Phys. Rev. D* 53 (1996) 4086.

The GERDA experiment

M. Agostiniⁿ, M. Allardt^c, E. Andreotti^e, A.M. Bakalyarov^l, M. Balata^a,
I. Barabanov^j, M. Barnabe-Heider^f, L. Baudis^s, C. Bauer^f, N. Becerici-Schmid^m,
E. Bellotti^{g,h}, S. Belogurov^{k,j}, S.T. Belyaev^l, A. Bettini^{o,p}, L. Bezrukov^j,
T. Bruch^s, V. Brudanin^d, R. Brugnera^{o,p}, D. Budjas^f, A. Caldwell^m,
C. Cattadori^{g,h}, F. Cossavella^m, E.V. Demidova^k, A. Denisov^j, S. Dinter^m,
A. Domula^c, V. Egorov^d, F. Faulstich^m, A. Ferella^s, K. Freund^r, F. Froberg^s,
N. Frodyma^b, A. Gangapshev^j, A. Garfagnini^{o,p}, S. Gazzana^{f,a}, P. Grabmayr^r,
V. Gurentsov^j, K.N. Gusev^{l,d}, W. Hampel^f, A. Hegai^r, M. Heisel^f, S. Hemmer^{o,p},
G. Heusser^f, W. Hofmann^f, M. Hult^e, L. Ioannucci^a, L.V. Inzhechik^j, J. Janicskoⁿ,
J. Jochum^r, M. Junker^a, S. Kianovsky^j, I.V. Kirpichnikov^k, A. Kirsch^f,
A. Klimenko^{d,j}, K.T. Knöpfle^f, O. Kochetov^d, V.N. Kornoukhov^{k,j}, V. Kusminov^j,
M. Laubenstein^a, V.I. Lebedev^l, B. Lehnert^c, S. Lindemann^f, M. Lindner^f,
X. Liu^q, A. Lubashevskiy^f, B. Lubsandorzhev^j, A.A. Machado^f, B. Majorovits^m,
G. Marissens^e, G. Meierhofer^r, I. Nemchenok^d, S. Nisi^a, C. O'Shaughnessy^m,
L. Pandola^a, K. Pelczar^b, F. Potenza^a, A. Pulliaⁱ, M. Reissfelder^f, S. Riboldiⁱ,
F. Ritter^r, C. Sada^{o,p}, J. Schreiner^f, U. Schwan^f, B. Schwingenheuer^f,
S. Schönertⁿ, H. Seitz^m, M. Shirchenko^{l,d}, H. Simgen^f, A. Smolnikov^f, L. Stanco^p,
F. Stelzer^m, H. Strecker^f, M. Tarka^s, A.V. Tikhomirov^l, C.A. Ur^p, A.A. Vasenko^k,
O. Volynets^m, M. Wojcik^b, E. Yanovich^j, P. Zavarise^a, S.V. Zhukov^l,
D. Zinatulina^d, F. Zoccaⁱ, K. Zuber^c, and G. Zuzel^b.

^a) INFN Laboratori Nazionali del Gran Sasso, LNGS, Assergi, Italy

^b) Institute of Physics, Jagellonian University, Cracow, Poland

^c) Institut für Kern- und Teilchenphysik, Technische Universität Dresden, Dresden, Germany

^d) Joint Institute for Nuclear Research, Dubna, Russia

^e) Institute for Reference Materials and Measurements, Geel, Belgium

^f) Max Planck Institut für Kernphysik, Heidelberg, Germany

^g) Dipartimento di Fisica, Università Milano Bicocca, Milano, Italy

^h) INFN Milano Bicocca, Milano, Italy

ⁱ) Dipartimento di Fisica, Università degli Studi di Milano e INFN Milano, Milano, Italy

^j) Institute for Nuclear Research of the Russian Academy of Sciences, Moscow, Russia

^k) Institute for Theoretical and Experimental Physics, Moscow, Russia

^l) National Research Center Kurchatov Institute, Moscow, Russia

^m) Max-Planck-Institut für Physik, München, Germany

ⁿ) Physik Department E15, Technische Universität München, Germany

^o) Dipartimento di Fisica dell'Università di Padova, Padova, Italy

^p) INFN Padova, Padova, Italy

^q) Shanghai Jiaotong University, Shanghai, China

^r) Physikalisches Institut, Eberhard Karls Universität Tübingen, Tübingen, Germany

^s) Physik Institut der Universität Zürich, Zürich, Switzerland

Spokesperson: S. Schönert (*Stefan.Schoenert@ph.tum.de*)

Deputy Spokesperson: C. Cattadori (*Carla.Cattadori@lngs.infn.it*)

Technical Coordinator: K.T. Knöpfle (*Karl-Tasso.Knoepfle@mpi-hd.mpg.de*)

URL: <http://www.mpi-hd.mpg.de/GERDA/>

Abstract

The GERmanium Detector Array (GERDA) experiment searches for neutrinoless double beta decay ($0\nu\beta\beta$) of the isotope ^{76}Ge . In 2010, the construction of the experiment was finished. The muon veto was commissioned and data taking started with 3 low background detectors from natural germanium. An unexpectedly large background from ^{42}Ar was identified by the observation of the 1525 keV line from the subsequent ^{42}K decay. Peaks from the natural decay chains have low intensities. The ^{42}Ar contamination was also identified in our liquid argon scintillation test setup LArGe. Studies on the composition of the background around $Q_{\beta\beta}$ are ongoing.

1 Introduction

The construction of the GERmanium Detector Array (GERDA) [1] in Hall A has been completed and its commissioning has started. Inaugurated on November 9, 2010, the experiment will search for neutrinoless double beta decay ($0\nu\beta\beta$) of the germanium isotope ^{76}Ge . Its observation would establish that the neutrino is its own antiparticle.

GERDA uses a novel shielding concept (Fig. 1). Bare Ge diodes are operated in a 65 m^3 cryostat filled with high purity liquid argon which acts as coolant for the detectors and as shield against the radioactivity of the cryostat and the underground environment. The shielding is supplemented by a 3 m thick water buffer. The diodes are both source and detector for $0\nu\beta\beta$ decay. Since no neutrino is emitted, the signal is a line at the Q value of the decay. The water is instrumented with photomultipliers (PMT) to detect the Cherenkov light of muons passing through the water tank. On top is a clean room for diode handling and at its center a lock for transferring the detectors to the argon atmosphere. Next to the water tank is the GERDA building which houses the cryogenic infrastructure and the electronics for data taking.

The aim of GERDA is to scrutinize the claim of discovery of neutrinoless double beta decay [2] and in a second phase to achieve a background index of 10^{-3} cts/(keV·kg·y) which is two orders of magnitude lower than achieved so far. This will allow to probe half-lives of about $T_{1/2}=1.4\cdot 10^{26}$ y (at 90% C.L.) with an exposure of 100 kg·y.

This report summarizes the progress in the construction of GERDA and presents first results from the still ongoing commissioning. In addition, the preparations for the second phase are discussed and recent laboratory results concerning active background suppression methods with the LArGe cryostat are reported. Further detailed information is available in the biannual progress reports to the LNGS scientific committee [3].

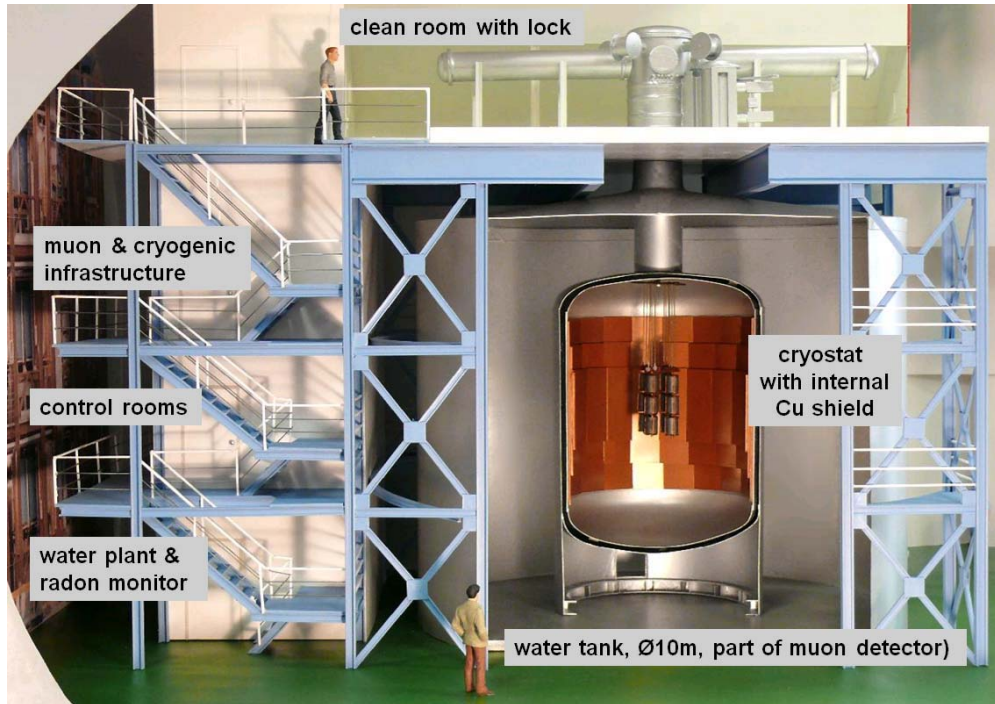


Figure 1: Model of the GERDA experiment.

2 Completion of construction

Cryostat, water tank and steel structure of the GERDA building had been already delivered in 2008 and the installation continued in 2009 with the construction of the clean room on top of the GERDA building. Afterwards the internal cryogenic infrastructure like the active cooling system was installed. By the end of August 2009, the Cherenkov muon veto with its 66 PMTs had been installed.

In the following we discuss individual activities during 2010.

Cryostat

Two reviews with external experts and the LNGS staff verified in October 2009 the readiness of GERDA and LNGS for cryogenic operation, and on November 2, GERDA received green light to start the cryostat operation. The cool down process and the subsequent filling worked very smoothly. During cool down the pressure of the insulation vacuum dropped by almost three orders of magnitude to its present value of $3 \cdot 10^{-8}$ mbar. A turbo pump is running continuously to keep this value.

After a short tuning period for the active cooling we achieved a stable liquid argon temperature of 88 K with practically no evaporation loss. Hence no liquid argon was refilled since January 2010. The entire system is regulated by a PLC. All sensor data and parameters are stored in a database and a monitoring program issues alarms with notification via email and SMS.

Starting in January 2010 continuous 24 hour safety shifts have been established. Since its filling the operation of the cryostat has been found to be very stable.

Water tank

LNGS required for the operation of GERDA with both cryostat and water tank filled to establish that in emergency the water tank can be drained within 2 hours, which corresponds to a constant drainage rate of about 90 ℓ/s . In several tests we verified that the new pipe below the TIR tunnel could take a flow rate of up to 75 ℓ/s without interfering with other installations. The full functioning of this setup has been proven by a simulated emergency alarm in May 2010, when under PLC control the water level was lowered from 8.2 m to 1.2 m within 2 hours. Additional drainage lines to two former GNO pits via the grid surrounding the water tank at up to 16 ℓ/s and via a dedicated pump at 20 ℓ/s will result in a total drainage rate of more than 100 ℓ/s .

The last important milestone for GERDA has been passed in June 2010 when the water tank was completely filled with ultrapure water delivered from the BOREXINO water plant. Since then, the water is cleaned constantly in the GERDA purification plant with a rate of 2.5 m^3/h . At the output of a filter (4.5 μm pore size) and an ionic resin, the resistivity is above 17 $M\Omega\cdot cm$. The gas volume above the water is kept at an overpressure of 30 mbar and is constantly flushed with nitrogen gas. This system is running smoothly and maintains a very good water quality as can be judged by the high light yield found by the muon veto.

Cleanroom

A simpler version of the lock (called commissioning lock) was built and used for a first diode assembly test in 2009. Some improvements have been implemented and this lock together with a glove box was installed in 2010 in the GERDA cleanroom. In addition a gas system for the lock was assembled. The germanium detectors are assembled in the glove box in a nitrogen atmosphere and then transferred to the lock. The latter can be evacuated and purged with argon gas before a shutter is opened and the diodes are lowered into the cryostat. The entire system has worked reliably about a dozen times and will be used for Phase I.

Material screening

The cleaning of surfaces is crucial for many experiments. In GERDA we investigated the removal of radon daughters from germanium surfaces. With etching we achieved a factor of about 100 reduction for ^{210}Po , ^{210}Bi and ^{210}Pb . A redeposition from the acid to the surface was observed which shows the importance of ultrapure chemicals.

Radon is emanated from surfaces to the environmental gas. When the surface and the gas is however at liquid nitrogen/argon temperature, radon freezes out at the surface. We investigated whether this behavior is also true if the surface is embedded in liquid argon. In this case radon goes to the liquid. Therefore any radon emanated from the cryostat walls will be in the argon.

An electrostatic radon monitor was successfully installed. With a detection limit of typically $200 \mu\text{Bq}/\text{m}^3$ it will be used to monitor continuously the radon content at the argon gas exhaust line of the GERDA cryostat.

Plastic muon veto

To veto also muons going through the center of the experiment the central 4 m^2 will be covered with two layers of plastic scintillator panels. The first ones have been placed on top of the cleanroom during 2010 and are now read out together with the Cherenkov PMTs.

Slow control and computing hardware

The slow control hardware was installed and large parts of the infrastructure integrated into the monitoring process and archive database. This system is working since one year without any interruption and a graphical user interface allows a fast access to historical data.

For computing, a data server for intermediate storage underground is available and 40 TB of disk space was bought and mounted on the LNGS Linux cluster. The DAQ systems for the muon veto and germanium detectors have been installed and are running. These include also power supplies for low and high voltage and a pulser.

Frontend electronics

The charge sensitive amplifier for the germanium detectors is a combination of an input transistor, a BF862 JFET, and an operational amplifier. For the latter we have built a custom chip. Since it had some drawbacks we investigated again commercial components as alternatives. It turned out that the now available AD8651 from Analog Devices can also work in liquid argon. The overall performance of this component and the ease of using it lead us to the decision to use this amplifier.

A circuit called CC2 (Fig. 2), which integrates three channels, was built and a large effort was placed to reduce the radioactivity of it. The base material is cuflon (copper on teflon) and all components have been screened individually as well as the assembled circuits. Capacitors containing barium had to be replaced since they had a large radium contamination. The feedback capacitors and test pulse coupling capacitors have been implemented on board using stray capacitances.

The total measured activity with gamma ray screening for three channels is $150 \mu\text{Bq}$ for ^{228}Th and $290 \mu\text{Bq}$ for ^{226}Ra . At a distance of 30 cm to the closest diode this corresponds to a background of less than $10^{-3} \text{ cts}/(\text{keV}\cdot\text{kg}\cdot\text{y})$ which is sufficient for Phase I.

The intrinsic equivalent noise charge (ENC) of the circuit at cryogenic temperatures and 0 pF input capacitance has been measured to be $110 e^-$ (r.m.s.), raising to $150 e^-$ for $C_{det} = 33 \text{ pF}$, corresponding to 0.8 and 1.0 keV resolution (FWHM) in Ge, respectively. The measured FWHM of the circuit connected to a BEGe detector operated in liquid argon is 1.8 keV at 1.3 MeV (^{60}Co line).

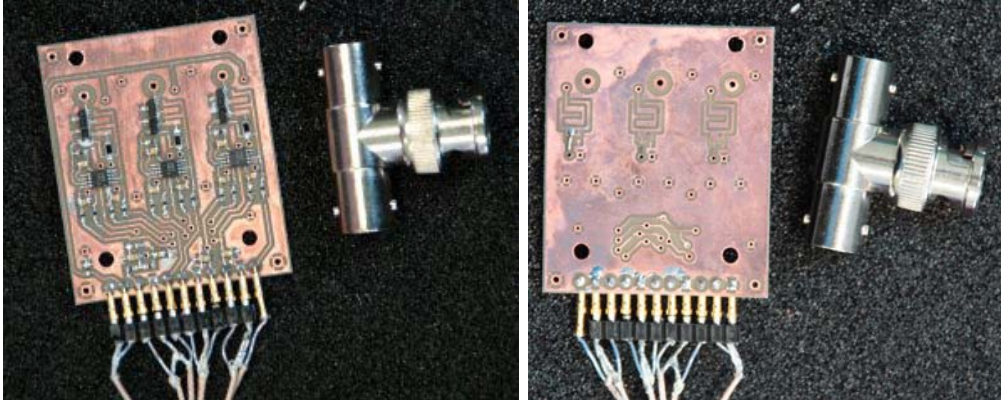


Figure 2: The CC2 circuit top (left) and bottom (right) views.

Calibration system

For energy calibration GERDA has produced a ^{228}Th source embedded in gold. Since commercial companies do not disclose the material composition of the source encapsulation, we were worried about the neutron flux from (α, n) reactions in the ceramic. For gold the threshold for this reaction is higher than the α energies of the Th decay chain. A neutron flux measurement with a ^3He counter showed that our custom source has a neutron flux of about 10^{-3} n/s per kBq source activity. A Li(Eu)I detector was acquired to cross check the flux.

The activity of several sources were cross checked at IRMM. The error on the activities could be reduced to about 3%.

The mechanics for lowering the sources into the cryostat showed some problem during the 2010 operation. A new design is available with features like a measurement of the real source position and end switches.

3 GERDA commissioning

The data taking started in June 2010 using three low background detectors made from germanium with natural isotope composition (Fig. 3). These diodes had been operated before in the Genius Test Facility (GTF) and were modified by Canberra in the same way as the enriched detectors and the prototype detector [4]. The latter has been used during the last years to establish the feasibility of long term operation of bare diodes in liquid argon and nitrogen [5].

In parallel the muon veto was commissioned which will be discussed first.

3.1 Muon veto

Of the 66 installed water tank PMTs one is currently not working. For all others the analog signals are digitized with a 100 MHz flash ADC (FADC). Each FADC card has 8 channels and provides a trigger if one of the channels is above 50% of the single photon peak. If at least 5 of the 10 FADC cards trigger within 60 nsec, the event is read out. Fig. 4

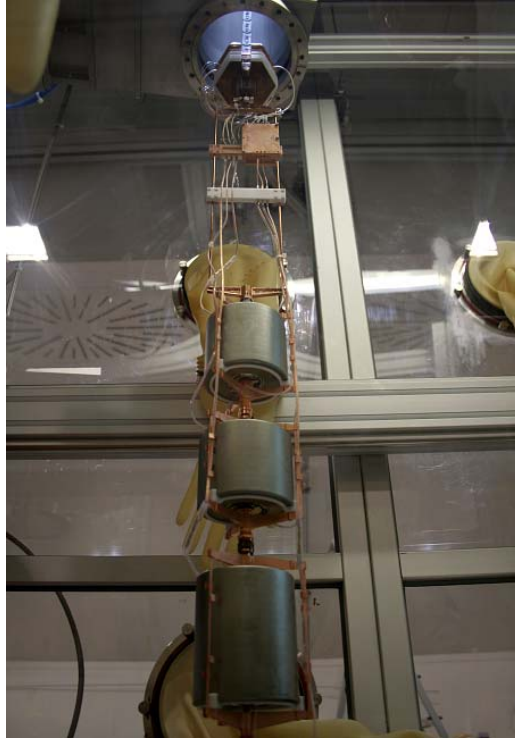


Figure 3: String of three refurbished GTF Ge diodes ready for being lowered into the cryostat. 30 cm above the diodes inside a copper box is the charge sensitive preamplifier.

shows an event with 54 water tank PMTs fired and with with an additional coincidence from 2 plastic panels (in green) on the roof of the cleanroom.

Various trigger conditions have been studied. The trigger threshold can be lowered and the number of coincidences can be changed. The result is that there are two types of events: one class with low multiplicity and low total pulse height and a second class with very high multiplicity like the one shown above. We interpret the former one as coming from environmental radioactivity or random coincidences while the latter one is due to muons.

With the current trigger setting the rate is about 140 triggers per hour which corresponds roughly to the expected muon rate in Hall A of one per hour per m^2 .

3.2 Germanium detectors

The main purposes of this commissioning run is to study the background level in GERDA and the electronic performance of the setup. For the latter we achieve for a pulser 2.8 keV energy resolution (FWHM) and 3.8 keV for the 2.6 MeV line of ^{208}Tl . These numbers can be converted to a resolution of 3.3 keV for the reference 1.3 MeV line of a ^{60}Co source. This value is 0.5 keV higher than the one we achieved for these detectors with commercial electronics. Such a performance is a success although there is room for improvement. Some modifications have been studied already like modifications on the grounding scheme and the knowledge gained will be used for the deployment of the enriched detectors.

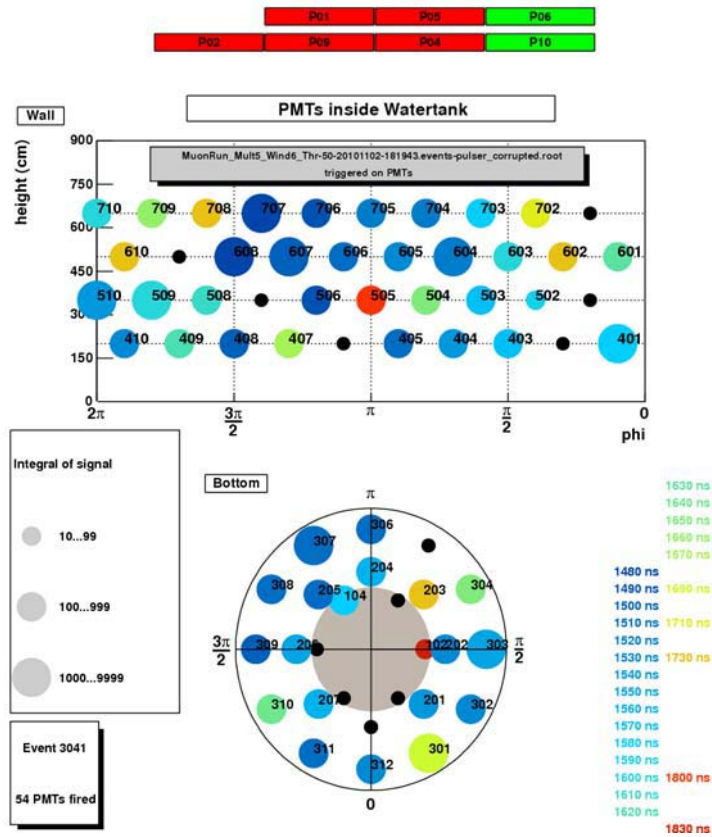


Figure 4: Event in the plastic scintillator panels (top part), the water tank PMTs mounted on the cylindrical wall (middle part) and on the tank bottom surface (bottom). The size of the circles decodes the pulse height and the color the arrival time of the hits. The green panels have a hit.

The main focus of the current data taking is on the study of the background level. Fig. 5 shows the spectrum for a statistics of 1.7 kg·y. The data for different running conditions and of all detectors have been added and an anti-coincidence cut among the germanium diodes and also with the muon veto is applied. The most prominent feature is a line at 1525 keV originating from the β decay of ^{42}K ($T_{1/2} = 12$ h, see Fig. 6), the progeny of ^{42}Ar ($T_{1/2} = 33$ y). Other possible peaks are indicated by dashed lines. These are at 511 keV from positron annihilation photons and at 2615 keV from ^{208}Tl decays - the highest energy line in any natural decay chain. The detection of other lines below 1525 keV is obscured due to Compton events from this line. No high energy lines from the ^{238}U decay chain (e.g. at 1764 keV or 2204 keV) are visible. The count rate at $Q_{\beta\beta} = 2039$ keV depends on the settings of experimental conditions. For some, values which are significantly below 0.11 cts/(keV·kg·y) - the level seen by the Heidelberg-Moscow experiment without pulse shape analysis cuts [2] - have been measured. Precise rates are difficult to determine at this time because of the small numbers of events involved and the changing conditions. The rate is however still higher than the Phase I design goal of 0.01 cts/(keV·kg·y). There appear to be several sources for the currently observed

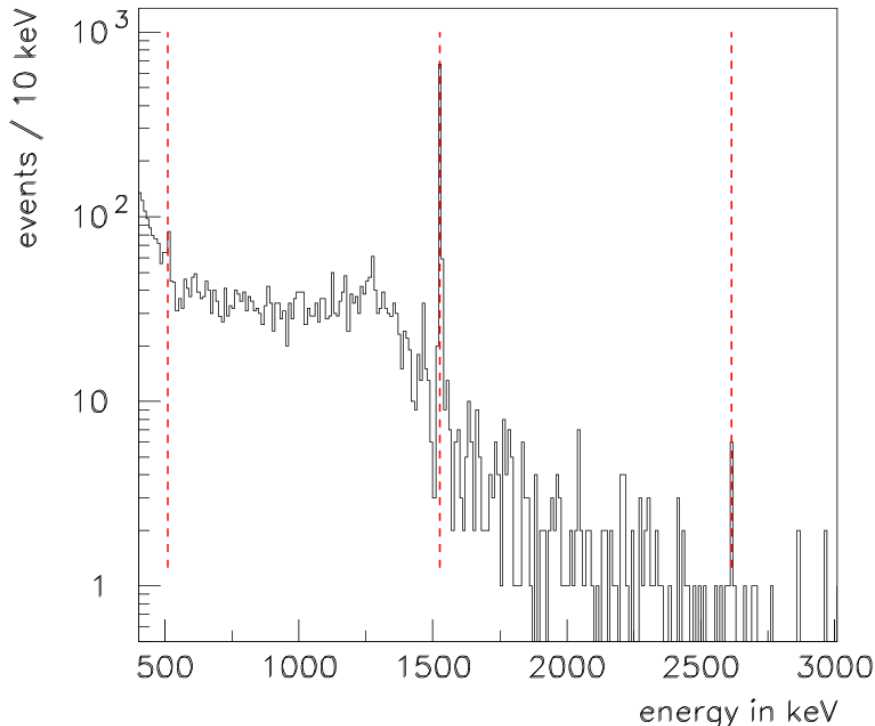


Figure 5: GERDA background spectrum after an exposure of 1.7 kg·y. Data with different running conditions are added in this plot.

background. The natural decay chains are not the dominating ones since the intensities of the corresponding gamma lines is too low. Also the high number of events above 2615 keV suggests a different origin. Other possible sources are intrinsic contaminations and β decays of ^{42}K with a Q value of 3.5 MeV. Beta particles originating close to the detector can contribute to the background at $Q_{\beta\beta}$.

The ^{42}Ar background was initially studied at the time of the proposal [1] using the best upper limits available for the $^{42}\text{Ar}/^{nat}\text{Ar}$ concentration of $3 \cdot 10^{-21}$ g/g [6]. We observe in GERDA that this value could be almost an order of magnitude higher by analyzing the count rate in the 1525 keV line. In addition, ^{42}K must drift to the detector surfaces before it decays to explain the high count rate above the line. This can occur if potassium originating from ^{42}Ar β decay is charged and drifts in the electric field surrounding the germanium diodes.

Currently, we are studying different hypothesis for the origin of the background and at the same time we search for options for its mitigation.

4 LArGe test facility

In Phase I of GERDA liquid argon (LAr) is used as a passive shield only. For the next phases additional methods of background reductions are required. One option is the measurement of an energy deposition in LAr by the detection of scintillation light. The

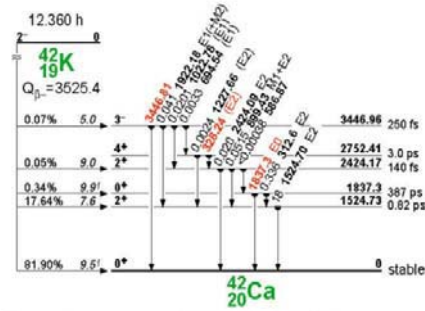


Figure 6: ^{42}K decay scheme. ^{42}K is the progeny of ^{42}Ar which is a β emitter with $Q = 599$ keV and $T_{1/2} = 32.9$ y.

pilot setup Mini-LArGe (19 kg of LAr) had been constructed and successfully operated to demonstrate the power of this concept. A long-term stability (about 2 years) with constant light yield of 1300 photoelectrons per MeV was achieved. In addition, a pulse shape discrimination (PSD) of the light was developed which allows to perform gamma / alpha / neutron selection with a strong ($> 10^5$) discrimination factor [15]. Based on the obtained experience an up-scaled facility (LArGe) with 1.4 tons of LAr was constructed.

In LArGe, 9 PMTs are used for light detection. The high purity copper cryostat is lined with the wavelength shifting reflector foil used previously in Mini-LArGe. The setup uses a shield consisting of (from outside to inside) 20 cm polyethylene, 23 cm steel, 10 cm lead and 15 cm copper of increasing radio-purity. Assembly and installation of the LArGe setup in the underground GERDA detector laboratory at LNGS have been finished by the end of 2009; only the top part of the shield has still to be installed (Fig. 7). The cryostat is equipped with an active cooling system using liquid nitrogen to subcool LAr to 86.2 K. The operation is stable without any loss of LAr.

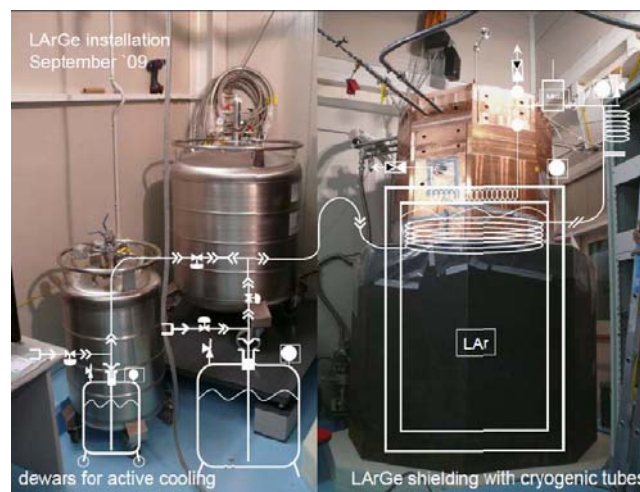


Figure 7: View of the LArGe set up inside its multilevel shield. An overlaid schematic drawing shows the active cooling system.

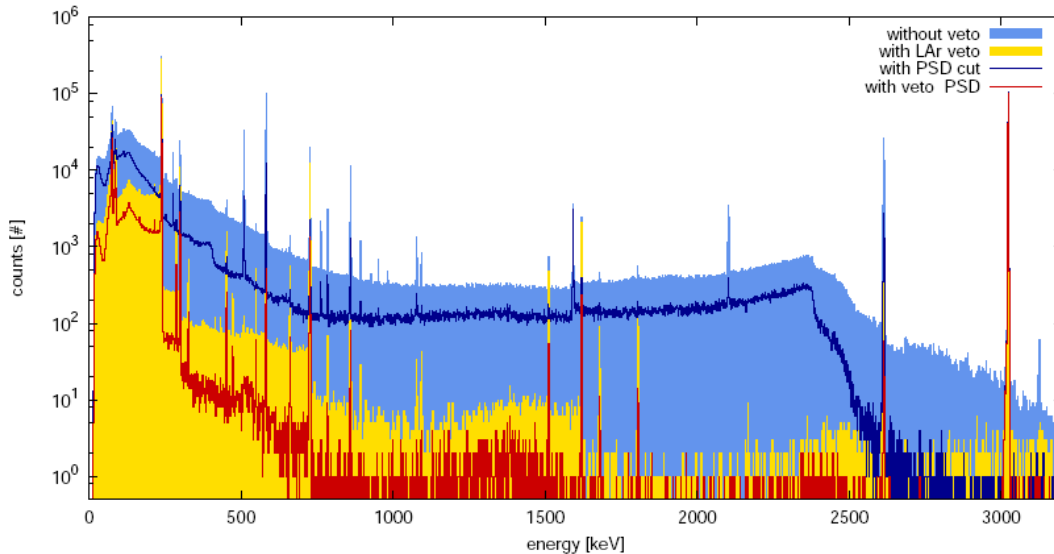


Figure 8: Response of the BEGe detector to the ^{228}Th inner source irradiation in LArGe: the spectrum prior to any cut (blue), with liquid argon veto (yellow), with PSD analysis (ultramarine), and with both liquid argon veto and PSD (red).

The main goal of LArGe is the development of methods to reduce internal backgrounds of Ge detectors by using an anti-coincidence with the LAr scintillation signal. During 2010, a wide program of measurements with a bare BEGe detector in LArGe has been carried out. Calibration sources (^{228}Th , ^{226}Ra , ^{60}Co , ^{137}Cs) have been placed in- and outside of the cryostat. The efficiency of the scintillation veto was optimized and determined as well as the background reduction factor due to PSD of signals from the BEGe detector. For instance, it could be demonstrated that the background from decays of the ^{228}Th chain occurring close to the Ge detector can be suppressed by a factor of 6000 (Fig. 8).

Another task for LArGe emerged recently after the first GERDA commissioning runs which showed the actual need to study concentration and volume distribution of the cosmogenic isotope ^{42}Ar and its daughter ^{42}K in liquid argon. Beta decays of ^{42}K will create signals in both the germanium detector as well as in LAr. The simultaneous detection of the scintillation light together with the germanium detector signal is therefore a powerful tool to identify and reject these events. Investigations in this direction started at the end of 2010 using a similar natural p-type Ge diode as the ones deployed in GERDA. The PMT veto reduces the background at $Q_{\beta\beta}$ by about one order of magnitude to a value which is comparable to the one currently reached in GERDA. Additional information about possible effects of the purity of the liquid argon will be obtained by running sequentially with LAr 5.0 and LAr 6.0.

5 Phase II detector R&D

In the second phase, GERDA aims at a background which is a factor of 10 lower than the one of Phase I. We follow two options to reach this goal. The $0\nu\beta\beta$ events normally

deposit energy only at one location in a detector (single-site event, SSE) while the large majority of backgrounds will deposit energy also in the liquid argon and/or will scatter at several locations in a diode (multi-site events, MSE). The former creates scintillation light which can be detected with PMTs (see the section about LArGe). The latter can be detected by an analysis of the detector current pulse (pulse shape discrimination, PSD) or by segmenting a contact of a diode and searching for coincidences among the segments.

Research on BEGe detectors

During the last years it was discovered that point contact detectors offer good PSD power [7] and similar diodes have also been studied in GERDA [8, 9, 10, 11]. They are commercially available like the Broad Energy Germanium (BEGe) detector from Canberra. A BEGe is a p-type detector of cylindrical shape which has on one planar surface a small area p^+ contact (≈ 15 mm diameter) at the center (Fig. 9). The outer part of this plane and all other surfaces are the n^+ contact. The field strength is maximal close to the p^+ contact. Consequently, the current signal from drifting holes has a sharp maximum when they reach this electrode. This is largely independent from their starting position in the diode. Several interactions in the detector (MSE) will cause several such maxima if the drift times are different. SSE events have only one maximum. Hence the ratio A/E of the maximum of the current signal (A) over the total energy (E) turns out to be a powerful discrimination variable. The pulse shape identification capability is uniform in the detector volume except for a relatively small region close to the p^+ contact (a few percent of the total volume).

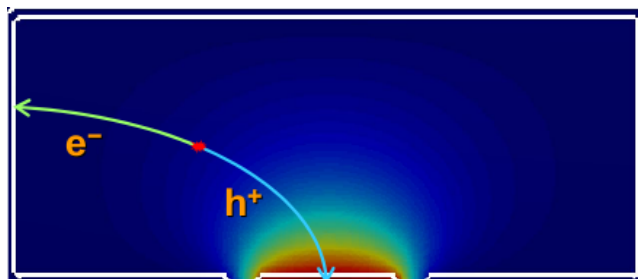


Figure 9: Cross section of a BEGe detector with the electric field distribution.

To better understand the performance and the features of BEGe detectors, a complete simulation was developed of the detector response to ionizing particle interactions [12]. The simulation was validated by directly comparing simulated and measured charge pulse shapes and by comparing the distribution of the rise time and the A/E parameter for different energies. The PSD performance on decays inside Ge detectors, which are difficult to study experimentally, was then evaluated with the simulation.

The estimated cut survival probability in the $Q_{\beta\beta}$ region is 1% for ^{60}Co , 5% for ^{68}Ga (progeny of ^{68}Ge) and 86% for $0\nu\beta\beta$ decays when the acceptance of the double escape peak is adjusted to 90%. The ^{60}Co and ^{68}Ga , produced by cosmic ray interactions in Ge, are amongst the most challenging backgrounds in GERDA. The simulation results show

that both can be significantly reduced by PSD while keeping a large acceptance for $0\nu\beta\beta$ decay.

One BEGe detector was removed from its vacuum cryostat and operated as a bare detector in liquid argon. An energy resolution of 1.8 keV FWHM for the 1.3 MeV ^{60}Co line was achieved and the PSD performance was found to be unaltered as compared to the results obtained in the vacuum cryostat [13].

Production chain test

To demonstrate that working BEGe detectors can be produced from the procured enriched Ge material, a full production chain validation was initiated at the beginning of 2009. The test was performed with depleted (in ^{76}Ge) germanium (34 kg of GeO_2) left over from the enrichment process. The oxide was refined to 6N-grade germanium at PPM, Langelsheim, Germany. Crystal pulling occurred at Canberra, Oak Ridge, USA and the diode fabrication took place at Canberra, Olen, Belgium. Four Ge crystals (17.7 kg total mass) were grown from which five detectors were manufactured. Up to now, four detectors (with masses between 700 g and 930 g) underwent a comprehensive testing campaign [14] to characterize their charge collection, spectroscopic and pulse shape discrimination performance, as well as long-term stability. The results are summarized in Fig. 10. The different detectors were produced from various slices of the grown crystals and underwent different machining steps in order to learn how to maximize the detector yield for the upcoming production from enriched material. All aspects of the performance of the detectors are as good as of reference BEGe detectors from standard production.

Def.	Diam. \times length [mm \times mm]	Mass [g]	Dead layer [mm]	FWHM @ 1.3 MeV [keV]	2.6 MeV peak PSD acc. [%]
Ref.	81 \times 32	878	0.43	1.63	7.7 \pm 0.4
1	74 \times 33	760	0.7	1.61	6.1 \pm 0.5
2	74 \times 32	700	0.45	1.66	6.4 \pm 0.5
3	75 \times 31	730	0.5	1.6	7.4 \pm 0.6
4	74 \times 41	930	0.4	1.7	5.7 \pm 0.5
5	70 \times 28	350	operational, to be tested		

Figure 10: The performance of various BEGe detectors from the GERDA Phase II production chain using the depleted germanium material. As reference the data for a 81 mm diameter BEGe detector from the standard factory production is included.

Research with segmented coaxial detectors

Two additional 18-fold segmented detectors have been purchased to study more details of this technology. One had larger metalization areas for the segment contacts to study effects on the signal quality. No change was found. A second one had an additional contact on one of the planar surfaces of the diode. This detector allowed to determine the dead layer on these surfaces to be 1 mm.

PSA is also possible for coaxial detectors. A simulation program for pulse shapes was written and the results compare well with the data [16].

The standard cable for the signal contacts is made out of Kapton. Since we did not identify a sample clean enough for our application, cables made out of polyethylene naphthalate (PEN) have been produced and successfully tested with a detector. This material is cleaner and we are now in the process to identify a clean production chain for its metalization.

Crystal growing at IKZ

Since no commercial company was willing to grow n-type crystal from enriched material for us, we contacted Institut für Kristallzüchtung (IKZ) in Berlin.

During the last years IKZ has made big progress towards growing a crystal good enough for detector production. In 2010 the previously dominating arsenic contamination of the Czochraski puller was removed by electro-polishing the puller. To further reduce the impurity level a quartz glass surrounding the crucible was recently added.

IKZ has grown in total about 30 crystals. The net impurity levels are now at the $10^{11}/\text{cm}^3$ level and for part of the latest crystal a factor of 2-3 lower and thus at the value required for detector production.

Decision for Phase II technology

In summer 2010 the collaboration selected BEGe detectors as the nominal technology for Phase II. This decision is based on the achieved performances and on the fact that IKZ could not deliver n-type crystals in due time. BEGe detectors are at least as efficient in background rejection as segmented detectors while having a better nominal energy resolution. They need less cabling and should hence contribute less to the background. In the meantime the advantages of segmented detector technology are further explored. These include the position sensitivity to background sources and the exploitation of segmentation to determine crystal properties important for the understanding of pulse shapes.

The ^{76}Ge enriched material for Phase II detectors recently underwent reduction to metallic form and purification at PPM Pure Metals. The total yield of 6N material was 94% resulting in 35.4 kg. The GERDA collaboration has started negotiations with Canberra for the production of about 20 kg of ^{76}Ge enriched BEGe detectors.

6 Summary

In 2010, data taking started in GERDA. All systems are running and allow continuous data taking. The background at $Q_{\beta\beta}$ is smaller than for previous experiments but unexpectedly large. The natural decay chains are not the dominating contributions because of the low intensities of the corresponding gamma lines. Other sources like ^{42}Ar are under study.

In LArGe the background rejection power of argon scintillation detection together with pulse shape analysis of a BEGe detector could be demonstrated. ^{42}Ar was also identified here. Thus we have two setups where this background can be studied.

For Phase II the detector technology was decided to be BEGe. The test production of BEGe detectors from depleted material was successful and the enriched material was converted into metal and zone-refined to 6N material. Negotiations with Canberra for the detector production are ongoing.

7 List of GERDA related publications in 2010

1. I. Abt et al, *Pulse shape simulation for segmented true-coaxial HPGe detectors*, Eur. Phys. J. C 68 (2010) 609.
2. P. Grabmayr, GERDA: *Verändert das Neutrino das Standardmodell?*, Welt der Physik 1 (2010) 5098.
3. M. Barnabé Heider et al, *Operation and performance of a bare broad-energy germanium detector in liquid argon*, J. Instrum. 5 (2010) p10007.
4. B. Majorovits, *Segmented HPGe detectors for the search of neutrinoless double β -decay*, Prog. Part. and Nucl. Phys. 64 (2010) 264.
5. G. Meierhofer et al, *Thermal neutron capture cross section of Ge-74*, Phys. Rev. C 81 (2010) 027603.
6. A. Pullia et al, *Cryogenic Performance of a Low-Noise JFET-CMOS Preamplifier for HPGe Detectors*, IEEE Trans. Nucl. Sci. 57 (2010) 737.
7. F. Ritter et al, *The calibration system of the GERDA muon veto Cherenkov detector*, Nucl. Instr. Methods A 617 (2010) 420.
8. A. Smolnikov and P. Grabmayr, *Conversion of experimental half-life to effective electron neutrino mass in $0\nu\beta\beta$ decay*, Phys. Rev. C 81 (2010) 028502.

References

- [1] Letter of Intent, 2004, hep-ex/04040390; Proposal to the LNGS, 2004, <http://www.mpi-hd.mpg.de/gerda>
- [2] H.V. Klapdor-Kleingrothaus et al., Nucl. Instr. Meth. A522, 371-406 (2004)
- [3] <http://www.mpi-hd.mpg.de/gerda/reportsLNGS/progress-reports.html>
- [4] M. Barnabé Heider, Dissertation, Univ. Heidelberg, 2009
- [5] M. Barnabé Heider et al., IEEE Nuclear Science Symposium, Oct 19-25, 2008, N68-7.
- [6] A.S. Barabash, Proc. Int. Workshop on technique and application of Xenon detectors, Japan Dec. 2001, World Scientific (2002), p. 101-114.
- [7] P.S. Barbeau et al, 2007 JCAP 0709 P009.

- [8] D. Budjáš, Dissertation, Univ. Heidelberg, 2009.
- [9] D. Budjáš et al., 2009 JINST 4 P10007.
- [10] M. Agostini et al., arXiv:1012.5200v2, submitted to JINST.
- [11] R. Gonzáles et al., J Radioanal Nucl Chem 286, 477-482 (2010).
- [12] M. Agostini et al., arXiv:1012.4300v2, submitted to JINST.
- [13] M. Barnabé Heider et al., 2010 JINST 5 P10007.
- [14] S. Georgi, Bachelor thesis, Univ. Heidelberg, 2010.
- [15] P. Peiffer et al., 2008 JINST 3 P08007.
- [16] I. Abt et al, Eur. Phys. J. C 68 (2010) 609.

The ICARUS Experiment

The ICARUS Collaboration

M. Antonello^a, P. Aprili^a, B. Baiboussinov^b, M. Baldo Ceolin^b, P. Benetti^c, E. Calligarich^c,
N. Canci^a, F. Cavanna^r, S. Centro^b, A. Cesana^e, K. Cieřlik^f, D.B. Cline^g, A.G. Cocco^d,
A. Dabrowska^f, N. Deniskina^d, D. Dequal^b, A. Dermenev^h, R. Dolfini^c, C. Farnese^b, A. Fava^b,
A. Ferrariⁱ, G. Fiorillo^d, D. Gibin^b, A. Gigli Berzolari^c, S. Gninenko^h, T. Golan^l, A. Guglielmi^b,
M. Haranczyk^f, J. Holeczekⁿ, M. Kirsanov^h, J. Kisielⁿ, I. Kochanekⁿ, J. Lagoda^m, S. Maniaⁿ,
G. Mannocchi^o, A. Menegolli^c, G. Meng^b, C. Montanari^c, S. Otwinowski^g, O. Palamara^a,
T.J. Palczewski^m, L. Periale^o, G. Piano Mortari^r, P. Picchi^o, F. Pietropaolo^b, P. Plonski^p,
P. Przewłocki^m, A. Rappoldi^c, G.L. Raselli^c, M. Rossella^c, C. Rubbia^{1a,i}, P. Sala^e, E. Scantamburlo^a,
A. Scaramelli^e, E. Segreto^a, F. Sergiampietri^q, J. Sobczyk^l, D. Stefan^f, J. Stepaniak^m, R. Sulej^m,
M. Szarska^f, M. Terrani^e, F. Varanini^b, S. Ventura^b, C. Vignoli^a, T. Wachala^f, H.G. Wang^g, X. Yang^g,
A. Zalewska^f, K. Zaremba^p, J. Zmuda^l

^aINFN - Laboratori Nazionali del Gran Sasso, Assergi, Italy

^bUniversità di Padova e INFN, Padova, Italy

^cUniversità di Pavia e INFN, Pavia, Italy

^dUniversità Federico II di Napoli e INFN, Napoli, Italy

^ePolitecnico di Milano e INFN, Milano, Italy

^fH.Niewodniczański Institute of Nuclear Physics, Kraków, Poland

^gDepartment of Physics, UCLA, Los Angeles, USA

^hInstitute for Nuclear Research of the Russian Academy of Sciences, Moscow, Russia

ⁱCERN, Geneva, Switzerland

^lInstitute of Theoretical Physics, Wrocław University, Wrocław, Poland

^mA. Sołtan Institute for Nuclear Studies, Warszawa, Poland

ⁿInstitute of Physics, University of Silesia, Katowice, Poland

^oINFN Laboratori Nazionali di Frascati, Frascati, Italy

^pInstitute for Radioelectronics, Warsaw Univ. of Technology, Warsaw, Poland

^qUniversità di Pisa e INFN, Pisa, Italy

^rUniversità dell'Aquila, L'Aquila, Italy

¹Spokesman of the ICARUS Collaboration

1 ICARUS T600 detector

The idea of a Liquid Argon Time Projection Chamber (LAr-TPC - calorimetric measurement of particle energy together with three dimensional particle track reconstruction from the electrons drift in an electric field in a sufficiently pure LAr), proposed in 1977 by C. Rubbia [1], finally resulted in the construction of a cryostat of mass of 600 tons of LAr - the ICARUS T600 detector.

The ICARUS T600 LAr detector is split into two identical, adjacent T300 half-modules, each with internal dimensions $3.6 \times 3.9 \times 19.6 \text{ m}^3$ and filled with about 380 t of ultra-pure liquid Argon. Each half-module houses two TPCs separated by a common cathode, a field shaping system, monitors and probes, and two arrays of photo-multipliers. Externally the cryostat is surrounded by a set of thermal insulation layers. The detector layout is completed by a cryogenic plant made of a liquid Nitrogen cooling circuit and a system of LAr purifiers. Each TPC is made of three parallel planes of wires, 3 mm apart, facing the drift region, with wires oriented at 0° and $\pm 60^\circ$ from the horizontal direction. Globally 54272 wires with length up to 9 m are installed in the detector.

By appropriate voltage biasing, the first two planes (induction planes) provide signals in non-destructive way, whereas the charge is finally collected in the last one (collection plane). The maximum drift path, i.e. the distance between the cathode and the wire planes, is 1.5 m and the nominal electric field $E_D = 500 \text{ V/cm}$.

The signals coming from each wire are independently digitized every 400 ns. The measurement of the time of the ionizing event, the T_0 time, which can be determined via the prompt scintillation light produced by ionizing particles in LAr, together with the knowledge of the electron drift velocity $v_D \simeq 1.6 \text{ mm}/\mu\text{s}$ at $E_D = 500 \text{ V/cm}$, provides the absolute time and hence the position of the tracks along the drift co-ordinate.

A schematic view of the T600 module is shown in Fig. 2. The detailed description of the T600 ICARUS detector design, construction and test on the surface in Pavia (Italy) can be found in [2].

The installation of ICARUS at the LNGS Gran Sasso Underground Laboratories required additional modification and improvement of the experimental setup, with respect to the on-surface technical run [2]. In order to fulfill the efficiency, safety and reliability requirements for long underground operations, new solutions for the cooling and insulation systems have been adopted and dedicated infrastructures have been developed.

The commissioning in underground at LNGS of the ICARUS T600 detector has been successfully performed in the course of 2010. The ICARUS experiment at the Gran Sasso Laboratory is so far the most important milestone for the LAr-TPC technology.

1.1 Detector Cryogenic plant

The T600 Module, shown in Fig. 1, is installed in LNGS Hall-B on 20 seismic adsorbers.

The two T300 half-modules are independent from the point of view of LAr containment and purification systems while they are cryogenically interdependent having the Nitrogen cooling system and the thermal insulation in common (see Fig. 2).

A thermal insulation layer surrounds the two half-modules: it is realized by evacuated insulating honeycomb panels (0.4 m thick NomexTM) assembled together to realize a tight

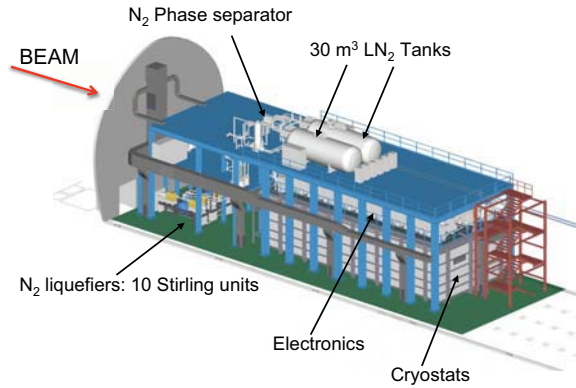


Figure 1: *Schematic view of the whole ICARUS T600 plant.*

containment in case of liquid spillage, with nominal heat losses of about 10 W/m^2 . Between the insulation and the aluminum containers a thermal shield is placed, with boiling Nitrogen circulation inside, to intercept the heat load through the thermal insulation box, in order to maintain uniform and stable the cryostat bulk temperature.

Each semi-module is equipped with two gas and one liquid recirculation systems, both required to attain a very high free-electron lifetime (several ms) in less than one month. The continuously active gas recirculation units (maximum rate $25 \text{ GAr Nm}^3/\text{h}$ each) collect the gas from the chimneys that host the cables for the wire chamber read-out on top of the detector. The re-condensed gas drops into OxysorbTM filters placed below the re-condenser and is sent back into the LAr containers just below the LAr surface. Liquid recirculation units consist of an immersed, cryogenic, liquid transfer pump placed inside an independent dewar. The circulated LAr goes through standard Oxysorb/HydrosorbTM filters before being re-injected into the cryostats ($\sim 2 \text{ m}^3/\text{h}$, corresponding to a full volume recirculation in about 6 days).

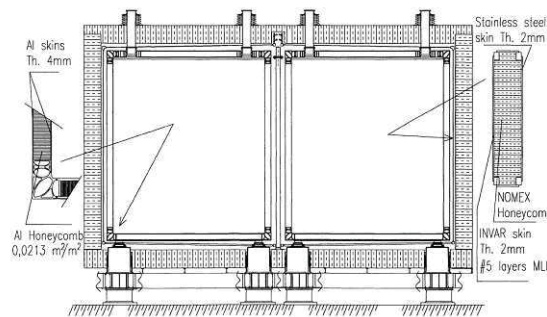


Figure 2: *Vertical cross section of the ICARUS T600 module.*

In steady state conditions, liquid Argon is maintained in stable conditions by Nitrogen screens and GAR recirculation at a typical working pressure of about 1.1 bar abs (89 K).

Nitrogen used to cool the T300 half-modules and their Ar purification systems is sent back into two 30 m³ LN₂ storage tanks, located on the top of the supporting structure. Nitrogen temperature is fixed by the equilibrium pressure in the LN₂ storage tanks (\approx 2.1 bar abs which corresponds to about 84 K), which is kept stable by a dedicated re-liquefaction system composed by ten cryocoolers (about 40 kW global cold power at 84 K), thus guaranteeing a safe operation in closed-loop. The circulation speed is defined by the request to maintain a thermal uniformity within 1 K in the LAr bulk.

1.1.1 Commissioning

In January 2010 the T600 cryogenic plant commissioning started. The procedure consisted in four subsequent phases including cryostats vacuuming, cooling down, LAr filling and finally LAr forced purification start up.

The vacuum phase, essential to reach an acceptable initial LAr purity, lasted for a period of three months. Eight dry pumping systems, composed of primary dry scroll pump and turbo molecular pump, were used to reach a pressure better than 10^{-4} mbar. The molecular regime was maintained over a long period of time, during which materials and surfaces of the inner detector had the proper outgassing. Ultimately the pressure stabilized around the value of $3.8 \cdot 10^{-5}$ mbar in the East cryostat and $4.5 \cdot 10^{-5}$ mbar in the West cryostat (Fig. 3), with residual leak rates of $0.06 \text{ mbar} \cdot \text{l/s}$ and $0.04 \text{ mbar} \cdot \text{l/s}$ respectively (mainly due to out-gassing). A residual gas analysis revealed, in both cryostats, a major 70% water content which is expected to stick over internal surfaces and freeze during the cooling down phase thus not affecting the LAr purity. The Oxygen contribution was measured to be the 10% at most of the total pressure of the residual gas. During the whole vacuum phase the mechanical deformations of the cryostat inner walls were monitored to keep under control the effects of the load due to vacuum forces. Vacuum was broken with ultra-pure GAR (6.0 grade) to begin the cooling-down phase. LN₂ circulation was started inside the cooling screens using LN₂ from the 30 m³ storage. A constant overpressure of +100 mbar (w.r.t. ambient pressure) was maintained by means of continuous injection of purified gas argon. During the transient phase all the 10 Stirling cryogenerators were fully operative while N₂ vapor not managed by Stirling units was warmed-up through a 50 kW electrical heater and safely evacuated from Hall B via the ventilation system. The use of the Stirling cryogenerators was the key for a LN₂ total consumption (55800 l) reduced to a factor 1/4 w.r.t. expectations. LN₂ cooling was slowed-down when required to keep the internal temperature gradients on the wire chamber mechanics within specifications (50K). Fig.4 shows the temperature trend and gradients in the Right Chamber of West cryostat. At conclusion of the 7-days cooling-down phase the temperature target value of 90 K was reached.

Starting from April 29th, cryostats were filled in about 2 weeks fluxing commercial LAr through a two-stages purification system of standard Oxysorb/Hydrosorb cartridges. LAr purity was continuously monitored after the first purification stage. The filling rate in the 2 weeks was $\sim 1\text{m}^3/\text{hour}$ per cryostat for a total downloaded 610511 Argon liters (47 trucks), including the 30 m³ storage tank filling. During the whole period the four gaseous re-circulations were operating at maximum speed to intercept the degassing impurities. In steady state conditions 8 cryocoolers out of 10 are operating (32 KWatt) smoothly. One

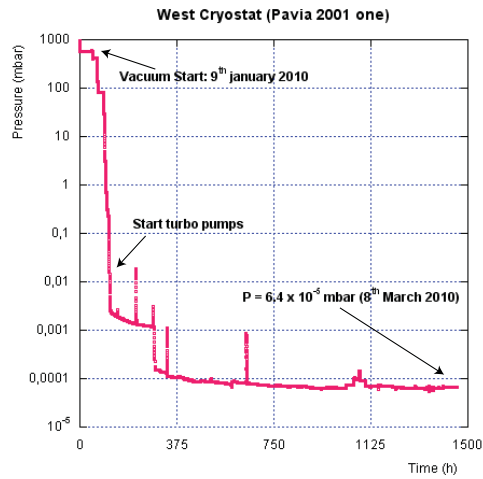


Figure 3: Vacuum phase. Pressure as a function of time inside West cryostat.

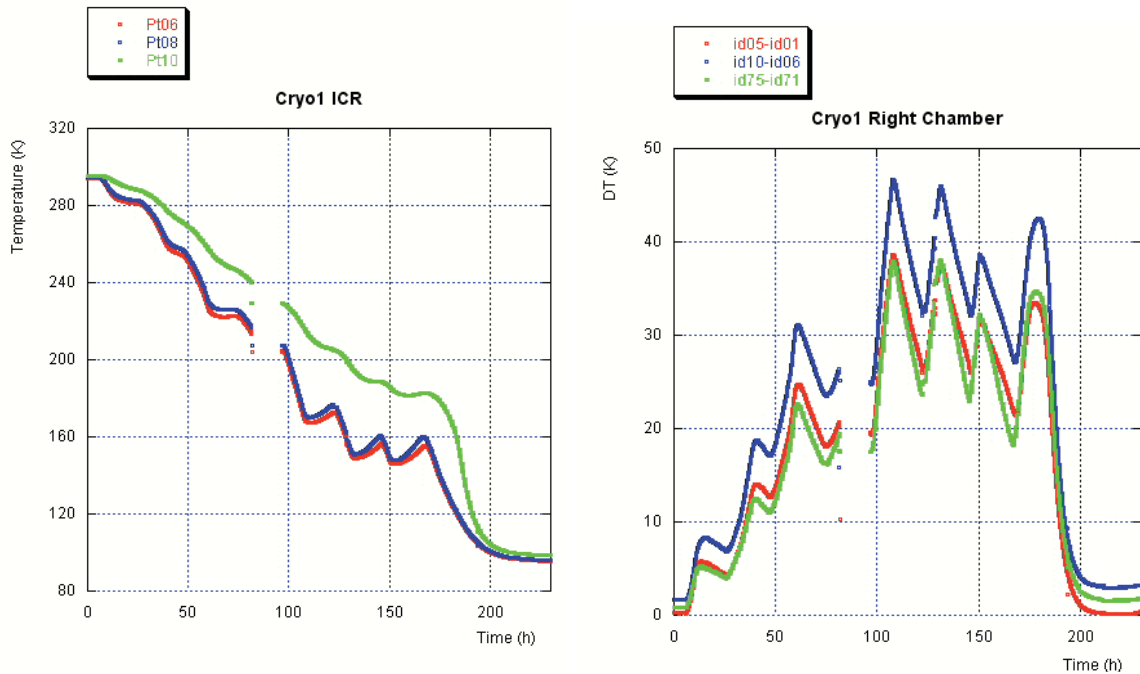


Figure 4: [Left] Cooling phase. Temperature trend on three different verticals on Right wire chamber structure, West Cryostat. [Right] Temperature Gradients on the same verticals.

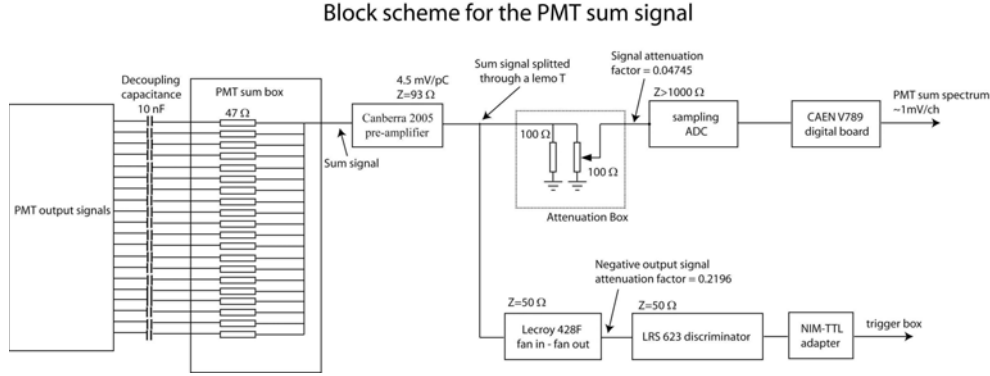


Figure 5: *Scheme of the PMT signal treatment to generate a trigger signal.*

and a half month after filling, the forced liquid recirculation started on both cryostats at rate of $\sim 1 \text{ m}^3/\text{hour}/\text{cryostat}$.

1.2 Internal PMT system

The two T300 half modules employ arrays of Photo Multiplier Tubes (PMTs) directly immersed in the LAr to detect the prompt ($< 2 \mu\text{s}$) photon emission in the VUV spectrum with $\lambda = 128 \text{ nm}$ produced by charged particles interacting in the LAr volume, which produce scintillation light through the recombination and de-excitation processes of the ionized and excited Ar molecular states [3]. In this way PMTs provide an absolute time measurement for drift coordinate reconstruction and a trigger for ionizing events occurring in LAr.

The devices employed are large surface 9357FLA Electron Tubes PMTs, which are made sensitive to the 128 nm scintillation light by a coating of their windows with tetraphenyl-butadiene (TPB) that acts as a wavelength shifter [4].

A total of 20 and 54 PMTs are installed in the West and East cryostats respectively. PMTs are deployed along three horizontal rows of nine devices each behind the two TPCs wire planes.

As a starting layout, for each of the four chambers, the analog sum of the PMT signals is exploited. The response of the PMTs has been equalized for each chamber. The PMT signals are treated as sketched in Fig. 5: the sum signal is pre-amplified, with an integration time constant of $30 \mu\text{s}$ to collect the full scintillation light yield and split into two parallel chains. One is used to feed the input of a sampling ADC, allowing the measurement of its amplitude for the light spectrum acquisition, the other is discriminated and used for trigger purposes.

1.3 Electronics and DAQ

The electronics was designed to allow continuous read-out, digitization and independent waveform recording of signals from each wire of the TPC. The read-out chain is organized on a 32 channel modularity principle [2].

A Decoupling Board receives the signals from the chamber and passes them to a Analogue Board via decoupling capacitors; it also provides wire biasing voltage and the distribution of the test signals.

The Analogue Board hosts the front-end amplifiers and performs 16:1 channel multiplexing and 10-bit ADC digitization at 400 ns sampling time per channel. The overall gain is about 1000 electrons per ADC count, setting the signal of minimum ionizing particles to ~ 15 ADC counts with a dynamic range of about 100 mip's. A $3 \mu\text{s}$ time constant is used for the unipolar signals from Collection and Induction1 wires, while $100 \mu\text{s}$ time constant is used for the bipolar current signals (Induction2 wires).

The average electronic noise is measured to be well within expectations on practically all the 54272 channels: 1500 electrons rms to be compared with ~ 15000 free electrons produced by m.i.p. over 3 mm ($S/N \geq 10$).

Gain uniformity within 3% has been obtained with test-pulse calibration signals injected in both the decoupling and analog boards. This value corresponds essentially to the fluctuation of the test capacitance values, indicating that the actual channel-to-channel fluctuations of the electronic gain are even smaller.

A Digital Board acts as a 10-bit-wide waveform recorder. It continuously reads the data, stores them in multi event circular buffers, each covering a full drift distance; when a trigger signal occurs, the active buffer is frozen, writing operations are moved to the next free buffer, and the stored data are read out by the DAQ.

To increase the bandwidth of the DAQ system with respect to the 2001 technical run, a new on-line lossless factor-4 data compression has been implemented [7]. This is performed by storing the difference between the signal amplitude value for a t-sample and the previous one. Given the slow signal variation, only 4 bits instead of 16 are in general sufficient, allowing to store ± 7 ADC count differences. For the rare signals with slope exceeding this value, the full difference is stored in a 16 bit word and flagged for unambiguous reconstruction. This configuration guarantees no dead time, at least until the maximum DAQ throughput (1 full-drift event per second) is reached.

DAQ and event builder architecture is completed by DAQ computers (10 servers), storage (160 TB on disk and 100 TB on tape), networking (cabling, switches and fibers to control room and to external labs).

The same DAQ system also stores the signals from the Internal PMT's with a sampling time of 50 ns (using a modified Analogue board receiving 4 channels and bypassing the multiplexer).

1.4 Trigger

The ICARUS-T600 scientific program addresses the neutrino physics with the CNGS beam from CERN, cosmic neutrinos and proton-decay search. The trigger system relies on the scintillation light signals provided by the internal PMTs and on the CNGS proton extraction time.

The trigger set-up is based on a controller crate, hosting a FPGA-board for signals processing, interfaced to a PC in the Control Room for data communication and parameter setting. It can handle different trigger sources such as signals from internal photomultipliers, CNGS proton extraction time and test pulses for electronic channel calibration.

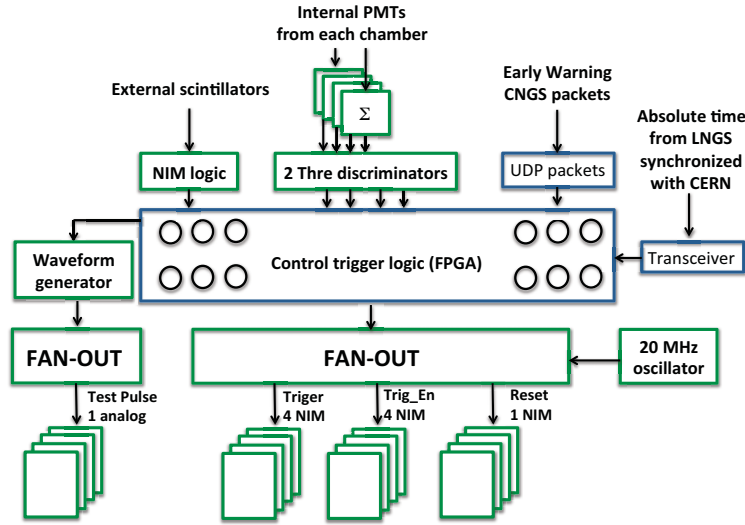


Figure 6: *The general scheme of the signals handled by the trigger controller.*

Moreover it provides the absolute time stamp for the recorded events and the opening of the CNGS proton spill gate. The handling by the FPGA controller of the different input signals, of the absolute timing generated by CNGS atomic clock, of the beam extraction early warning packets from CERN and the distribution of the trigger to the electronic crates is shown in Fig. 6. For every CNGS cycle two proton spills, lasting $10.5 \mu\text{s}$ each, separated by 50 ms , are extracted from the SPS machine. An "early warning" packet is sent from CERN to LNGS via Ethernet 80 ms before the first proton spill extraction, allowing to open two $\sim 50 \mu\text{s}$ gates in correspondence to the predicted extraction times. A $\sim 35 \mu\text{s}$ precision has been measured, due to a jitter in the extraction time prediction.

The most accurate timing inside the controller is realized by a 40 MHz counter, reset every 1 ms by a synchronization signal containing absolute time infos, generated by the master clock unit of the LNGS external Laboratories (GPS unit and 10 MHz atomic clock) synchronized to CERN SPS accelerator clock (the propagation delay to Hall B, $\sim 44 \mu\text{s}$, is not accounted for).

The discrimination thresholds for the PMT sum signals have been set at a threshold around 90 phe and 110 phe for the West and East half-module respectively, during a $60 \mu\text{s}$ spill gate in coincidence with each CNGS extraction. Therefore the CNGS-type trigger is generated when a signal from the internal PMTs of a TPC chamber is present within the CNGS gate. As a result about 80 events per day are recorded with a trigger rate of about 1 mHz . The analysis of the recorded neutrino interactions in LAr, shows a synchronization between ICARUS and the actual proton extraction time as written in the CNGS-database, sufficient to reconstruct the $10.5 \mu\text{s}$ width of the two proton spills (Fig. 7). The residual 2.4 ms delay is in agreement with the neutrino time of flight (2.44 ms).

The trigger for cosmic events requires a low discrimination threshold in order to max-

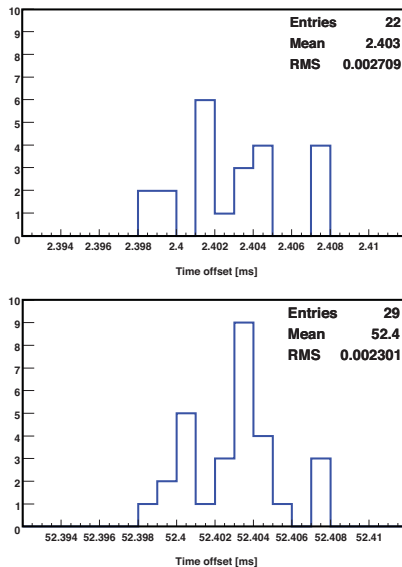


Figure 7: *Time difference between neutrino interaction absolute time in ICARUS T600 and the corresponding CNGS proton extraction time of the first spill. The two spills are $10.5\mu\text{s}$ wide and are separated by 50 ms.*

imize the low energy event detection down to tens of MeV. An efficient reduction of the spurious signals is provided exploiting the coincidence of the PMTs sum signals of the two adjacent chambers in the same module, relying on the 50 % cathode transparency.

As a preliminary result, a trigger rate of about 12 mHz per cryostat has been achieved leading to about 83 cosmic event rate per hour collected on the full T600 (only 6 % of the events are classified as empty by a visual scanning).

2 Early operations of ICARUS-T600 at LNGS

During the first months of 2010 the detector commissioning took place, leading to the successful filling with liquid Argon, DAQ and trigger activation and detection of the first events from the CNGS neutrino beam and cosmic rays.

Optimization of the detector performance - including cryogenic plant, signal and noise of wire chambers and PMTs, tuning of trigger and DAQ systems - has been performed with real events. The software for event visualization and reconstruction has been commissioned, including automatic procedures for event scanning and initial classification, based on the actual T600 running conditions. Some details of the ICARUS T600 operation in 2010 are described in this section.

2.1 Electron Lifetime measurements in ICARUS T600

The liquid Argon purity is a key issue for the detector imaging capability and to obtain a correct estimation of the ionization charge of events at any depth along the drift path [8].

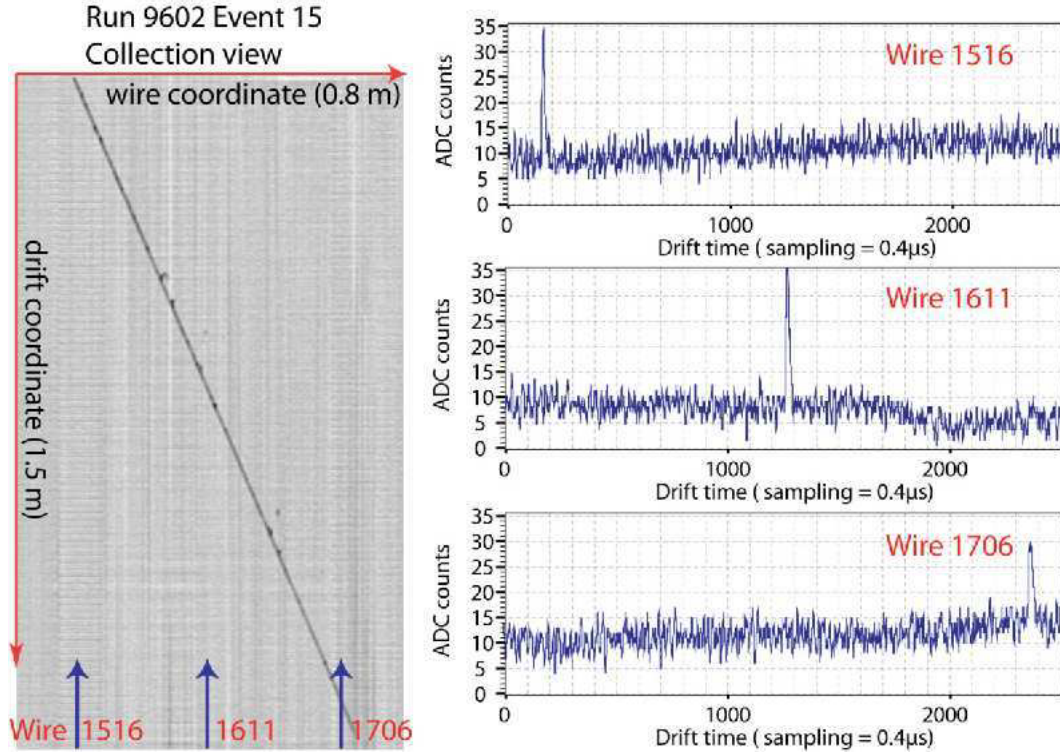


Figure 8: A muon track candidate for the purity measurement. Contributions of delta rays at large angle are rejected by the analysis.

Therefore a continuous monitoring of the electron lifetime is essential and it is performed measuring the charge attenuation of ionizing events.

Electron lifetime is measured directly by the charge signal attenuation in Collection view along through-going clean muon tracks, i.e. a track without evident associated δ -rays and γ 's, that extend at least 50 wires and 1200 time samples in both Collection and Induction2 views (Fig. 8). Only hits at less than 3 mm distance from the reconstructed track (linear fit) are retained. For each selected hit, the pulse area, proportional to the collected charge, is calculated over the signal baseline. At present the associated uncertainty is 3% given by the pre-amplifier gain uniformity. However, the precision of the lifetime measurement is dominated by the Landau fluctuations in the 10-20 % range depending on the effective sampling pitch determined by the track direction.

To further improve the measurement precision the following "truncation" method is adopted: 10% of the hit signals, with the largest energy deposition of the Landau tail of the dE/dx distribution, are rejected as well as 10% of smallest charge values with the worse signal to noise ratio. To ensure a uniform hit signal selection along the track, this method is applied to 8 equal length sub-segments. The RMS of the residual quasi-gaussian charge distribution, 14 % on average, is assigned as effective uncertainty on single hit charge measurement. Finally an exponential fit of the survived hit signals versus drift time provides the value of τ_T associated to the selected track

The electron lifetime τ_{ele} in each T300 module is the average of τ_T for a ~ 50 muon

sample selected during a day. The starting value in the West half-module was measured to be $\tau_{ele} \sim 650 \mu\text{s}$ with only gaseous re-circulation system active, sufficient to visualize tracks over the full drift distance (1.5 m equivalent to 1 ms drift time). In the East half-module the initial value was substantially lower due to a necessary short opening of the HV feed-through flange after LAr filling completion. A precise and systematic measurement of the electron lifetime in LAr was initiated soon after the beginning of the liquid recirculation in the two half-modules (Fig. 9). With the liquid recirculation turned on, the LAr purity steadily increased well above the 1.8 ms, the value obtained in the 2001 technical run, reaching 6.8 ms (West half-module) and 2.8 ms (East half-module) after 4 months of operation. This corresponds to a maximum free electron yield attenuation of 14 % and 30 % respectively, at the maximum drift distance of 1.5 m. Pumps maintenance required a couple of stops of the LAr recirculation lasting several days, resulting in a sudden degradation of the purity, which however never went below 1 ms. The different asymptotic values of the LAr purity in the two half-modules is currently under investigation.

3 Software and scanning

The software for event visualization and reconstruction is an evolution of what was originally developed for the 2001 test[9]. Developments were oriented both to add functionalities for reconstruction, and to improve the interface with the user and data.

The 3D track reconstruction starts from a 2D track finding algorithm based on an automatic clustering over an angle-position matrix. An approach based on principal curve analysis has been developed for three dimensional reconstruction [6]. Both algorithms have been developed and tested on Monte Carlo data and are now in the commissioning phase on real data. The information from track reconstruction fed the algorithms for muon momentum determination through multiple scattering [5], and for particle identification through neural networks trained on the shape of the dE/dx energy behavior. The initial effort at the beginning of the data taking has been put in the implementation and operation of a method for the determination of LAr purity from muon tracks, as described in section 2.1. Calibration data from test pulses have also been analyzed, providing a database table for wire equalization. A noise monitoring procedure, that automatically analyzes events as they are collected, is an important support to hardware debugging and fixing. Tools developed for this procedure are also implemented in the hit fitting stage, in order to exclude noisy wires from the reconstruction. This last item has proven to be an essential pre-requisite for data analysis at least in the initial phase of data tacking. The track finding and PID algorithms are in the commissioning phase, having been developed on MC events they need to be checked on real data. An example of a ν_μ CC candidate event is shown in Fig. 10(top). The long muon track, about 14 meters, is impressive. As another example, a low energy neutrino interaction as seen in the collection view is shown in Fig. 10(middle top).

In the initial phase of the commissioning a visual scanning of the collected events has been performed. The output of this scan is used to validate automatic algorithm for event pre-selection and noise rejection. An automatic procedure for event scanning and

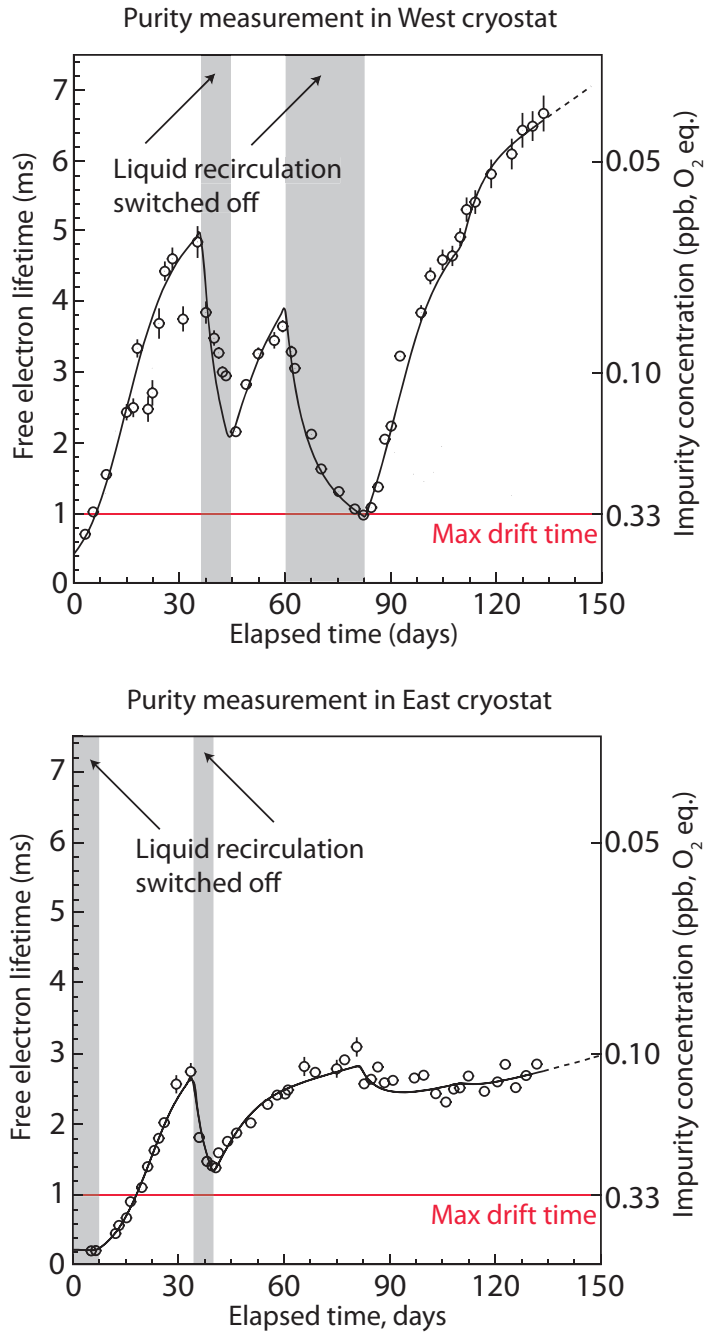


Figure 9: *Electron lifetime evolution in the West and East cryostats.*

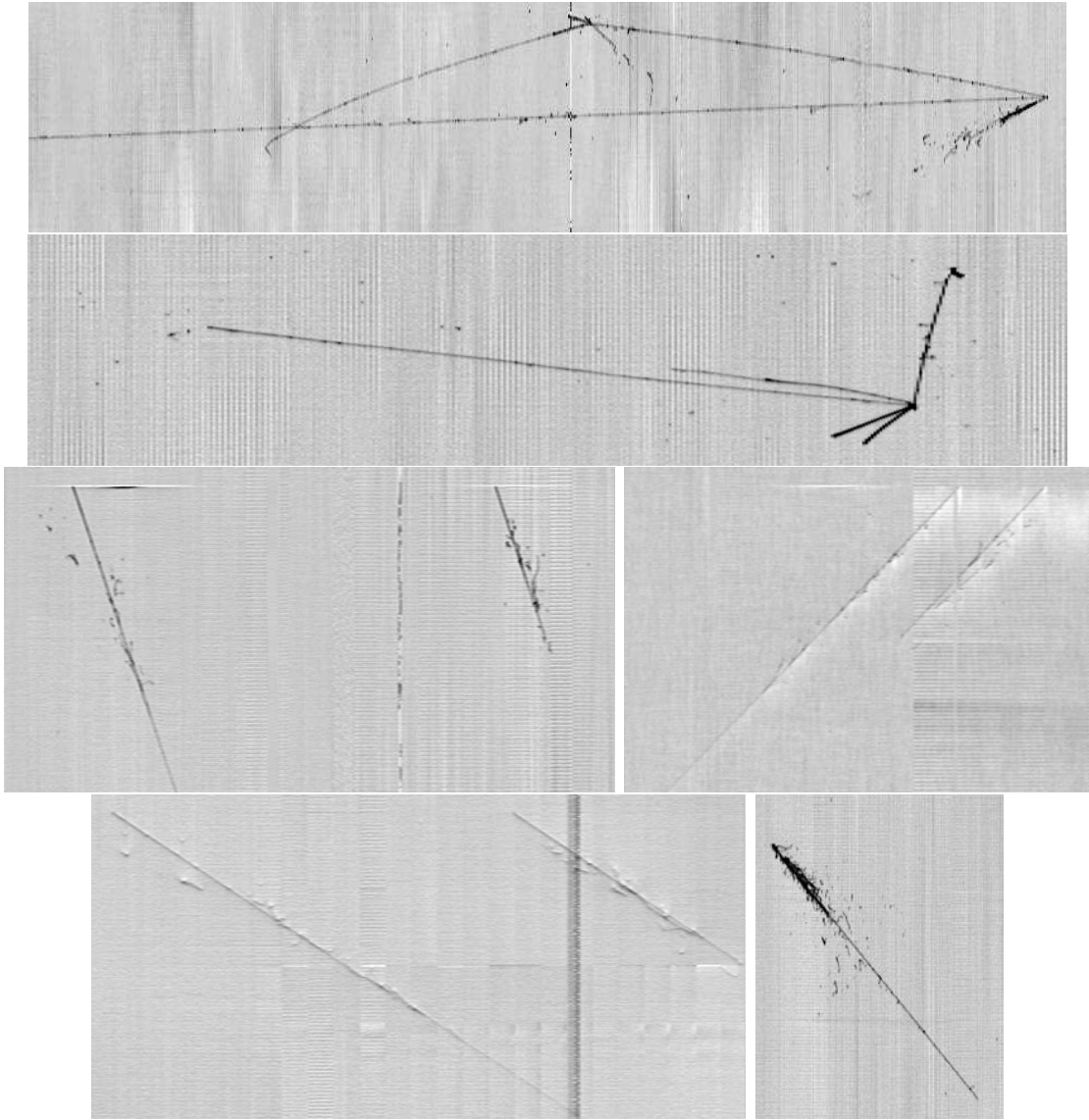


Figure 10: *Event gallery. From top to bottom: candidate ν_μ CC event in collection view, low-energy neutrino interaction, muon bundle in three projections (middle bottom and bottom left) and cosmic muon with e.m. activity (bottom right). Figures not to scale.*

initial classification has been developed and included in the official reconstruction and visualization code. A data sample of 11227 events collected in about 47 days during June and July and been distributed to the collaborating institutes to be visually classified to identify different event topologies. The event classification from the scanning is shown in the following table 1. About 55% of the events show physical activity. As can be seen

Empty	5032	(45%)
physical	6195	(55%)
muon	2462	
muon with e.m. activity	3042	
e.m. showers	282	
multiple muons	119	
charged primary interaction	63	
Hadronic shower	5	
neutrino interactions (CNGS)	38	
CNGS muon	87	
Other	97	

Table 1: *Classification of scanned events*

about 90% of the events are cosmic muons, in more than half of all cases accompanied by sizeable electromagnetic activity. Several examples of such events are shown in Fig. 8 and Fig. 10 (bottom right). Some interactions involving multiple muons are also observed as shown in the Fig. 10 (middle bottom and bottom left), where the redundancy in the 3D reconstruction provided by three independent stereo views, can also be appreciated. Most of the events classified as “other” are tails of cosmic interactions outside of the detector, or, in few cases, correspond to very noisy events.

4 Conclusions

The commissioning at the Gran Sasso Laboratory of the ICARUS T600 detector has been successfully performed in the course of 2010. The detector has smoothly reached optimal working conditions and is presently taking cosmic data, ready for its second year of CNGS neutrino beam. The successful assembly and operation of the ICARUS-T600 LAr-TPC demonstrate that the technology is mature and well suited for future massive detectors. The ICARUS experiment at the Gran Sasso Laboratory is so far the most important milestone for this technology and acts as a full-scale test-bed located in a difficult underground environment.

Acknowledgements

The ICARUS Collaboration would like to warmly thank the LNGS staff and in particular the cryogenic group, which contributed to the detector commissioning and operation. A special thank goes to Arnaldo Di Cesare, Luca Scarcia and Marco Brugnolli for their

efficient technical support. Finally, we wish to acknowledge the valuable contribution of Andrea Triossi to the setup of the trigger system.

List of Publications

1. D. Stefan, Acta Phys. Pol. B41, 2010, 1547-1553.
2. A. Guglielmi, Neutrino 2010 Conference Proceeding. Submitted for publication.
3. P. Sala, NOW 2010 Conference Proceeding. Submitted for publication.
4. C. Rubbia, NNN 2010 Conference Proceeding. Submitted for publication.
5. C. Farnese, DISCRETE 2010 Conference Proceeding. Submitted for publication.

References

- [1] C.Rubbia, CERN-EP/77-08 (1977).
- [2] S. Amerio et al., Nucl. Instr. Meth. **A527**, (2004) 329.
- [3] T. Doke et al., Nucl. Instr. Meth. **A269**, (1988) 291.
- [4] A. Ankowski et al., Nucl. Instr. Meth. **A556**, (2006) 146.
- [5] A. Ankowski et al., Eur. Phys. J. **C48**, (2006),667.
- [6] B. Kegl, A. Krzyzak, T. Linder, K. Zeger, IEEE Transactions on Pattern Analysis and Machine Intelligence **22 no. 3** (2000), 281 .
- [7] B. Baibussinov et al., JINST **5**, (2010), 12006.
- [8] B. Baibussinov et al., JINST **5**, (2010), 03005.
- [9] S.Amoruso et al., Eur. Phys. J. **C33**, (2004) 233.

LUNA: Laboratory for Underground Nuclear Astrophysics

M. Anders^a, D. Bemmerer^a, A. Bellini^b, C. Broggini^c, A. Cacioli^{c,d,e}, P. Corvisiero^b,
H. Costantini^f, Z. Elekes^{a,g}, M. Erhard^c, A. Formicola^h, Zs. Fülöp^g, G. Gervinoⁱ,
A. Guglielmetti^j, C. Gustavino^{h,k}, Gy. Gyürky^g, G. Imbriani^l, M. Junker^h, B. Limata^l,
M. Marta^a, C. Mazzocchi^j, R. Menegazzo^c, P. Prati^b, V. Roca^l, C. Rolfs^m, C. Rossi
Alvarez^c, E. Somorjai^g, O. Stranieroⁿ, F. Strieder^m, T. Szücs^g, F. Terrasi^o,
H.P. Trautvetter^m, D. Trezzi^p

SPOKESPERSON: A. GUGLIELMETTI

^aHelmholtz-Zentrum Dresden-Rossendorf, Dresden, Germany

^bUniversità degli Studi di Genova and INFN, Genova, Italy

^cINFN, Padova, Italy

^dUniversità di Siena, Siena, Italy

^eCentro di GeoTecnologie, San Giovanni Valdarno, Italy

^fINFN, Genova, Italy

^gInstitute of Nuclear Research (ATOMKI), Debrecen, Hungary

^hINFN, Laboratori Nazionali del Gran Sasso (LNGS), Assergi (AQ), Italy

ⁱUniversità degli Studi di Torino and INFN, Torino, Italy

^jUniversità degli Studi di Milano and INFN, Milano, Italy

^kINFN, Roma 1, Italy

^lUniversità degli Studi di Napoli “Federico II”, and INFN, Napoli, Italy

^mInstitut für Experimentalphysik III, Ruhr-Universität Bochum, Bochum, Germany

ⁿOsservatorio Astronomico di Collurania, Teramo, and INFN Napoli, Italy

^oSeconda Università di Napoli, Caserta and INFN, Napoli, Italy

^pINFN, Milano, Italy

Abstract

Aim of the LUNA experiment is the measurement of thermonuclear fusion cross sections relevant for stellar nucleosynthesis. In the course of the year 2010, analysis of the results obtained for the $^{14}\text{N}(p,\gamma)^{15}\text{O}$ reaction studied with a clover composite detector and of the results obtained for the $^{15}\text{N}(p,\gamma)^{16}\text{O}$ reaction studied with enriched solid targets and a high efficiency detecting apparatus were completed. The experimental set-up used for the measurement of the the $\text{D}(\alpha,\gamma)^6\text{Li}$ reaction was finalized and a complete characterization of the beam induced background was

obtained. Moreover, a first data taking of three weeks was performed. The target preparation procedure for the measurement of the $^{17}\text{O}(p,\gamma)^{18}\text{F}$ reaction was finalized and a complete study on targets produced with ^{18}O enriched water using a well known resonance of the $^{18}\text{O}(p,\gamma)^{19}\text{F}$ reaction was performed. A feasibility study of the $^{17}\text{O}(p,\gamma)^{18}\text{F}$ resonance at 193 keV using the activation technique was also undertaken. The LUNA-MV project was discussed with the LNGS Scientific Committee and with a dedicated committee. As a consequence, an improved and better specified project came out. This was judged by the Scientific Committee as very positive and worthwhile to be further pursued.

1 The $^{14}\text{N}(p,\gamma)^{15}\text{O}$ reaction studied with the clover detector

The CNO cycle is responsible for most of the energy produced in stars heavier than the Sun. Its stellar rate is given by the slowest process, the $^{14}\text{N}(p,\gamma)^{15}\text{O}$ reaction. It contributes less than 1% to our Sun's luminosity [1], nevertheless it produces neutrinos via the β^+ decay of ^{13}N and ^{15}O , that could bring direct information of the physics conditions in the solar core. They can in principle be measured on Earth in underground experiments like Borexino [2]. It has been suggested [3] to use the expected CNO neutrino fluxes to determine the carbon and nitrogen abundances in the solar core, but precise $^{14}\text{N}(p,\gamma)^{15}\text{O}$ reaction rate is required. That would help solving the solar metallicity problem [4], i.e. a recent discrepancy between solar models and helioseismological data.

The $^{14}\text{N}(p,\gamma)^{15}\text{O}$ cross section is the sum of the contributions from capture to different excited levels E_x and to the ground state in ^{15}O . It has been previously studied at LUNA [5, 6, 7]. The discrepancy of a factor two between LUNA [5] and TUNL [8] groups with respect to the extrapolated S-factor for the capture to the ground state triggered a new study, described here.

This experiment was done at three proton energies $E_p = 359, 380, 399$ keV, with solid titanium nitride targets. Using a Clover composite germanium detector, the systematic uncertainty due to the true coincidence summing-in correction was reduced by a factor 30. The target degradation was monitored regularly by scanning the $E_p = 278$ keV resonance.

As a first step, the ground state data have been obtained relative to the well-known capture to the 6792 keV excited state in ^{15}O . A new R-matrix fit has been performed that yielded $S_{\text{GS}} = 0.20 \pm 0.05$ keV barn [9]. That solved the discrepancy in literature in favour of the previous LUNA result of 0.25 ± 0.06 keV barn [5] and ruled out the TUNL conclusion $S_{\text{GS}} = 0.49 \pm 0.08$ keV barn [8]. The ground state capture now contributes less than 4% uncertainty to the total $S_{\text{tot}}(0)$, instead of the previous 15%.

In a second phase, the cross sections for capture to the ground state and to the 5181, 6172, and 6792 keV excited states have been determined with an absolute method [10]. The target stoichiometry and profile and the measured beam charge were considered, that made the systematic uncertainties of final results larger than in the relative case. The obtained S-factors are plotted in figure 1. They provide an additional independent data set with competitive uncertainties.

Furthermore, new precise branching ratios for the decay of the $E_p = 278$ keV resonance

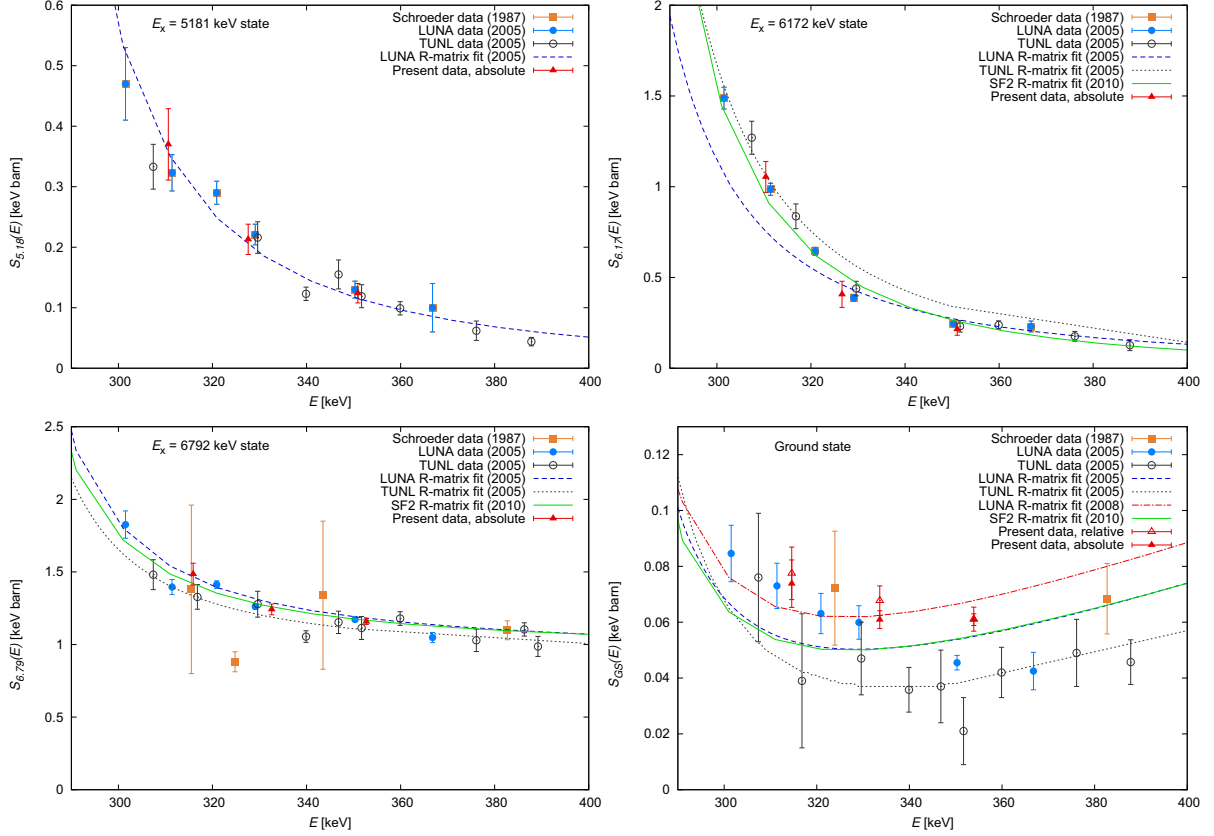


Figure 1: S-factors for the four most important transitions: capture to the ground state and to the excited states at $E_x = 6792$, 6172 , and 5181 keV. The data and fits are from Schröder et al. [11], LUNA 2005 [5, 6], TUNL [8] and present [9, 10]. The recent fits SF2 from the review [13] are also included.

have been obtained.

These results are included in the recently updated solar model [4]. More details are discussed in a Ph.D. thesis [12]. This work has been supported by DFG (BE4100/2-1).

2 The $^{15}\text{N}(p,\gamma)^{16}\text{O}$ reaction: a new measurement with enriched solid target and a high efficiency detecting apparatus

The $^{15}\text{N}(p,\gamma)^{16}\text{O}$ reaction is an important reaction belonging to the CNO cycles. As a matter of fact, it links the first CNO cycle to the second one allowing for the production of the oxygen isotopes and giving access also to the third and fourth cycles that are responsible for the production of the elements until neon. The astrophysical S-factor of the $^{15}\text{N}(p,\gamma)^{16}\text{O}$ reaction is dominated by the resonant capture to the ground state through the interference of two resonances at $E_R = 312$ keV and $E_R = 964$ keV with $J^\pi = 1^-$ where E_R is the resonance energy in the center of mass system. This reaction has been

studied previously by Hebbard in 1960 [14] and Rolf and Rodney in 1974 [15]. Hebbard reported an S-factor extrapolated to zero energy $S(0) = 32.0 \pm 5.8$ keV barn while Rolfs and Rodney published a value of $S(0) = 64 \pm 6$ keV barn. The NACRE [16] database uses the most recent Rolfs and Rodney value for the extrapolated S-factor. Recently, two new R-matrix fits [17, 18] have been published on these two measurements reporting different extrapolated S-factor with respect to the one quoted in NACRE. LUNA already performed an intensive study of this reaction in the last years [19, 20]. Moreover, a new experiment has been designed to measure the $^{15}\text{N}(p,\gamma)^{16}\text{O}$ reaction at the energies of the Gamow peak in nova explosion and in AGB stars, never explored before.

The experiment was done using a dedicated high efficiency setup (see Fig. 2).

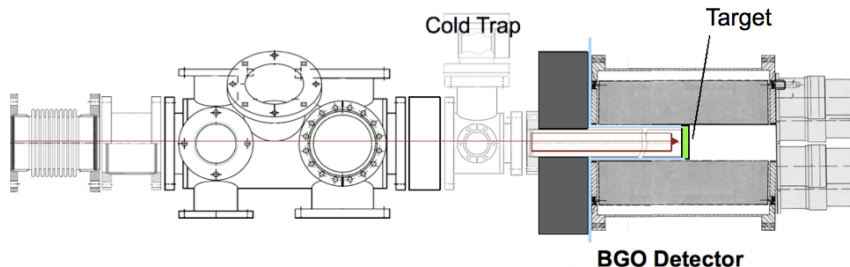


Figure 2: Experimental apparatus used for the $^{15}\text{N}(p,\gamma)^{16}\text{O}$ reaction measurement.

The beam passed through three apertures (10.0 mm, 3.0 mm, and 5.0 mm in diameter, respectively) which allowed to focus it each time on the same area on the target surface. The third collimator was placed at 1 m distance from the target, oriented at 90° with respect to the beam direction. The target was water-cooled to reduce the deterioration due to the impinging beam since a typical beam intensity of $150 \mu\text{A}$ was delivered onto it by the accelerator. A cold trap, filled with liquid nitrogen, minimized the carbon build-up on target: a 1 m long copper tube (28 mm diameter) was placed in between the last collimator and the target and it was connected thermally to the cold trap. It extended to within 2 mm from the target. A negative voltage (300 V) was applied between this tube and the target to suppress the secondary electrons escape both from the last aperture and from the target. The detection efficiency was enhanced by choosing a 4π -BGO detector with a cylindrical shape and a coaxial hole where the target was hold in order to cover most of the total solid angle. The detector response was determined with a simulation code which was checked with data taken with radioactive sources and the study of the $E = 163$ keV resonance of the $^{11}\text{B}(p,\gamma)^{12}\text{C}$ reaction. Another solution adopted to increase the statistic was the selection of TiN targets enriched in ^{15}N up to a nominal value of 98%. In this way, the contribution from beam induced background on boron deposited on the beam line or target was proven to be negligible. In fig. 3 the sum spectrum acquired at 80 keV in the laboratory system shows how these solutions allowed to measure with good statistic at energies never reached before.

The final S-factor (see Fig. 4 for the preliminary data) cover for the first time the whole Gamow peak in nova scenarios and investigate the region of energies relative to the hydrogen burning shell in AGB stars. A factor 2 reduction in the cross section was found, confirming the previous LUNA works.

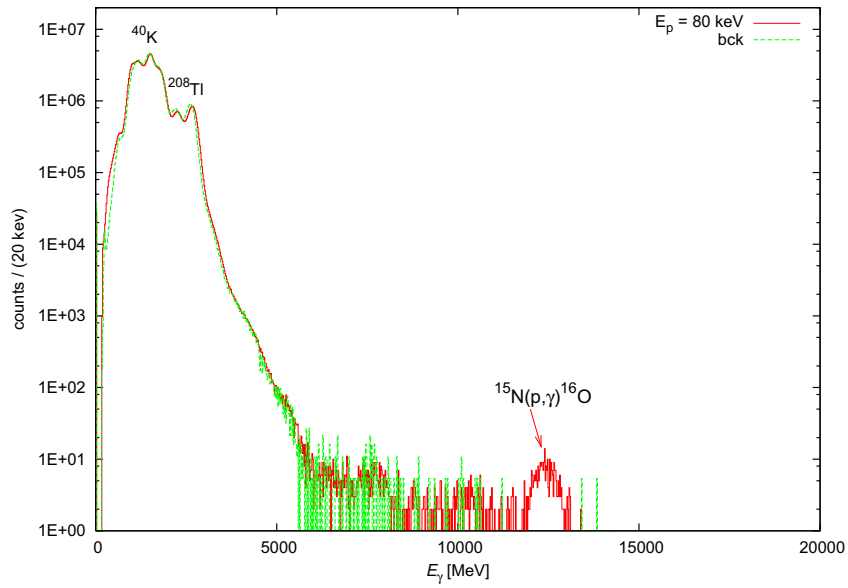


Figure 3: Sum spectrum acquired at $E_p = 80\text{keV}$. A background spectrum is also shown normalized to the same measurement time.

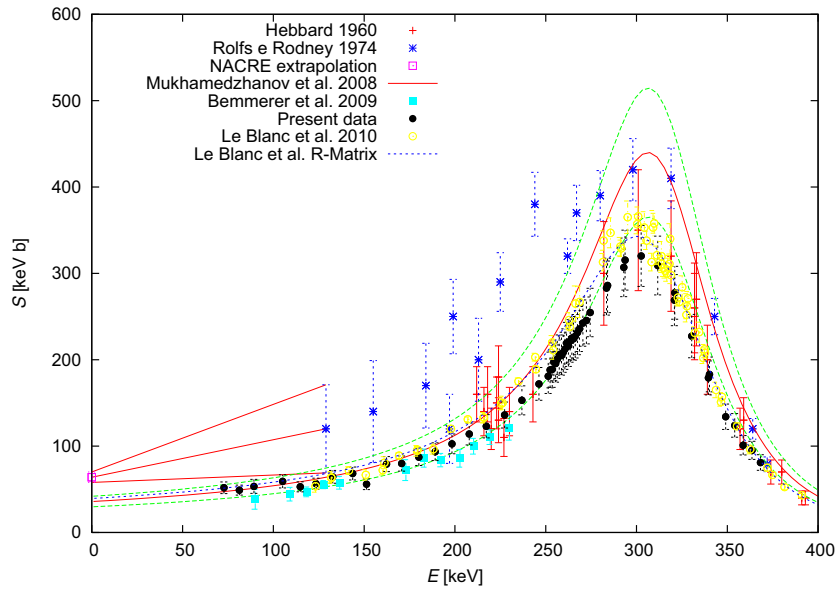


Figure 4: S-factor of the $^{15}\text{N}(p,\gamma)^{16}\text{O}$ reaction and R-Matrix fits. Black points refer to the last data (preliminary) obtained with enriched solid targets and a BGO detector.

3 Measurement of the ${}^2\text{H}(\alpha,\gamma){}^6\text{Li}$ reaction

It is well-known that the lithium abundance observed in the so-called Spite plateau for metal-poor stars [21] is about a factor three lower than the prediction of big-bang nucleosynthesis [22, 23], with the standard nuclear physics inputs. The recent LUNA data on the ${}^3\text{He}(\alpha,\gamma){}^7\text{Be}$ reaction [24, 25] show a cross section that is a few percent higher than previously believed, actually worsening the problem. This reaction dominates ${}^7\text{Li}$ production through radioactive ${}^7\text{Be}$ decaying to ${}^7\text{Li}$.

This situation (fig. 5) is made more complex by the discovery of the less abundant stable lithium isotope ${}^6\text{Li}$ (7.6% isotopic abundance on Earth) in the spectra of metal-poor stars [26]. These data have been criticized, but several detections of the isotope ${}^6\text{Li}$ in metal-poor stars remain [27]. As it is difficult to devise cosmic-ray scenarios that both destroy ${}^7\text{Li}$ and produce ${}^6\text{Li}$ [28], the only approach solving both lithium problems at the same time seems to lie in new physics [29, 30].

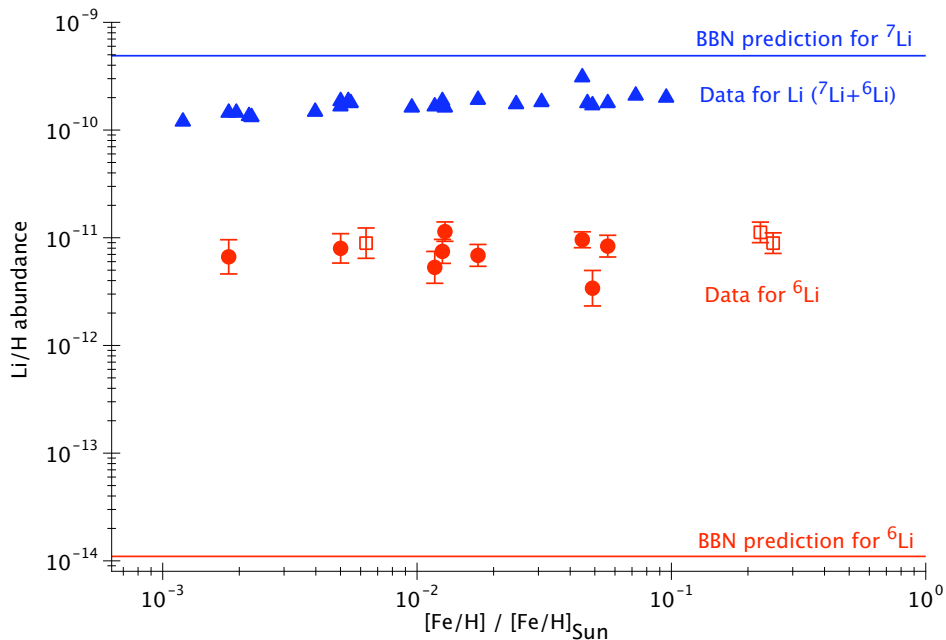


Figure 5: Abundances for lithium (mainly ${}^7\text{Li}$) and ${}^6\text{Li}$ as predicted by big-bang nucleosynthesis [22], and as observed in metal-poor halo stars [26, and references therein].

However, before exotic scenarios can be pursued, it is necessary to first rule out a standard physics solution, in this case a much higher production of ${}^6\text{Li}$ in big-bang nucleosynthesis. As is the case for ${}^7\text{Li}$, also ${}^6\text{Li}$ production in big-bang nucleosynthesis is dominated by one single reaction. This is the ${}^2\text{H}(\alpha,\gamma){}^6\text{Li}$ reaction [22].

The ${}^2\text{H}(\alpha,\gamma){}^6\text{Li}$ reaction has been studied previously in direct experiments at energies far above the big-bang window of interest [31, and references therein]. Due to the exceedingly low cross section at big-bang energies, it has been attempted to study it by Coulomb dissociation of 26 A MeV ${}^6\text{Li}$ projectiles at Karlsruhe, and cross section data have been presented [32]. However, a more recent Coulomb dissociation experiment

with 150 AMeV ${}^6\text{Li}$ beam at GSI concluded that even at the much higher energy, nuclear breakup dominated the observed yield, and no cross section could be extracted [33]. This means the Karlsruhe data [32] should be interpreted as an upper limit, containing mainly nuclear breakup. Even so, a fit of the angular distribution of the GSI data showed Coulomb-nuclear interference, and a theoretical S-factor curve has been presented [33]. A measurement of the cross section is therefore only possible with the direct method, using a low-background environment such as LUNA.

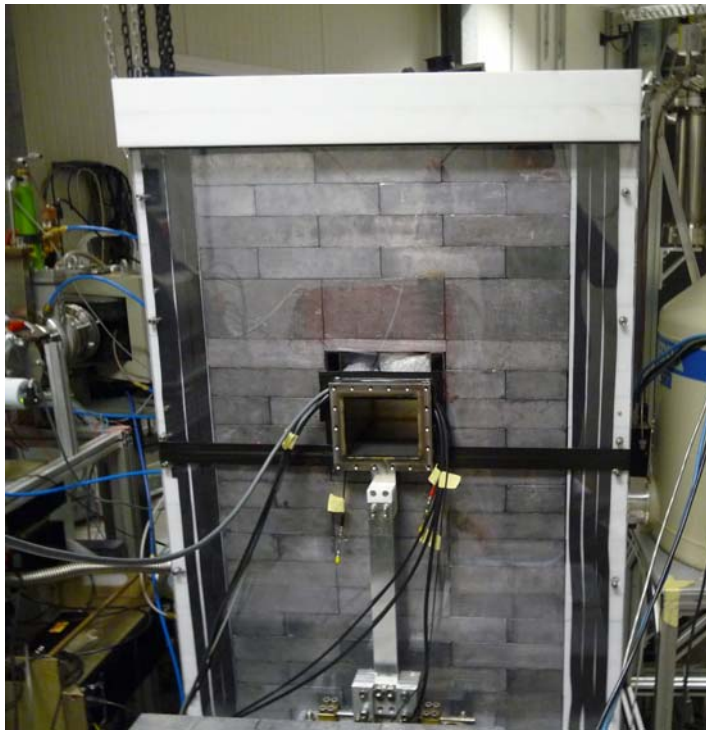


Figure 6: Photo of the setup, taken from the downstream end. The borated polyethylene shielding on the sides and on the top is well visible. The shielding on the downstream end is open to allow this view.

The LUNA study of the ${}^2\text{H}(\alpha,\gamma){}^6\text{Li}$ cross section was ongoing during the 2010 calendar year. It is hampered by background indirectly induced by the ion beam: the α -beam produces energetic deuterons by Rutherford scattering in the ${}^2\text{H}$ gas. The energetic deuterons, in turn, collide with other deuterons in the gas or in the walls of the vacuum chamber, and the ${}^2\text{H}(\text{d},\text{n}){}^3\text{He}$ reaction can occur. The neutrons released by this reaction then produce a beam induced background in the HPGe detector.

Based on extensive simulations and some in-beam tests, this process is now well-understood, and the resulting neutron yield has been reduced. In order to limit possible effects on other experiments in the Gran Sasso underground facility, the neutron production rate has been limited to less than 10 s^{-1} at all times, and the effective beam-on running time of the experiment was limited to three weeks in 2010. A neutron shield of borated polyethylene was built around the experimental setup (fig.6), and no neutron signal above background has been detected in a neutron counter placed in the immediate

vicinity of the experiment.

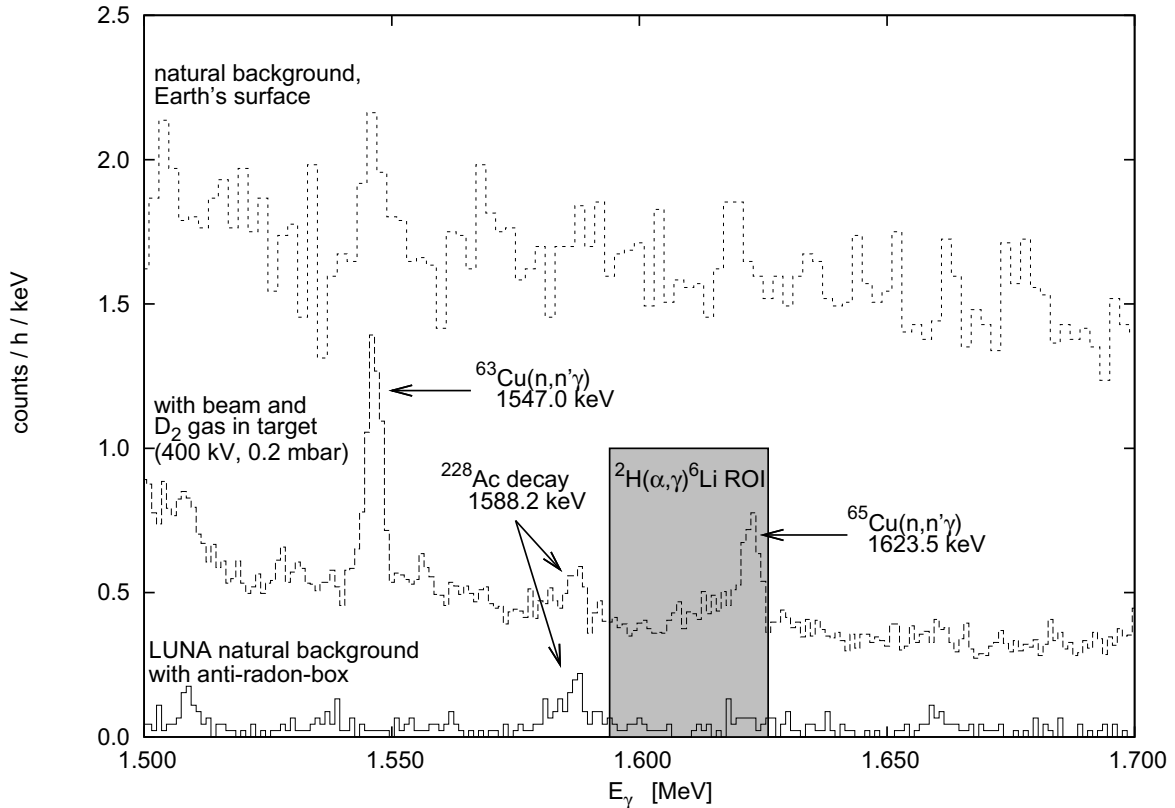


Figure 7: Observed spectrum in the γ -ray detector.

As expected, the preliminary γ -ray spectrum does not yet show the signature of the expected ${}^2\text{H}(\alpha,\gamma){}^6\text{Li}$ γ -peak (fig. 7). In order to correctly subtract the neutron-induced background in the spectrum, new experiments using ${}^3\text{He}$ beam are planned for 2011. Monte Carlo simulations show that with ${}^3\text{He}$ beam, the neutron-induced background in the HPGe detector should be the same as with ${}^4\text{He}$ beam. However, no ${}^2\text{H}(\alpha,\gamma){}^6\text{Li}$ signal can be produced with ${}^3\text{He}$ beam, so this experiment will produce a pure background spectrum that can then be subtracted. The permission to produce ${}^3\text{He}$ beam in the LUNA 400 kV accelerator is expected to be granted by the responsible authorities in early 2011.

4 Measurement of the ${}^{17}\text{O}(\text{p},\gamma){}^{18}\text{F}$ reaction

The ${}^{17}\text{O}+\text{p}$ thermonuclear reaction rate is relevant to hydrogen burning in a variety of astrophysical sites, including red giant stars, massive stars, Asymptotic Giant Branch (AGB) stars, and classical novae. Indeed, the precise knowledge of CNO reaction rates is of crucial importance for the interpretation of new astronomical observations. For example, the determination of the age of old globular clusters strongly depends on the adopted

rate of CN-cycle reactions while star's surface element abundances during AGB phase depend both on convection and on CNO reaction rates. AGB stars are important sites for the chemical evolution of the galaxies. A low- or medium-mass star reaches the AGB phase when it develops a carbon-oxygen core, surrounded by helium and hydrogen shells. Observations of the surface composition of Red Giant stars show wide ranges of the $^{16}\text{O}/^{17}\text{O}$ ratios that reveal an important enrichment of ^{17}O relative to the solar value. Similarly, recent discoveries of pre-solar meteoritic grains allow O-isotopic ratios to be measured with a precision unavailable in typical stellar observations, linking ^{17}O abundances to nuclear ^{17}O -destruction rates. AGB stars are also one of the sites where fluorine can be synthesized. The origin of fluorine is a longstanding problem in nuclear astrophysics, as it shows an enhancement factor (2 to 30 with respect to the solar abundance) that no stellar model has been able to reproduce. Another opportunity to test nucleosynthesis models is offered by classical novae through direct observations of the composition of the ejected matter and the detection of gamma rays emitted by suitably long-lived radioisotopes such as ^{18}F . Detection of such gamma rays can then put constraints on current nova models and the associated nucleosynthesis processes. The synthesis of ^{18}F crucially depends on the $^{17}\text{O}(\text{p},\gamma)^{18}\text{F}$ reaction and its competition with the $^{17}\text{O}(\text{p},\alpha)^{14}\text{N}$ as an alternative branching route. Unfortunately, a detailed interpretation of all these observations suffers from uncertainties in the $^{17}\text{O}(\text{p},\gamma)^{18}\text{F}$ and $^{17}\text{O}(\text{p},\alpha)^{14}\text{N}$ reaction rates at relevant stellar energies. For example, it has been estimated that a variation of their rates within current uncertainties will lead to more than a factor of 2 change in the abundances of ^{17}O and ^{18}F in novae events. Only improved measurements will help to put firmer constraints on existing models. The energy level scheme of the ^{18}F compound nucleus is quite complex (fig. 8): the low resonances located at $E_{R,\text{lab}} = 70$ and 193 keV are believed to dominate the Novae energy region.

In the framework of the LUNA program the measurement of the resonance at $E_{R,\text{lab}} = 193$ keV will be performed at the 400 kV accelerator in a complementary approach: the detection of the prompt gamma-ray using an HPGe detector, and the activation method looking for the ^{18}F β^+ activity ($T_{1/2}=110$ min). The strength of this resonance has been measured by different authors ([35],[36]) but still there is a disagreement by more than one standard deviation. New data are highly desirable, as also pointed out by the same authors. The measurements of the $^{17}\text{O}(\text{p},\gamma)^{18}\text{F}$ cross section demands the fulfillment of various requirements: first of all the quality of the solid target used. High density, high purity and high stability are requested. The targets are produced in the LNGS chemistry laboratory by an anodization process (see fig. 9 for a photo of the apparatus) of thick tantalum backings in 70% ^{17}O enriched water ($^{18}\text{O} \simeq 0.6\%$). This procedure [34] results in targets (see fig. 10) with well defined stoichiometry: Ta_2O_5 . An extensive study was dedicated to the purity of the target: light element impurities can produce, due to their relatively low Coloumb barrier, intense γ -ray lines which give rise to a background that hampers the analysis of ^{17}O spectra. Gamma-ray lines from proton capture reactions on ^{11}B , ^{12}C , ^{19}F were investigated. A precise knowledge of target composition, stoichiometry, and density profile is an essential ingredient for an absolute cross section measurement. Moreover, these proprieties have to be stable under beam bombardments. Repeated measurements of the resonance profile during long term high power bombardments allow for monitoring the target quality and stability. A sample of the excitation function obtained

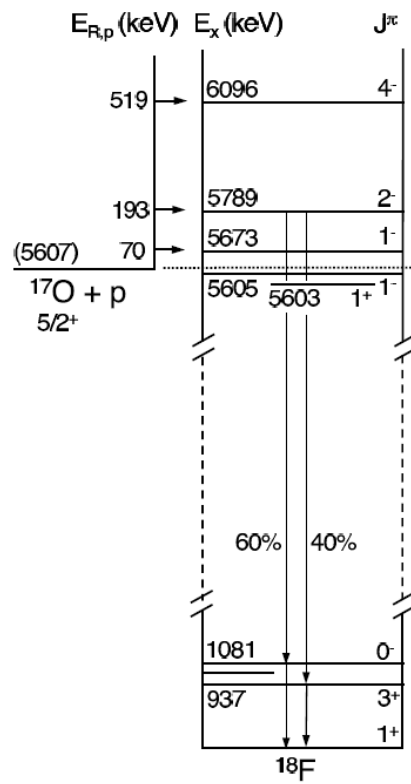


Figure 8: The level structure of ^{18}F

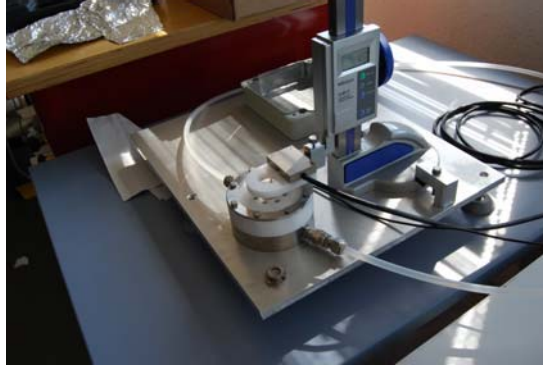


Figure 9: Anodizing apparatus



Figure 10: Tantalum Oxide target: brilliant color due to the oxide/metal interface interference were observed. Each color is related to a different thickness.

with ^{18}O anodized target, out of a large number of test performed with different treated backings in order to remove some of the impurities, is shown in fig. 11. First tests for the activation feasibility were also concluded using the STELLA (Sub Terranean Low Level Assay) apparatus at LNGS. A preliminary half life analysis confirmed the detection of the radioactive ^{18}F nuclei (see fig. 12). This experimental project of the LUNA collaboration is also supported by Corrado Salvo (INFN-LNGS), Matthias Laubenstein (INFN-LNGS), Marialuisa Aliotta and David Scott (University of Edinburgh), Antonino Di Leva (INFN-Na).

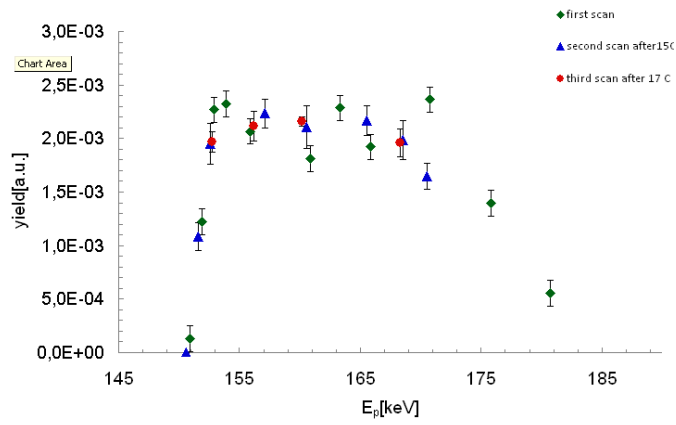


Figure 11: The excitation function of the $^{18}\text{O}(p,\gamma)^{19}\text{F}$ reaction at $E_{R,\text{lab}}=153$ keV, with a total charge of 32C (red points)

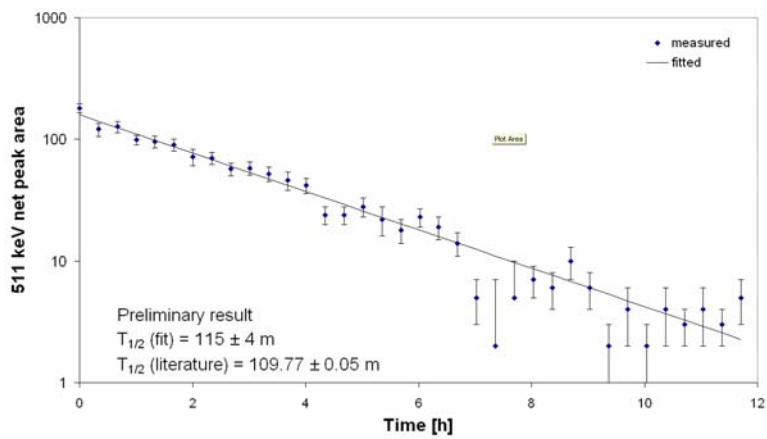


Figure 12: The half life of ^{18}F β^+ activity

5 The LUNA-MV project

In 2007 the LUNA collaboration submitted a Letter of Intent (LoI) to the LNGS Scientific Committee (SC) for the installation of a MV machine underground at LNGS. This document contained a list of reactions belonging to the Helium burning that cannot be studied with the present LUNA 400 kV accelerator since the requested energy range is higher than the maximum reachable by such machine. This is due to the fact that such reactions are important in stellar environment at higher temperatures corresponding to higher energies with respect to those involved in the hydrogen burning reactions studied so far. This document was integrated in autumn 2007 by an addendum requested by the SC (LoI addendum), better specifying aims of the project and neutron pollution issues. In November 2009, following the recommendation of SC "*The committee recommends that the director set up a small committee to address the issue of possible neutron generation and the operation of the experiment, in order to ensure that the neutron backgrounds are at a suitable level.*" a committee was formed. Different expertises in the field of nuclear astrophysics, neutron shielding, accelerators, safety and radioprotection were covered by this committee formed by five scientists. The collaboration and the committee interacted over several months on different issues. Upon request, the collaboration provided a document (LoI update) with updated calculations of the neutron production rates obtained with the most recent results for the respective cross sections, showing that the maximum neutron production rate is 1800 n/s. Realistic values for the beam intensity and target stoichiometry, isotopic ratio and areal density were considered, while the maximum beam energy was chosen in order to reach a good overlap with existing literature data. The maximum alpha beam intensity is due to the technical characteristics of the foreseen accelerator, which have now been better specified with respect to the original LoI. The machine would be a closed, single-ended positive-ion accelerator with a maximum terminal voltage of 3.5 MV. Following the submission of LoI update, several questions were raised by the committee and addressed by the collaboration. The possible location of the facility turned out to be one the major issues which influences all the other technical decisions (shielding, pollution, safety,...). The interferometric node was identified as the best possible solution due to its size and distance from the other LNGS experiments. For this solution a few more problems have still to be addressed among which the presence of another experiment in situ and the water uptake inlet for the Teramo aqueduct. At the SC meeting of May 2010 the review of the committee on the LUNA MV project was presented and brought to a very positive recommendation by the SC to further pursue the realization of the project. Therefore, the first steps of a close interaction with the LNGS management were undertaken. With the help of the engineers working at the Laboratory a technical project of the accelerator + shielding is going to be finalized in the next months. The technical study of the site for the LUNA MV project as well as contacts with possibly interested groups have been inserted as key issues in the financing request of the LUNA collaboration to INFN for 2011.

6 List of Publications

- “*Constraining the S factor of $^{15}\text{N}(p,\gamma)^{16}\text{O}$ at Astrophysical Energies*”,
P. J. LeBlanc, G. Imbriani, J. Goerres, M. Junker, R. Azuma, M. Beard, D. Bemmerer, A. Best, C. Brogгинi, A. Caciolli, P. Corvisiero, H. Costantini, M. Couder, R. deBoer, Z. Elekes, S. Falahat, A. Formicola, Zs. Fulop, G. Gervino, A. Guglielmetti, C. Gustavino, Gy. Gyurky, F. Kaeppler, A. Kontos, R. Kuntz, H. Leiste, A. Lemut, Q. Li, B. Limata, M. Marta, C. Mazzocchi, R. Menegazzo, S. O’Brien, A. Palumbo, P. Prati, V. Roca, C. Rolfs, C. Rossi Alvarez, E. Somorjai, E. Stech, O. Straniero, F. Strieder, W. Tan, F. Terrasi, H.P. Trautvetter, E. Uberseder, M. Wiescher,
Phys. Rev. C 82, 055804 (2010)
- “*New experimental study of low-energy (p,γ) resonances in magnesium isotopes*”,
B. Limata, F. Strieder, A. Formicola, G. Imbriani, M. Junker, H.W. Becker, D. Bemmerer, A. Best, R. Bonetti, C. Brogгинi, A. Caciolli, P. Corvisiero, H. Costantini, A. DiLeva, Z. Elekes, Zs. Fulop, G. Gervino, A. Guglielmetti, C. Gustavino, Gy. Gyurky, A. Lemut, M. Marta, C. Mazzocchi, R. Menegazzo, P. Prati, V. Roca, C. Rolfs, C. Rossi Alvarez, C. Salvo, E. Somorjai, O. Straniero, F. Terrasi, H.-P. Trautvetter,
Phys. Rev. C 82, 015801 (2010)
- “*An actively vetoed Clover γ -detector for nuclear astrophysics at LUNA*”,
T. Szucs, D. Bemmerer, C. Brogгинi, A. Caciolli, F. Confortola, P. Corvisiero, Z. Elekes, A. Formicola, Zs. Fulop, G. Gervino, A. Guglielmetti, C. Gustavino, Gy. Gyurky, G. Imbriani, M. Junker, A. Lemut, M. Marta, C. Mazzocchi, R. Menegazzo, P. Prati, V. Roca, C. Rolfs, C. Rossi Alvarez, E. Somorjai, O. Straniero, F. Strieder, F. Terrasi, and H.P. Trautvetter (The LUNA collaboration),
Eur. Phys. J. A 44, 513-519 (2010)
- “*LUNA: Nuclear Astrophysics Deep Underground*”,
C. Brogгинi, D. Bemmerer, A. Guglielmetti, and R. Menegazzo,
Annual Review of Nuclear and Particle Science, 60 (2010) p.53.
- “*Underground study of $^{15}\text{N}(p,\gamma)^{16}\text{O}$ at stellar energies*”,
A. Caciolli,
PhD thesis, Università degli studi di Padova, 2010.
- “*Study of the $^{15}\text{N}(p,\gamma)^{16}\text{O}$ reaction at the LUNA accelerator with a gas target setup*”,
A. Caciolli for the LUNA collaboration,
AIP Conf. Proc. 1213, (2010) 192.
- “*Study of the $^{15}\text{N}(p,\gamma)^{16}\text{O}$ Reaction at LUNA with a Solid Target*”,
V. Capogrosso for the LUNA collaboration,
AIP Conf. Proc. 1213, (2010) 195.

- “*Study of the $^{15}\text{N}(p,\gamma)^{16}\text{O}$ reaction at the LUNA accelerator with a BGO detector*”,
A. Caciolli for the LUNA collaboration,
J. Phys.:Conf. Ser. 202, (2010) 012036.
- “*Nuclear Physics Underground*”,
D. Bemmerer for the LUNA collaboration,
AIP conference proceedings 1265, (2010) 121.
- “*Progress of LUNA*”,
A. Guglielmetti for the LUNA collaboration,
J. Phys.:Conf. Ser. 202, (2010) 012031.
- “*Nuclear astrophysics deep underground: the LUNA experiment*”,
C. Mazzocchi for the LUNA collaboration,
Proceedings of Science PoS (Bormio2010) 055.
- “*Nuclear astrophysics deep underground: the case of the $^{15}\text{N}(p,\gamma)^{16}\text{O}$ reaction at LUNA*”,
C. Mazzocchi for the LUNA collaboration,
Proceedings of the 12th Int.Conf. on Nuclear Reaction Mechanisms, Varenna, Italy,
2009, CERN-Proceedings-2010-001, p. 495.
- “*Reaction rate measurements in underground laboratories*”,
H. Costantini for the LUNA collaboration,
Proceedings of Science PoS (NIC XI) 014.
- “*Study of the BBN reaction $D(\alpha,\gamma)^6\text{Li}$ deep underground at LUNA*”,
M. Erhard for the LUNA collaboration,
Proceedings of Science PoS (NIC XI) 003.

7 Conference and seminar contributions

- M. Marta, “Updated $^{14}\text{N}(p,\gamma)^{15}\text{O}$ data from LUNA”, German Physical Society,
Spring Meeting, Bonn 15.-19.03.2010
- M. Marta, “Experimental study of the $^{14}\text{N}(p,\gamma)^{15}\text{O}$ reaction”, 15th Workshop on
Nuclear Astrophysics, Ringberg, March 22 - 27 2010
- M. Marta: “Experimental study of the $^{14}\text{N}(p,\gamma)^{15}\text{O}$ reaction”, International
School of Nuclear Physics (32nd Course) Particle and Nuclear Astrophysics, Erice-
Sicily, 16 - 24 September 2010
- A. Caciolli: “The $^{15}\text{N}(p,\gamma)^{16}\text{O}$ reaction”, GIANTS2010 , Catania, 29-31 March 2010
- A. Caciolli: “Study of the $^{15}\text{N}(p,\gamma)^{16}\text{O}$ reaction”, poster, 11th Symposium on Nuclei
in the Cosmos, Heidelberg, Germany, July 19-23

- D. Bemmerer, “Nuclear data needs for underground accelerators”, Workshop on Data Requirements in Nuclear Astrophysics, Darmstadt 27.-28.07.2010
- D. Bemmerer, “Underground accelerators in Europe” Origins of the elements and nuclear history of the universe, Dubrovnik 24.-26.11.2010
- A. Guglielmetti, “LUNA at LNGS”, Nupecc meeting, Catania, 12 March 2010
- A. Guglielmetti, “Stato dell’arte dell’esperimento LUNA”, GIANTS2010 , Catania, 29-31 March 2010
- A. Guglielmetti, “LUNA: present and future”, Underground nuclear-reaction experiments for astrophysics and applications, Dresden, 29-31 April 2010
- A. Guglielmetti, “The LUNA experiment at LNGS”, From the Big bang to the nucleosynthesis , Varenna, 19-24 July 2010
- Zs. Fülöp, “Nuclear astrophysics underground: The LUNA experiment.”, Seminar, Universitat Basel. Basel, Switzerland, 18. March, 2010
- C. Mazzocchi, “Nuclear astrophysics deep underground: the LUNA experiment”, talk at the Zakopane Conference on Nuclear Physics “Extremes of the Nuclear Landscape”, August 30 - September 5, 2010, Zakopane, Poland
- C. Mazzocchi, “Nuclear astrophysics deep underground: the LUNA experiment”, invited talk at the XLVIII International Winter Meeting on Nuclear Physics, Bormio, Italy, January 2010
- C. Mazzocchi, “Measurement of the ${}^2\text{H}(\alpha,\gamma){}^6\text{Li}$ reaction at LUNA”, GIANTS2010, Catania, 29-31 March 2010
- F. Strieder, “Experimental Quests for Nuclear Astrophysics with stable Beams”, 7th Russbach Workshop, Austria, 17.03.2010
- F. Strieder, “LUNA - Nuclear Astrophysics Underground”, Annual Spring Meeting of the German Physical Society, Bonn, Germany, 18.03.2010
- C. Brogini, “Twenty years of LUNA and solar neutrinos”, XXIV International Conference on Neutrino Physics and Astrophysics, Athens, June 14-19
- C. Brogini, “20 years of LUNA”, International School of Nuclear Physics, 32nd Course Particle and Nuclear Astrophysics, Erice, September 16-24.
- G. Imbriani, “Direct Measurements of Cross Section of Astrophysical Interest”, INPC 2010, Vancouver, Canada, July 4 - 9, 2010
- G. Imbriani, “Underground measurements of cross section of astrophysical”, American Physical Society, 2010 Fall Meeting of the APS Division of Nuclear Physics, November 2-6, 2010

- G. Imbriani, “Nucleosynthesis in AGB Stars: ^{19}F Production”, seminar, Notre Dame University, United States, November 8, 2010
- C. Gustavino, “The LUNA experiment at LNGS”, Vulcano Workshop 2010, Vulcano (Italy) 24-29 May 2010
- C. Gustavino, “The LUNA experiment at LNGS”, Finustar 3rd International Conference on Frontiers in Nuclear Structure, Astrophysics and Reactions, Rhodes, Greece, August 23-27
- C. Gustavino, “The LUNA experiment at LNGS”, seminar, Laboratori Nazionali Frascati (Italy), November 24.
- C. Gustavino, “Nuclear astrophysics deep underground: the LUNA experiment”, seminar (Italy), Università Roma1, September 30.
- H. Costantini, “Reaction rate measurements in underground laboratories”, 11th Symposium on Nuclei in the Cosmos, Heidelberg, Germany, July 19-23
- M. Erhard, “Study of the BBN reaction $\text{D}(\alpha,\gamma)^6\text{Li}$ deep underground at LUNA”, 11th Symposium on Nuclei in the Cosmos, Heidelberg, Germany, July 19-23
- A. Formicola, “Best values and uncertainties of the nuclear reaction cross sections important to solar burning”, The Physics of the Sun and the Solar Neutrinos, Gran Sasso, Italy, 4-5 October 2010

References

- [1] J. N. Bahcall, A. M. Serenelli, and S. Basu. *Astrophys. J.* **621**, L85–L88 (2005)
- [2] C. Arpesella, et al. *Phys. Rev. Lett.* **101**, 091302 (2008)
- [3] W. C. Haxton and A. M. Serenelli. *Astrophys. J.* **687**, 678–691 (2008)
- [4] A. M. Serenelli, S. Basu, J. W. Ferguson, and M. Asplund. *Astrophys. J. Lett.* **705**, L123–L127 (2009)
- [5] A. Formicola et al. *Phys. Lett. B* **591**, 61–68 (2004)
- [6] G. Imbriani et al. *Eur. Phys. J. A* **25**, 455–466 (2005)
- [7] A. Lemut et al. *Phys. Lett. B* **634**, 483 (2006)
- [8] R. C. Runkle et al. *Phys. Rev. Lett.* **94**, 082503 (2005)
- [9] M. Marta et al. *Phys. Rev. C* **78**, 022802(R) (2008)
- [10] M. Marta et al. Submitted to *Phys. Rev. C*
- [11] U. Schröder et al. *Nucl. Phys. A* **467**, 240–260 (1987)

- [12] M. Marta Ph.D. thesis, Technische Universität Dresden (2011)
- [13] E. Adelberger et al. Rev. Mod. Phys. **in press** (2010). arXiv: 1004.2318
- [14] D. Hebbard, Nucl. Phys. 15(1960)289.
- [15] C. Rolfs and W. S. Rodney, Nucl. Phys. A 235(1974)450.
- [16] C. Angulo et al., Nucl. Phys. A 656(1999)3.
- [17] F. C. Barker, Phys. Rev. C 78(2009)044612.
- [18] A. M. Mukhamedzhanov et al., Phys. Rev. C 78(2008)015804.
- [19] D. Bemmerer et al., J. of Phys. G 36(2009)045202.
- [20] P. J. LeBlanc et al., Phys. Rev. C, 82(2010)055804.
- [21] M. Spite and F. Spite, Nature **297**, 483 (1982).
- [22] P. D. Serpico *et al.*, J. Cosmol. Astropart. Phys. **2004**, 010 (2004).
- [23] F. Iocco *et al.*, Phys. Rep. **472**, 1 (2009), 0809.0631.
- [24] D. Bemmerer *et al.*, Phys. Rev. Lett. **97**, 122502 (2006).
- [25] F. Confortola *et al.*, Phys. Rev. C **75**, 065803 (2007).
- [26] M. Asplund *et al.*, Astrophys. J. **644**, 229 (2006).
- [27] M. Steffen *et al.*, Convection and ${}^6\text{Li}$ in the atmospheres of metal-poor halo stars, in *IAU Symposium*, edited by C. Charbonnel, M. Tosi, F. Primas, & C. Chiappini, , IAU Symposium Vol. 268, pp. 215–220, 2010, 1001.3274.
- [28] N. Prantzos, Astron. Astrophys. **448**, 665 (2006).
- [29] M. Kusakabe *et al.*, Phys. Rev. D **74**, 023526 (2006).
- [30] K. Jedamzik and M. Pospelov, New Journal of Physics **11**, 105028 (2009), 0906.2087.
- [31] P. Mohr *et al.*, Phys. Rev. C **50**, 1543 (1994).
- [32] J. Kiener *et al.*, Phys. Rev. C **44**, 2195 (1991).
- [33] F. Hammache *et al.*, Phys. Rev. C **82**, 065803 (2010), 1011.6179.
- [34] D. Phillips et al., Nucl. Inst. Meth. A135 (1976) 389
- [35] A. Chafa et al., Phys. Rev. C 75 (2007) 035810
- [36] C. Fox et al., Phys. Rev. C 71 (2005) 055801

2010 LVD STATUS REPORT

The LVD Collaboration

N.Yu.Agafonova⁹, M.Aglietta¹⁴, E.D.Alyea⁷, P.Antonioli¹, G.Badino¹⁴, G.Bari¹,
M.Basile¹, V.S.Berezinsky⁹, M.Bertaina¹⁴, R.Bertoni¹⁴, V.V.Boyarkin⁹, A. Bonardi¹⁴,
G.Bruni¹, G.Bruno⁵, G.Cara Romeo¹, A.Chiavassa¹⁴, J.A.Chinellato³, L.Cifarelli¹,
F.Cindolo¹, A.Contin¹, V.L.Dadykin⁹, E.A. Dobrynina⁹, L.G.Dos Santos³, R.I.Enikeev⁹,
W.Fulgione¹⁴, P.Galeotti¹⁴, M.Garbini¹, P.L.Ghia^{5,14}, P.Giusti¹, F.Gomez¹⁴, F.Grianti⁴,
G.Jacobucci¹, E.Kemp³, E.V.Korolkova⁹, V.B.Korchaguin⁹, V.V.Kuznetsov⁹,
M.Luvisetto¹, A.A.Machado⁵, A.S.Mal'gin⁹, H.Menghetti¹, N.Mengotti Silva³,
B.Miguez³, A.Molinario¹⁴, C.Morello¹⁴, R.Nania¹, K.Okei¹⁰, L.Periale¹⁴, R.Persiani¹,
A.Pesci¹, P.Picchi¹⁴, I.A.Pless⁸, A.Porta¹⁴, A.Romero¹⁴, V.G.Ryasny⁹,
O.G.Ryazhskaya⁹, O.Saavedra¹⁴, K.Saitoh¹³, G.Sartorelli¹, M.Selvi¹, N.Taborgna⁵,
N.Takahashi¹², V.P.Talochkin⁹, G.C.Trincherro¹⁴, S.Tsuji¹¹, A.Turtelli³, P.Vallania¹⁴,
S.Vernetto¹⁴, C.Vigorito¹⁴, L.Votano⁴, R.Weinstein⁶, M.Widgoff², V.F.Yakushev⁹,
G.T.Zatsepin⁹, A.Zichichi¹

¹*University of Bologna and INFN-Bologna, Italy*

²*Brown University, Providence, USA*

³*University of Campinas, Campinas, Brazil*

⁴*INFN-LNF, Frascati, Italy*

⁵*INFN-LNGS, Assergi, Italy*

⁶*University of Houston, Houston, USA*

⁷*Indiana University, Bloomington, USA*

⁸*Massachusetts Institute of Technology, Cambridge, USA*

⁹*Institute for Nuclear Research, Russian Academy of Sciences, Moscow, Russia*

¹⁰*Okayama University, Okayama, Japan*

¹¹*Kawasaki Medical School, Kurashiki, Japan*

¹²*Hirosaki University, Hirosaki, Japan*

¹³*Ashikaga Institute of Technology, Ashikaga, Japan*

¹⁴*IFSI-INAF, Torino; University of Torino and INFN-Torino, Italy*

Abstract

The Large Volume Detector (LVD) at the INFN Gran Sasso National Laboratory (LNGS), Italy, is an underground neutrino observatory mainly designed to study core-collapse supernovae. The experiment has been monitoring the Galaxy since June 1992 with increasing active mass up to the final configuration $M = 1$ kt that has been reached on January 2001. No burst candidate has been found over 6013 days of live-time, the resulting 90% c.l. upper limit to the rate of gravitational stellar collapses in the Galaxy ($D \leq 20$ kpc) is 0.14 y^{-1} .

Since July 2005 LVD has taken part to the Supernovae Early Warning System (SNEWS), the network of SN neutrino observatories whose main goal is to provide the astronomical community with a prompt alert for the next galactic core-collapse supernova explosion.

Since 2006 LVD has acted as a far monitor for the Cern Neutrinos to Gran Sasso (CNGS) high energy, wide band ν_μ beam, set up at Cern and sent towards the LNGS.

The study of the seasonal modulation of the cosmic muon flux during 2001-2008 has been completed. An annual modulation with average amplitude 1.5% and maximum intensity in July has been found, in agreement with previous measurements at LNGS.

The low threshold channel of the LVD electronics, dedicated to the detection of gammas from (n,p) capture, is continuously monitored to keep under control the detector performance during long periods allowing to measure the environmental conditions. The analysis of these data during 1997-2009 shows the existence of a seasonal modulation with the maximum occurring at the end of August due to radon concentration variations in the experimental hall.

1 The LVD experiment

The Large Volume Detector (LVD), located in the hall A s of the INFN Gran Sasso National Laboratory, Italy, is made of 1000 tons of liquid scintillator arranged in a modular geometry. The major goal of LVD is to search for neutrinos from Gravitational Stellar Collapses (GSC) in our Galaxy [1].

The detector is a three-dimensional array of 840 scintillator counters, 1.5 m^3 each. The whole array is split into three identical parts (towers) with independent power supply, trigger and data acquisition. In turn, each tower consists of 35 cluster of 8 counters (modules). Each counter is viewed from the top by three photomultipliers (PMTs).

The main neutrino reaction in LVD¹ is $\bar{\nu}_e p \rightarrow e^+ n$, which gives two detectable signals: the prompt one, due to the e^+ , followed by the signal from the (n,p) capture ($E_\gamma = 2.2$ MeV) with a mean delay of $\simeq 185 \mu\text{s}$.

The trigger logic is optimized for the detection of both products of the inverse beta decay and is based on the three-fold coincidence of the PMTs of a single counter. Each PMT is discriminated at two different thresholds resulting in two possible levels of coincidence

¹LVD is also sensitive to $\bar{\nu}_i + e^- \rightarrow \nu_i + e^-$ scattering; $(\nu_e + \bar{\nu}_e)$ c.c. interactions and $\bar{\nu}_i$ n.c. interactions with carbon.

between a counter's PMTs: H and L, corresponding respectively to $\mathcal{E}_H \simeq 4$ MeV and $\mathcal{E}_L \simeq 500$ KeV.

The iron support structure of the detector can also act as target for neutrinos and antineutrinos. The products of the interaction can escape from iron and be detected in the liquid scintillator. The amount of neutrino-iron interactions can be as high as about 20% of the total number of interactions.

The observable signal in LVD, in different reactions and due to different kinds of neutrinos, besides providing astrophysical information on the nature of the collapse, is sensitive to intrinsic ν properties, as oscillation of massive neutrinos and can give an important contribution to define some of the neutrino oscillation properties still missing. We have studied [2] how neutrino oscillations affect the signal detected by LVD and also evaluated the impact on the signal of the astrophysical parameters of the supernova explosion mechanism, such as the total energy emitted in neutrinos, the star distance, the neutrino-sphere temperatures and the partition of the energy among the neutrino flavors.

However, being aware of the fact that the astrophysical parameters of the supernova mechanism are up to now not well defined, to compute the detector sensitivity expressed in terms of source distance or emitted neutrino flux we adopted the following conservative values for the astrophysical parameters [3], [4]: average $\bar{\nu}_e$ energy $\langle E_{\bar{\nu}_e} \rangle = 14$ MeV;

total radiated energy $E_b = 2.4 \cdot 10^{53}$ erg and average non-electron neutrino energy 10% higher than $\bar{\nu}_e$ [5]. Concerning neutrino oscillations we conservatively assumed direct mass hierarchy. Taking into account Poisson fluctuations in the cluster multiplicity, we derived the trigger efficiency shown in figure 1 as a function of the distance (lower scale) for LVD working stand-alone (the trigger efficiency, as a function of neutrino luminosity in terms of percentage of SN1987A one is shown in the upper scale). The trigger efficiency for LVD working in the SNEWS network [6] is shown in figure 2 [7].

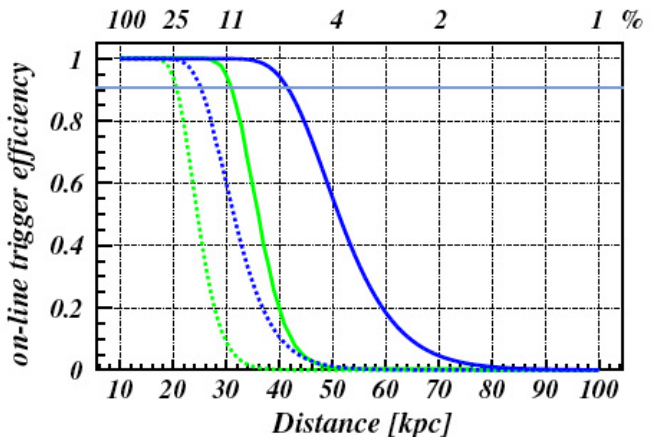


Figure 1: *On-line trigger efficiency versus distance (lower scale) and percentage of SN1987A-like signal at 10 kpc (upper scale) for $E_{cut}=7-10$ MeV (light green and dark blue lines, respectively) and $M=300t$ (dotted) and $1000t$ (continuous) for LVD stand alone.*

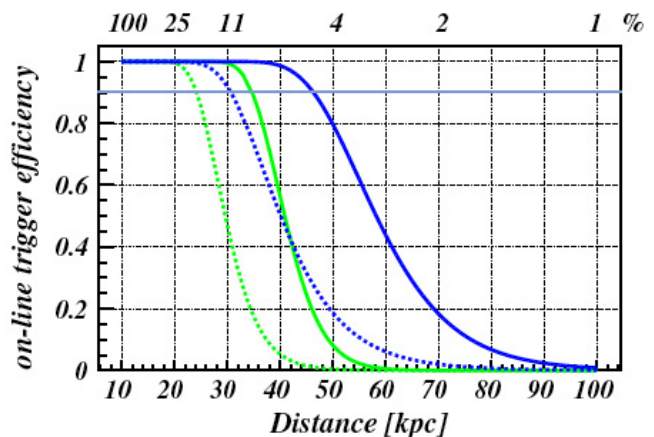


Figure 2: *Same as figure 1 for LVD in the SNEWS.*

2 LVD: experimental activity

2.1 Supernova physics

2.1.1 Monitoring the Galaxy

LVD has been taking data since June 1992 with increasing mass configurations (sensitive mass being always greater than 300 t), enough to monitor the whole Galaxy ($D \leq 20$ kpc)². In figure 3 we show sensitive mass and duty cycle of the experiment during the period 1992-2010. The LVD duty cycle, in the entire period, is greater than 92%. The search for ν burst candidates is performed by studying the temporal sequence of triggers and looking for clusters. Preliminary cuts are applied to reject muons and events with an energy release lower than 7 MeV or higher than 100 MeV. The off-line neutrino burst candidate selection, widely discussed in [10], consists of the analysis of each cluster of triggers of duration up to 200 seconds.

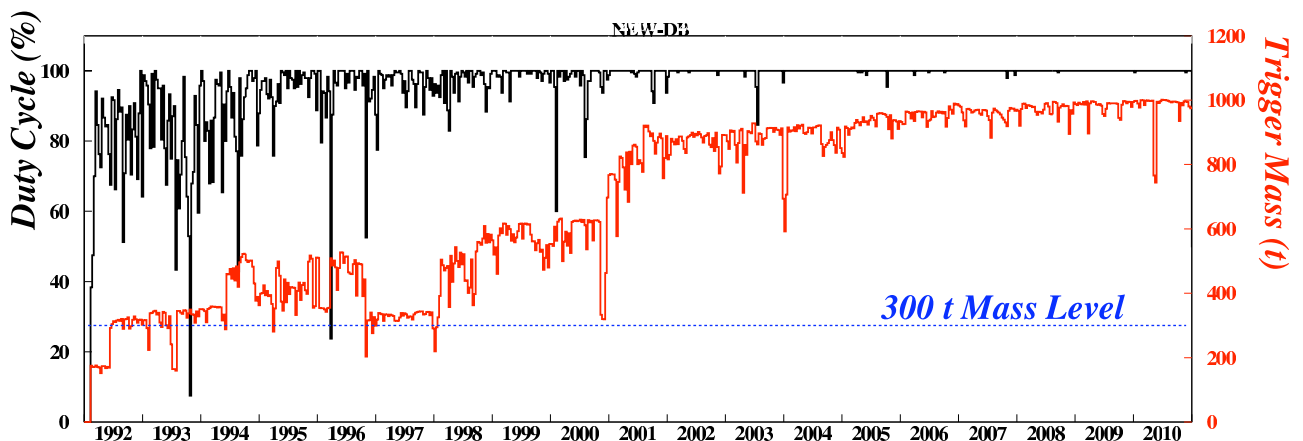


Figure 3: *LVD sensitive mass and duty cycle during 1992-2010.*

For each cluster, with multiplicity m and duration Δt , the imitation frequency F_{im} is calculated as a function of the background rate. A complete analysis of each detected cluster with $F_{im} \leq 1 \text{ y}^{-1}$ is performed, to test its consistency with a ν burst through the study of the topological distribution of pulses inside the detector. Additional information will come from the study of: *a)* the energy spectrum of the events in the cluster; *b)* the time distribution of the events in the cluster and *c)* the time distribution of delayed low energy pulses.

²The results of this search have been periodically updated and published in the ICRC and Neutrino Conference Proceedings, since 1993 till 2010. [8].

No candidates have been found since 1992, see details in table 1. Since the LVD sensitivity is higher than what is expected from GSC models (even if the source is at a distance of 20 kpc and for soft neutrino energy spectra), the resulting 90% c.l. upper limit to the rate of gravitational stellar collapses in the Galaxy ($D \leq 20$ kpc) is 0.14 y^{-1} (to be compared with the result obtained by SuperKamiokande of 0.32 y^{-1} ($D \leq 100$ kpc)[11].

Table 1: LVD run.

Run	start	end	days	up (%)	mass (t)
1	6-6-1992	5-31-1993	285	60	310
2	8-4-1993	3-11-1995	397	74	390
3	3-11-1995	4-30-1997	627	90	400
4	4-30-1997	3-15-1999	685	94	415
5	3-16-1999	12-11-2000	592	95	580
6	12-12-2000	3-24-2003	821	98	842
7	3-25-2003	2-4-2005	666	> 99	881
8	2-4-2005	5-31-2007	846	> 99	936
9	5-31-2007	4-30-2009	669	> 99	967
10	5-1-2009	5-31-2010	395	> 99	976
Σ	6-6-1992	5-31-2010	6013		

2.1.2 The Supernova On-line Monitor and SNEWS

The first, and unique, observation of ν 's from gravitational stellar collapse was driven by optical observation (SN1987A), but, since the probability of such an event for a stellar collapse in our Galaxy is only of 20%, the detector capabilities of identifying a ν burst in the absence of an "external trigger" must be carefully demonstrated. In the presence of an electromagnetic counterpart, on the other hand, the prompt identification of the neutrino signal could alert the worldwide network of observatories allowing study of all aspects of the rare event from its onset.

The SNEWS (SuperNova Early Warning System) [6] project is an international collaboration including several experiments sensitive to a core-collapse supernova neutrino signal in the Galaxy and neighbourhood. The goal is to provide the astronomical community with a prompt and reliable alert of the occurrence of a Galactic supernova event, generated by the coincidence of two or more active detectors. In July 2005, after a few years of tuning, the charter members of SNEWS (i.e., LVD, Super-K and SNO³) together with the newly joined Amanda/IceCube, started the effective operation of the network, which means that the alert is really sent to the list subscribers, in the case of an at least two-fold coincidence (subscribe at <http://snews.bnl.gov> to get your own SN alert !). Since 2009 also Borexino joined the network.

³At present the SNO experiment is stopped and decommissioned.

Since 2001 a fast and reliable on-line ν -burst monitor has been implemented, the algorithm is based on the search for clusters of triggers within a fixed time window, $\Delta t=20$ s. The candidate is simply characterized by its multiplicity m , i.e. the number of pulses detected in Δt . All the other characteristics of the cluster are left to a subsequent independent analysis. The search for burst candidates is performed, on-line, simultaneously for two values of the energy threshold: $E_{cut} = 7$ MeV ($f_{bk} = 0.2$ Hz) and $E_{cut} = 10$ MeV ($f_{bk} = 0.03$ Hz). The chosen imitation frequencies, F_{im} , below which the detected cluster will be an on-line candidate supernova event, is 1 per 100 year working stand-alone while it is relaxed to 1 per month working in coincidence with other detectors (SNEWS), and 1 per day for monitoring task. The corresponding detection efficiency are shown in figure 1 and 2, details are discussed in [7].

2.2 CNGS beam monitor

The Cern Neutrinos to Gran Sasso (CNGS) program is a high energy, wide band ν_μ beam set up at Cern and sent towards the LNGS. Its main goal is the observation of the ν_τ appearance, through neutrino flavour oscillation. As shown in [12], due to its large area and active mass, LVD can act as a beam monitor, detecting the interaction of neutrinos inside the detector and the muons generated by the ν interaction in the rock upstream the detector. The monitor capabilities have been confirmed during the first CNGS run in August 2006 [13], fall 2007 and 2008 [14].

2.2.1 MC simulation of the expected events

The CNGS events in LVD can be subdivided into two main categories:

- ν_μ charged current (CC) interactions in the rock upstream the LNGS; they produce a muon that can reach LVD and be detected,
- ν_μ CC and neutral current (NC) interactions in the material (liquid scintillator and iron of the support structure) of LVD.

A full Montecarlo simulation has been developed including the generation of the neutrino interaction products, the propagation of the muon in the Gran Sasso rock and the response of the LVD detector. The details of the simulation are described in [12]. The resulting number of expected events, at the nominal intensity $4.5 \cdot 10^{19}$ p.o.t./y is 33400/y, equivalent to $7.422 \cdot 10^{-16}$ events per p.o.t. (considering 200 effective days per year it corresponds to ~ 165 CNGS events per day): 78% are muons from the rock, 17% are CC interactions in the detector and 5% are NC.

During 2010 the total intensity was $4.04 \cdot 10^{19}$ p.o.t., corresponding to about 30000 expected events in LVD.

2.2.2 CNGS detected events

The LVD events are filtered using a very loose selection cut: we require to have at least one scintillation counter with an energy release larger than 100 MeV. The resulting rate is quite stable, with an average value of about 0.13 Hz, and it is mainly due to cosmic

muon events. Among this data sample the selection criteria is based on the correlation of the LVD event time with the beam spill time written in the DB:

we search for the CNGS events in the interval $[-15, +25] \mu s$ around the start time of the beam spill. An example of this distribution, corresponding to the data collected during 2008, is shown in figure 4: it reflects the $10.5 \mu s$ width of the beam spill. The number of detected events is 30311.

The background, estimated considering: the 0.13 Hz rate of events among which the CNGS events are searched for, the time window around the beam spill time, $40 \mu s$ wide, and the number of useful spills in the DB, is practically negligible.

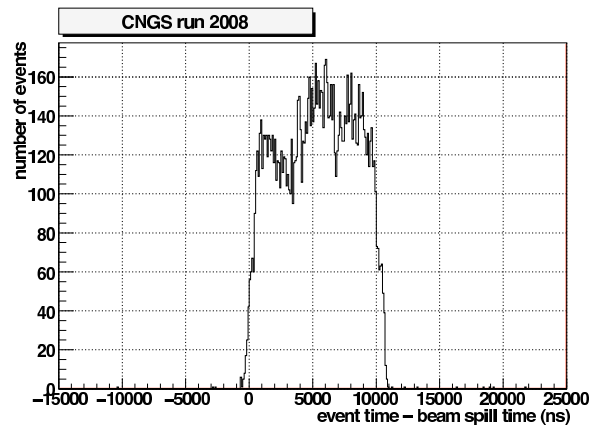


Figure 4: *Distribution of the detection time of the CNGS events, with respect to the initial time of the beam spill.*

3 List of publications in 2010

- *Neutrino bursts from gravitational stellar collapses with LVD*
A. Molinaro and C. Vigorito On behalf of the LVD Collaboration, *Astrophys. Space Sci. Trans.*, 7, 4952, 2011
- *Neutrino bursts from gravitational stellar collapses with LVD*
W. Fulgione, A. Molinaro and C. Vigorito for the LVD Collaboration, *Mem. S.A.It. Vol. 75*, 282
- *Neutrino bursts from gravitational stellar collapses with LVD*
A. Molinaro and C. Vigorito On behalf of the LVD Collaboration, *Proceedings of Neutrino 2010*, to be published in *Nuclear Physics B Proceedings Supplement*

References

- [1] LVD Collaboration, *Il Nuovo Cimento* **A105** (1992) 1793
- [2] N. Yu. Agafonova *et al.*, *Study of the effect of neutrino oscillations on the supernova neutrino signal in the LVD detector*, *Astropart. Phys.* **27**, 254-270 (2007) [arXiv: hep-ph/0609305].
- [3] G. Pagliaroli, F. Vissani, M. L. Costantini, and A. Ianni, *Astropart. Phys.* **31**, 163 (2009)

- [4] M.L. Costantini, A. Ianni and F. Vissani, Phys. Rev. D **70** (2004) 043006.
- [5] M.T.Keil, G.G.Raffelt and H.T.Janka, Astrophys. J. **590** (2003) 971.
- [6] P. Antonioli *et al.*, New Journal of Physics **6** (2004) 114; <http://hep.bu.edu/~snnet/>
- [7] N. Yu. Agafonova *et al.*, *On-line recognition of supernova neutrino bursts in the LVD detector*, Astropart. Phys. **28**, 516-522 (2008) [arXiv:0710.0259].
- [8] LVD Collaboration, Astrophys. Space Sci. Trans., 7, 4952, 2011 and reference therein.
- [9] LVD Collaboration, Proceedings of the 31st ICRC, 2009 and reference therein.
- [10] W.Fulgione, N.Mengotti-Silva, L.Panaro NIM A 368 (1996)
- [11] M.Ikeda *et al.*, The Astrophysical Journal, 669:519-524, 2007
- [12] M. Aglietta et al., *CNGS beam monitor with the LVD detector*, Nuclear Instruments and Methods in Physics Research **A 516**, 96 (2004).
- [13] N. Yu. Agafonova et al., *First CNGS events detected by LVD*, Eur. Phys. J. **C 52**, 849-855 (2007) [arXiv:0710.1536 hep-ex].
- [14] N. Yu. Agafonova et al., *The Large Volume Detector*, in the 2007 and 2008 LNGS Annual Report, p. 114 (2007).

OPERA

N. Agafonova¹, A. Aleksandrov², O. Altinok³, A. Anokhina⁴, S. Aoki⁵, A. Ariga⁶,
T. Ariga⁶, D. Autiero⁷, A. Badertscher⁸, A. Bagulya⁹, A. Bendhabi¹⁰, A. Bertolin^{11,*},
C. Bozza¹², T. Brugière⁷, R. Brugnera^{13,11}, F. Brunet¹⁴, G. Brunetti^{15,16,7},
S. Buontempo², A. Cazes⁷, L. Chaussard⁷, M. Chernyavskiy⁹, V. Chiarella¹⁷,
A. Chukanov¹⁸, N. D'Ambrosio¹⁹, F. Dal Corso¹¹, G. De Lellis^{20,2}, P. del Amo Sanchez¹⁴,
Y. Déclais⁷, M. De Serio²¹, F. Di Capua², A. Di Crescenzo^{20,2}, D. Di Ferdinando¹⁶,
N. Di Marco^{22,a}, S. Dmitrievski¹⁸, M. Dracos²³, D. Duchesneau¹⁴, S. Dusini¹¹,
T. Dzhatdov⁴, J. Ebert²⁴, O. Egorov²⁵, R. Enikeev¹, A. Ereditato⁶, L. S. Esposito⁸,
J. Favier¹⁴, T. Ferber²⁴, R. A. Fini²¹, D. Frekers²⁶, T. Fukuda²⁷, A. Garfagnini^{13,11},
G. Giacomelli^{15,16}, M. Giorgini^{15,16,b}, C. Göllnitz²⁴, J. Goldberg²⁸, D. Golubkov²⁵,
L. Goncharova⁹, Y. Gornushkin¹⁸, G. Grella¹², F. Grianti^{29,17}, A. M. Guler³,
C. Gustavino^{19,c}, C. Hagner²⁴, K. Hamada²⁷, T. Hara⁵, M. Hierholzer²⁴, A. Hollnagel²⁴,
K. Hoshino²⁷, M. Ieva²¹, H. Ishida³⁰, K. Jakovcic³¹, C. Jollet^{23,*}, F. Juliet⁶,
M. Kamiscioglu³, K. Kazuyama²⁷, S. H. Kim^{32,d}, M. Kimura³⁰, N. Kitagawa²⁷,
B. Klicek³¹, J. Knuesel⁶, K. Kodama³³, M. Komatsu²⁷, U. Kose^{13,11}, I. Kreslo⁶,
H. Kubota²⁷, C. Lazzaro⁸, J. Lenkeit²⁴, I. Lippi¹¹, A. Ljubicic³¹, A. Longhin^{13,11,e},
P. Loverre³⁴, G. Lutter⁶, A. Malgin¹, G. Mandrioli¹⁶, K. Mannai¹⁰, J. Marteau⁷,
T. Matsuo³⁰, V. Matveev¹, N. Mauri^{15,16,e}, E. Medinaceli¹⁶, F. Meisel⁶, A. Mereaglia^{23,*},
P. Migliozzi², S. Mikado³⁰, S. Miyamoto²⁷, P. Monacelli²², K. Morishima²⁷, U. Moser⁶,
M. T. Muciaccia^{35,21}, N. Naganawa²⁷, T. Naka²⁷, M. Nakamura²⁷, T. Nakano²⁷,
D. Naumov¹⁸, V. Nikitina⁴, K. Niwa²⁷, Y. Nonoyama²⁷, S. Ogawa³⁰, N. Okateva⁹,
A. Olchevski¹⁸, M. Paniccia¹⁷, A. Paoloni¹⁷, B. D. Park^{32,f}, I. G. Park³², A. Pastore^{35,21},
L. Patrizii¹⁶, E. Pennacchio⁷, H. Pessard¹⁴, K. Pretzl⁶, V. Pilipenko²⁶, C. Pistillo⁶,
N. Polukhina⁹, M. Pozzato^{15,16}, F. Pupilli²², R. Rescigno¹², T. Roganova⁴, H. Rokujo⁵,
G. Romano¹², G. Rosa³⁴, I. Rostovtseva²⁵, A. Rubbia⁸, A. Russo^{20,2}, V. Ryasny¹,
O. Ryazhskaya¹, O. Sato²⁷, Y. Sato³⁶, A. Schembri¹⁹, W. Schmidt-Parzefall²⁴,
H. Schroeder³⁷, L. Scotto Lavina^{20,2,g}, A. Sheshukov¹⁸, H. Shibuya³⁰, G. Shojiyeov⁴,
S. Simone^{35,21}, M. Sioli^{15,16}, C. Sirignano¹², G. Sirri¹⁶, J. S. Song³², M. Spinetti¹⁷,
L. Stanco¹¹, N. Starkov⁹, M. Stipcevic³¹, T. Strauss^{8,h}, P. Strolin^{20,2}, S. Takahashi²⁷,
M. Tenti^{15,16}, F. Terranova¹⁷, I. Tezuka³⁶, V. Tioukov², P. Tolun³, A. Trabelsi¹⁰,
T. Tran⁷, S. Tufanli^{3,h}, P. Vilain³⁸, M. Vladimirov⁹, L. Votano¹⁷, J. L. Vuilleumier⁶,
G. Wilquet³⁸, B. Wonsak²⁴, V. Yakushev¹, C. S. Yoon³², T. Yoshioka²⁷, J. Yoshida²⁷,
Y. Zaitsev²⁵, S. Zemskova¹⁸, A. Zghiche¹⁴ and R. Zimmermann²⁴.

1. INR-Institute for Nuclear Research of the Russian Academy of Sciences, RUS-117312 Moscow, Russia
2. INFN Sezione di Napoli, I-80125 Napoli, Italy
3. METU-Middle East Technical University, TR-06531 Ankara, Turkey
4. SINP MSU-Skobeltsyn Institute of Nuclear Physics of Moscow State University, RUS-119992 Moscow, Russia
5. Kobe University, J-657-8501 Kobe, Japan
6. Albert Einstein Center for Fundamental Physics, Laboratory for High Energy Physics (LHEP), University of Bern, CH-3012 Bern, Switzerland
7. IPNL, Université Claude Bernard Lyon 1, CNRS/IN2P3, F-69622 Villeurbanne, France
8. ETH Zurich, Institute for Particle Physics, CH-8093 Zurich, Switzerland
9. LPI-Lebedev Physical Institute of the Russian Academy of Sciences, RUS-117924 Moscow, Russia
10. Unité de Physique Nucléaire et des Hautes Energies (UPNHE), Tunis, Tunisia
11. INFN Sezione di Padova, I-35131 Padova, Italy
12. Dipartimento di Fisica dell'Università di Salerno and INFN, I-84084 Fisciano, Salerno, Italy
13. Dipartimento di Fisica dell'Università di Padova, I-35131 Padova, Italy
14. LAPP, Université de Savoie, CNRS/IN2P3, F-74941 Annecy-le-Vieux, France
15. Dipartimento di Fisica dell'Università di Bologna, I-40127 Bologna, Italy
16. INFN Sezione di Bologna, I-40127 Bologna, Italy
17. INFN - Laboratori Nazionali di Frascati dell'INFN, I-00044 Frascati (Roma), Italy
18. JINR-Joint Institute for Nuclear Research, RUS-141980 Dubna, Russia
19. INFN - Laboratori Nazionali del Gran Sasso, I-67010 Assergi (L'Aquila), Italy
20. Dipartimento di Scienze Fisiche dell'Università Federico II di Napoli, I-80125 Napoli, Italy
21. INFN Sezione di Bari, I-70126 Bari, Italy
22. Dipartimento di Fisica dell'Università dell'Aquila and INFN, I-67100 L'Aquila, Italy
23. IPHC, Université de Strasbourg, CNRS/IN2P3, F-67037 Strasbourg, France
24. Hamburg University, D-22761 Hamburg, Germany
25. ITEP-Institute for Theoretical and Experimental Physics, RUS-117259 Moscow, Russia
26. University of Münster, D-48149 Münster, Germany
27. Nagoya University, J-464-8602 Nagoya, Japan
28. Department of Physics, Technion, IL-32000 Haifa, Israel
29. Università degli Studi di Urbino "Carlo Bo", I-61029 Urbino, Italy
30. Toho University, J-274-8510 Funabashi, Japan
31. IRB-Rudjer Boskovic Institute, HR-10002 Zagreb, Croatia
32. Gyeongsang National University, ROK-900 Gazwa-dong, Jinju 660-300, Korea
33. Aichi University of Education, J-448-8542 Kariya (Aichi-Ken), Japan
34. Dipartimento di Fisica dell'Università di Roma "La Sapienza" and INFN, I-00185 Roma, Italy
35. Dipartimento di Fisica dell'Università di Bari, I-70126 Bari, Italy
36. Utsunomiya University, J-321-8505 Tochigi-Ken, Utsunomiya, Japan
37. Fachbereich Physik der Universität Rostock, D-18051 Rostock, Germany
38. IIHE, Université Libre de Bruxelles, B-1050 Brussels, Belgium
- a. Now at INFN - Laboratori Nazionali del Gran Sasso, I-67010 Assergi (L'Aquila), Italy
- b. Now at INAF/IASF, Sezione di Milano, I-20133 Milano, Italy
- c. Now at Dipartimento di Fisica dell'Università di Roma "La Sapienza" and INFN, I-00185 Roma, Italy
- d. Now at Pusan National University, Geumjeong-Gu Busan 609-735, Korea
- e. Now at INFN - Laboratori Nazionali di Frascati dell'INFN, I-00044 Frascati (Roma), Italy
- f. Now at Asan Medical Center, 388-1 Pungnap-2 Dong, Songpa-Gu, Seoul 138-736, Korea
- g. Now at SUBATECH, CNRS/IN2P3, F-44307 Nantes, France
- h. Now at Albert Einstein Center for Fundamental Physics, Laboratory for High Energy Physics (LHEP), University of Bern, CH-3012 Bern, Switzerland

*Corresponding Authors:

Email addresses: bertolin@pd.infn.it (A. Bertolin), cecile.jollet@cern.ch (C. Jollet), anselmo.meregaglia@cern.ch (A. Mereaglia)

Abstract

The OPERA neutrino detector at the underground Gran Sasso Laboratory (LNGS) was designed to perform the first detection of neutrino oscillations in appearance mode through the study of $\nu_\mu \rightarrow \nu_\tau$ oscillations. The apparatus consists of a lead/emulsion-film target complemented by electronic detectors. It is placed in the high-energy long-baseline CERN to LNGS beam (CNGS) 730 km away from the neutrino source. Runs with CNGS neutrinos were successfully conducted in 2007 and 2008 for a total luminosity of 1.864×10^{19} p.o.t. (*proton on target*). In 2009 a new CNGS run has been conducted, from the end of May till November 23rd. In 2010, the CNGS facility accumulated 4.03×10^{19} proton-on-target. After a brief description of the beam and of the experimental apparatus we report on the data and related analysis results and first tau candidate.

1 Introduction

The solution of the long-standing solar and atmospheric neutrino puzzles has come from the hypothesis of neutrino oscillations. This implies that neutrinos have non vanishing and non-degenerate mass eigenstates, and that their flavor eigenstates involved in weak interaction processes are a superposition of the mass eigenstates.

Several experiments carried on in the last decades with solar and reactor neutrinos, as well as with atmospheric and accelerator neutrinos, contributed to build-up our present understanding of neutrino mixing. Atmospheric neutrino oscillations have been studied mainly by the Kamiokande, MACRO, Super-Kamiokande and SOUDAN2 experiments. Long baseline experiments with accelerator neutrinos (K2K and MINOS) confirmed the oscillation scenario first pointed out by the Super-Kamiokande experiment supporting the $\nu_\mu \rightarrow \nu_\tau$ oscillation channel for atmospheric neutrinos, while the CHOOZ and Palo Verde reactor experiments excluded the $\nu_\mu \rightarrow \nu_e$ channel as the dominant one.

However, the direct appearance of a different neutrino flavor is still an important open issue. This is the main goal of the OPERA experiment [1, 2] that uses the long baseline (L=730 km) CNGS neutrino beam from CERN to LNGS. The challenge of the experiment is to measure the appearance of ν_τ from ν_μ oscillations in an almost pure muon-neutrino beam. This requires the detection of the short-lived τ lepton ($c\tau = 87.11 \mu\text{m}$) produced in the charged-current interaction of a ν_τ . This sets two conflicting requirements: a large target mass needed to have sufficient statistics and an extremely high accuracy detector technique to observe the short-lived τ lepton.

The τ is identified by the detection of its characteristic decay topologies either in one prong (electron, muon or hadron) or in three prongs. The τ track is measured with a large-mass active target made of 1 mm thick lead plates (target mass and absorber material) inter-spaced with thin nuclear emulsion films (high-accuracy tracking devices). This detector is historically called Emulsion Cloud Chamber (ECC). Among past applications it was successfully used in the DONUT experiment for the first direct observation of the ν_τ .

The OPERA detector [2] is made of two identical Super Modules (SM) each consisting of a target section of about 625 tons made of lead/emulsion-film ECC modules (hereafter called "bricks"), of a scintillator tracker detector (TT) needed to trigger the read-out and

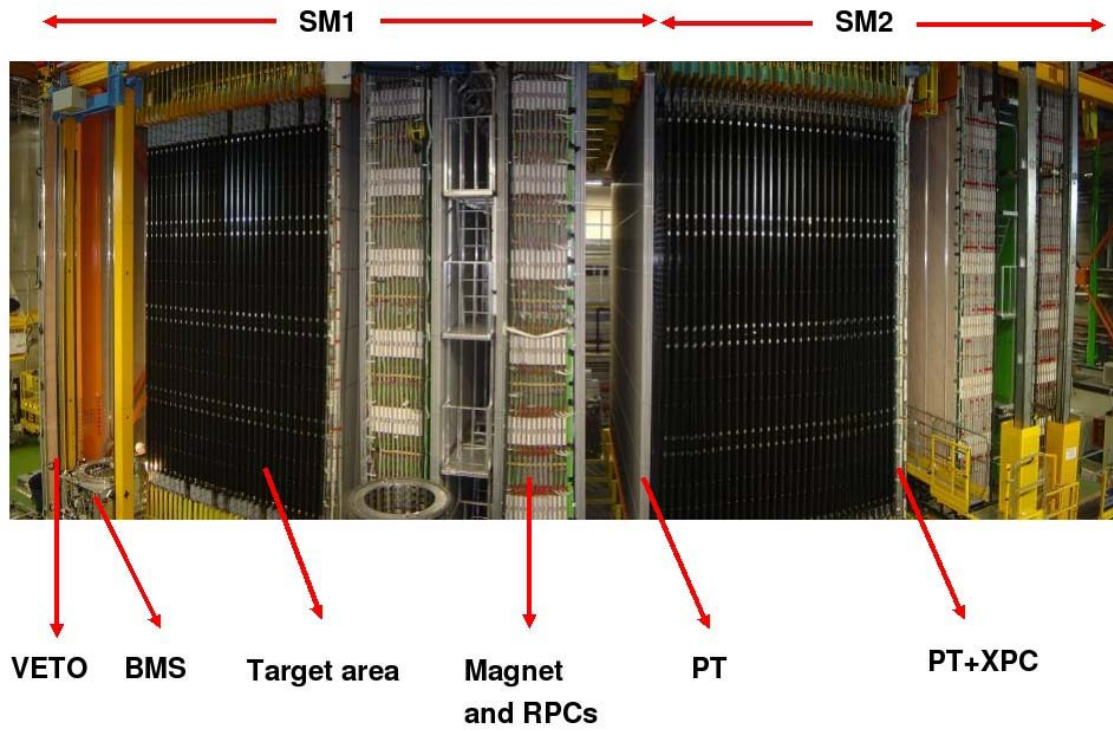


Figure 1: Fish-eye view of the OPERA detector. The upper horizontal lines indicate the position of the two identical supermodules (SM1 and SM2). The "target area" is made of walls filled with ECC bricks interleaved with planes of plastic scintillators (TT). Arrows also show the position of the VETO planes, the drift tubes (PT), the RPC with diagonal strips (XPC), the magnets and the RPC installed between the magnet iron slabs. The Brick Manipulator System (BMS) is also visible. See [2] for more details.

pre-localize neutrino interactions within the target, and of a muon spectrometer (Figure 1). A single SM has longitudinal dimensions of about 10 m. The detector is equipped with an automatic machine (the Brick Manipulator System, BMS) that allows the on-line removal of bricks from the detector. Ancillary facilities exist for the handling, the development and the scanning of the emulsion films. The film scanning is performed with two independent types of scanning microscopes: the European Scanning System (ESS) in Europe and the S-UTS in Japan.

A target brick consists of 56 lead plates of 1 mm thickness interleaved with 57 emulsion films [4]. The plate material is a lead alloy with a small calcium content to improve its mechanical properties [5]. The transverse dimensions of a brick are $12.8 \times 10.2 \text{ cm}^2$ and the thickness along the beam direction is 7.9 cm (about 10 radiation lengths). The construction of more than 150,000 bricks for the neutrino target has been accomplished by an automatic machine, the Brick Assembly Machine (BAM) operating underground in order to minimize the number of background tracks from cosmic-rays and environmental radiation. The BAM was delivered at LNGS in July 2006 and made operational in September 2006. The production lasted from March 2007 to June 2008 with an average rate of 650 assembled bricks/day. In this period, the brick production at the BAM was based on two shifts/day of 8 hours each, 5 working days a week. Each shift involved 7 operators plus 1 site manager. At the end of mass production the BAM had assembled 146621 bricks (June 2008). A few thousand more have been produced at the beginning of 2009 after the delivery of the remaining lead, delayed by an accident which occurred at lead producing factory (JL Goslar, Germany) in June 2008. The bricks have been inserted in the detector target by BMS and housed in a light support structure placed between consecutive TT walls. The support structure has been designed with the requirement of minimizing the material along the neutrino beam direction in order to reduce to the 0.1% level the number of interactions in regions not instrumented with emulsion films or scintillators.

In order to reduce the emulsion scanning load the use of Changeable Sheets (CS) [6], successfully applied in the CHORUS experiment, was extended to OPERA. Tightly packed doublets of emulsion films are attached to the downstream face of each brick and can be removed without opening the brick. Charged particles from a neutrino interaction in the brick cross the CS and produce a trigger in the TT scintillators. Following this trigger the brick is extracted and the CS developed and analyzed in the scanning facilities at LNGS and in Nagoya. The information of the CS is used for a precise prediction of the position of the tracks in the most downstream films of the brick, hence guiding the so-called *scan-back* vertex finding procedure.

The brick, CS and TT layout [6] is schematically shown in Figure 2.

First data were collected by the OPERA detector in 2006 with the electronic detectors alone, in 2007 with reduced target and in 2008, 2009 and 2010 with the full target installed (around 150000 bricks).

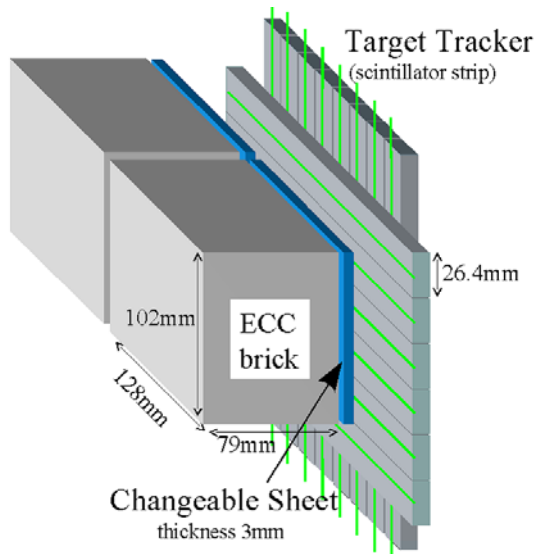


Figure 2: Schematic view of two bricks with their Changeable Sheet and target tracker planes.

Run 2008 status			
	0mu	1mu	All
Events predicted by electronic detector	406	1292	1698
Found CS	275	1053	1328
Neutrino interactions in the bricks	166	825	991
Located in dead material	26	94	120
Interaction in the upstream brick	6	34	40
Decay search performed	159	791	950

Table 1: Event location in the bricks for the 2008 Run

2 Real time detection of CNGS Beam

The CNGS neutrino beam was designed and optimized for the study of $\nu_\mu \rightarrow \nu_\tau$ oscillations in appearance mode, by maximizing the number of charged current (CC) ν_τ interactions at the LNGS site. For a detailed description of the CNGS beam we refer to [2].

After the beam commissioning run in 2006, the CNGS run started on September 2007 at rather low intensity. The first event inside the OPERA target was observed on October 3rd.

A longer run took place in 2008 [3] when 1.782×10^{19} protons were delivered on the CNGS target. OPERA collected about 10100 events on time with the arrival of the beam at the Gran Sasso and among them around 1700 interactions in the bricks. The other events originate outside the target region (spectrometer, OPERA supporting structures, rock surrounding the cavern, hall structures). The scanning of these events is completed and the status of the measurements is shown in TABLE I. In 2009 the CNGS beam started

on May the 30th and lasted until November the 23rd. The final integrated intensity was 3.522×10^{19} p.o.t. The total number of events recorded in time with the CNGS spill was 21428, of which 3693 are tagged as internal events. The 2010 run is described in the last paragraph

3 Event Identification: from ECC Extraction to Kinematical Reconstruction

In the following the breakdowns of the different steps which are carried out to analyze the neutrino interaction events are described: from the identification of the "fired" brick up to the detailed kinematical analysis of the vertex in the emulsion films.

Once a trigger in the electronic detectors is selected to be compatible with an interaction inside the brick, the following procedure, named "Brick Handling", is applied:

1. the whole electronic detector data are processed by the reconstruction program and the most probable brick, inside which the neutrino interaction may have occurred, is selected;
2. the brick is removed from the detector by the BMS and exposed to X-rays for film-to-film alignment. There are two independent X-ray exposures: the first one ensures a common reference system to the CS films doublet and the brick (frontal exposure); the second produces thick lateral marks on the brick edges used for internal alignment and film numbering;
3. after first X-ray exposures the CS doublet is detached from the brick and developed underground while the brick is stored underground in a box with 5 cm thick iron shielding to reduce the radioactivity background.
4. if the CS scanning is successful in locating tracks compatible with those reconstructed in the electronic detectors, the brick is brought to the surface laboratory and exposed to cosmic-rays for about 24 hours inside a pit. The pit has been built to select high-energy particles in order to provide straight tracks in the bricks for a refined (sub-micrometric) film-to-film alignment;
5. the brick emulsion films are then developed in the OPERA developing laboratory at LNGS (Figure 3) and dispatched to the various scanning laboratories. Half of the removed bricks are sent to Japan for emulsion measurement, the other half is measured in the European laboratories. The CS of the European bricks are all measured at the LNGS Scanning Station (Figure 3) for event confirmation and localization.

The overall efficiency for the selection of bricks with neutrino interactions inwards depends of the convolution of several effects and measurements. We address here the issues on the two most important ones, the Changeable Sheet measurement and the Brick Finding. For the time being preliminary results have been obtained from the analysis of the first samples of events in 2007, 2008 and 2009 runs.



Figure 3: Left: Two of the six chains of the film development facility at the LNGS external laboratory. Right: The European CS Scanning Station at LNGS.

The ability in selecting the "fired" brick is the convolution of several effects and measurements. Here we discuss the two most important ones, the Brick Finding procedure and the Changeable Sheet measurement, for which preliminary results have been obtained from the analysis of partial samples of already scanned events.

The tracking efficiency of single emulsion films can be measured by exposure to high-energy pion beams [7]. However, the measurement of the CS doublet efficiency in situ, in the OPERA detector, is by far more challenging, given the coarse resolution in the extrapolation of tracks from the electronic detectors to the CS.

At the present, we are studying the CS tracking efficiency by two independent approaches: (a) all tracks produced in already located neutrino vertices are followed downstream and searched for in the corresponding CS doublet; (b) muon tracks reconstructed by the electronic detectors and found in the CS are normalized to the total number of CC events where at least one track (not necessarily the muon) is found in the CS. The two methods yield a preliminary efficiency for finding a track in both films of the CS doublet which is compatible with the conservative expectation of $\sim 90\%$ on a single film.

The brick finding algorithm exploits the tracking capabilities of the OPERA electronic detectors and, by combining this information with the output of a Neural Network for the selection of the most probable wall where the interaction occurred, provides a list of bricks with the associated probability that the interaction occurred therein. A preliminary estimate of the brick finding efficiency, limited to the extraction of the most probable brick, is compatible with the Monte Carlo estimate of $\sim 70\%$ computed for a standard mixture of CC and NC events. A higher efficiency can be obtained by extracting also bricks ranked with lower probabilities.

All tracks measured in the CS are sought for in the most downstream films of the brick and followed back until they are not found in three consecutive films. The stop is considered as the signature of a primary or secondary vertex. The vertex is then confirmed by scanning a volume with a transverse size of 1 cm^2 for 11 films in total, upstream and downstream of the stopping point. Preliminary results on the vertex location efficiency as measured with the data are in agreement with the Monte Carlo expectations of $\sim 90\%$ and $\sim 80\%$ for CC and NC events, respectively. In the subsample of located

neutrino interactions charm and tau decay topologies were searched for. This search is systematically going on.

4 Overview of the OPERA activities in 2010

2010 has been a very special year for OPERA. In June, the first tau analysis - covering about 30% of the 2009-2009 statistics- has been published together with the first tau candidate event [10]. In addition, the 2010 run has been extremely successful. In terms of duration and accumulated statistics it has been the longest since the CNGS startup. In 2010, the CNGS facility accumulated 4.03×10^{19} proton-on-target, corresponding to about 4250 events in the bricks, with an overall duty-cycle for the accelerator complex of 82%. The run started on April 29 and finished on November 22: the OPERA subdetectors were, thus, active and in nominal conditions for about 7 months. On the data analysis side, the 2008 sample has been fully studied, together with a large fraction of the 2009 data; the analysis includes the extraction of the candidate bricks, the scanning of the CS, the vertex localization and the search for a decay topology. The analysis of 2009 data is well advanced and it will be completed by spring 2011 the situation is shown in TABLE II. The event analysis status of 2010 run is shown in TABLE III.

Before the publication of the tau candidate, very important milestones have been achieved. In particular, together with ancillary cosmic ray measurements [11], OPERA has published the first analysis of a high purity charm sample [10], which represents a crucial benchmark for the tau and demonstrates appropriate knowledge of the detector efficiencies. The charm sample studied in [10] corresponds to the same integrated statistics as for the tau candidate. Here, 20 events were observed, to be compared with a MC expectation of 16 events. Significant improvements have also been achieved in the study of systematics from hadron rescattering and charm contamination in the tau sample. Such achievements were mainly boosted by the analysis of the tau candidate, interpreted as a $\tau \rightarrow \text{hadron}$ (1-prong) event (see Fig.4). In order to avoid post-processing biases, data have been analyzed using the same selection cuts as for the experiment Proposal [9]. However, a complete reevaluation and tuning of the selection criteria is in progress: the new analysis takes advantage of the large statistics accumulated so far and allows for a data-driven evaluation of the detector efficiencies.

References and list of publications

- [1] R. Acquafredda *et al.* [OPERA Collaboration], "First events from the CNGS neutrino beam detected in the OPERA experiment," *New J. Phys.* **8** (2006) 303 [arXiv:hep-ex/0611023].
- [2] R. Acquafredda *et al.* [OPERA Collaboration] "The OPERA experiment in the CERN to Gran Sasso neutrino beam", *JINST* 4:P04018,2009.

Run 2009 status			
	0mu	1mu	All
Events predicted by electronic detector	1097	2460	3557
CS scanned	989	2326	3315
Found CS	694	2009	2703
Neutrino interactions in the bricks	318	1304	1622
Located in dead material	16	102	118
Interaction in the upstream brick	27	142	169
Decay search performed	260	1098	1358

Table 2: Event location in the bricks for the 2009 Run (emulsion scanning still in progress)

Run 2010 status			
	0mu	1mu	All
Events predicted by electronic detector	1165	2747	3912
CS scanned	754	1897	2651
Found CS	391	1090	1481
Neutrino interactions in the bricks	104	384	488
Decay search performed	66	232	298

Table 3: Event location in the bricks for the 2010 Run (emulsion scanning still in progress)

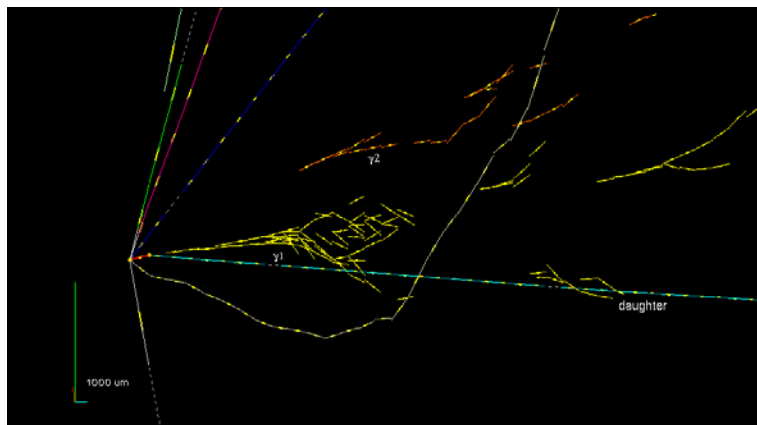


Figure 4: The first OPERA tau candidate (see [10] for details).

- [3] N. Agafonova *et al.* [OPERA Collaboration] "The Detection of neutrino interactions in the emulsion/lead target of the OPERA experiment", JINST 4:P06020,2009.
- [4] T. Nakamura *et al.*, "The Opera Film: New Nuclear Emulsion For Large-Scale, High-Precision Experiments," Nucl. Instrum. Meth. A **556** (2006) 80.
- [5] A. Anokhina *et al.* [OPERA Collaboration], "Study of the effects induced by lead on the emulsion films of the OPERA experiment," JINST **3** P07002 (2008).
- [6] A. Anokhina *et al.* [OPERA Collaboration], "Emulsion sheet doublets as interface trackers for the OPERA experiment," JINST **3** (2008) P07005
- [7] L. Arrabito *et al.*, "Track reconstruction in the emulsion-lead target of the OPERA experiment using the ESS microscope," JINST **2** (2007) P05004
- [8] K. Kodama *et al.*, "Momentum measurement of secondary particle by multiple Coulomb scattering with emulsion cloud chamber in DONuT experiment," Nucl. Instrum. Meth. A **574** (2007) 192.
- [9] M. Guler *et al.*, OPERA proposal, CERN/SPSC 2000-028, SPSC/P318, LNGS P25/2000.
- [10] N. Agafonova *et al.* [OPERA Collaboration], "Observation of a first ν_τ candidate in the OPERA experiment in the CNGS beam," Phys. Lett. *B691* , 138 (2010).
- [11] N. Agafonova, *et al.* [OPERA Collaboration], "Measurement of the atmospheric muon charge ratio with the OPERA detector," Eur. Phys. J. *C67* , 25 (2010).

THEORY GROUP

The research is organized in the six working groups: FA51, GS51, CT51, PD51, PI12, PI21, that are generically denoted as IS (from “Iniziativa Specifiche”). It concerns as main areas: astroparticle physics (mainly FA51), phenomenology of Planck scale physics (GS51), supernova neutrinos (CT51), cosmology, large scale structures and dark matter (PD51), computer simulations of gauge theories (PI12), particle physics phenomenology (mainly PI21). There is a tradition of collaboration between the LNGS theory group and several experimental groups. In this report, we describe the activities of the theory group in 2010.

Members of the group: R. Aloisio, Z. Berezhiani, V. Berezhinsky, D. Boncioli, G. Di Carlo, A. Gazizov, A.F. Grillo, E. Luzio, A. Maiezza, M. Mitra, G. Pagliaroli, P. Panci, L. Pilo, N. Rossi, F. Rossi-Torres, F. Tortorici, F.L. Villante, F. Vissani.

Updated information and further info at: <http://theory.lngs.infn.it/index.html> .

Markov Prize 2010!

The Institute for Nuclear Research (INR) of the Russian Academy of Sciences in Moscow has awarded the 2010 M.A. Markov Prize to a member of our group: V.S. Berezhinsky, who received the award at the 8th Markov Readings in Moscow on May. He is recognized for his “outstanding contribution to the physics of cosmic rays and development of the theory of cosmogenic neutrinos at ultra-high energies”. Our congratulations, Venya!

_____ Theoretical Astroparticle Physics (FA51) _____

The Astroparticle group of LNGS in 2010 included R. Aloisio, **V. Berezhinsky**, A. Gazizov, F. Vissani and visitors V. Dokuchaev (Institute for Nuclear Research, Moscow), Yu. Eroshenko (Institute for Nuclear Research, Moscow), B. Hnatyk (Lviv University, Ukraine), S. Grigorieva (Institute for Nuclear Research, Moscow). The group worked in close collaboration with F. Aharonian (Dublin IAS), P. Blasi (Arcetri Observatory, Firenze), A. Vilenkin (Tufts University, USA), M. Kachelrieß (NUST, Trondheim, Norway) and S. Ostapchenko (Karlsruhe, Germany).

Nagoya, Japan.

V. Berezhinsky presented invited talks:

at M.A. Markov Readings 2010, 20 May 2010, Moscow,

at Int. Conferences “Neutrino 2010” (14-19 June 2010, Athens, Greece,

at 31st Russian Federation Cosmic Ray Conference, 4-10 July 2010, Moscow,

at symposium “Highlights of Astroparticle Physics” 30 September.

F. Vissani gave talks on “Progresses in Neutrino Astronomy” at the 2nd Galileo-Xu Guangqi meeting *The sun, the stars, the universe and general relativity*, Ventimiglia, Italy, July; on “High Energy Neutrino Astronomy: From the Hope for Surprises to Predictions,” at the *National meeting of the Italian Physics Society (SIF)*, Bologna, Italy, September; and the summary talk “PHYSUN-II: Impressions and Conclusive Remarks,” at the *Second PHYSUN Workshop*, LNGS, Italy, October.

Publications in journals, proceedings and preprints

- [1] R. Aloisio, V. Berezhinsky, A. Gazizov,
“Ultra High Energy Cosmic Rays: The disappointing model.”
Revised and extended version of preprint arXiv:0907.5194 v2 (2010), *Astropart.Phys.*
34 (2011) 620626.
- [2] R. Aloisio, V. Berezhinsky, S. Grigorieva,
“Analytic calculations of the spectra of ultra high energy cosmic ray nuclei. II. The
general case of background radiation.”
Revised and extended version of preprint arXiv:arXiv:1006.2484 v2 (2010) submitted
to *Phys. Rev. D*
- [3] R. Aloisio, D. Boncioli,
“Ultra High Energy Cosmic Rays: Anisotropies and Spectrum.”
arXiv:1002.4134
- [4] V. Berezhinsky, V. Dokuchaev, Yu. Eroshenko, M. Kachelrieß, M.Aa. Solberg,
“Superdense cosmological dark matter clumps.”
Phys. Rev. D 81:103529, 2010
- [5] V. Berezhinsky, V. Dokuchaev, Yu. Eroshenko, M. Kachelrieß, M.Aa. Solberg,
“Annihilations of superheavy dark matter in superdense clumps.”
Phys. Rev. D 81:103530, 2010
- [6] V. Berezhinsky, A. Gazizov, M. Kachelrieß, S. Ostapchenko,
“Restricting UHECRs and cosmogenic neutrinos with Fermi-LAT.”
Phys. Lett. B 695, 13, 2011 (arXiv:1003.1496)
- [7] F. Vissani, F. Aharonian, N. Sahakyan,
“On the Detectability of High-Energy Galactic Neutrino Sources.”
arXiv:1101.4842 (to be published in *Astrop. Phys.*).

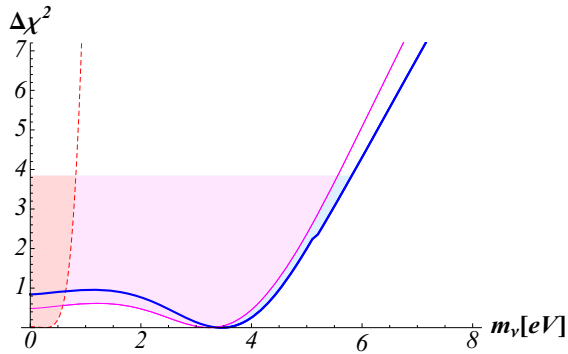


Figure 2: $\Delta\chi^2$ for various neutrino masses, as obtained from SN1987A data and from the simulated events of a future supernova, using the model for electron antineutrino emission described in Pagliaroli et al., *Astropart.Phys.* 31, 163. From [4].

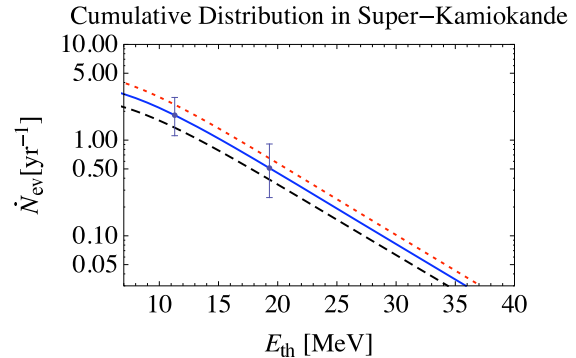


Figure 3: Yearly counting rate in 22.5 kton of water due to relic supernova neutrinos, as a function of the energy threshold of the detector, as derived from SN1987A data. The 3 lines correspond to different cosmic distributions of supernovae. From [1].

Supernova Neutrinos (CT51)

Members: G. Pagliaroli, F. Rossi-Torres and **F. Vissani**. In 2010, the group worked with E. Coccia (Rome U.), M.L. Costantini (ICRANet), W. Fulgione (Turin U.) and A. Ianni.

Scientific work

In Pagliaroli et al., *Astropart.Phys.* 31 (2009) 163, a parameterized model for the emission of electron antineutrinos from a standard supernova—that improves on the earlier proposal by Loredò & Lamb, *Phys.Rev.* D65 (2002) 063002—has been developed.

The analysis of SN1987A events showed that the model describes the data of Kamio-kande-II, IMB and Baksan significantly better than the simpler model of Bahcall, “Neutrino Astrophysics” (Cambridge U. Press, 1989), or the one of Jegerlehner, Neubig, Raffelt, *Phys. Rev.* D54 (1996) 1194. This holds true even keeping into account the increased number of free parameters, and independently from the fact that the new model it is better motivated by the general theory of the standard emission.

In 2010 new applications of the improved model were considered. They further demonstrate its utility and flexibility. Some of them are illustrated in Figs. 2 and 3 and Tab. 1.

Conferences, seminars and other activities

Talks by F. Vissani: May: *Frontier Objects in Astrophysics and Particle Physics* (Vulcano 2010 Workshop) Vulcano, Italy, talk on “What is the Issue with SN1987A Neutrinos?”. December: *5th Symposium on Large TPC for Low Energy Neutrino Detection and Workshop on Neutrinos from Supernovae*, talk on “A Parameterized Model for Electron Antineutrino Emission and its Applications.”

Analysis of SN1987A	Duration of the accretion	$\tau_a = 0.55$ s	[2, 3]
	Neutrinosphere radius	$R_c = 16$ km	[2, 3]
	Neutrino mass	$m_\nu < 5.8$ eV	[4]
Future supernova	Duration of the accretion	$\delta\tau_a/\tau_a=10\%$	[5]
	Neutrino mass	$m_\nu < 1$ eV	[4]
Gravity Wave Burst	Time of the burst	$\delta t < 15$ ms	[5]
Diffuse Background	Counting rate in SK	(0.3-0.9)/yr	[1]
	Counting rate in SK+	(1.1-2.9)/yr	[1]

Table 1: Sample results based on the model of Pagliaroli et al., *Astropart.Phys.* 31, 163.

Other commitments of F. Vissani: Coordinator of the LNGS theory group; Co-organizer of the LNGS seminar series; SIF referent person at LNGS; Coordinator for LNGS of the Virgo-EGO Science Forum (VESF); Member of the scientific committee for the ICRANet-INFN agreement; INFN representative in the Science Advisory Committee of ApPEC/ASPERA; co-holder with G. Bellini of a PhD course on neutrinos at Milan U. He worked on high energy neutrinos and gamma rays together with Narek Sahakyan, PhD student at Rome U. and followed A. Lami (Rome 3 U.) in his “laurea” thesis [7].

Publications in journals, proceedings and preprints

- [1] F. Vissani and G. Pagliaroli,
“The diffuse supernova neutrino background: Expectations and uncertainties derived from SN1987A.”
LNGS-TH-02-10 (Oct 2010) arXiv:1102.0447.
- [2] F. Vissani, M.L. Costantini, W. Fulgione, A. Ianni, G. Pagliaroli,
“What is the issue with SN1987A neutrinos?”
Proc. of the Vulcano 2010 workshop, arXiv:1008.4726.
- [3] F. Vissani, G. Pagliaroli, F. Rossi-Torres,
“Using supernova neutrinos to monitor the collapse, to search for gravity waves and to probe neutrino masses.”
Proc.of the 1st Galileo Xu Guangqi meeting, arXiv:1005.3682.
- [4] G. Pagliaroli, F. Rossi-Torres, F. Vissani,
“Neutrino mass bound in the standard scenario for supernova electronic antineutrino emission.”
Astropart. Phys. 33 (2010) 287.

- [5] G. Pagliaroli,
 “Using neutrinos to search for gravity waves.”
 J. Phys. Conf. Ser. 203 (2010) 012080.
- [6] I. Leonor et al. (with G. Pagliaroli and F. Vissani),
 “Searching for prompt signatures of nearby core-collapse supernovae by a joint analysis of neutrino and gravitational-wave data.”
 Class. Quant. Grav. 27 (2010) 084019
- [7] Thesis by A. Lami,
 “Interazioni deboli semileptoniche e loro applicazioni in fisica astroparticellare.”
 Rome 3 University, 2010, advisors V. Lubicz and F. Vissani.

_____ Cosmology and Dark Matter (PD51) _____

Members: Z. Berezhiani, P. Panci, L. Pilo, F. Tortorici, **F.L. Villante** and F. Vissani. They worked in collaboration with L. Canton and C. Brogini (INFN-Padova), A. Serenelli (UAM-Barcellona), D. Comelli and F. Nesti (INFN-Ferrara), A. Riotto (CERN and INFN-Padova), M. Cirelli (CERN and CNRS), A. Drago (University of Ferrara), D. Blas (IPT, Lausanne), M. Nemevšek (IJS, Ljubljana), G. Senjanovic (ICTP, Trieste).

Scientific work

The research activity has been focused on the following topics:

i) Modifications of gravity. Using an effective field theory approach we have studied how one of the benchmark solutions of general relativity, namely the Schwarzschild solution, is modified in massive gravity. The modification found is twofold: renormalization of the total mass of the body and non-analytic term r^γ , $\gamma < -1$, whose size depends on the size of the body.

The metric has the form

$$ds^2 = -J(r)dt^2 + J^{-1}(r)dr^2 + r^2d\Omega^2 .$$

The typical form of the solution is shown in figure (4). For the equation of state for matter inside the self-gravitating body of radius R we have used $\rho = \rho_0 = 3M_0/4\pi R^3$. The solution depends also on an effective mass parameter μ that encodes the details of the massive deformation.

ii) Direct and Indirect dark matter search. We have discussed some astrophysical implications of the dark matter interpretation of the PAMELA e^+/e^- excess. Moreover, we have considered the effect of reionization and heating of the primordial gas that can be produced by Dark Matter annihilations after recombination and during the epoch of structure formation. Finally, we have compared the gamma ray fluxes predicted by Dark

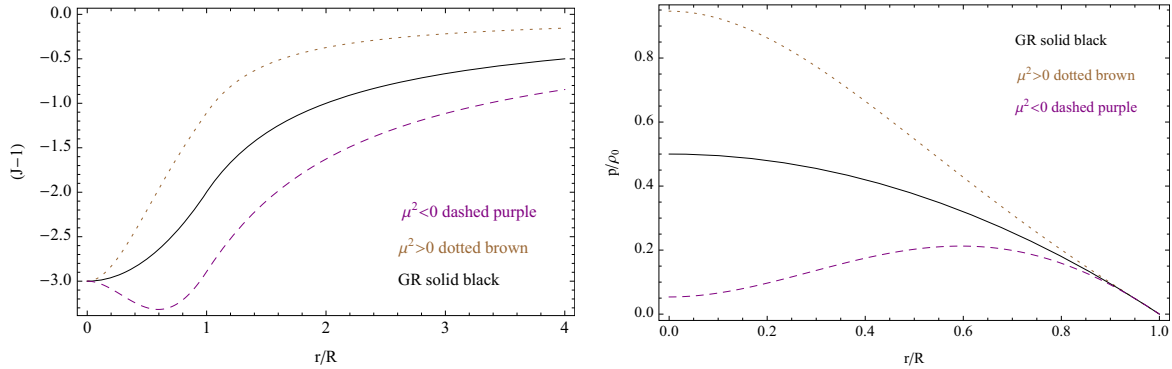


Figure 4: Plot, in the linear regime, of $J - 1$ and the pressure p/ρ_0 inside of a self-gravitating body. The case of massive gravity and standard GR are shown. The numerical values used are: $\mu^2 R^2 = \pm 3.06$, $R_s/R = 8.6 \times 10^{-7}$ and $\gamma = -2.5$. The units are such that $GM_0/R = 1$. From [6].

Matter annihilation or decay (both from prompt emission and from Inverse Compton Scattering) with the Fermi first year observations, excluding large regions of the Dark Matter parameter space.

Conferences, seminars and other activities

International Workshop on *Hot topics in cosmology* SW34, Cargese, France, May 2010 (talks by Z. Berezhiani, L. Pilo).

Int. Workshop “Dark Matter: Its Origin, Nature and Prospects for Detection”, June 2010, Galileo Galilei Institute for Theoretical Physics, Florence, Italy (seminar by Z. Berezhiani).

International Workshop on *Long-Baseline Neutrino Physics and Astrophysics*, Seattle, USA, August 2010 (talk by F.L. Villante).

International *Neutrino Oscillation Workshop* NOW2010, Otranto (LE), Italy, September 2010 (talk by F.L. Villante).

F.L. Villante gave seminars in Padova (October 2010) and Madrid (November 2010).

F. Vissani organized the meeting in honor of G. Senjanovic “The Joy of Making Physics (Goranfest)” June 2010, Split, Croatia.

Publications in journals, proceedings and preprints

- [1] M. Cirelli, P. Panci, P. D. Serpico,
“Diffuse gamma ray constraints on annihilating or decaying Dark Matter after Fermi.”
Nucl.Phys.B840:284-303,2010.
- [2] F.L. Villante and B. Ricci.
“Linear Solar Models.”
Astrophys.J.714:944-959,2010.

- [3] Zurab Berezhiani, Luigi Pilo, Nicola Rossi,
“Mirror Matter, Mirror Gravity and Galactic Rotational Curves.”
Eur. Phys. J. C70:305-316, 2010.
- [4] F.L. Villante,
“Linear Solar Models: a simple tool to investigate the properties of solar interior.”
J.Phys.Conf.Ser.203:012084,2010.
- [5] F.L. Villante,
“Constraints on the opacity profile of the sun from helioseismic observables and solar neutrino flux measurements.”
Astrophys.J.724:98-110,2010.
- [6] D. Comelli, F. Nesti, L. Pilo,
“Stars and (Furry) Black Holes in Lorentz Breaking Massive Gravity.”
arXiv:1010.4773 (Oct 2010).
- [7] M. Cirelli, G. Corcella, A. Hektor, G. Hutsi, M. Kadastik, P. Panci, M. Raidal, F. Sala, A. Strumia.
“PPPC 4 DM ID: A Poor Particle Physicist Cookbook for Dark Matter Indirect Detection.”
arXiv:1012.4515, CERN-PH-TH-2010-057 (Dec 2010).
- [8] V. Tello, M. Nemevsek, F. Nesti, G. Senjanovic, F. Vissani,
“Left-Right Symmetry: from LHC to Neutrinoless Double Beta Decay.”
arXiv:1011.3522 (Nov 2010).

Non-Perturbative QCD (PI12)

Member: **Giuseppe Di Carlo**, in collaboration with Vicente Azcoiti, Eduardo Follana e Alejandro Vaquero from Departamento de Fisica Teorica - Universidad de Zaragoza.

Scientific work

The activity of PI12 concerns non perturbative aspects of lattice gauge theories and in particular the study of topological structures and of QCD at finite temperature and density.

The main interest of our group is the study of lattice theories with sign problem, in particular Lattice QCD at non-zero baryon density; we are also working on a class of possible new geometric algorithms for simulating fermion models. Another field of interest are non abelian gauge theories with theta term in the action.

Our activity during 2010 mainly regarded the study of the realization of parity and flavour symmetries in QCD from first principles. Some recent results obtained with

fermions in the Ginsparg-Wilson regularization have been presented in a paper published in JHEP. Preliminary results on the characterization of the structure of the Aoki phase have been presented by A. Vaquero at the Lattice 2010 Conference.

Publications in journals, proceedings and preprints

- [1] V. Azcoiti, G. Di Carlo, E. Follana, A. Vaquero,
“Parity Realization in Lattice QCD with Ginsparg-Wilson Fermions.”
JHEP 1007 (2010) 047
- [2] V. Azcoiti, G. Di Carlo, E. Follana, A. Vaquero,
“The Aoki phase revisited.”
PoS(Lattice 2010)091,2010

———— Particle Physics Phenomenology (PI21) ————

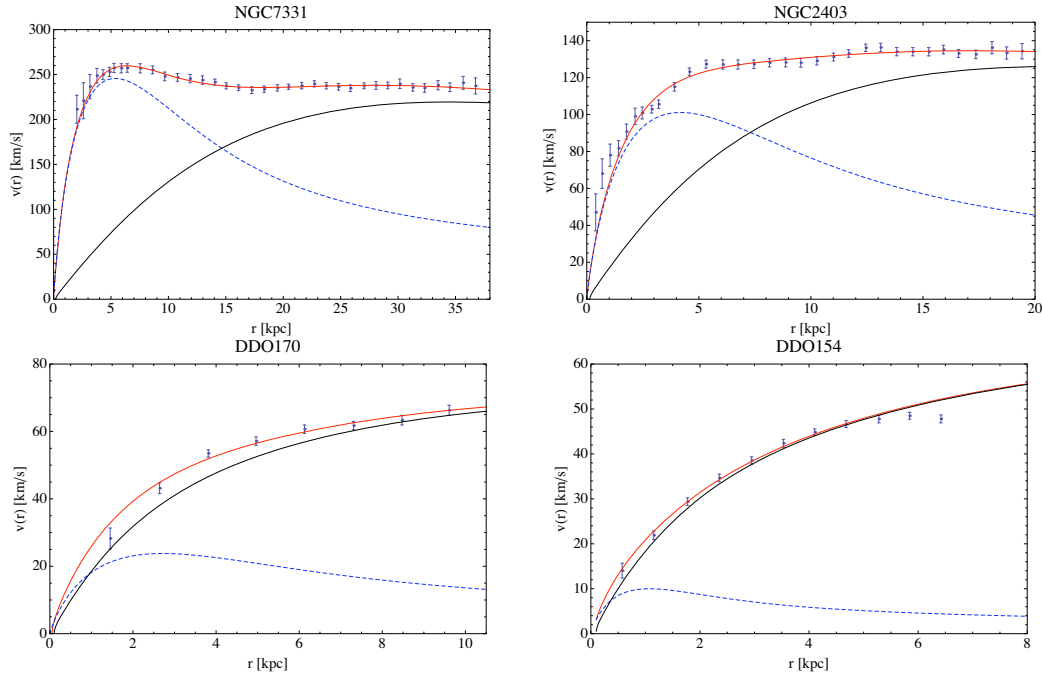
Members: **Z. Berezhiani**, A. Maiezza, P. Panci, L. Pilo, N. Rossi, F. Villante.

Scientific work

One line of the research was devoted to the large distance modifications of gravity (also known as massive gravity) that can change our views on the problem of dark matter and dark energy. In particular, we studied the massive phase of gravity realized by coupling the metric of the general relativity to additional twin metric related to the twin (mirror) matter, in conditions the Lorentz symmetry breaking. Thus, the two matter components, visible (ordinary) and dark (mirror), couple to separate gravitational fields that mix to each other through small Lorentz-breaking mass terms. There are two spin-2 eigenstates: the massless graviton that induces universal Newtonian attraction, and the massive one that gives rise to the Yukawa-like potential which is repulsive between the ordinary and dark bodies. Namely, a source composed of both type 1 and type 2 masses, M_1 and M_2 , induces the following gravitational potential for an ordinary test particle:

$$\phi(r) = -\frac{G_N(1 + e^{-\frac{r}{r_m}})M_1}{2r} - \frac{G_N(1 - e^{-\frac{r}{r_m}})M_2}{2r}, \quad (1)$$

where G_N is the Newton constant. As a result the distances much smaller than the Yukawa radius r_m the gravitation between the two types of matter becomes vanishing, while at large cosmological distances it becomes universal but with *halved* Newton constant $G_N/2$. If $r_m \sim 10$ kpc, a typical size of a galaxy, there are interesting implications for the nature of dark matter. In particular, one can avoid the problem of the cusp that is typical for the cold dark matter halos. Moreover, the flat shape of the rotational curves can be explained even in the case of the collisional and dissipative dark matter (as mirror matter)



	NGC7331	NGC2403	DDO170	DDO154
r_1	4.5 kpc	2.0 kpc	1.1 kpc	0.50 kpc
M_L	$54 M_9$	$7.9 M_9$	$0.18 M_9$	$0.05 M_9$
M_1	$98 M_9$	$12.6 M_9$	$0.4 M_9$	$0.03 M_9$
$\gamma = M_1/M_L$	1.8	1.6	2.2	0.6
M_2	$103 M_{10}$	$26 M_{10}$	$7.6 M_{10}$	$6.0 M_{10}$
$\beta = M_2/M_1$	10.5	20.6	190	2000
r_2	9.0 kpc	3.2 kpc	0.87 kpc	0.66 kpc
$\alpha = r_2/r_1$	2.0	1.6	0.8	1.3
$\chi^2_{d.o.f.}$	0.8	1.3	1.5	0.6

Figure 5: Fitting the rotational curves (solid) for different galaxies using the modified potential and disc-like distribution for dark matter. We also show contributions from dark matter v_{dm} and from luminous matter v_{vis} (dotted). In all cases the Yukawa radius is fixed as $r_m = 10$ kpc.

that cannot give the extended halos but instead must form galactic discs similarly to the visible matter. The observed rotational curves for the large, medium-size and dwarf galaxies, with masses from $10^{11} M_\odot$ down to $10^7 M_\odot$ can be nicely reproduced – see Fig. 5. Their optical disc scales r_1 and the “luminosity” masses $M_L = (L/L_\odot) M_\odot$ shown in the Table are taken from observations, in units of $M_9 = 10^9 M_\odot$, etc.; the ordinary and dark masses M_1, M_2 and the dark disc radius r_2 are the best fit parameters [1].

In other line of research, the diffuse gamma ray data from FERMI first year observations were analyzed and compared to the gamma ray fluxes predicted by Dark Matter annihilation or decay (both from prompt emission and from Inverse Compton Scattering), for different observation regions of the sky and a range of Dark Matter masses, annihilation/decay channels and Dark Matter galactic profiles [6]. We have found that the data exclude large regions of the Dark Matter parameter space not constrained otherwise and discuss possible directions for future improvements. Also, we further constrain Dark

Matter interpretations of the e^+e^- PAMELA/FERMI spectral anomalies, both for the annihilating and the decaying Dark Matter case: under very conservative assumptions, only models producing dominantly $\mu^+\mu^-$ and assuming a cored Dark Matter galactic profile can fit the lepton data with masses around 2 TeV.

Conferences, seminars and other activities

- Int. Workshop SW4 “*Hot topics in Modern Cosmology*”, 10-15 May 2010, Cargese, France; talks of Z. Berezhiani ”Looking glass house: Dark matter, dark gravity” and L. Pilo ”Recent developements in massive gravity”.
- Int. Conf. “*The Dark Matter Connection: Theory and Experiment*”, 17-21 May 2010, GGI, Florence; invited talk of Z. Berezhiani on ”Mirror dark matter”
- Int. Workshop “*Dark Matter: Its Origin, Nature and Prospects for Detection*”, 1-19 June 2010, GGI, Florence; seminar talk of Z. Berezhiani on Neutron oscillations
- Int. Workshop Multi³ “*A Cubic Approach to Dark Matter*”, 1-5 March 2010, Padua, Italy; invited talk of P. Panci on “Diffuse gamma Ray Constraints on Annihilating or Decaying Dark Matter after FERMI”
- Int. Workshop Planck 2010, “*From the Planck Scale to the Electroweak Scale*”, 31 May - 4 June 2010, CERN, Geneve, Switzerland, P. Panci participant.
- Int. Conf. TeVPA, “*TeV Particles Astrophysics*”, 19-23 July 2010, Paris, France; talk of P. Panci on “Diffuse gamma Ray Constraints on Annihilating or Decaying Dark Matter after FERMI”
- 4th UniverseNet School, “*Frontiers of Particle Cosmology*”, 13-18 Sept. 2010, Lecce, Italy; talk of P. Panci on “Diffuse gamma Ray Constraints on Annihilating or Decaying Dark Matter after FERMI”
- Int. Workshop on “*Long-Baseline Neutrino Physics and Astrophysics*”, Aug. 2010, Seattle, USA; talk of F. Villante on Linear solar models.
- Int. *Neutrino Oscillation Workshop* NOW2010, 4-11 Sept. 2010, Otranto, Italy, talk of F. Villante on “Helioseismic and neutrino constraints on solar composition and opacity”.
- Z. Berezhiani gave seminars on ”Mirror matter and mirror Gravity” in EPFL, Lausanne, Switzerland, February 2010; on Dark Matter, ETHZ, Zurich, Switzerland, April 2010; on ”Mirror Matter as dark matter” and ”Ordinary-mirror particle mixing phenomena” in JINR, Dubna, Russia, Oct.- Nov. 2010; and invited lecture on ”Parallel mirror world” at the Tbilisi State University (TSU), Georgia, Sept. 2010
- F. L. Villante gave seminars in Padova (Oct. 2010) and Madrid (Nov. 2010).

Z. Berezhiani was the organizer, together with R. Triay (Univ. Marseille), and A.D. Dolgov (Univ. Ferrara) of the Int. Workshop SW4 “*Hot Topics in Modern Cosmology*”, Cargese, France, May 2010.

Publications in journals, proceedings and preprints

- [1] Z. Berezhiani, L. Pilo, N. Rossi,
“Mirror Matter, Mirror Gravity and Galactic Rotational Curves.”
Eur. Phys. J C 70, 305-316 (2010).
- [2] A. Maiezza, M. Nemevsek, F. Nesti, G. Senjanovic,
“Left-Right Symmetry at LHC.”
Phys. Rev. D 82, 055022 (2010).
- [3] F.L. Villante and B. Ricci,
“Linear Solar Models.”
Astrophys. J. 714, 944-959 (2010).
- [4] F.L. Villante,
“Constraints on the opacity profile of the sun from helioseismic observables and solar neutrino flux measurements.”
Astrophys. J. 724, 98-110 (2010).
- [5] F.L. Villante,
“Linear Solar Models: a simple tool to investigate the properties of solar interior.”
J. Phys. Conf. Ser. 203, 012084 (2010).
- [6] M. Cirelli, P. Panci, P.D. Serpico,
“Diffuse gamma ray constraints on annihilating or decaying Dark Matter after Fermi.”
Nucl. Phys. B840, 284-303 (2010).
- [7] M. Cirelli, G. Corcella, P. Panci et al.
“PPPC 4 DM ID: A Poor Particle Physicist Cookbook for Dark Matter Indirect Detection.”
e-Print: arXiv:1012.4515 [hep-ph], Dec 2010. 52pp.
- [8] D. Comelli, F. Nesti, L. Pilo,
“Stars and (Furry) Black Holes in Lorentz Breaking Massive Gravity.”
e-Print: arXiv:1010.4773 [hep-th], Oct 2010. 22pp.

Theory Group and LNGS

As illustrated in this report, there are several direct connections between the research at the LNGS Theory Group and the INFN experiments on astroparticle physics: this applies to cosmic rays, high energy neutrinos, indirect search for dark matter, gravity, etc. Here, we mention two more results obtained in 2010 that have a rather direct connection with the existing experimental activities hosted at the LNGS: in fact, they are concerned with solar neutrinos and neutrinoless double beta decay.

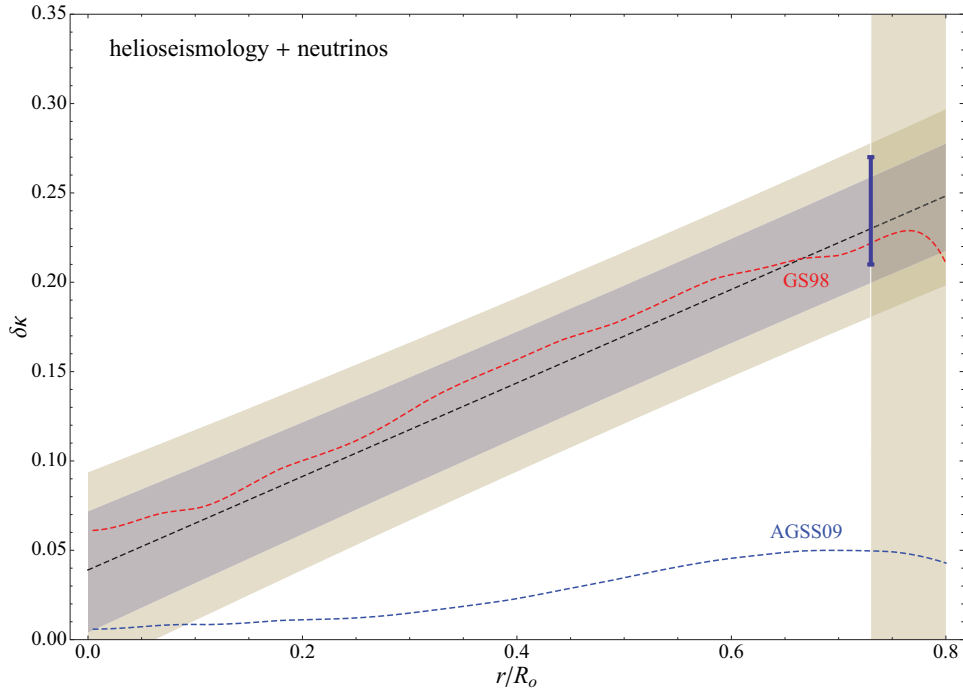


Figure 6: Constraints on the opacity profile of the sun obtained from helioseismic and solar neutrino data. The dark (light) area shows the opacity variation required to reproduce at 1σ (2σ) level the helioseismic determination of the solar surface helium abundance and convective radius and the experimental information on the boron and beryllium neutrino flux. The red (blue) dashed lines correspond to the composition opacity changes obtained when we replace the AGS05 composition with the GS98 (AGSS09) admixture. From F.L. Villante, *Astrophys.J.*724 (2010) 98.

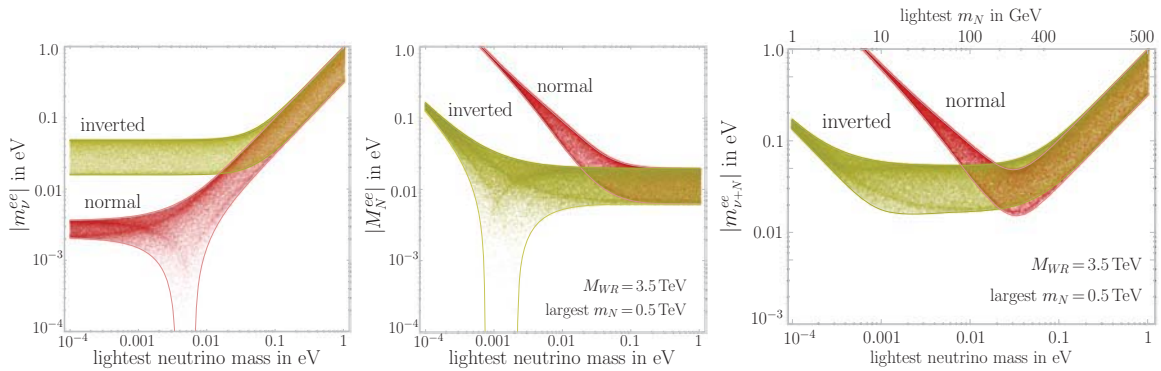


Figure 7: Impact of the left-right symmetry at TeV on the neutrinoless double beta decay. First panel, contribution to the transition from light neutrino exchange. Second panel, new contribution from the exchange of heavy neutrinos and simultaneous emission of charged-bosons coupled to the right currents, whose masses are denoted as m_N and M_{W_R} , respectively. Last plot, sum of the two contributions. Note the possibility to have a relatively large decay rate, even when the light neutrinos are non-degenerate thus playing a marginal role in cosmology. From V. Tello *et al.*, [arXiv:1011.3522](https://arxiv.org/abs/1011.3522).

WArP

The WArP Collaboration

R.Acciarri^a, M.Antonello^b, B. Baibussinov^c, M.Baldo-Ceolin^d, P.Benetti^e, F. Boffelli^e, F.Calaprice^f, E.Calligarich^g, M.Cambiaghi^e, N.Canci^a, F.Carbonara^h, F.Cavanna^a, S. Centro^d, A.G.Coccoⁱ, N.Deniskina^h, F.Di Pompeo^a, G.Fiorillo^h, C.Galbiati^f, L.Grandi^b, A.Menegolli^e, G. Meng^c, C.Montanari^g, O.Palamara^b, L.Pandola^b, F.Perfetto^h, F. Pietropaolo^c, G.L.Raselli^g, M.Roncadelli^g, M.Rossella^g, C.Rubbia^{1b}, E.Segreto^b, A.M.Szelc^{j,b}, S. Ventura^c, C.Vignoli^{g,b}, A. Zani^e

^a *Università dell'Aquila e INFN, L'Aquila, Italy*

^b *INFN - Laboratori Nazionali del Gran Sasso, Assergi, Italy*

^c *INFN - Sezione di Padova, Padova, Italy*

^d *Università di Padova e INFN, Padova, Italy*

^e *Università di Pavia e INFN, Pavia, Italy*

^f *Princeton University - Princeton, New Jersey, USA*

^g *INFN - Sezione di Pavia, Pavia, Italy*

^h *Università di Napoli e INFN, Napoli, Italy*

ⁱ *INFN - Sezione di Napoli, Napoli, Italy*

^j *IFJ PAN, Krakow, Poland*

¹Spokesman of the WArP Collaboration

Abstract

The WArP programme is a graded programme intended to search for cold Dark Matter in the form of WIMPs. These particles may produce via weak interactions nuclear recoils in the energy range 10 - 100 keV.

A cryogenic noble liquid like Argon permits the simultaneous detection of both ionization and scintillation induced by an interaction, allowing the possibility of discriminating at high efficiency between nuclear recoils signals and background electrons events.

The WArP 100 lt detector, after assembly has been activated in February 2010 in HallB at the underground LNGS site. Due to technical problems however the run was stopped in June 2010. The main outcomes from this run will be summarized here, together with the reasons that led to its interruption.

In parallel, the WArP R&D activity continued all throughout the year with small scale prototypes, aiming at extending the detection capabilities of the two-phase LAr technology for DM search. The most relevant results from this activity are here also briefly summarized.

1 WArP -100 detector: Technical run in 2010

The WArP -100 detector layout is composed by an external passive shield (a polytene 70 cm thick layer as n-shield and a lead 10 cm thick shield for γ 's) sustained by a stainless steel anti-seismic structure, inside the external shield a large 15 ton LAr cryostat (a double wall cryogenic vessel insulated with vacuum and super-insulation and made of stainless steel selected for low radioactive contamination) contains (1) the Inner Detector (100 lt of active LAr target), (2) the active VETO detector formed by about 8 ton of LAr around the inner detector and (3) externally to the active veto, also immersed in LAr, a 10 cm thick shield of polyethylene.

The Inner Detector volume is delimited by a cylindrical field-shaping system for the formation of the drift field inside the LAr internal volume, by a grid system on the top for the extraction of ionization electrons from the liquid Argon volume into the a gas volume above it and for the proportional light production in gas, and by an array of 37 PMTs for the readout of the primary and secondary light signals on top of the gas volume. The boundary surfaces of the Inner Detector volume are lined with a highly reflecting layer coated by a thin wavelength-shifting film (TPB - TetraPhenilBoutadiene). The reflector layer is a polymeric multi-layer plastic mirror totally dielectric and with highest specular reflectivity and the TPB film on it is obtained by deposition with vacuum evaporation technique (about 250 g/cm²). In this way, scintillation VUV photons from energy deposition in the LAr volume propagate inside the LAr volume, then are w-shifted into visible photons when hitting the TPB film on the surface boundaries and finally the visible photons are reflected (several times) from the mirror surfaces beneath, up to collection from the active (photo-cathodic) area of the PMT coverage. The TPB film is, in first approximation, transparent to the visible photons. In addition, the PMT

windows are also coated with a very thin TPB layer (TPB embedded in a polystyrene matrix) whose characteristics are optimized to maximize the transmission of the blue shifted photons and to (at least partially) convert the VUV light emission component that directly hits the photo-sensitive area of the detector.

The Inner Detector is suspended at the center of the LAr volume of the active VETO detector.

This volume works as active shield against residual gamma and neutron backgrounds. Minimum thickness of the active LAr shield is 60 cm. The active VETO detector consists of a set of 270 photomultipliers that are held in place by PEEK supports that are connected to a thin copper structure that delimits the external surface of the active shield volume. The Cu structure is also internally lined with waveshifting/reflecting layers.

The inner detector and the active shield are optically separated (to avoid vetoing of events occurring in the central volume).

The construction and assembly of the WArP -100 detector has been completed in fall 2008. A first activation of the system has been carried out in 2009.

As a consequence of the damage of the high voltage feed-through and cable for the drift field, the WArP 100lt detector was partially disassembled for the necessary repairs (end 2009). During the technical stop the optical system (reflector surfaces with wavelength shifter deposit) of the inner detector was also replaced.

After reassembly and re-positioning inside the cryostat (January 2010), the commissioning of the detector was promptly initiated: vacuum pumping, cooling and LAr filling followed the same procedures of the first run. The filling phase with ultra-purified argon ended on March 16, 2010.

A preliminary test of the HV system was successfully performed (-45 kV applied to the cathode of the inner detector from the new voltage feed-through and cable).

As a second step, the photomultipliers of both the inner detector (37 units) and the external veto system (270 units) were activated, with a slow voltage ramp procedure. When the photomultipliers of the inner detector reached the nominal working conditions the efficiency of the light collection system was evaluated, as in our standardized procedure, from the features of the beta decay spectrum of ^{39}Ar present in concentration of 1 Bq/kg in the natural Ar filling the detector. The scintillation light yield at null field resulted in about 1.5 phe/keV, a value comparable to that achieved during the previous run, Fig.1

The next step, to move into a two-phase operation of the 100lt detector, was the full activation of the electric fields [HV polarization of cathode (-57 kV) and field shaping rings in the LAr volume and of the grids in the gas pocket on top of the liquid Argon surface]. Stable working conditions have been reached recording nominal values of the drain current (through the voltage distribution chain of the field shaping system). The counting rates of the PMTs (inner detector) were also quite stable and within expectations. A first measurement of the LAr purity (determined as ionization electron lifetime in LAr) as been performed thanks to the two-phase operation of the inner detector (primary-to-secondary light signal ratio as a function of depth, induced by ionizing events in the active LAr volume). The electron lifetime was found to be rather modest, in the range of 10

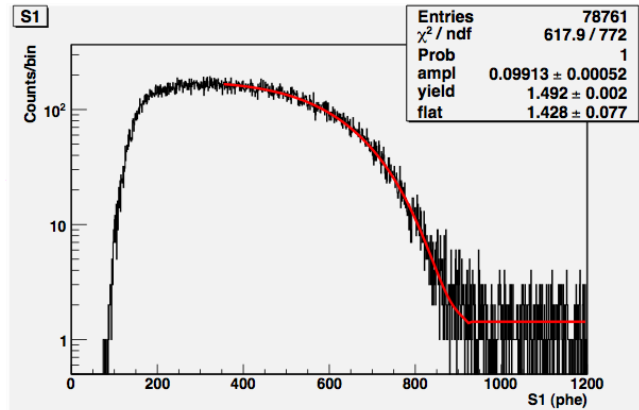


Figure 1: Primary scintillation γ spectrum from ^{39}Ar with the superimposed fit function.

μs , corresponding to a total content of electronegative impurities (Oxygen equivalent) of about 10 ppb.

The activation of the fast LAr purification system (forced LAr circulation through the filter by means of an immersed pump) has been then started as the final step of the detector commissioning (beginning of May 2010).

At this stage a series of unforeseen events have been recorded: the current in the circuit of the high voltage distribution for the drift field became unstable and finally dropped to zero, the counting frequency of individual photoelectrons in the PMTs significantly increased (more than tens of kHz per PMT, as possibly due to occurrence of light discharges in the active volume), the consumption of cryogenics (low quality LAr) in the cooling system increased by about 30%.

Immediately the high voltage system was shut down and all the photomultipliers were powered off.

After that, all the attempts to restore the EF in the inner detector failed: apparently the electric continuity of the resistive chain for the voltage distribution in the field shaping system was interrupted. The need to access the inner detector for inspection of the HV system appeared as necessary and therefore the run had to be halted.

Before stopping, however, a test of the response of the detector active shield (VETO system) has been performed. For this test the readout electronics of the inner detector (38 channels available for direct anode signal digitization and recording) has been used. The study was performed on groups of 38 neighboring VETO PMTs at a time. From the detected light signals (sum of 38 PMTs) of alphas from residual radon decay, by crude extrapolation (to 280 PMTs of the VETO system), a preliminary information on the light collection efficiency of the VETO system has been inferred: ≤ 0.7 phe/keV (assuming a perfect homogeneity of the detector response and taking into account the correction to the collection efficiency due to the light quenching for alpha particles). Moreover, a check of the fast-to-slow signals (Ar recoil-to-background electron) separation capability based

on the F_p criteria has been performed showing a satisfactory level of discrimination, Fig.2.

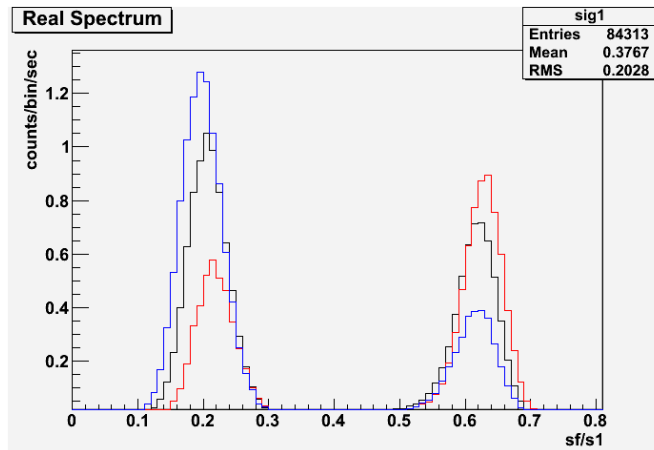


Figure 2: F-prompt distributions for runs 155, 156 and 157 (black, red and blue respectively), obtained with different trigger logics.

Around mid-June 2010 the run was ended, the detector components were all switched off and the main cryostat was emptied. This last operation was carried out by pouring part of the liquid Argon into the storage tank (of the cooling system), by means of the LAr recirculation pump. The insulation vacuum of the main cryostat was then broken and the residual Argon was left to evaporate. The emptying was completed in about 10 days. It took another 10 days to allow the detector returning to room temperature.

In July 2010 the detector (inner detector and surrounding VETO system) was extracted from the main cryostat and brought into the WArP clean room (located nearby, in Hall-B). We then proceeded to a partial disassembly of the detector to access the high voltage divider chain inside the detector. It was found that 6 of the ceramic resistances of the high-voltage divider were indeed broken, presumably due to a mechanical failure resulting from contraction occurred during cooling. The resistive voltage divider was replaced with a parallel of 3 resistors per voltage step. The new layout of the resistor chain allows for a better mechanical flexibility of the anchors. The detector was then moved back into the cryostat and put under vacuum, to avoid further exposure of the wavelength-shifter surfaces to air and light.

The program for a prompt re-activation of the 100 lt detector has been defined, following the recommendations of the funding agencies and of the LNGS Scientific Committee. A technical run will be performed in 2011 after a number of intervention on the detector layout will be completed. These include the test of the new resistive voltage divider, the replacement of the gas Ar recirculation/purification lines with thermally insulated lines to lower the cryogen consumption of the cooling system, interventions on the electronic

boards of the VETO system to better matching the signal read-out sensitivity to the actual experimental conditions, the implementation of an optical screen around the PMTs of the VETO system to reduce PMT instability problems experienced during the test performed during the 2010 run.

2 The WArP R&D activity and results in 2010

Within the WArP R&D program a series of prototype tests has been carried out during 2010 aiming at extending the detection capabilities of the two-phase LAr technology for DM search. In particular this has been achieved by adopting new last generation, high Quantum Efficiency photomultipliers recently made available on the market.

The most significative test has been performed in December 2010 and the results are here briefly summarized.

The experimental set-up is composed with the WArP 2.3 lt chamber equipped with 4 HQE Hamamatsu PMTs (Mod. R11065), contained in the a low-radioactivity st. steel vessel, filled with purified LAr and immersed in a LAr bath of an open cryostat.

The 4 PMT anode signals are directly digitized by two Acqiris Boards (Mod. U 1080 A, 2-chs. each with 8-bit dynamic range) at 1 GHz over a $15\mu\text{s}$ time interval (standard WArP read-out chain, DAQ and off-line codes). The voltage divider is custom made on a G10 printed circuit, with components selected for operation at cryogenic temperature. The boundary surfaces (lateral and bottom) of the 2.3 lt active volume is lined with a TPB coated VIKUITI ESR reflector layer (about $250\ \mu\text{g}/\text{cm}^2$, freshly produced at LNGS with the standard vacuum evaporation technique), the PMT glass windows are instead naked. The photo-cathodic surface is 13% of the total boundary surface (\sim equivalent to the coverage of the 100 lt Inner Detector). In Fig.3 a picture of the detector set-up is shown (vessel and inner 2.3 lt chamber).

After detector assembly the activation of the experimental set-up started on Dec. 13, 2010. It consisted in a vacuum pumping phase (4 days) of the vessel down to few 10^{-5} mbar, followed by a warm GAr flushing phase (24 h) and again by a vacuum pumping phase (2 days, back to 10^{-5} mbar). After immersion of the vessel in the LAr bath water outgassing is halted by temperature drop below freezing point and the residual pressure in the chamber quickly dropped down in the 10^{-6} mbar range. At this stage the LAr filling procedure through an in-line set of filtering cartridges (Oxygen reactant and molecular sieve, Trigon and Zeolite) was started and smoothly completed in about three hours (Dec. 19).

It was decided to completely fill the 2.3 lt vessel, up to full immersion of the PMTs and their bases in LAr. Therefore, the results reported below refer to measurements in single (liquid) phase.

The PMTs (DC coupling) are biased with a low ripple power supply and after a period left for thermalization of the PMTs at LAr temperature (several hours), the bias voltage (negative) on the PMTs cathode was slowly raised up to the working point $\text{HV}=-1400\ \text{V}$ corresponding to a gain of about 3×10^6 .



Figure 3: *Layout of the vessel and inner 2.3 lt chamber. In the present test the LAr level inside the vessel is above the PMT bases (i.e. the detector is operated in single liquid-phase).*

Operation of the detector lasted about 4 days only (Dec. 19 to Dec. 22, 2010). The detector has been exposed to a ^{241}Am source with monochromatic gamma emission at 59.54 keV. A short exposure to a ^{57}Co source (main γ emission line at 122 keV) has been also performed at the end of the run period. The source is located inside a collimator holder positioned outside the 2.3 lt vessel in a fixed position. Data acquisition runs with the sources have been alternated to blank runs (background from ambient radiation).

Scintillation events are detected when the pulse from one of the four PMTs is above threshold (corresponding to 20 *phel*). In this case the four signal waveforms from the PMTs are individually recorded.

During each source (or blank) run, single photo-electron (SER) pulses are selected from out-of-trigger parts of the recorded waveforms, in order to provide with photo-electron data (SER) useful for calibration [from ADC·ns to *phel*].

Measurement of the light yield (LY) attainable in the 2.3 lt chamber with the use of these new PMTs characterized by a high QE at LAr temperature was the main issue of this test.

The LY [*phel/keV* units], primarily depends on the PMT Quantum Efficiency but also upon several other factors, including the detector geometry and the actual operation conditions of the experimental set-up. Among these, the LAr purity and the TPB wavelength-shifting efficiency play a significant role. The detector geometry of the 2.3 lt is a scaled-down version of the WArP 100 lt detector; therefore the results from the 2.3 lt can be assumed to be somehow predictive of the LY from the WArP Inner Detector, when operated under equivalent conditions.

The quality of the TPB coating on VIKUITI ESR reflector has been carefully considered. The set of TPB coated reflector foils showed the expected maximum light output and were installed in the 2.3 lt chamber.

By integration, after local baseline evaluation and subtraction, of each PMT waveform (in a DAQ run) the event signal amplitude is obtained ($S1 = \sum_{i=1,\dots,4} s1_i$ in *phel* units). The pulse amplitude $S1$ is proportional to the electron energy deposited in the LAr cell. Pulse amplitude spectra have been thus obtained for each source run. Blank runs have been also acquired, alternated to the source runs. These are used for ambient background subtraction. Gamma rays from the ^{241}Am source induce photo-electric interactions in the

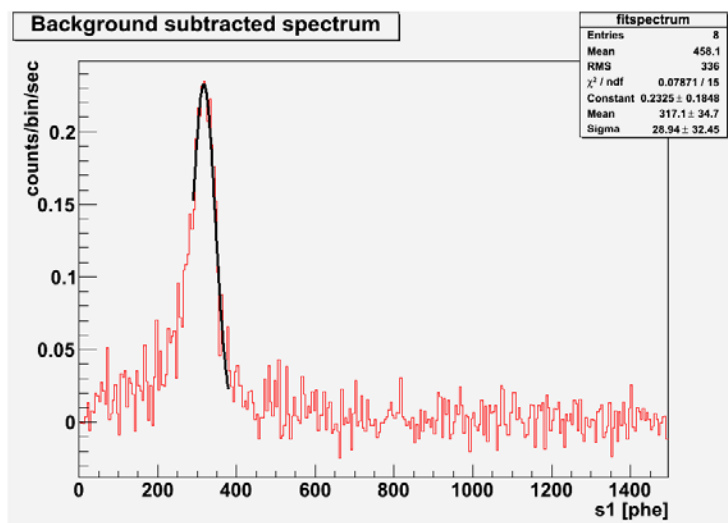


Figure 4: ^{241}Am spectrum (background subtracted). Peak value determined by fit (superimposed)

LAr cell active volume, with electron emission in the *mip* range. The Pulse Amplitude spectrum ($S1$ distribution) shows the expected full absorption peak whose value (in [phe] units) is determined from the gaussian fit of the (run) spectrum and corresponds to 59.54 keV of deposited energy. As example, a ^{241}Am spectrum is shown in Fig.4 (background subtracted), with the full absorption peak at 317 *phel*. Therefore, the Light Yield of the detector can be evaluated as:

$$LY = 5.3 \frac{\text{phel}}{\text{keV}} \pm 5\% \quad (1)$$

The LY value from the spectrum of the ^{57}Co source is less precisely determined, but confirms the above LY value [$LY(\text{Co}) = 5.6 \text{ phel/keV}$].

This LY result, though much higher than any other determined with the 2.3 lt set-up in all previous tests (2005-2010), is lower than expected from simulations and calculations. The LAr purity has been considered as a possible cause of loss of light. The average waveform of the collected signals (in a DAQ run) has been determined and fitted. This

is shown in Fig.5. The exponential fit yields a time constant of the slow component of the scintillation light $\tau_T \simeq 1000$ ns, definitively lower than the value of about $1.3 \mu\text{s}$ expected for pure LAr.

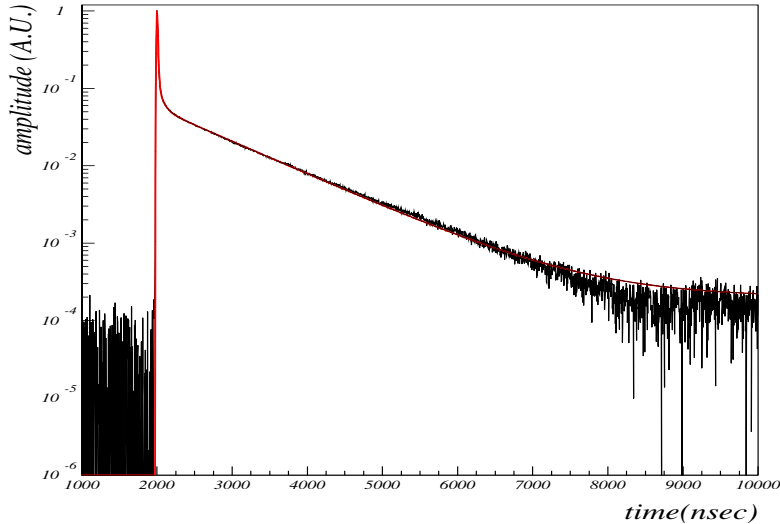


Figure 5: *Average waveform and exponential fit for τ_T determination.*

The filter for O_2 removal used during the filling of the detector was nearly exhausted (as known from previous fillings that showed a decreased LAr purity). There was no time for a regeneration cycle of the filter (considering the limited time available for the run before the Xmas period) and it was decided to use the present filter with the risk of lack of purification performance.

A loss of light of the order of about 20% due to residual Oxygen contamination is envisaged from the actual determination of the τ_T value (and in agreement with LY expectations in case of pure LAr).

The LY result reported from this last test of the 2.3 lt chamber (4 HQE Hamamatsu PMTs) is the highest value ever found, since the first operation of the 2.3 lt prototype (the last two runs with the 2.3 lt PTFE structure with 4 ETL PMTs yielded 0.9 phel/keV - *depAr test* in 2008, and 1.6 phel/keV - *AmBe test* for n/γ PSD studies in 2009). In first approximation this result is approaching the result obtained with the 0.7 lt detector (single liquid-phase) equipped with one HQE Hamamatsu PMT ($\text{LY} \simeq 7$ phel/keV), characterized by an equivalent photo-cathodic coverage ($\sim 13\%$ in both chambers). The difference is attributed to a higher O_2 concentration in LAr, due to lack of filtering performance during filling in this last test.

The 2.3 lt has been smoothly emptied at the end of the run (Dec. 23) and left in GAR atmosphere. A new filter is now available and a new test is foreseen, by refilling the

chamber without any other intervention on the set-up (i.e. same PMTs, same TPB coated reflector surfaces). The aim is to check under (possibly) identical operation conditions the effect of an increased (optimal) LAr purity.

References

- [1] C. Rubbia *et al.*, A programme to search for WIMP particles in Liquid Argon at the LNGS, Letter of intent, Univ. of Pavia, July 1999.
- [2] WArP Collaboration, Status Report of the current progress of the WArP Experiment, Addendum to Proposal **LNGS-EXP 32/05** (2005);
- [3] WArP Collaboration, First results from a dark matter search with liquid argon at 87 K in the Gran Sasso underground laboratory, *Astropart. Phys.* **28** (2008), 495.
- [4] WArP Collaboration, Measurement of the specific activity of ^{39}Ar in natural argon, *Nuclear Instruments and Methods in Physics Research A* 574, 83 (2007).
- [5] D. Acosta-Kane *et al.* (WArP Collaboration), Discovery of underground argon with low level of radioactive ^{39}Ar and possible applications to WIMP Dark Matter detectors, arXiv:0712.0381v1 [astro-ph] (Dec 2007), *Nucl. Instr. and Meth. A* 587 (2008), 46.
- [6] WArP Collaboration, Oxygen contamination in liquid Argon: combined effects on ionization electron charge and scintillation light, *Journal of Instrumentation* **JINST-5-P05003**, 2010.
- [7] WArP Collaboration, Effects of Nitrogen contamination in Liquid Argon, *Journal of Instrumentation* **JINST-5-P06003**, 2010.
- [8] WArP Collaboration, The WArP Experiment, *Journal of Physics: Conference Series* 203 (2010) 012006.

The XENON100 Dark Matter Experiment

E. Aprile^{a *}, K. Arisaka^g, F. Arneodo^c, A. Askin^b, C. Balan^e, L. Baudis^b, M. Beck^h, A. Behrens^b, K. Bokeloh^h, E. Brown^h, G. Bruno^{c,o}, J. Cardoso^e, W.T. Chenⁱ, B. Choi^a, D. Cline^g, J.-P. Cussonneauⁱ, M.P. Decowski^p, S. Fattori^l, A. Ferella^b, F. Gao^j, M. Garbiniⁿ, K.L. Giboni^j, C. Grignon^l, E. Gross^q, V. Hannen^h, F. Kahlhöfer^m, A. Kish^b, C. W. Lam^g, J. Lamblinⁱ, R.F. Lang^a, C. Levy^h, K.E. Lim^a, Q. Lin^j, F. Linde^p, S. Lindemann^m, M. Lindner^m, J.A.M. Lopes^e, K. Lung^g, T. Marrodan-Undagoitia^b, Y. Mei^d, A.J. Melgarejo^a, Y. Meng^g, K. Ni^j, U. Oberlack^{l,d}, S.E.A. Orrigo^e, E. Pantic^g, V. Patricio^e, R. Persianiⁿ, G. Plante^a, G. Sartorelliⁿ, J. M. F. dos Santos^e, R. Schoen^p, M. Schumann^b, M. Selviⁿ, P. Shagin^d, H. Simgen^m, A. Teymourian^g, D. Thersⁱ, O. Vitells^q, H. Wang^g, M. Weber^m, C. Weinheimer^h

^a Department of Physics, Columbia University, New York, NY 10027, USA

^b Physics Department, University of Zurich, Switzerland

^c INFN, Laboratori Nazionali del Gran Sasso, Assergi, 67100, Italy

^d Department of Physics and Astronomy, Rice University, Houston, TX 77251, USA

^e Department of Physics, University of Coimbra, R. Larga, 3004-516, Coimbra, Portugal

^f Dipartimento di Fisica, Università de L'Aquila, Italy

^g University of California, Los Angeles

^h Institut für Kernphysik, Westfälische Wilhelms-Universität, 48149 Münster, Germany

ⁱ Subatech Laboratory, University of Nantes, 44307 Nantes, France

^j Shanghai Jiao Tong University, Shanghai, China

^l Institut für Physik, Johannes Gutenberg Universität Mainz, 55099 Mainz, Germany

^m Max-Planck-Institut für Kernphysik, Saupfercheckweg 1, 69117 Heidelberg, Germany

ⁿ University of Bologna and INFN-Bologna, Bologna, Italy

^o University of L'Aquila, Coppito, 67100 AQ Italy

^p Nikhef, Sciencepark 105, 1098XG Amsterdam, the Netherlands

^q Weizmann Institute of Science, 76100 Rehovot, Israel

* Spokesperson

Abstract

This report summarizes the status of the XENON100 Dark Matter experiment together with the progress achieved in 2010. First results from the search for Dark Matter were rapidly published in Physical Review Letters. These are based on only 11 live days of data, taken during the commissioning of the detector in autumn of 2009. Meanwhile, with more than five months of uninterrupted data taking during spring, more than 100 live days of high-quality low-background data have been acquired. This constitutes an unprecedented data set in the search for Dark Matter. The signal region of this data set is still blinded to allow for an unbiased analysis, with unblinding expected in March 2011. Over the summer, data taking was interrupted to allow for necessary maintenance works on the cryogenic system, which had been running continuously for almost three years. At the time of writing, the detector is filled again with xenon that has been purified even further through our cryogenic krypton distillation column. After verifying the even lower background due to the reduced ^{85}Kr content, Dark Matter data taking will continue well into 2011. Advances in some of the R&D activities at the institutes of the collaboration are also summarized.

1 Introduction

XENON100 is a two-phase liquid/gas time projection chamber (TPC) for the direct detection of WIMP Dark Matter by observing nuclear recoils from WIMPs scattering off xenon nuclei. A two-phase xenon TPC is a very powerful tool for rare event searches. Signal and background discrimination are possible based on the simultaneous detection of the scintillation light (S1) and the electrons released in an interaction. These electrons are drifted in an electric field and extracted into the gas phase, where the charge yields an amplified secondary light signal (S2) due to proportional scintillation. In addition, XENON100 combines the excellent self-shielding capabilities of xenon with event position reconstruction in three dimensions based on the drift time and the hit pattern of the S2 signal.

XENON100 is located in the interferometer tunnel of LNGS in the same location as its predecessor XENON10 (1). While XENON10 has already established some of the best limits on WIMP-nucleon interactions to-date (2; 3), XENON100 improves the sensitivity of this technology even further. XENON100 uses the passive lead/polyethylene shield of XENON10, with the addition of a 5 cm copper layer on the inside as well as additional neutron shielding with 20 cm thick water canisters around the lead shield. With 161 kg of liquid xenon in total and 62 kg in the TPC, XENON100 has 4.5 times more target mass than XENON10 and 6–9 times more fiducial mass. The gamma background was improved by two orders of magnitude by means of an optimized detector design and a careful selection for radiopurity of all materials employed inside the shield. Thus XENON100 is currently the most sensitive detector to observe elastic, spin-independent scattering of weak-scale Dark Matter.

2 Results from the Commissioning Run

Figure 1 (left) shows the calibration of XENON100 with Compton-scattered gammas from a ^{60}Co source as well as neutrons from a $^{241}\text{Am}/\text{Be}$ source. These data sets define the background region due to electronic recoils and the signal region due to nuclear recoils, respectively. Data taken during commissioning was not blinded, but our first analysis was strictly defined on these two calibration sets only. Using this same analysis on 11.17 days live time of background data resulted in the events shown in figure 1 (right).

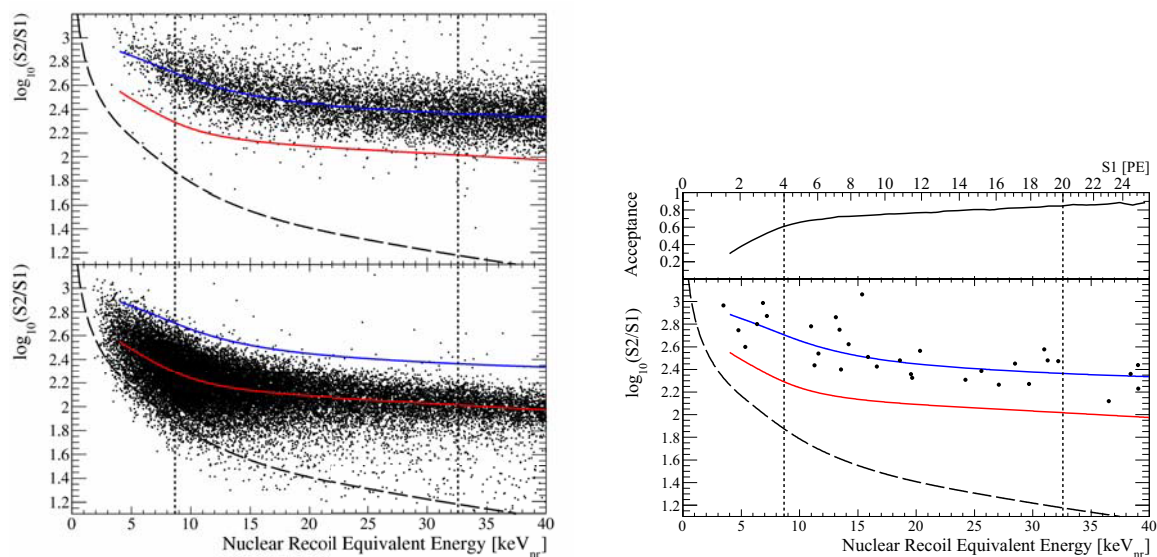


Figure 1: Left: Electronic (top) and nuclear (bottom) recoil bands from ^{60}Co and $^{241}\text{Am}/\text{Be}$ calibration data, respectively, after data selection and the 40 kg fiducial volume cut. Colored lines correspond to the median $\log_{10}(\text{S2}/\text{S1})$ values of the electronic (blue) and nuclear (red) recoil bands. The WIMP search energy window 8.7–32.6 keV_{nr} (vertical, dashed) and S2 software threshold of 300 PE (long dashed) are shown. Right: Cut acceptance (top, not including 50% acceptance from S2/S1 discrimination) and $\log_{10}(\text{S2}/\text{S1})$ (bottom) as functions of nuclear recoil energy for events observed in the 40 kg fiducial volume during 11.17 live days.

In the selected fiducial target of 40 kg, and within the pre-defined signal region, we observe no events and hence exclude spin-independent WIMP-nucleon elastic scattering cross-sections above $3.4 \times 10^{-44} \text{ cm}^2$ for 55 GeV/c^2 WIMPs at 90% confidence level. As shown in figure 2, this result places one of the most stringent limits on the elastic spin-independent WIMP-nucleon scattering cross-section and is already published in Physical Review Letters (4). Even this small data set has caused a stir in the community and triggered much work by various groups on the understanding of liquid noble gas detectors, also of high relevance for liquid argon or liquid neon detectors.

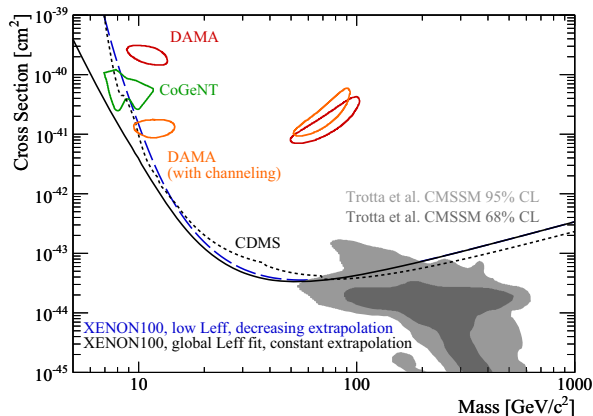


Figure 2: 90% confidence limit on the spin-independent elastic WIMP-nucleon cross section (solid and long dashed), together with the best limit to date from CDMS (dotted) (5), re-calculated assuming an escape velocity of 544 km/s and $v_0 = 220$ km/s. Expectations from a theoretical model (6), and the areas (90% CL) favored by CoGeNT (green) (7) and DAMA (red/orange) (8) are also shown.

3 Dark Matter Search and Upcoming Analyses

In mid-January 2010, we started a Dark Matter run until summer, see figure 3. With more than 100 live days of data, and given our low background level, we now have a data set on tape that is unprecedented in the search for Dark Matter. Additional calibrations with low anode voltages, dedicated to light-pattern based likelihood algorithms, were taken. Analysis of this data set is in full progress and we are anticipating unblinding of the signal region in early 2011. This data will for the first time probe the next order of magnitude in cross section of spin-independent WIMP-nucleon interactions. In parallel to this analysis, we are working on further physics interpretations of the already-published data set as well as publications dedicated to the detector, our extensive screening efforts, and the background simulation.

4 Preparations for Lower Background Search

The pulse tube refrigerator (PTR) together with its associated systems (helium compressor, motor valve, etc.) as well as the recirculation/purification system have been in continuous operation since early 2008 and maintenance became necessary. Having enough data on tape to reach the next order of magnitude in probed WIMP-nucleon cross-sections, we decided to recuperate the xenon to allow these necessary works. Helium compressor, motor valve and helium lines were exchanged. The PTR was also replaced, which, thanks to the design of the XENON100 cooling tower, was possible while leaving a xenon gas atmosphere inside the TPC. On the gas recirculation system, we replaced the membrane pump, installed a new getter cartridge and changed the flow controller for one that is calibrated for xenon gas.

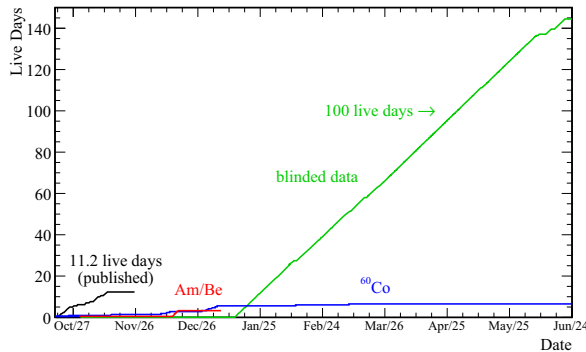


Figure 3: Data taking of run 7 (black) and run 8 (green). More than 100 live days to search for Dark Matter were acquired in run 8 during spring 2010 and are currently being studied.

In the published analysis, we observe 22 electronic recoil events in the energy range of interest and attribute eight of these to a krypton contamination of ~ 150 ppt. This is consistent with a detailed comparison of the observed spectral shape with the simulated background spectrum, as well as a dedicated delayed-coincidence analysis. This summer, we thus processed the xenon through our cryogenic krypton distillation column to lower the background from ^{85}Kr even further, and filled the detector again. This should render the background from ^{85}Kr negligible and enable us to go for a Dark Matter run under even cleaner background conditions, which will bring us well into 2011. We aim to continue this Dark Matter search until we are dominated by other radioactive backgrounds, such as from the photomultipliers (PMTs), thus further improving the sensitivity of XENON100.

5 R&D Efforts at Collaborating Institutions

5.1 Reflectivity of Polytetrafluoroethylene and Quantum Efficiency of Photomultipliers

In xenon experiments, certain optical parameters such as the reflectivity of Polytetrafluoroethylene (PTFE) and the quantum efficiency (QE) of PMTs are important for the understanding the detector response to light. For our simulations, we estimate the QE from the cathode blue sensitivity (SKB) provided by Hamamatsu Co., and use literature values for the PTFE reflectivity measured at higher wavelengths. At the Westfälische Wilhelms-Universität Münster, a setup offering the possibility to measure both quantities under vacuum conditions has been built and is now jointly being operated at Columbia University. A monochromator allows to set various wavelengths, and the temperature can be set with the help of a Pulse Tube Refrigerator (PTR). Inside the setup, a R8520-06-AL Hamamatsu PMT is mounted on a manipulator allowing the adjustment of two angles and linear movement in three directions. PTFE pieces can be placed on a second manipulator, controlling the angle of incident light. The chamber is operating and first results are anticipated in time to allow a simulation-aided design of various details for an

upgraded TPC for XENON100 as well as the XENON1T inner chamber.

5.2 Calibration with ^{83m}Kr

^{83m}Kr can be uniformly distributed in the liquid xenon, diffusing from a ^{83}Rb source placed in the XENON100 gas recirculation system, in order to calibrate the detector response down to the lowest de-excitation energy of 9.40 keV. A potential emanation of ^{83}Rb isotopes from the source would compromise the low background of XENON100 and hence needs to be avoided. Thus we measured the emanation by exposing, at the Westfälische Wilhelms-Universität of Münster, a low-activity OFHC copper tube for 256 hours to a 1.8 MBq ^{83}Rb source deposited in Zeolite beads. After shipment to LNGS, the emanated tube was measured by the University of Zürich with the Gator High Purity Germanium spectrometer for 18.9 days. There was no detectable evidence of γ -lines from ^{83}Rb in the measured spectrum. Hence, the final result is an upper limit of 0.2 mBq to the emanation of the source, which would give a negligible background count rate in the XENON100 region of interest when such a source is used for the calibration of XENON100.

5.3 Light and Charge Yield of Nuclear and Electronic Recoils

A 0.1 kg double-phase xenon TPC is available for R&D studies at the University of Zürich. It has demonstrated the successful use of ^{83m}Kr as a uniform calibration source for liquid xenon detectors (9). The detector is now being used to measure the scintillation efficiency \mathcal{L}_{eff} and the charge yield of low-energy nuclear recoils in double phase mode using a deuterium-deuterium fusion neutron generator that is available at the University of Zürich.

A new liquid xenon detector has been designed and built at the Columbia University Nevis laboratories specifically to measure \mathcal{L}_{eff} in the energy range of a few keV. The active volume of this detector is a $2.5 \times 2.5 \times 2.5 \text{ cm}^3$ cube surrounded by six $2.5 \times 2.5 \text{ cm}^2$ Hamamatsu R8520-406 SEL high QE PMTs. By using this maximized photocathode coverage configuration, we achieved an unprecedented scintillation light yield of 22 PE/keV_{ee} for 122 keV_{ee} γ -rays in single phase operation. The scintillation efficiency of nuclear recoils is obtained by recording fixed-angle elastic scatters of monoenergetic neutrons from a deuterium-deuterium neutron generator, tagged by multiple organic liquid scintillator cells. The detector vessel has also been designed to minimize the amount of materials where neutrons could scatter near the active xenon volume and thus contaminate the fixed-energy elastic nuclear recoil spectrum. Data taking is currently underway and results obtained so far indicate that the apparatus will allow us to measure the scintillation efficiency of nuclear recoils with greater precision, and to very low energies never probed before. Two-phase operation will allow to measure the charge yield also.

In addition, the same systems will subsequently be operated to measure the light and charge yield of electronic recoils. This measurement is a crucial input to determine the electron-equivalent keV_{ee}-energy scale down to very low energies. Using Compton scattered electrons from monoenergetic gamma-rays, and a precise energy selection with a HPGe detector, it will allow to define this energy scale to test hypothetical electronic scatterings from Dark Matter in XENON100, and allow for a direct test of the DAMA annual modulation.

5.4 Performance of Photosensors

The QUPID is an innovative new photon detector whose whole structure is based on synthetic quartz (fused silica), fabricated with extremely low radioactivity and with good transparency for UV light (175 nm from xenon scintillation). The total gain of the QUPID includes contributions from the avalanche photodiode (APD) gain, and the bombardment gain from the electrons accelerated from the photocathode to the APD. At maximum APD bias voltage and photocathode voltage, a gain of 10^6 was achieved and verified at UCLA. At lower temperatures, the gain increases for a given bias voltage, but the maximum gain achievable stays relatively constant. The leakage current was also measured at UCLA for various temperatures. As the temperature decreases, the leakage current also decreases, with a value of 1 nA at the temperature of liquid xenon. In addition, single photoelectron spectra have been measured, with clear peaks for 0, 1, 2, and 3 photoelectrons. The cathode and anode uniformity of the QUPID was checked with a dedicated scanner system and shows good uniformity over most of the photocathode surface. Finally, the QUPID has been successfully operated under liquid xenon in a cryogenic system built at UCLA. The existing system for single-phase liquid xenon operation is currently being upgraded to include xenon gas purification that would allow dual phase operation, and a system for operating seven QUPIDs simultaneously under liquid xenon is also being developed, along with a readout system. In parallel, UCLA is developing a low temperature vacuum UV spectrophotometer in order to measure the QE of the QUPIDs down to liquid xenon temperature.

Further improvements on the QUPID continue at Hamamatsu as well. The APD within the QUPID has been changed to a back-illuminated setup that allows for more stable operation of the QUPID. Recently, several QUPIDs have been manufactured with QE above 40%.

In addition, various photosensors for XENON1T are being tested and characterized at the University of Zürich. A facility to measure dark current, single photon spectrum, and other relevant properties for several sensors simultaneously has been set up. It already lead to first results for the new Hamamatsu R11410 PMT. A chamber to test photosensors in liquid xenon is also under construction.

5.5 Radon Assay

Using HD-II type miniaturized low-background proportional counters developed at the Max-Planck-Institut für Kernphysik Heidelberg, with their extremely low background of about 1 count/day of ^{222}Rn -like events, it is possible to quantify ^{222}Rn at the single-atom level. Combined with a specially developed gas-handling apparatus (gasline), ^{222}Rn emanation pure vessels and a special tool to handle larger amounts of gases and cryogenic liquids (MoREx), it is possible to perform such a ^{222}Rn emanation assay of assembly pieces of various sizes. In the context of the XENON100 experiment, a spare of the Viton o-ring used to seal the cryostat has been measured to have a ^{222}Rn emanation activity (in saturation) of (2.3 ± 0.1) mBq. A neoprene membrane, similar to the one used in the recirculation pump, had a measured emanation activity (again in saturation) of (250 ± 50) μBq .

5.6 Krypton Assay

To quantify the amount of ^{85}Kr in xenon used for XENON100, a gas chromatography (gc) setup was hooked up to a inert gas mass spectrometer at the Max-Planck-Institut für Kernphysik Heidelberg. It was already shown for the BOREXINO experiment that this spectrometer can detect krypton at the sub-ppt level in nitrogen. The gc hook-up is used to separate the krypton from the biggest part of a xenon gas sample taken from the experiment, before it can be measured with the spectrometer. The spectrometer then quantifies the more abundant isotopes ^{84}Kr and ^{86}Kr , and the amount of radioactive ^{85}Kr is then inferred using the isotope ratio. To infer this ratio, a method was developed to measure the ^{85}Kr activity of air, using the above-mentioned HD-II type counters. A program was launched to monitor the LNGS for this isotope in regular periods. In a first measurement, it was found that this activity is $(1.33 \pm 0.16) \text{ Bq/m}^3$.

The Atom Trap Trace Analysis (ATTA) project is single-atom detection experiment being set up at Columbia University to measure the abundance of ^{84}Kr in a xenon sample to the ppt level. The levels of other isotopes of krypton, including radioactive ^{85}Kr , will then be inferred using previously measured relative abundances. A high-power all-diode laser system has been constructed and robustly locked to 811 nm using the heterodyne spectroscopy technique. The construction of the ultra high vacuum system is nearly complete, and pressures of $< 3 \times 10^{-9}$ torr have already been reached. Also, the tapered solenoid that plays a vital role in slowing the atoms has been built and tested. The next phase of development is the discharge source which excites the atoms to the metastable state, and the magneto-optical trap which finally traps the atoms, so that the first atom trapping can occur early in 2011.

6 XENON1T - a ton-scale LXe experiment

The XENON collaboration is preparing for the XENON1T experiment, with lower backgrounds and an order of magnitude more fiducial mass than XENON100, to reach a sensitivity of about $5 \times 10^{-47} \text{ cm}^2$. We would like to continue this program at LNGS and have submitted a proposal for XENON1T (April 2010) and a Technical Design Report (October 2010) to the LNGS Scientific Committee. We propose to locate the XENON1T experiment in Hall B of LNGS, next to the ICARUS experiment. Based on recommendation from the Scientific Committee, we are presently writing a joint XENON100 and XENON1T Memorandum of Understanding (MoU). As part of the MoU, we are arranging for a *Common Fund* that will cover XENON100 operations and general (infrastructure) XENON1T expenditures.

7 List of Publications during 2010

- E. Aprile et. al., First Dark Matter Results from the XENON100 Experiment, Phys. Rev. Lett. 105 (2010) 131302 [1005.0380]
- The XENON100 dark matter experiment at LNGS: Status and sensitivity. By Xenon Collaboration (Elena Aprile for the collaboration). 2010. 6pp. Prepared

for 11th International Conference on Topics in Astroparticle and Underground Physics (TAUP 2009), Gran Sasso, Assergi, Italy, 1-5 Jul 2009. Published in J.Phys.Conf.Ser.203:012005,2010.

- Design and Performance of the XENON10 Dark Matter Experiment. (E. Aprile et al.) *Astroparticle Physics* 34 (2011), pp. 679-698

References

- [1] E. Aprile *et. al.*, *Design and performance of the xenon10 dark matter experiment*, *Astroparticle Physics* **34** (Apr, 2011) 679–698.
- [2] J. Angle *et. al.*, *First Results from the XENON10 Dark Matter Experiment at the Gran Sasso National Laboratory*, *Phys. Rev. Lett.* **100** (2008) 021303 [0706.0039].
- [3] J. Angle *et. al.*, *Constraints on inelastic dark matter from XENON10*, *Phys. Rev.* **D80** (2009) 115005 [0910.3698].
- [4] E. Aprile *et. al.*, *First Dark Matter Results from the XENON100 Experiment*, *Phys. Rev. Lett.* **105** (2010) 131302 [1005.0380].
- [5] Z. Ahmed *et. al.*, *Results from the Final Exposure of the CDMS II Experiment*, *Science* **327** (2010), no. 5973 1619–1621 [0912.3592].
- [6] R. Trotta, F. Feroz, M. P. Hobson, L. Roszkowski and R. Ruiz de Austri, *The Impact of priors and observables on parameter inferences in the Constrained MSSM*, *JHEP* **12** (2008) 024 [0809.3792].
- [7] C. E. Aalseth *et. al.*, *Results from a Search for Light-Mass Dark Matter with a P-type Point Contact Germanium Detector*, 1002.4703.
- [8] C. Savage, G. Gelmini, P. Gondolo and K. Freese, *Compatibility of DAMA/LIBRA dark matter detection with other searches*, *JCAP* **0904** (2009) 010 [0808.3607].
- [9] A. Manalaysay *et. al.*, *Spatially uniform calibration of a liquid xenon detector at low energies using 83m-Kr*, *Rev. Sci. Instrum.* **81** (2010) 073303 [0908.0616].

ERMES

Uranium groundwater anomalies and L'Aquila earthquake: a possible scenario

The ERMES Collaboration

W. Plastino^{a,b}, P. Aprili^c, M. Balata^c, F. Bella^a, A. Cardarelli^c, M. Cozzella^{d,b}, P. De Felice^{d,b}, C. Doglioni^e, M. Frezzotti^f, B. Gallese^c, L. Ioannucci^c, M. De Vincenzia^b, M. Laubenstein^c, S. Nisi^c, G. Panza^{g,h}, A. Peccerilloⁱ, F. Ruggieri^b, L. Tortora^b

^a *Dept. of Physics, Univ. of Roma Tre, I-00146 Rome, Italy*

^b *INFN, Section of Roma Tre, I-00146 Rome, Italy*

^c *INFN, Gran Sasso National Laboratory, I-67010 Assergi (AQ), Italy*

^d *ENEA - INMRI, Rome, Italy*

^e *Dept. of Earth Sciences, Univ. of Roma "La Sapienza", Rome, Italy*

^f *Dept. of Earth Sciences, Univ. of Siena, Siena, Italy*

^g *Dept. of Earth Sciences, Univ. of Trieste, Trieste, Italy*

^h *Abdus Salam International Centre for Theoretical Physics, Trieste, Italy*

ⁱ *Dept. of Earth Sciences, Univ. of Perugia, Perugia, Italy*

Abstract

The use of radon as a possible earthquake's precursor is not clearly linked to crustal deformation. It is shown in this paper that uranium groundwater anomalies, which were observed in cataclastic rocks crossing the underground Gran Sasso National Laboratory, can be used as a possible strain meter in domains where continental lithosphere is subducted. Measurements evidence clear, sharp anomalies from July, 2008 to the end of March, 2009, related to a preparation phase of the seismic swarm, which occurred near L'Aquila, Italy, from October, 2008 to April, 2009. On April 6th, 2009 an earthquake ($M_w = 6.3$) occurred at 01:33 UT in the same area, with normal faulting on a NW-SE oriented structure about 15 km long, dipping toward SW. In the framework of the geophysical and geochemical models of the area, these measurements indicate that uranium may be used as a possible strain meter in extensional tectonic settings similar to those where the L'Aquila earthquake occurred.

1 Introduction

Radon (Rn) as a possible candidate for earthquake's precursor has been studied for a long time, but there is no clear evidence that it is really a precursor [1]. It has been suggested as one of several possible early signals, and its air or groundwater anomalies associated with earthquakes and air-rock or water-rock interactions were detected in several seismogenic areas worldwide. The physical processes associated with Rn anomalies are based on the changes of Rn emanation rates occurring due to strain signal near to the earthquake's nucleation point. Particularly, its behaviour before, during and after the main shock, considering the consolidated scheme for Rn release due to stress-strain processes in the rock is unclear. In the geological environment, the Rn concentration depends on the isotopic abundance of its parent radionuclides (^{238}U and ^{226}Ra), and on their geochemical patterns with reference to environmental redox and pH characteristics. The geodynamic processes induced by earthquakes can modify Rn migration patterns as a potential indicator of strain. However, the activity of Rn in fractured lithologies is difficult to predict, and the Rn concentration does not uniquely constrain the rock deformation or the chemical inhomogeneity nor its relationship with the transient crustal strain signals from 'aseismic' fault slip, near to the earthquake's nucleation point [1].

2 Results and Discussion

The uranium (U) groundwater monitoring started on June 2008 with the aim of better defining the Rn groundwater transport processes through the cataclastic rocks [2], as well as to check its contribution to the neutron background at the LNGS-INFN [3]. The U measurements carried out between June 2008 and December 2010 at four different sites (E1, E4 and E3, E3dx) show the presence of two different water groups, whose existence is confirmed by stable isotope of hydrogen and oxygen ($\delta^2\text{H}, \delta^{18}\text{O}$), ^{14}C and ^3H analyses [4].

Simultaneous measurements of the following parameters were performed for each water sample at the monitoring sites inside the LNGS-INFN: U, sodium (Na), magnesium (Mg), potassium (K), calcium (Ca), electrical conductivity (EC), oxidation-reduction Potential (ORP), and pH. The U, Na, Mg, K and Ca readings show a long-term variability, around the unit value, limited to $\pm 20\%$. In addition to this background, in the period A, from 23rd June 2008 to 31st March 2009, these readings show a clear short-term 40-80% peak structure. Readings of EC, ORP and pH show relatively smooth fluctuations within $\pm 10\%$. A different situation can be observed in period B, from 10th April 2009 to 31st December 2010. The systematic peak structure for U, Na, Mg, Ca and K readings is no longer present, and only few isolated peaks of K and Na can now be observed. Period B readings of EC, ORP and pH show a similar behavior as in period A. The water-rock interaction, modulated by percolation processes (due to meteoric events) above the water table of the Gran Sasso aquifer, do not justify the U anomalies [4]. Therefore, the progressive marked increase of U, along with the enrichment in Ca, Mg, and Na observed in groundwater located close to the main fault, crossing the deep underground LNGS-INFN during the preparation phases of the recent L'Aquila earthquake of 6th April 2009, is interpreted as chemical interactions with endogenic, upper mantle-derived carbon dioxide (CO₂) fluids, generated by recycling and melting of carbonaceous sediments during the ongoing subduction of the continental Adriatic plate beneath the Italian peninsula [5].

3 Conclusion

We propose that the U groundwater anomalies observed before the seismic swarm and the main shock, which occurred on 6th April, 2009 in L'Aquila, provide a key geochemical signal of a progressive increase of deep CO₂ fluxes at middle-lower crustal levels. Repeated sharp U enrichments in groundwater, that can be directly associated with the geodynamics of the earthquake, represent a much more precise strain-meter than Rn, whose presence could be modulated by U content during the preparation phase of the earthquake, and only successively released by microfracturing, during the main shock and aftershocks.

4 Acknowledgments

The authors want to thank Prof. Lucia Votano, Director of the Gran Sasso National Laboratory, for her kind collaboration.

References

- [1] E. Roeloffs, Nature 399, 104 (1999)
- [2] W. Plastino, F. Bella, Geophys. Res. Lett. 28, 2675 (2001)
- [3] W. Plastino et al., J. Radioanal. Nucl. Chem. 813, 809 (2009)

- [4] W. Plastino et al., *J. Environ. Radioactiv.* 101, 45 (2010)
- [5] A. Peccerillo, *A Plio-Quaternary volcanism in Italy. Petrology, geochemistry, geodynamics.* Springer, Heidelberg, pp 1-365 (2005)

GIGS. The Interferometric Station at LNGS

Antonella Amoruso^{a,b}, Luca Crescentini^{a,b,c}

^a Dip.to di Fisica Univ. di Salerno, Salerno - Italy

^b INFN - Gruppo collegato di Salerno, Salerno - Italy

^c Spokeperson

Abstract

During 2010 the activity has been devoted to the completion of the analysis of the data produced by the interferometers before the occurrence of the April 6th earthquake. We have given tight limits on the size and strength of a possible preparatory zone and on the amount of released pre-seismic slip. Data related to the post-seismic phase are still under investigation. We have also studied the impact of the earthquake on groundwater flow in the Gran Sasso carbonate aquifer. Further investigations are in progress.

1 Introduction

Since several years two geodetic extensometers are working at LNGS. Both instruments are unequal-arm Michelson interferometers, using a 90-m long measurement arm and a <40-cm long reference arm, and sharing the same stabilized HeNe laser source. Nominal strain ($\Delta l/l$) sensitivity is better than 10^{-12} and, in the present configuration, recording rate is 600Hz. The two interferometers are monitoring extension along two orthogonal directions, striking N66E (BC interferometer) and N24W (BA interferometer).

Several phenomena have been proposed as diagnostic precursors of earthquakes, including strain-rate changes, changes in seismic wave velocities, electromagnetic signals, changes in groundwater levels and flow, radon anomalies, and acoustic emissions. Most, if not all, those phenomena are ascribed to deformation processes. “In many cases of purported precursory behavior, the reported observational data are contradictory and unsuitable for a rigorous statistical evaluation. One related problem is a bias towards publishing positive rather than negative results, so that the rate of false negatives (earthquake but no precursory signal) cannot be ascertained. A second is the frequent lack of baseline studies that establish noise levels in the observational time series.” (International Commission on Earthquake Forecasting for Civil Protection, Operational Earthquake Forecasting: State of Knowledge and Guidelines for Utilization, Italian Civil Protection Department, 2009) The long-anticipated 2004 Parkfield earthquake was monitored by a wealth of scientific instrumentation (including water wells, high-resolution strain, electric field, magnetic field,

and seismic-wave detectors) designed to record it, most of which was part of the Parkfield Earthquake Prediction Experiment. However, “nothing unusual (statistically significant) was recorded before the mainshock” ([13], and references therein). As regards the 2009 L’Aquila earthquake, claimed earthquake precursors and preparation-phase-related phenomena include radon anomalies ([11]), radio anomalies ([6]), and uranium groundwater anomalies ([19]).

We show results ([3], [4]) from the analysis of pre-seismic deformation data recorded our paired high-sensitivity laser extensometers, which are located about 20 km NE of the epicenter. During the two years before the event, no anomalous signal larger than a few tens of nanostrains is visible, limiting the volume of the possible earthquake preparation zone to less than 100 km³; moreover, earth tidal response is stable within 0.5% in amplitude and 0.5° in phase. Thus, reality of large-scale precursory phenomena seems unlikely. During the last few days, there is some evidence of dilatancy of saturated rock over the earthquake causative fault, maybe related to the foreshocks. Seconds before the event, strain is stable at the 10⁻¹² level and prerupture nucleation slip in the hypocentral region is constrained to have a moment less than 2 × 10¹² Nm, i. e. 0.00005% of the main shock seismic moment.

2 Earthquake preparation zones?

Most large-scale precursory phenomena are assumed to result from changes in the elastic properties of the crustal rock in some large enough “earthquake preparation” zone. The appearance of such an inclusion affects the deformation field caused by the regional tectonic stress ([10]). In order to assess the sensitivity of our data to possible inclusions in the source area, we have computed strain changes at the interferometer site generated by small inclusions on a regular grid around the hypocenter, for an extensional tectonic stress acting perpendicularly to the fault strike. Using the small perturbation method, an approximate solution of the superficial displacement caused by an inclusion for an otherwise homogeneous isotropic elastic half-space is:

$$w_r(x_0, y_0) = - \left[\frac{\Delta K}{K^0} \frac{\sigma_{ij}^0}{3} \delta_i^j + \frac{\Delta \mu}{\mu^0} (\sigma_{ij}^0 - \frac{\sigma_{ij}^0}{3} \delta_i^j) \right] \int \int \int_V v_{i,j}^r dV$$

where w is the displacement vector at (x_0, y_0) ; $K^0(\mu^0)$ is the bulk (shear) modulus outside the inclusion; $K^0 + \Delta K$ ($\mu^0 + \Delta \mu$) is the bulk (shear) modulus inside the inclusion; v_i^r is the displacement tensor at (x, y, z) of a unit point force acting on (x_0, y_0) and computed in an elastic half-space (e. g. [16]); σ_{ij}^0 is the tectonic stress field (uniform at large distances). Hereinafter we use $\mu^0 = 30$ GPa and consider the rock outside the inclusion as a Poisson solid (i. e., $K^0 = 5\mu^0/3$). Crack density (Φ) and water saturation affect both the bulk and shear moduli, even if at different levels. The shear modulus depends on the crack density only, while the presence of a very small amount of air (or gas) within the pore space is sufficient to induce a drastic decrease of the bulk modulus ([15]). In order to assess the sensitivity of our data to possible inclusions in the source area, we have computed strain changes at the interferometer site generated by small inclusions on a regular grid around the hypocenter, for an extensional tectonic stress $\sigma^0 = 10^8$ Pa acting perpendicularly to

the fault strike, and $V = 1 \text{ km}^3$. We assume $\Phi = 0.1$ (implying about 7% decrease of shear wave velocity), consequently $\Delta\mu/\mu^0$ is about -0.13, while $\Delta K/K^0$ is about -0.05 for saturated rock and about -0.26 for unsaturated rock ([15]). Computed strain changes are at the $n\epsilon$ level for both interferometers (Figure 1).

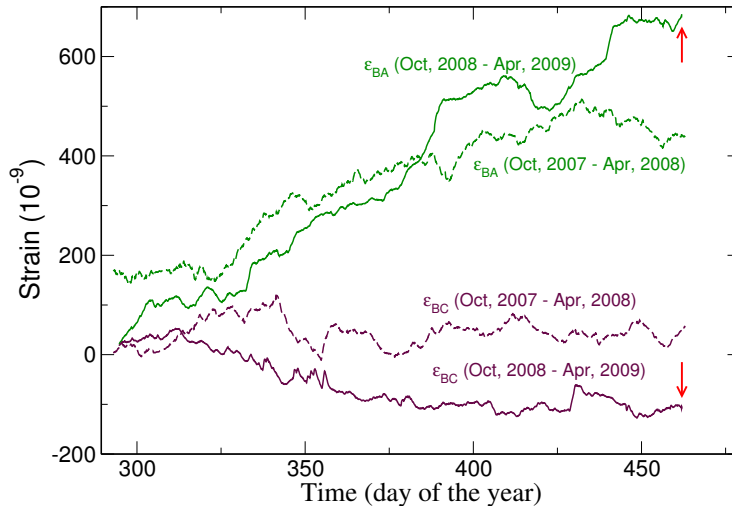


Figure 1: Comparison of strain recorded at both interferometers during the periods October 2008 to April 6th, 2009, and October 2007 to April 2008. Zero-strain level for each time series is arbitrary. Arrows, occurrence time of the earthquake.

There is no indication of coherent anomalous signals larger than a few tens of nanostains thus limiting the volume of the possible inclusion to less than 100 km^3 . Although we can not completely exclude that a large-scale pre-seismic phenomenon took place, it seems unlikely. We verify this result by searching for changes in earth tidal response before the earthquake, that were suggested as a possible means for earthquake prediction ([17]). Also recently, strain tidal changes up to 20% in amplitude have been reported several tens of kms from the epicenter of magnitude-6 earthquakes ([24]). Signal-to-noise ratio of the Gran Sasso extensometers in the tidal band is very high, thus we determine the tidal response for the two years prior to L'Aquila earthquake. Amplitude and phase of M2 (BA interferometer) as a function of time from 2007 to summer 2009 show that no change in the tidal response is visible before the earthquake, within 0.5% in amplitude and 0.5° in phase (Figure 2). The analyses of the M2 tidal response for BC and O1 tidal response for both interferometers lead to the same conclusion, but with a lower signal-to-noise ratio.

2.1 Precursory slip?

Strain recorded during the last 10 days before the earthquake shows some hints of coherent (but opposite in sign) changes in the last 3 to 4 days preceding the earthquake (Figure 3).

It is difficult to provide a quantitative evaluation of how likely such variations relate to the earthquake. Nevertheless, these changes are significant in this section of record and

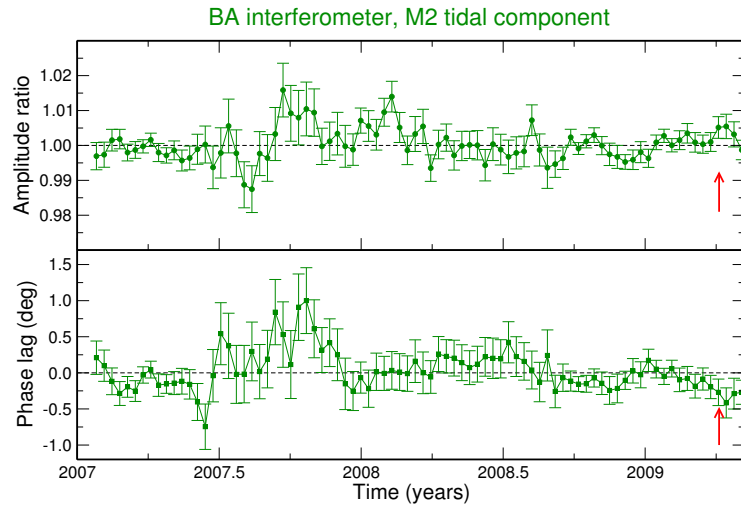


Figure 2: Tidal analyses carried out using VAV2003 ([22]) on sliding 2-month time blocks with a 10-day overlap between blocks. Error bars are 1 standard deviation. Amplitude normalized to the weighted mean value; phase lag given with respect to the weighted mean value. Time tag associated with each analysis is taken as the midpoint of the window. Higher noise from June 2007 to February 2008 reflects anthropic activity close to the interferometers. Arrows, occurrence time of the earthquake.

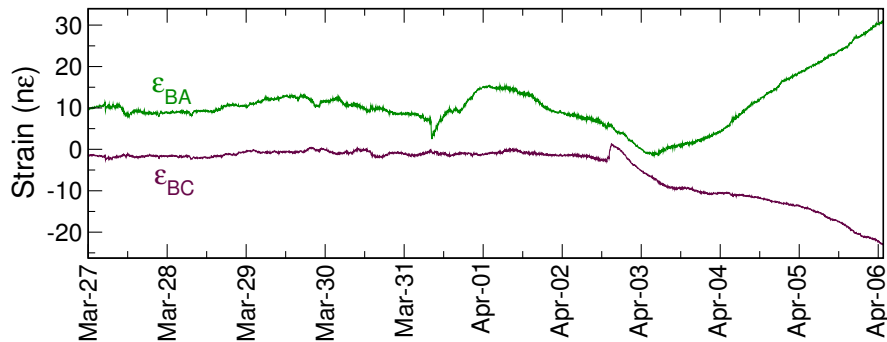


Figure 3: Strain data recorded the last ten days before the earthquake, after removal of Earth tides, environmental effects, and offsets (to to foreshocks). Data have been low-pass filtered with a 10-pole butterworth filter with a high cut of 1.67 mHz and the linear trend of the first 6 days has been removed. Seeming anomalies in BA(BC), occurred about 5.7(3.5) days before the earthquake, are due to anthropic activity close to BA(BC) end monuments.

the possibility that they may result from some pre-seismic or post-seismic (with respect to the M 4.1 foreshock occurred on March 30th close to the April 6th mainshock) process cannot be precluded (Figure 4). In particular, an about 5% increase of V_P/V_S along the path between the seismic stations AQU and FAGN, which is parallel to the NW-SE striking earthquake causative fault, has been reported ([9]) during the days preceding the main shock. Changes along the NE-SW striking path between AQU and FIAM were certainly much smaller or null. Such observations are ascribed to the movement of fluids along fault planes. We model the increase of V_P/V_S through fluid migration and crack opening in saturated rocks (case A) or saturation of partially saturated rock (case B). In case A, the shear modulus (μ) would decrease by about 22% and the bulk modulus (K) by about 8%, while in case B, μ would remain unchanged and K would increase by about 20% (see e.g. Figure 5 in [15]).

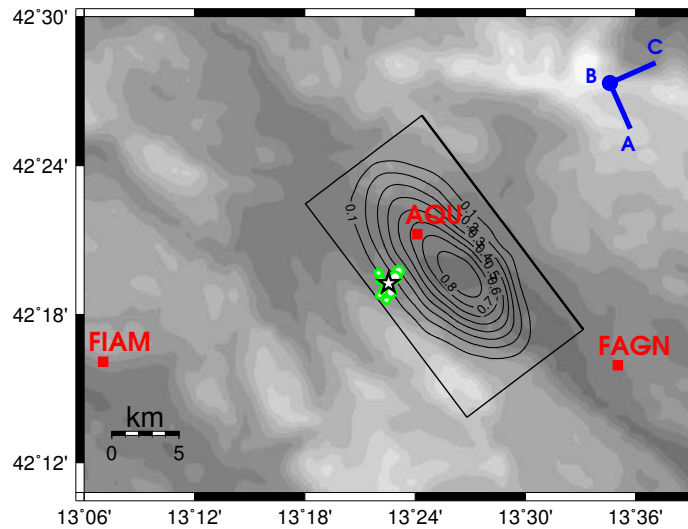


Figure 4: Map of the epicentral region of the 2009/04/06 L'Aquila earthquake with the fault geometry and slip distribution from the work by [23]. Blue large solid circle (B), location of the two interferometers; blue solid lines (BA and BC), directions of the interferometers. Black star, epicenter of the March 30th M 4.1 foreshock; green circles, epicenters of the succeeding foreshocks with $M > 2.5$ [<http://iside.rm.ingv.it>]. Red squares, seismic stations.

We compute the amplitude and sign of deformation at both interferometers due to small inclusions ($V=10^9 \text{ m}^3$) located in different positions on the April 6th fault plane, for both cases A and B (Figure 5). Because of the model simplicity, we do not take into account siting effects, that produce small coupling among the different strain components. Saturated-rock crack opening in the region surrounding the March 30th foreshock causes negative BC strain and positive BA strain, of about the same amount (nanostains), consistently with the strain changes (about 10 ne in amplitude) observed during the days preceding the earthquake. This implies a dilatant volume of about 10 km^3 , which is

quite small and unable to justify the observations in [9] if quasi-spherical in shape, but consistent with them if confined to a thin sheet over the fault plane. Sudden dilation, and the corresponding changes in porosity, permeability and fluid pressure, could have occurred because of the M 4.1 foreshock (March 30th) and/or the succeeding foreshocks, causing fluid to flow into and along the fault. Case B can not fit our observations because of sign mismatch.

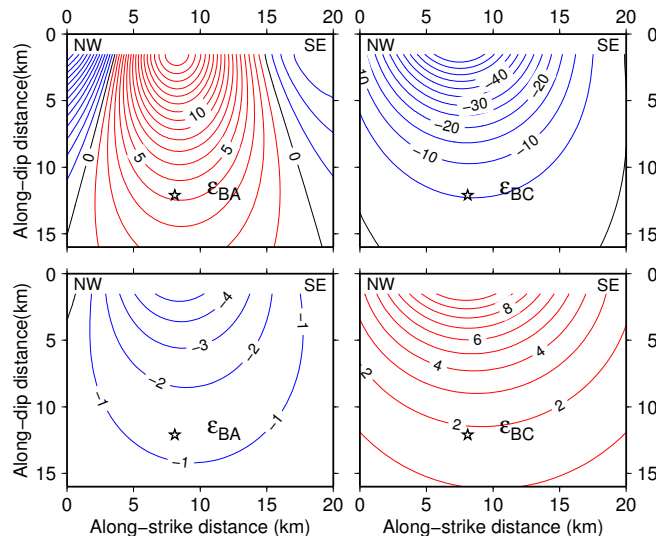


Figure 5: Strain (nanostains; blue contours, negative values; red contours, positive values) generated at the interferometers by a small inclusion ($V = 1 \text{ km}^3$) located in different positions on the fault plane causative of the April 6th earthquake. Star, hypocenter of the March 30th foreshock. Top panels: case A (dilatancy of saturated rock). Bottom panels: case B (saturation of unsaturated cracked rock).

2.2 Earthquake nucleation

Precursory strain could be detectable as rapid acceleration of strain near instability, either because of local dilatancy (days before the earthquake; [21]) or nucleation zone expansion (tens to hundreds of seconds before the earthquake; e. g. [12]). A closer look at the data recorded before the earthquake can put limits to the nucleation phase. To be linked to nucleation, the strain history should be exponential-like with the largest strain changes occurring at the last stages of failure and the amplitude or size of the strain change relating to nucleation patch moment release. Moreover, changes have to be present in both (BA and BC) strain time series. If nucleation occurs at the earthquake hypocenter, a 10^{16} Nm normal-faulting source produces $\epsilon_{BA} \approx 5n\epsilon$ and $\epsilon_{BC} \approx -5n\epsilon$ (see Figure 3 in [2]).

Laser frequency fluctuations can give apparent strain signals, which are coherent in the two interferometers but disappear in the difference between the two measured strains. Consequently, we show $\epsilon_{BC} - \epsilon_{BA}$ just before the earthquake (Figures 6 to 8).

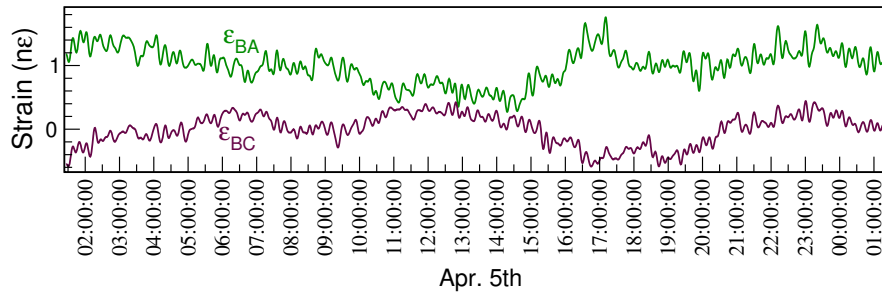


Figure 6: Strain data recorded the last day before the earthquake, after the removal of Earth tides and environmental effects. Data have been low-pass filtered with a 10-pole butterworth filter with a high cut of 1.67 mHz and detrended. No coherent exponential-like changes larger than $1n\epsilon$ are apparent.

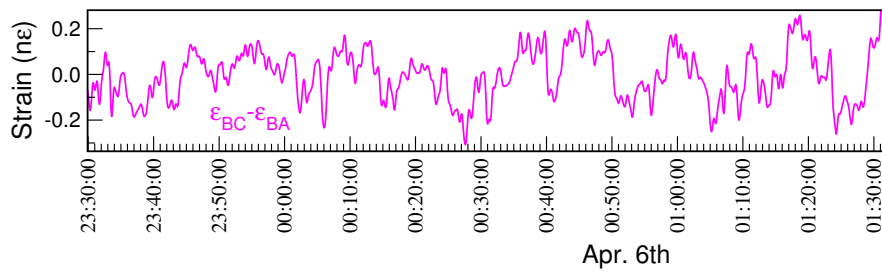


Figure 7: Strain data recorded the last two hours before the earthquake, after removal of Earth tides and environmental effects. Data have been low-pass filtered with a high cut of 33 mHz and detrended. Standard deviation is $0.1 n\epsilon$.

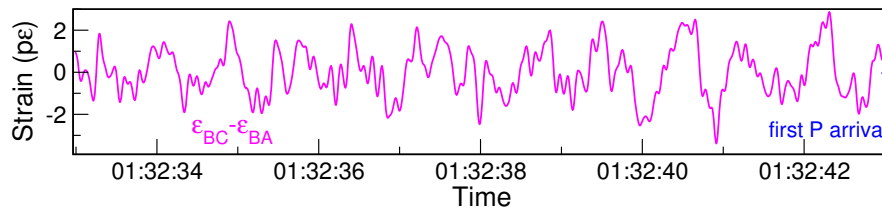


Figure 8: Strain data recorded the last ten seconds preceding the first P arrival. Data have been low-pass filtered with a 10-pole butterworth filter with a high cut of 10 Hz; 6 harmonics in the microseism band have been removed, at periods of 1.3, 2.0, 2.2, 3.7, 4.5, and 5.0 secs. Standard deviation is $1 p\epsilon$.

The largest moment release that could go undetected is 2×10^{15} Nm during one day before the event, 2×10^{14} Nm during two hours, 2×10^{12} Nm during ten seconds before the event. As a comparison, the earthquake seismic moment was about 3.5×10^{18} Nm ([8]). This lack of detectable pre-seismic moment release confirms the results and lowers the limits from previous strain measurements ([14]).

2.3 Remarks about published pre-seismic anomalies

Some recently-published pre-seismic anomalies do not necessarily conflict with our conclusions. Reported radio anomalies ([6]) might be due to an interruption of the broadcasting from the transmitter (RMC, France) (P. Tognolatti, personal communication, and [7]). As regards the reported uranium (U) anomalies in the groundwater collected weekly from June 2008 inside the LNGS ([19], [20]), figures in [18] show that normalized (with respect to each background value) U time series are very similar at all monitoring sites – the only exception being two spikes at one site during summer 2008 – and that each U time series strictly mimics those of Na, Ca, and Mg at the same site, both in shape and relative concentration changes. These characteristics suggest possible changes in water recharge and dilution and/or rock dissolution, e. g. because of the addition of CO₂. However, the ionic content time series appear inconsistent with the electrical conductivity ones, and the CO₂ increase seems unsupported by the pH time series (see plots in [18] and [19], and Table 1 in [20]).

3 Impact of the earthquake on groundwater flow in the Gran Sasso area

Changes observed over space and time in the Gran Sasso carbonate aquifer immediately after the mainshock indicate that the aquifer discharge generally increased to varying degrees while displaying an inverse relationship between discharge increase and distance from the Paganica fault (where the main shock was located) ([5]). At the regional scale, the rise of the groundwater table can be attributed to the pore pressure change effect. Near the Paganica fault, the pore pressure changes of negative sign determine a quick decrease of the discharge of the closest springs, as observed in Tempera springs.

The general increase in discharge recorded throughout the aquifer during the months following the mainshock cannot be attributed to pore pressure changes and is likely caused by permeability changes in the recharge area, located no far from the Paganica fault. An increase in the bulk hydraulic conductivity of the recharge area of the aquifer lowers the local hydraulic gradient – as testified by the spot measurements of hydraulic head on the horizontal piezometer inside the highway tunnels – and triggers a discharge increase on the regional scale. Because of the additional flow coming from the recharge area, water table levels close to the aquifer boundaries are elevated above pre-mainshock values, as observed. We have validated the above exposed conceptual model through numerical modelling, taking into account the pore pressure changes due to the coseismic strain and the effects of possible changes of the hydraulic conductivity.

The model is based on the 1D crustal structure in [8] (see curves labelled LVZ in Figure 2 of their auxiliary material). Hydraulic diffusivity is assumed constant (1 or 100 m^2/s ; [1]) in the shallowest 1.5-km -thick layer, then decreases linearly down to 0.01 m^2/s at a depth of 4 km, is 0.01 m^2/s between 4 and 8 km in depth, and 0.001 m^2/s below 8 km. Skempton's coefficient is 0.25 at all depths, and Biot's coefficient is 0.7 . As regards the seismic fault, different slip distributions have been proposed (e.g. [8]; [23]); details of pore pressure coseismic changes close to the fault depend on the slip distribution, but general features do not. Our results were obtained using a smooth distributed-slip source model ([23]), because its smoothness avoids possible local artefacts from non-robust small features of the distribution itself. Other slip distributions and reasonable crustal profiles (elastic, poroelastic and hydraulic parameters) were tested, obtaining very similar results.

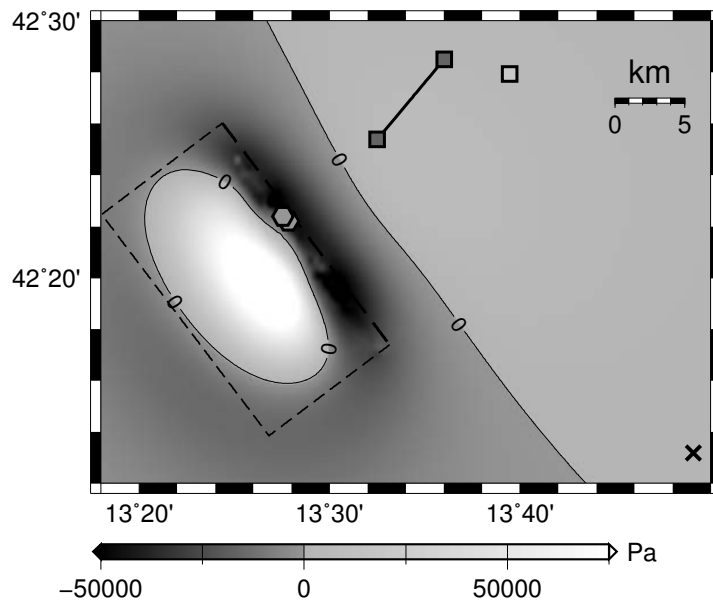


Figure 9: Simulation of coseismic pore pressure changes due to L'Aquila earthquake. Dashed rectangle, horizontal projection of the fault, the thickest side being its surface trace; grey hexagons, Tempera springs; light grey square, Vacelliera spring group; thick solid line and dark grey squares, highway tunnel (sketch) and drainages. Cross, well field (WF). The contour lines labelled 0 separate regions of positive (increase) and negative (decrease).

A large coseismic pore pressure decrease is predicted along the fault surface trace, inside a 3-km -wide strip where the Tempera spring group is located. On the contrary, pore pressure increase is predicted NE of the fault, in the recharge area of the highway tunnel and northern springs. A positive pore pressure change is also observed in the main discharge area, where WF monitoring wells are located (Figure 9). These results reflect the observed field data for the after-mainshock period, including the discharge shortage and spring disappearing near the Paganica fault, the quick increase at the tunnel drainages and at the northern springs, and the first part of the water table rise at the discharge area.

Direct poroelastic response cannot explain the gradual persistent water level rise at WF. To test if it could be caused by changes in the bulk hydraulic properties of the groundwater aquifer, the recharge area of WF has been modelled as an unconfined heterogeneous annular-sectored axisymmetric aquifer, consistently with its main features from the literature. We assumed a smooth pattern of the hydraulic conductivity changes, with maximum magnitude in the recharge area of the Gran Sasso carbonate aquifer, where the effects of the mainshock are expected to be greater than in the discharge area, which is farther from the Paganica fault. Permeability changes can be induced by fracture cleaning and unblocking of pre-existing fractures. Both magnitude and shape of the first 60 days of the simulated time histories of the hydraulic head change are consistent with field observations. As regards the subsequent evolution of the water table, simulations show that the hydraulic head should increase for about 3 years after the event, and a progressive return of the hydraulic conductivity towards pre-seismic values is required in order to match recent measurements.

Further investigations focussed on the LNGS area, and considering the local changes of hydraulic conductivity, are in progress.

This part of the activity is in co-operation with R. Adinolfi Falcone, A. Falgiani, M. Petitta, and M. Tallini.

4 Acknowledgments

The Interferometric Station at Gran Sasso is the object of the related Accordo di Programma between Istituto Nazionale di Fisica Nucleare and Istituto Nazionale di Geofisica e Vulcanologia.

5 List of Publications

1. Amoruso, A., and L. Crescentini, *Geophys. Res. Lett.*, **37**, L10307, doi:10.1029/2010GL043308, 2010.
2. Amoruso, A., L. Crescentini, M. Petitta, S. Rusi, and M. Tallini, *Hydrol. Process.*, doi: 10.1002/hyp.7933, 2011.
3. Amoruso, A., and L. Crescentini, *Boll. Geof. Teor. Appl.*, in press.

References

- [1] Adinolfi Falcone, R., A. Falgiani, B. Parisse, M. Petitta, M. Spizzico, and M. Tallini, *J. Hydrol.*, **357**, 368–388, 2008.
- [2] Amoruso, A., and L. Crescentini, *Geophys. Res. Lett.*, **36**, L24306, doi:10.1029/2009GL041503, 2009.
- [3] Amoruso, A., and L. Crescentini, *Geophys. Res. Lett.*, **37**, L10307, doi:10.1029/2010GL043308, 2010.

- [4] Amoruso, A., and L. Crescentini, *Boll. Geof. Teor. Appl.*, in press.
- [5] Amoruso, A., L. Crescentini, M. Petitta, S. Rusi, and M. Tallini, *Hydrol. Process.*, doi: 10.1002/hyp.7933, 2011.
- [6] Biagi, P. F., L. Castellana, T. Maggipinto, D. Loiacono, L. Schiavulli, T. Ligonzo, M. Fiore, E. Suciù, and A. Ermini, *Nat. Hazards Earth Syst. Sci.*, **9**, 1551–1556, 2009.
- [7] Biagi, P. F., L. Castellana, T. Maggipinto, D. Loiacono, L. Schiavulli, T. Ligonzo, M. Fiore, E. Suciù, and A. Ermini, *Nat. Hazards Earth Syst. Sci.*, **10**, 215–216, 2010.
- [8] Cirella, A., A. Piatanesi, M. Cocco, E. Tinti, L. Scognamiglio, A. Michelini, A. Lomax, and E. Boschi, *Geophys. Res. Lett.*, **36**, L19304, doi:10.1029/2009GL039795, 2009.
- [9] Di Luccio, F., G. Ventura, R. Di Giovambattista, A. Piscini, and F. R. Cinti, *J. Geophys. Res.*, doi:10.1029/2009JB007190, 2010.
- [10] Dobrovolsky, I.P., S.I. Zubkov, and V.I. Miachin, *Pure Appl. Geophys.*, **117**, 1025–1044, 1979.
- [11] Giuliani, G. G., R. Giuliani, G. Totani, G. Eusani, and F. Totani, *Eos Trans. AGU*, **90(52)**, Fall Meet. Suppl., Abstract U14A-03, 2009.
- [12] Fang, Z., J. H. Dieterich, and G. Xu, *J. Geophys. Res.*, doi:10.1029/2009JB006558, 2010.
- [13] Harris R. A., and J.R. Arrowsmith, *Bull. Seism. Soc. Am.*, **96** (4B), S1–S10, 2006.
- [14] Johnston, M. J. S., R. D. Borchardt, A. T. Linde, and M. T. Gladwin, *Bull. Seismol. Soc. Am.*, **96**, S56–S72, 2006.
- [15] Le Ravalec, M., Y. Gueguen, and T. Chelidze, *J. Geophys. Res.*, **101**, 11,217–11,223, 1996.
- [16] Mindlin, R. D., *Physics*, **7**, 195–202, 1936.
- [17] Nishimura, E., *Trans. Am. Geophys. Union*, **31**, 357–376, 1950.
- [18] Plastino W., S. Nisi, G. De Luca, M. Balata, M. Laubenstein, and F. Bella, *J. Radioanal. Nucl. Chem.*, **282**, 809–813, doi:10.1007/s10967-009-0151-2, 2009.
- [19] Plastino, W., P. P. Povinec, G. De Luca, C. Doglioni, S. Nisi, L. Ioannucci, M. Balata, M. Laubenstein, F. Bella, and E. Coccia, *J. Environ. Radioact.*, doi:10.1016/j.jenvrad.2009.08.009, 2010.
- [20] Plastino W., et al., *J. Radioanal. Nucl. Chem.*, doi:10.1007/s10967-010-0876-y, 2010.
- [21] Rice, J. R., and J. W. Rudnicki, *J. Geophys. Res.*, **84**, 2177–2184, 1979.
- [22] Venedikov, A. P., J. Arnoso, and R. Vieira, *Comput. Geosci.*, [**31**, 667–669, 2005.

- [23] Walters, R. J., J. R. Elliott, N. DAgostino, P. C. England, I. Hunstad, J. A. Jackson, B. Parsons, R. J. Phillips, and G. Roberts, *Geophys. Res. Lett.*, **36**, L17312, doi:10.1029/2009GL039337, 2009.
- [24] Zhang, Y., J. Jian, J. Qian, J. Chen, S. He, Y. Zhang, and P. He, *Acta Seismologica Sinica*, **15(1)**, 113–118, 2002.

TELLUS Experiment.

V. Sgrigna^a, L. Conti^a, D. Zilpimiani^b

^a Dipartimento di Fisica e Sezione INFN, Università Roma Tre, Rome - Italy

^b National Institute of Geophysics, Georgian Academy of Sciences, Tbilisi - Georgia

Abstract

A new technique with related patent has been proposed in the year 2010 by the TELLUS team for the signal waveform reconstruction by multichannel selection and variable feedback differential amplification (patent pending RM2009A000007). To this purpose a specific electronic board has been designed and constructed, which allows to any (often unknown) analog signal detected inside the geomagnetic cavity to be reconstructed by a conditioning technique based on filtering and tunable feedback differential amplification.

1 Introduction

Aim of the experiment is to detect signals inside the geomagnetic cavity due to solid earth and Sun activities to investigate the physical mechanisms underlying the main lithosphere-atmosphere-ionosphere-magnetosphere couplings. At this purpose specific instruments have been planned to be installed on board a LEO satellite and/or the International Space Station (ISS). They include electric and magnetic probes, optical-UV instruments (photometers and video cameras), as well as an X/ γ ray detector and a charged particle detector. A few of them have been designed and constructed as reported in previous LNGS annual reports [1]-[3] and in literature [4]-[7]. Original and specific signal conditioning techniques and data acquisition systems are necessary for an optimal use of these instruments. In the following section is reported an original component of such systems.

2 Instruments

The electronic board for the signal conditioning mentioned above is reported in figure 1. It may perform the preamplification of an input analog signal, dividing and filtering it in a discrete number (n) of different frequency channels using passive filters centered around these n adjacent frequency bands spaced in decades. Each frequency channel may be amplified separately by a specific electronic block of amplifiers constituted by two amplification stages controlled by a selector. The gain of each frequency channel may be tuned individually (just once or time by time) via an external digital control unit and a

feedback amplification procedure. Finally, the output signals from the n analog frequency channels may be added one each other in several selectable combinations.

The device allows the continuous variation of the gains in data acquisition systems devoted to waveform reconstruction or spectrogram analysis for any analog signal. In signal processing applications when the signal frequency and amplitude characteristics are unknown it is possible to set and reset the amplifications of the n conditioning blocks using digital selectors. The modular character of the electronic board also allows to combine (by jumpers) the channels analog outputs according to different selectable combinations.

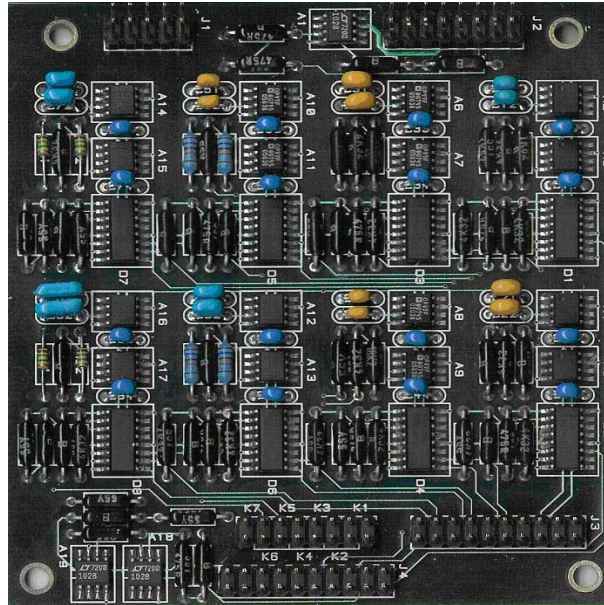


Figure 1: Signal conditioning electronic board.

3 Conclusions

An original signal conditioning system for specific near-Earth space applications has been proposed and constructed by the TELLUS team [8]. The device (patent pending) has low power consumption and minimum costs and overall dimensions.

References

- [1] Sgrigna, V., Conti, Zilpimiani, D., 2010. TELLUS Experiment. Detection of transient phenomena associated with thunderstorms, *Laboratori Nazionali del Gran Sasso, INFN, Annual Report 2009, LNGS/EXP-01/10*, May 2010, pp.199-204.
- [2] Sgrigna, V., Buzzi, A., Conti, L., Stagni L., Zilpimiani, D., 2009. TELLUS. A new electromagnetic strainmeter for the monitoring of ground field deformations, *Labora-*

tori Nazionali del Gran Sasso, INFN, Annual Report 2008, LNGS/EXP-01/09, June 2009, pp.187-192.

- [3] Sgrigna, V., Buzzi, A., Conti, L., Stagni L., Zilpimiani, D., 2008. TELLUS. Ground deformations and their effects in the near-Earth space, *Laboratori Nazionali del Gran sasso, INFN, Annual Report 2007, LNGS/EXP-01/08*, May 2008, pp.187-190.
- [4] Sgrigna, V. and Conti, L., 2010. Earthquake preparation and warning: science, methods and technologies, *In: Advances in Environmental Research Volume 7, Chapter 1 (Justin A. Daniels, Editor), 2010 Nova Science Publishers, Inc.* , ISBN 978-1-61728-774-9, pp. 1-38.
- [5] Sgrigna, V., A. Buzzi, L. Conti, P. Picozza, C. Stagni, D. Zilpimiani, 2008. The ESPERIA satellite project for detecting seismic-associated effects in the topside ionosphere. First instrumental tests in space, *Earth Planets and Space*, 60, 463-475.
- [6] Sgrigna, V., Buzzi, A., Conti, L., Picozza, P., Stagni, C., Zilpimiani, D., 2007. Seismo-induced Effects in the Near-Earth Space: Combined Ground and Space Investigations as a contribution to Earthquake Prediction, *Tectonophysics*, 431, 153-171.
- [7] Buzzi , A., Conti, L., Galper, A. M., Koldashov, S.V., Malvezzi, V., Murashov, A.M., Picozza, P., Scrimaglio, R., Sgrigna, V., Stagni, L., 2006. Sismo-electromagnetic emissions, *Proc. NATO Adv. Study Institute on "Sprites, Elves and Intense Lightning Discharges"*, Edited by M. Fullekrug, E.A. Mareev and M.J. Rycroft, Published by Springer, vol. 225, pp. 388-389, 2006. (NATO Science Series II: Mathematics, Physics and Chemistry- vol.225. ISBN-10 1-4020-4628-6 (PB)).
- [8] Patent pending *RM2009A000207*. Authors: Conti, L., Sgrigna, V., and Zilpimiani, D., Title: *Signal conditioning board for filtering and feedback multichannel amplification in data acquisition systems of analog signals*.

THE PIERRE AUGER EXPERIMENT

C. Di Giulio^a, A.F. Grillo^b, C. Macolino^a, S. Petrer^a,
V. Rizi^a, F. Salamida^a
for the Auger Collaboration

^a INFN and Dipartimento di Fisica, Università dell'Aquila - Italy

^b LNGS-INFN - Italy

Abstract

The Pierre Auger Project is an international Collaboration involving over 400 scientists from 17 countries, with the objective of studying the highest energy cosmic rays. Recent results from the Collaboration as well as further developments in the detector are presented in this report.

1 Introduction

Ultra-high energy cosmic rays are of intrinsic interest as their origin and nature are unknown. It is quite unclear where and how particles as energetic as $\simeq 10^{20}$ eV are accelerated. Over 40 years ago it was pointed out that if the highest energy particles are protons then a fall in the flux above an energy of about $\times 10^{19}$ eV is expected because of energy losses by the protons as they propagate from distant sources through the CMB radiation. At the highest energies the key process is photo-pion production in which the proton loses part of its energy in each creation of a Δ resonance. This is the Greisen-Zatsepin-Kuzmin (GZK) effect. It follows that at 10^{20} eV any proton observed must have come from within about 50 Mpc and on this distance scale the deflections by intervening magnetic fields in the galaxy and intergalactic space are expected to be so small that point sources should be observed. Despite immense efforts in the period since the prediction, the experimental situation remains unclear. The main problem in examining whether or not the spectrum steepens is the low rate of events which, above 10^{20} eV, is less than 1 per km^2 per century so that the particles are only detectable through the giant air showers that they create.

These showers have particle footprints on the ground of $\simeq 20 \text{ km}^2$ and suitably distributed detectors can be used to observe them. Also the showers excite molecules of atmospheric nitrogen and the resulting faint fluorescence radiation, which is emitted isotropically, can be detected from distances of several tens of kilometers.

The Pierre Auger Observatory has been developed by a team of over 400 scientists from 17 countries. The Observatory comprises about $1600 \text{ km}^2 \times 1.2 \text{ m}$ water-Cherenkov

detectors deployed over 3000 km² on a 1500 m hexagonal grid. This part of the Observatory (the surface detector, SD) is over-looked by 24 fluorescence telescopes in 4 clusters located on four hills around the SD area which is extremely flat. The surface detectors contain 12 tonnes of clear water viewed by 3 × 9" hemispherical photomultipliers. The fluorescence detectors (FD) are designed to record the faint ultra-violet light emitted as the shower traverses the atmosphere. Each telescope images a portion of the sky of 30° in azimuth and 1°-30° in elevation using a spherical mirror of 3 m² effective area to focus light on to a camera of 440 × 18 cm² hexagonal pixels, made of photomultipliers complemented with light collectors, each with a field of view of 1.5° diameter.

An important feature of the design of the Observatory was the introduction of the hybrid technique as a new tool to study airshowers. It is used here for the first time. The hybrid technique is the term chosen to describe the method of recording fluorescence data coincident with the timing information from at least one surface detector. Employing these two complementary observation methods provides the Auger Observatory with high quality information about angular reconstruction, determination of the core position of the shower and of the types of particles in the primary cosmic rays. Comparing results from the different types of detectors also helps scientists reconcile the two sets of data and produce the most accurate results about the energy of primary cosmic rays.

2 Recent results from the Pierre Auger Cosmic Ray Observatory

2.1 The Energy Spectrum

The energy spectrum of ultra-high energy cosmic rays at energies greater than 2.5×10^{18} eV has been derived using data from the surface detector array of the Pierre Auger Observatory [1]. This measurement provided evidence for the suppression of the flux above 4×10^{19} eV and is updated here. In 2009 we extended the previous measurements to lower energies by analysing air showers measured with the fluorescence detector that also triggered at least one of the stations of the surface detector array. Despite the limited event statistics due to the fluorescence detector on-time of about 13%, the lower energy threshold and the good energy resolution of these *hybrid* events allow us to measure the flux of cosmic rays in the region of the ankle.

The energy spectrum of hybrid events is determined from data taken between November 2005 and May 2008, during which the Auger Observatory was still under construction. Using selection criteria that are set out below, the exposure accumulated during this period was computed and the flux of cosmic rays above 10^{18} eV determined. The spectrum obtained with the surface detector array, updated using data until the end of December 2008, is combined with the hybrid one to obtain a spectrum measurement over a wide energy range with the highest statistics available.

The combined energy spectrum scaled with E^3 is shown in Fig. 1 in comparison with the spectrum obtained with stereo measurements of the HiRes instrument [2]. An energy shift within the current systematic uncertainties of the energy scale applied to one or both experiments could account for most of the difference between the spectra. The ankle

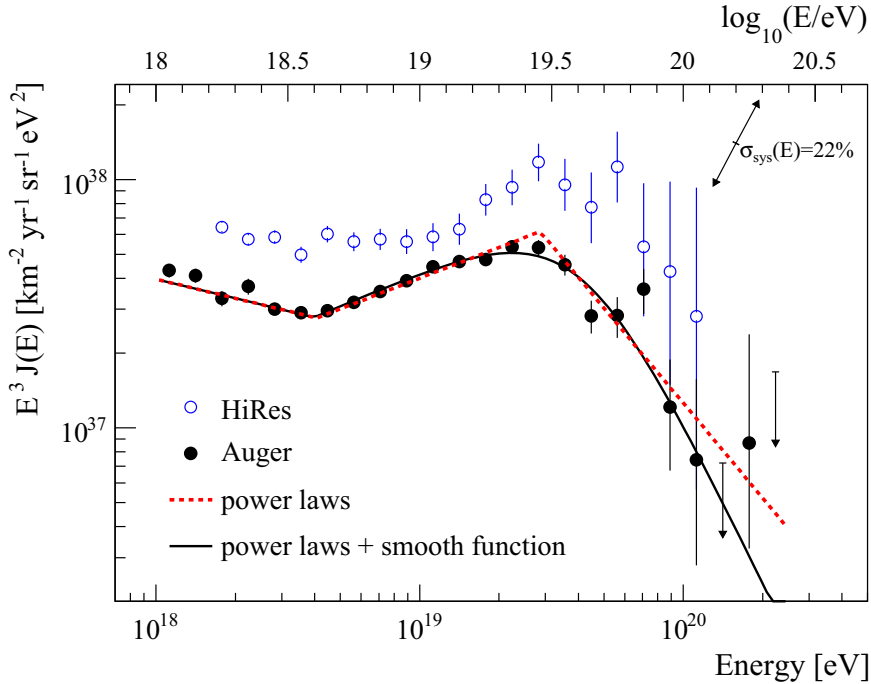


Figure 1: The combined energy spectrum is fitted with two functions (see text) and compared to data from the HiRes instrument [2]. The systematic uncertainty of the flux scaled by E^3 due to the uncertainty of the energy scale of 22% is indicated by arrows. A table with the Auger flux values can be found at [3].

feature seems to be somewhat more sharply defined in the Auger data. This is possibly due to a systematic energy offset between the experiments. However, for a complete comparison, care must also be taken to account for energy resolution and possible changes in aperture with energy.

The dominant systematic uncertainty of the spectrum stems from that of the overall energy scale, which is estimated to be 22%.

The position of the ankle at $\log_{10}(E_{\text{ankle}}/\text{eV}) = 18.61 \pm 0.01$ has been determined by fitting the flux with a broken power law $E^{-\gamma}$. An index of $\gamma = 3.26 \pm 0.04$ is found below the ankle. Above the ankle the spectrum follows a power law with index 2.55 ± 0.04 . In comparison to the power law extrapolation, the spectrum is suppressed by a factor two at $\log_{10}(E_{1/2}/\text{eV}) = 19.61 \pm 0.03$. The significance of the suppression is larger than 20σ . The suppression is similar to what is expected from the GZK effect for protons or nuclei as heavy as iron, but could in part also be related to a change of the shape of the average injection spectrum at the sources.

2.2 The Mass Composition

The atmospheric depth, X_{max} , at which the longitudinal development of a shower reaches its maximum in terms of the number of secondary particles is correlated with the mass of the incident cosmic ray particle. With the generalization of Heitlers model of electron-photon cascades to hadron-induced showers and the superposition assumption for nuclear

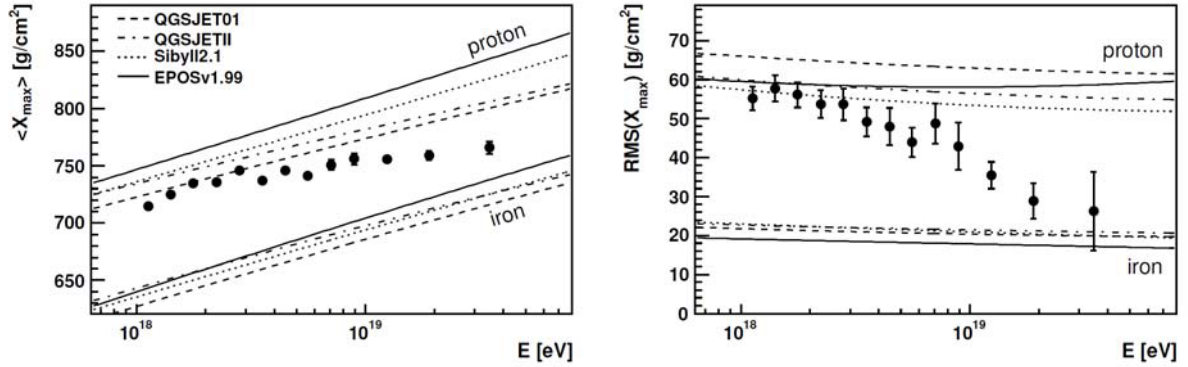


Figure 2: Measurements of X_{max} (left) and its RMS (right) as a function of energy [8].

primaries of mass A , the average depth of the shower maximum, X_{max} , at a given energy E is expected to follow [4]

$$\langle X_{max} \rangle = \alpha(\ln E - \ln \langle A \rangle) + \beta \quad (1)$$

where $\ln \langle A \rangle$ is the average of the logarithm of the primary masses. The coefficients α and β depend on the nature of hadronic interactions, most notably on the multiplicity, elasticity and cross-section in ultra-high energy collisions of hadrons with air, see e.g. [5]. At ultra high energies, the shower maximum can be observed directly with fluorescence detectors. Previously published X_{max} measurements [6], [7] as a function of energy had only limited statistics above 10^{19} eV.

A recent analysis [8] based on high quality and high statistics hybrid data collected with the southern site of the Pierre Auger Observatory has been addressed to the $\langle X_{max} \rangle$ measurement and its energy dependence.

The results of such measurements are presented in Fig. 2 together with predictions for proton and Fe primaries using different hadronic interaction models [8]. These models need to extrapolate the features of hadronic interactions well beyond the cms-energies accessible at man-made accelerators. Their uncertainties are correspondingly large and the wide distribution of predictions in the figure demonstrates that the systematic uncertainties in this analysis can be significant. With this caveat kept in mind, a transition from a light composition up to the ankle approaching the expectations for heavier nuclei up to 40 EeV is inferred from both the X_{max} values and from its RMS values.

2.3 The Cosmic Ray Anisotropy

Between January 2004 and December 2009 the Pierre Auger Observatory has detected 69 cosmic rays events with energy in excess of 55 EeV. Their arrival directions are reported in [9] This data set is more than twice as large as the one analyzed in [10], which provided evidence of anisotropy in CR arrival directions at the 99% confidence level. The anisotropy was tested with a priori parameters through the correlation between the arrival directions of CRs and the positions of nearby active galaxies from the 12th edition of the Veron-Cetty

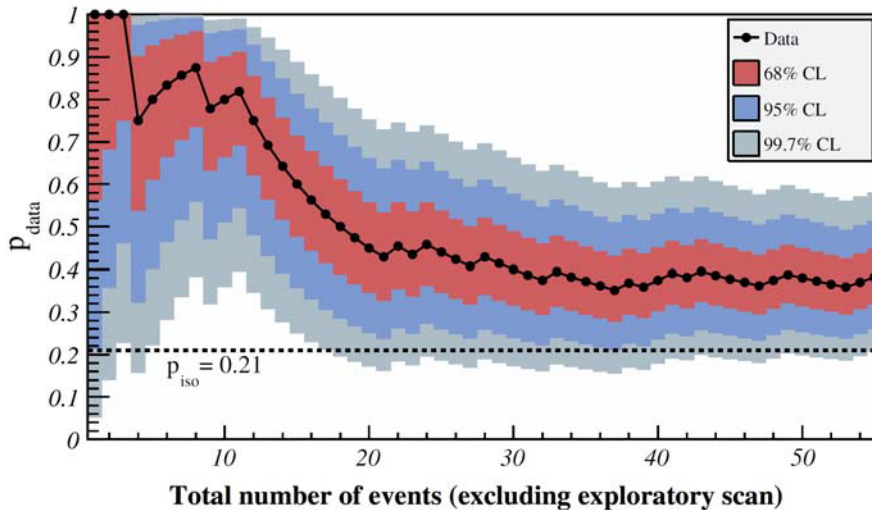


Figure 3: The most likely value of the degree of correlation $p_{data} = k/N$ is plotted with black circles as a function of the total number of time-ordered events (excluding those in period I). The 68%, 95% and 99.7% confidence level intervals around the most likely value are shaded. The horizontal dashed line shows the isotropic value $p_{iso} = 0.21$.

Veron catalog of quasars and active galactic nuclei. The degree of that observed correlation has decreased from $(69^{+11}_{-13})\%$ to $(38^{+7}_{-6})\%$, to be compared with the 21% expected to occur by chance if the flux were isotropic. More data are needed to determine this correlating fraction accurately. The evidence for anisotropy has not strengthened since the analysis reported in [10].

The correlation of recent data with objects in the VCV catalog is not as strong as that observed in 2007. If the evidence for anisotropy is substantiated by future data, then it should also become possible to discriminate between different astrophysical scenarios using techniques of the type that have been presented here to explore the compatibility of different models with the present set of arrival directions.

The time sequence of the correlations between events with energy exceeding 55 EeV and AGN in the VCV catalog is shown in Fig.3. Period I is the exploratory period [10] from 1 January, 2004 through 26 May, 2006. The data collected during this period was scanned to establish the parameters which maximize the correlation. Period II is from 27 May, 2006 through 31 August, 2007 when the correlation paper [10] was published and period III includes data collected after, from 1 September, 2007 through 31 December, 2009. The time sequence is shown in terms of p_{data} , the degree of correlation with objects in the VCV catalog as a function of the total number of time-ordered events after the exploratory period.

We have also compared the distribution of arrival directions with the positions of different populations of nearby extragalactic objects: galaxies in the 2MRS survey and AGNs detected in X-rays by Swift-BAT. These studies are a posteriori and do not constitute further quantitative evidence for anisotropy.

We have analyzed the region of the sky close to the location of the radiogalaxy Cen A, since this corresponds to the largest observed excess with respect to isotropic expectations.

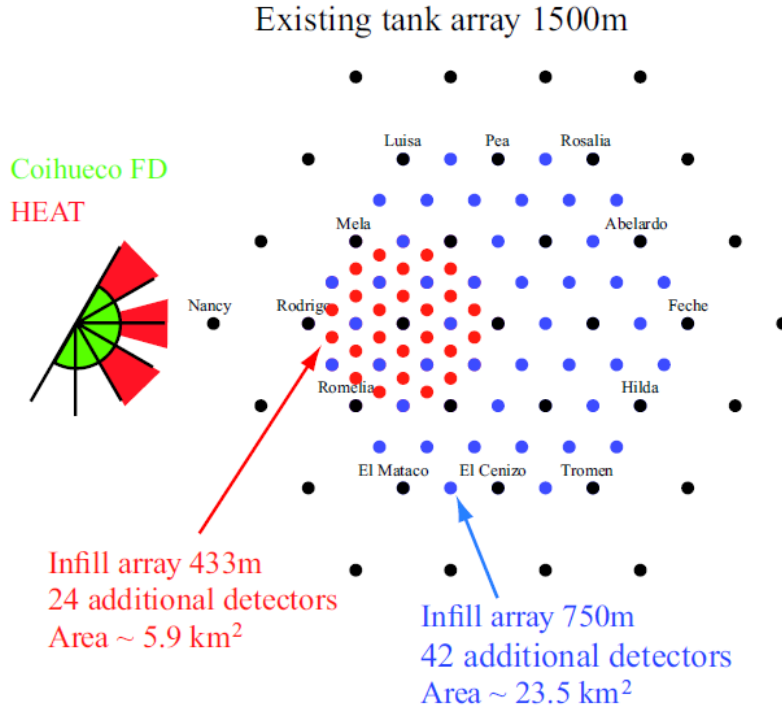


Figure 4: Layout of the enhancements AMIGA and HEAT for the southern site of the Pierre Auger Observatory.

The region of Cen A is densely populated with different types of nearby extragalactic objects. From all the arrival directions of CRs with $E \leq 55 \text{ EeV}$, 18.8% lie within 18° of Cen A, while 4.7% is the isotropic expectation. There are two arrival directions very close to the position of the Cen A nucleus. Aside from those two events, the excess is distributed rather broadly.

3 Enhancements of the Southern Observatory

After having completed the southern observatory, there are several enhancements under construction to improve the sensitivity of the observatory at low energy. Many of these activities are motivated by the interest in understanding the transition between galactic and extragalactic cosmic rays [11].

The extension of the surface detector is called AMIGA (“Auger Muons and Infill for the Ground Array”). It is itself a hybrid system containing an array of water Cherenkov detectors, called infill, each accompanied by a muon counter. Due to the higher flux for low energy cosmic rays, it is sufficient to only extend the surface detector in a small part of the whole ground array. This area is located close to the site of the HEAT extension to allow combined hybrid measurements. The infill part contains 66 new detector stations which will be deployed inside the 1.5 km grid to achieve a dense array with 61 stations on a 750 m grid and 24 stations on a 433 m grid (see Fig. 4). The design of these additional stations is the same as for the standard stations. Additionally, there are scintillators

buried next to each of the infill stations at a depth of about 3 m. These muon counters allow for a precise measurement of the showers electron to muon ratio at ground level, which is a direct indicator of the composition. The counter is sub-divided into three scintillator modules.

Moreover three new telescopes, called HEAT (“High Elevation Auger Telescope”), have been built and are taking data on a regular basis since September 2009. They have the same field of view as the current telescopes, but are mounted inside a tiltable housing, which can be inclined by 30° . The location of the telescopes is in the direct vicinity of the existing telescope station Coihueco. This allows two interesting ways of measuring: if the building is not tilted, which is the only position a person can enter the building for maintenance work, the field of view of HEAT and Coihueco is overlapped and the measurements can be used for cross calibrations; In the tilted position, which is intended to be the usual data taking position, HEAT and Coihueco see different parts of the same shower and a combined reconstruction could be done to gain a higher precision. Apart from the new housing, the basic design of the telescopes is the same as in the current ones. However, a few changes have been done in the DAQ electronics to use state-of-the-art technique with increased readout speed.

4 List of Publications

1. P.Abreu *et al.* [The Pierre Auger Collaboration], “Update on the correlation of the highest energy cosmic rays with nearby extragalactic matter,”
Astropart. Phys. **34**, 314-326 (2010).
([arXiv:1009.1855])
2. J.Abraham *et al.* [The Pierre Auger Collaboration], “Trigger and aperture of the surface detector array of the Pierre Auger Observatory,”
Nucl. Instrum. Meth. **A613**, 29-39 (2010).
3. J.Abraham *et al.* [The Pierre Auger Collaboration], “Measurement of the energy spectrum of cosmic rays above 10^{18} eV using the Pierre Auger Observatory,”
Phys. Lett. **B685**, 239-246 (2010).
(arXiv:1002.1975 [astro-ph.HE]).
4. J.Abraham *et al.* [The Pierre Auger Collaboration], “Measurement of the Depth of Maximum of Extensive Air Showers above 10^{18} eV,”
Phys. Rev. Lett. **104**, 091101 (2010).
(arXiv:1002.0699 [astro-ph.HE]).
5. J.Abraham *et al.* [The Pierre Auger Collaboration], “A Study of the Effect of Molecular and Aerosol Conditions in the Atmosphere on Air Fluorescence Measurements at the Pierre Auger Observatory,”
Astropart. Phys. **33**, 108-129 (2010).
(arXiv:1002.0366 [astro-ph.IM]).

References

- [1] J.Abraham *et al.* [The Pierre Auger Collaboration], Phys. Lett. **B685**, 239-246 (2010). (arXiv:1002.1975 [astro-ph.HE]).
- [2] [HiRes Collab.] R. U. Abbasi *et al.*, Astropart. Phys. 32 (2009) 53–60.
- [3] http://www.auger.org/combined_spectrum_icrc09.txt
- [4] W. Heitler, Oxford University Press, 1954;
J. Matthews, Astropart. Phys. **22** (2005), 387
- [5] T. Wibig, Phys. Rev. D **79**, 094008;
R. Ulrich *et al.* Proc. 31st Int. Cosmic Ray Conf. (Lodz, Poland) (2009) and arXiv:0906.0418
- [6] D.J. Bird, *et al.* [Fly’s Eye Coll.], Phys. Rev. Lett. **71** (1993), 3401.
- [7] R. U. Abbasi *et al.* [HiRes Coll.] Astrophys. J. **622** (2005),910.
- [8] Pierre Auger Collaboration [J. Abraham et al.], Phys. Rev. Lett. **104**, 091101 (2010). (arXiv:1002.0699 [astro-ph.HE]).
- [9] P.Abreu *et al.* [The Pierre Auger Collaboration], Astropart. Phys. **34**, 314-326 (2010). ([arXiv:1009.1855])
- [10] Pierre Auger Collaboration [J. Abraham et al.], Science 318 (2007) 938.
Astropart. Phys. 29 (2008) 188.
- [11] G. Medina-Tanco et al. for the Pierre Auger Collab., Proc. of 30th Int. Cosmic Ray Conf., Merida 5 (2007) 1101.

The Pierre Auger Collaboration

P. Abreu⁷², M. Aglietta⁵⁵, E.J. Ahn⁸⁸, I.F.M. Albuquerque^{17, 88}, D. Allard³¹, I. Allekotte¹, J. Allen⁹¹, P. Allison⁹³, J. Alvarez Castillo⁶⁵, J. Alvarez-Muñiz⁷⁹, M. Ambrosio⁴⁸, A. Aminaei⁶⁶, L. Anchordoqui¹⁰⁴, S. Andringa⁷², T. Antičić²⁵, A. Anzalone⁵⁴, C. Aramo⁴⁸, E. Arganda⁷⁶, F. Arqueros⁷⁶, H. Asorey¹, P. Assis⁷², J. Aublin³³, M. Ave^{39, 37}, M. Avenier³⁴, G. Avila¹⁰, T. Bäcker⁴³, M. Balzer³⁸, K.B. Barber¹¹, A.F. Barbosa¹⁴, R. Bardenet³², S.L.C. Barroso²⁰, B. Baughman⁹³, J.J. Beatty⁹³, B.R. Becker¹⁰¹, K.H. Becker³⁶, A. Bellétoile³⁵, J.A. Bellido¹¹, S. BenZvi¹⁰³, C. Berat³⁴, X. Bertou¹, P.L. Biermann⁴⁰, P. Billoir³³, F. Blanco⁷⁶, M. Blanco⁷⁷, C. Bleve³⁶, H. Blümer^{39, 37}, M. Boháčová^{27, 96}, D. Boncioli⁴⁹, C. Bonifazi^{23, 33}, R. Bonino⁵⁵, N. Borodai⁷⁰, J. Brack⁸⁶, P. Brogueira⁷², W.C. Brown⁸⁷, R. Bruijn⁸², P. Buchholz⁴³, A. Bueno⁷⁸, R.E. Burton⁸⁴, K.S. Caballero-Mora³⁹, L. Caramete⁴⁰, R. Caruso⁵⁰, A. Castellina⁵⁵, O. Catalano⁵⁴, G. Cataldi⁴⁷, L. Cazon⁷², R. Cester⁵¹, J. Chauvin³⁴, S.H. Cheng⁹⁴, A. Chiavassa⁵⁵, J.A. Chinellato¹⁸, A. Chou^{88, 91}, J. Chudoba²⁷, R.W. Clay¹¹, M.R. Coluccia⁴⁷, R. Conceição⁷², F. Contreras⁹, H. Cook⁸², M.J. Cooper¹¹, J. Coppens^{66, 68}, A. Cordier³², U. Cotti⁶⁴, S. Coutu⁹⁴, C.E. Covault⁸⁴, A. Creusot^{31, 74}, A. Criss⁹⁴, J. Cronin⁹⁶, A. Curutiu⁴⁰, S. Dagoret-Campagne³², R. Dallier³⁵, S. Dasso^{7, 4}, K. Daumiller³⁷, B.R. Dawson¹¹, R.M. de Almeida^{24, 18}, M. De Domenico⁵⁰, C. De Donato^{65, 46}, S.J. de Jong⁶⁶, G. De La Vega⁸, W.J.M. de Mello Junior¹⁸, J.R.T. de Mello Neto²³, I. De Mitri⁴⁷, V. de Souza¹⁶, K.D. de Vries⁶⁷, G. Decerprit³¹, L. del Peral⁷⁷, O. Deligny³⁰, H. Dembinski^{39, 37}, C. Di Giulio^{45, 49}, J.C. Diaz⁹⁰, M.L. Díaz Castro¹⁵, P.N. Diep¹⁰⁵, C. Dobrigkeit¹⁸, W. Docters⁶⁷, J.C. D’Olivo⁶⁵, P.N. Dong^{105, 30}, A. Dorofeev⁸⁶, J.C. dos Anjos¹⁴, M.T. Dova⁶, D. D’Urso⁴⁸, I. Dutan⁴⁰, J. Ebr²⁷, R. Engel³⁷, M. Erdmann⁴¹, C.O. Escobar¹⁸, A. Etchegoyen², P. Facal San Luis⁹⁶, I. Fajardo Tapia⁶⁵, H. Falcke^{66, 69}, G. Farrar⁹¹, A.C. Fauth¹⁸, N. Fazzini⁸⁸, A.P. Ferguson⁸⁴, A. Ferrero², B. Fick⁹⁰, A. Filevich², A. Filipčić^{73, 74}, S. Fliescher⁴¹, C.E. Fracchiolla⁸⁶, E.D. Fraenkel⁶⁷, U. Fröhlich⁴³, B. Fuchs¹⁴, R. Gaior³³, R.F. Gamarra², S. Gambetta⁴⁴, B. García⁸, D. García Gámez⁷⁸, D. Garcia-Pinto⁷⁶, A. Gascon⁷⁸, H. Gemmeke³⁸, K. Gesterling¹⁰¹, P.L. Ghia^{33, 55}, U. Giaccari⁴⁷, M. Giller⁷¹, H. Glass⁸⁸, M.S. Gold¹⁰¹, G. Golup¹, F. Gomez Albarracin⁶, M. Gómez Berisso¹, P. Gonçalves⁷², D. Gonzalez³⁹, J.G. Gonzalez³⁹, B. Gookin⁸⁶, D. Góra^{39, 70}, A. Gorgi⁵⁵, P. Gouffon¹⁷, S.R. Gozzini⁸², E. Grashorn⁹³, S. Grebe⁶⁶, N. Griffith⁹³, M. Grigat⁴¹, A.F. Grillo⁵⁶, Y. Guardincerri⁴, F. Guarino⁴⁸, G.P. Guedes¹⁹, A. Guzman⁶⁵, J.D. Hague¹⁰¹, P. Hansen⁶, D. Harari¹, S. Harmsma^{67, 68}, J.L. Harton⁸⁶, A. Haungs³⁷, T. Hebbeker⁴¹, D. Heck³⁷, A.E. Herve¹¹, C. Hojvat⁸⁸, V.C. Holmes¹¹, P. Homola⁷⁰, J.R. Hörandel⁶⁶, A. Horneffer⁶⁶, M. Hrabovský^{27, 28}, T. Huege³⁷, A. Insolia⁵⁰, F. Ionita⁹⁶, A. Italiano⁵⁰, C. Jarne⁶, S. Jiraskova⁶⁶, K. Kadija²⁵, K.H. Kampert³⁶, P. Karhan²⁶, P. Kasper⁸⁸, B. Kégl³², B. Keilhauer³⁷, A. Keivani⁸⁹, J.L. Kelley⁶⁶, E. Kemp¹⁸, R.M. Kieckhafer⁹⁰, H.O. Klages³⁷, M. Kleifges³⁸, J. Kleinfeller³⁷, J. Knapp⁸², D.-H. Koang³⁴, K. Kotera⁹⁶, N. Krohm³⁶, O. Krömer³⁸, D. Kruppke-Hansen³⁶, F. Kuehn⁸⁸, D. Kuempel³⁶, J.K. Kulbartz⁴², N. Kunka³⁸, G. La Rosa⁵⁴, C. Lachaud³¹, P. Lautridou³⁵, M.S.A.B. Leão²², D. Lebrun³⁴, P. Lebrun⁸⁸, M.A. Leigui de Oliveira²², A. Lemiere³⁰, A. Letessier-Selvon³³, I. Lhenry-Yvon³⁰, K. Link³⁹, R. López⁶¹, A. Lopez Agüera⁷⁹, K. Louedec³², J. Lozano Bahilo⁷⁸, A. Lucero^{2, 55}, M. Ludwig³⁹, H. Lyberis³⁰, M.C. Maccarone⁵⁴, C. Macolino³³, S. Maldera⁵⁵, D. Mandat²⁷, P. Mantsch⁸⁸, A.G. Mariazzi⁶, J. Marin^{9, 55}, V. Marin³⁵, I.C. Maris³³, H.R. Marquez Falcon⁶⁴, G. Marsella⁵², D. Martello⁴⁷, L. Martin³⁵, H. Martinez⁶², O. Martínez Bravo⁶¹, H.J. Mathes³⁷, J. Matthews^{89, 95}, J.A.J. Matthews¹⁰¹, G. Matthiae⁴⁹, D. Maurizio⁵¹, P.O. Mazur⁸⁸, G. Medina-Tanco⁶⁵, M. Melissas³⁹, D. Melo^{2, 51}, E. Menichetti⁵¹, A. Menshikov³⁸, P. Mertsch⁸⁰, C. Meurer⁴¹,

S. Mićanović²⁵, M.I. Micheletti², W. Miller¹⁰¹, L. Miramonti⁴⁶, S. Mollerach¹, M. Monasor⁹⁶, D. Monnier Ragainne³², F. Montanet³⁴, B. Morales⁶⁵, C. Morello⁵⁵, E. Moreno⁶¹, J.C. Moreno⁶, C. Morris⁹³, M. Mostafá⁸⁶, C.A. Moura^{22, 48}, S. Mueller³⁷, M.A. Muller¹⁸, G. Müller⁴¹, M. Münchmeyer³³, R. Mussa⁵¹, G. Navarra⁵⁵ †, J.L. Navarro⁷⁸, S. Navas⁷⁸, P. Necesal²⁷, L. Nellen⁶⁵, A. Nelles⁶⁶, P.T. Nhung¹⁰⁵, L. Niemietz³⁶, N. Nierstenhoefer³⁶, D. Nitz⁹⁰, D. Nosek²⁶, L. Nožka²⁷, M. Nyklicek²⁷, J. Oehlschläger³⁷, A. Olinto⁹⁶, P. Oliva³⁶, V.M. Olmos-Gilbaja⁷⁹, M. Ortiz⁷⁶, N. Pacheco⁷⁷, D. Pakk Selmi-Dei¹⁸, M. Palatka²⁷, J. Pallotta³, N. Palmieri³⁹, G. Parente⁷⁹, E. Parizot³¹, A. Parra⁷⁹, J. Parrisius³⁹, R.D. Parsons⁸², S. Pastor⁷⁵, T. Paul⁹², M. Pech²⁷, J. Peçkala⁷⁰, R. Pelayo⁷⁹, I.M. Pepe²¹, L. Perrone⁵², R. Pesce⁴⁴, E. Petermann¹⁰⁰, S. Petrera⁴⁵, P. Petrinca⁴⁹, A. Petrolini⁴⁴, Y. Petrov⁸⁶, J. Petrovic⁶⁸, C. Pfendner¹⁰³, N. Phan¹⁰¹, R. Piegai⁴, T. Pierog³⁷, P. Pieroni⁴, M. Pimenta⁷², V. Pirronello⁵⁰, M. Platino², V.H. Ponce¹, M. Pontz⁴³, P. Privitera⁹⁶, M. Prouza²⁷, E.J. Quel³, S. Querchfeld³⁶, J. Rautenberg³⁶, O. Ravel³⁵, D. Ravignani², B. Revenu³⁵, J. Ridky²⁷, S. Riggi^{79, 50}, M. Risse⁴³, P. Ristori³, H. Rivera⁴⁶, C. Rivière³⁴, V. Rizi⁴⁵, C. Robledo⁶¹, W. Rodrigues de Carvalho^{79, 17}, G. Rodriguez⁷⁹, J. Rodriguez Martino^{9, 50}, J. Rodriguez Rojo⁹, I. Rodriguez-Cabo⁷⁹, M.D. Rodríguez-Frías⁷⁷, G. Ros⁷⁷, J. Rosado⁷⁶, T. Rossler²⁸, M. Roth³⁷, B. Rouillé-d'Orfeuille⁹⁶, E. Roulet¹, A.C. Rovero⁷, C. Rühle³⁸, F. Salamida^{37, 45}, H. Salazar⁶¹, G. Salina⁴⁹, F. Sánchez², M. Santander⁹, C.E. Santo⁷², E. Santos⁷², E.M. Santos²³, F. Sarazin⁸⁵, B. Sarkar³⁶, S. Sarkar⁸⁰, R. Sato⁹, N. Scharf⁴¹, V. Scherini⁴⁶, H. Schieler³⁷, P. Schiffer⁴¹, A. Schmidt³⁸, F. Schmidt⁹⁶, T. Schmidt³⁹, O. Scholten⁶⁷, H. Schoorlemmer⁶⁶, J. Schovancova²⁷, P. Schovánek²⁷, F. Schröder³⁷, S. Schulte⁴¹, D. Schuster⁸⁵, S.J. Sciutto⁶, M. Scuderi⁵⁰, A. Segreto⁵⁴, D. Semikoz³¹, M. Settimo^{43, 47}, A. Shadkam⁸⁹, R.C. Shellard^{14, 15}, I. Sidelnik², G. Sigl⁴², H.H. Silva Lopez⁶⁵, A. Śmiałkowski⁷¹, R. Šmída^{37, 27}, G.R. Snow¹⁰⁰, P. Sommers⁹⁴, J. Sorokin¹¹, H. Spinka^{83, 88}, R. Squartini⁹, J. Stapleton⁹³, J. Stasielak⁷⁰, M. Stephan⁴¹, E. Strazzeri⁵⁴, A. Stutz³⁴, F. Suarez², T. Suomijärvi³⁰, A.D. Supanitsky^{7, 65}, T. Šuša²⁵, M.S. Sutherland^{89, 93}, J. Swain⁹², Z. Szadkowski^{71, 36}, M. Szuba³⁷, A. Tamashiro⁷, A. Tapia², M. Tartare³⁴, O. Taşcau³⁶, C.G. Tavera Ruiz⁶⁵, R. Tcaciuc⁴³, D. Tegolo^{50, 59}, N.T. Thao¹⁰⁵, D. Thomas⁸⁶, J. Tiffenberg⁴, C. Timmermans^{68, 66}, D.K. Tiwari⁶⁴, W. Tkaczyk⁷¹, C.J. Toderó Peixoto^{16, 22}, B. Tomé⁷², A. Tonachini⁵¹, P. Travnicek²⁷, D.B. Tridapalli¹⁷, G. Tristram³¹, E. Trovato⁵⁰, M. Tueros^{79, 4}, R. Ulrich^{94, 37}, M. Unger³⁷, M. Urban³², J.F. Valdés Galicia⁶⁵, I. Valiño^{79, 37}, L. Valore⁴⁸, A.M. van den Berg⁶⁷, B. Vargas Cárdenas⁶⁵, J.R. Vázquez⁷⁶, R.A. Vázquez⁷⁹, D. Veberič^{74, 73}, V. Verzi⁴⁹, M. Videla⁸, L. Villaseñor⁶⁴, H. Wahlberg⁶, P. Wahrlich¹¹, O. Wainberg², D. Warner⁸⁶, A.A. Watson⁸², M. Weber³⁸, K. Weidenhaupt⁴¹, A. Weindl³⁷, S. Westerhoff¹⁰³, B.J. Whelan¹¹, G. Wieczorek⁷¹, L. Wiencke⁸⁵, B. Wilczyńska⁷⁰, H. Wilczyński⁷⁰, M. Will³⁷, C. Williams⁹⁶, T. Winchen⁴¹, L. Winders¹⁰⁴, M.G. Winnick¹¹, M. Wommer³⁷, B. Wundheiler², T. Yamamoto⁹⁶ ^a, T. Yapici⁹⁰, P. Younk^{43, 86}, G. Yuan⁸⁹, A. Yushkov^{79, 48}, B. Zamorano⁷⁸, E. Zas⁷⁹, D. Zavrtnik^{74, 73}, M. Zavrtnik^{73, 74}, I. Zaw⁹¹, A. Zepeda⁶², M. Ziolkowski⁴³

¹ Centro Atómico Bariloche and Instituto Balseiro (CNEA- UNCuyo-CONICET), San Carlos de Bariloche, Argentina

² Centro Atómico Constituyentes (Comisión Nacional de Energía Atómica/CONICET/UTN-FRBA), Buenos Aires, Argentina

³ Centro de Investigaciones en Láseres y Aplicaciones, CITEFA and CONICET, Argentina

⁴ Departamento de Física, FCEyN, Universidad de Buenos Aires y CONICET, Argentina

⁶ IFLP, Universidad Nacional de La Plata and CONICET, La Plata, Argentina

- ⁷ Instituto de Astronomía y Física del Espacio (CONICET- UBA), Buenos Aires, Argentina
- ⁸ National Technological University, Faculty Mendoza (CONICET/CNEA), Mendoza, Argentina
- ⁹ Pierre Auger Southern Observatory, Malargüe, Argentina
- ¹⁰ Pierre Auger Southern Observatory and Comisión Nacional de Energía Atómica, Malargüe, Argentina
- ¹¹ University of Adelaide, Adelaide, S.A., Australia
- ¹² Centro Brasileiro de Pesquisas Físicas, Rio de Janeiro, RJ, Brazil
- ¹³ Pontifícia Universidade Católica, Rio de Janeiro, RJ, Brazil
- ¹⁴ Universidade de São Paulo, Instituto de Física, São Carlos, SP, Brazil
- ¹⁵ Universidade de São Paulo, Instituto de Física, São Paulo, SP, Brazil
- ¹⁶ Universidade Estadual de Campinas, IFGW, Campinas, SP, Brazil
- ¹⁷ Universidade Estadual de Feira de Santana, Brazil
- ¹⁸ Universidade Estadual do Sudoeste da Bahia, Vitória da Conquista, BA, Brazil
- ¹⁹ Universidade Federal da Bahia, Salvador, BA, Brazil
- ²⁰ Universidade Federal do ABC, Santo André, SP, Brazil
- ²¹ Universidade Federal do Rio de Janeiro, Instituto de Física, Rio de Janeiro, RJ, Brazil
- ²² Universidade Federal Fluminense, Instituto de Física, Niterói, RJ, Brazil
- ²³ Rudjer Bošković Institute, 10000 Zagreb, Croatia
- ²⁴ Charles University, Faculty of Mathematics and Physics, Institute of Particle and Nuclear Physics, Prague, Czech Republic
- ²⁵ Institute of Physics of the Academy of Sciences of the Czech Republic, Prague, Czech Republic
- ²⁶ Palacky University, RCATM, Olomouc, Czech Republic
- ²⁷ Institut de Physique Nucléaire d'Orsay (IPNO), Université Paris 11, CNRS-IN2P3, Orsay, France
- ²⁸ Laboratoire AstroParticule et Cosmologie (APC), Université Paris 7, CNRS-IN2P3, Paris, France
- ²⁹ Laboratoire de l'Accélérateur Linéaire (LAL), Université Paris 11, CNRS-IN2P3, Orsay, France
- ³⁰ Laboratoire de Physique Nucléaire et de Hautes Energies (LPNHE), Universités Paris 6 et Paris 7, CNRS-IN2P3, Paris, France
- ³¹ Laboratoire de Physique Subatomique et de Cosmologie (LPSC), Université Joseph Fourier, INPG, CNRS-IN2P3, Grenoble, France
- ³² SUBATECH, CNRS-IN2P3, Nantes, France
- ³³ Bergische Universität Wuppertal, Wuppertal, Germany
- ³⁴ Karlsruhe Institute of Technology - Campus North - Institut für Kernphysik, Karlsruhe, Germany
- ³⁵ Karlsruhe Institute of Technology - Campus North - Institut für Prozessdatenverarbeitung und Elektronik, Karlsruhe, Germany
- ³⁶ Karlsruhe Institute of Technology - Campus South - Institut für Experimentelle Kernphysik (IEKP), Karlsruhe, Germany
- ³⁷ Max-Planck-Institut für Radioastronomie, Bonn, Germany
- ³⁸ RWTH Aachen University, III. Physikalisches Institut A, Aachen, Germany

- 42 Universität Hamburg, Hamburg, Germany
- 43 Universität Siegen, Siegen, Germany
- 44 Dipartimento di Fisica dell'Università and INFN, Genova, Italy
- 45 Università dell'Aquila and INFN, L'Aquila, Italy
- 46 Università di Milano and Sezione INFN, Milan, Italy
- 47 Dipartimento di Fisica dell'Università del Salento and Sezione INFN, Lecce, Italy
- 48 Università di Napoli "Federico II" and Sezione INFN, Napoli, Italy
- 49 Università di Roma II "Tor Vergata" and Sezione INFN, Roma, Italy
- 50 Università di Catania and Sezione INFN, Catania, Italy
- 51 Università di Torino and Sezione INFN, Torino, Italy
- 52 Dipartimento di Ingegneria dell'Innovazione dell'Università del Salento and Sezione INFN, Lecce, Italy
- 54 Istituto di Astrofisica Spaziale e Fisica Cosmica di Palermo (INAF), Palermo, Italy
- 55 Istituto di Fisica dello Spazio Interplanetario (INAF), Università di Torino and Sezione INFN, Torino, Italy
- 56 INFN, Laboratori Nazionali del Gran Sasso, Assergi (L'Aquila), Italy
- 59 Università di Palermo and Sezione INFN, Catania, Italy
- 61 Benemérita Universidad Autónoma de Puebla, Puebla, Mexico
- 62 Centro de Investigación y de Estudios Avanzados del IPN (CINVESTAV), México, D.F., Mexico
- 64 Universidad Michoacana de San Nicolas de Hidalgo, Morelia, Michoacan, Mexico
- 65 Universidad Nacional Autonoma de Mexico, Mexico, D.F., Mexico
- 66 IMAPP, Radboud University, Nijmegen, Netherlands
- 67 Kernfysisch Versneller Instituut, University of Groningen, Groningen, Netherlands
- 68 NIKHEF, Amsterdam, Netherlands
- 69 ASTRON, Dwingeloo, Netherlands
- 70 Institute of Nuclear Physics PAN, Krakow, Poland
- 71 University of Łódź, Łódź, Poland
- 72 LIP and Instituto Superior Técnico, Lisboa, Portugal
- 73 J. Stefan Institute, Ljubljana, Slovenia
- 74 Laboratory for Astroparticle Physics, University of Nova Gorica, Slovenia
- 75 Instituto de Física Corpuscular, CSIC-Universitat de València, Valencia, Spain
- 76 Universidad Complutense de Madrid, Madrid, Spain
- 77 Universidad de Alcalá, Alcalá de Henares (Madrid), Spain
- 78 Universidad de Granada & C.A.F.P.E., Granada, Spain
- 79 Universidad de Santiago de Compostela, Spain
- 80 Rudolf Peierls Centre for Theoretical Physics, University of Oxford, Oxford, United Kingdom
- 82 School of Physics and Astronomy, University of Leeds, United Kingdom
- 83 Argonne National Laboratory, Argonne, IL, USA
- 84 Case Western Reserve University, Cleveland, OH, USA
- 85 Colorado School of Mines, Golden, CO, USA
- 86 Colorado State University, Fort Collins, CO, USA
- 87 Colorado State University, Pueblo, CO, USA
- 88 Fermilab, Batavia, IL, USA

- ⁸⁹ Louisiana State University, Baton Rouge, LA, USA
- ⁹⁰ Michigan Technological University, Houghton, MI, USA
- ⁹¹ New York University, New York, NY, USA
- ⁹² Northeastern University, Boston, MA, USA
- ⁹³ Ohio State University, Columbus, OH, USA
- ⁹⁴ Pennsylvania State University, University Park, PA, USA
- ⁹⁵ Southern University, Baton Rouge, LA, USA
- ⁹⁶ University of Chicago, Enrico Fermi Institute, Chicago, IL, USA
- ¹⁰⁰ University of Nebraska, Lincoln, NE, USA
- ¹⁰¹ University of New Mexico, Albuquerque, NM, USA
- ¹⁰³ University of Wisconsin, Madison, WI, USA
- ¹⁰⁴ University of Wisconsin, Milwaukee, WI, USA
- ¹⁰⁵ Institute for Nuclear Science and Technology (INST), Hanoi, Vietnam

(†) Deceased

(a) at Konan University, Kobe, Japan

Lasex. An X-ray source from 70 eV to 30 keV

L. Palladino^{a,c}, R. Gimenez De Lorenzo^{a,c}, G. Gualtieri^b

^a Physics Department of L'Aquila University - Italy

^b Science and Biomedical Technology Department of L'Aquila University - Italy

^c INFN, Laboratori Nazionali del Gran Sasso, Assergi (AQ) - Italy

Abstract

In this report, we present the activities of the LASEX experiment in the year 2010. The goal of the experiment LASEX is the realization of an X-ray source, with a spectrum of X-ray emission between 70 eV and 30 keV, based on the generation of a plasma obtained by focusing a laser beam on a target of a different material. This source is located in the PLASMA-X laboratory of the Physics Department of LAquila University.

1 Introduction

Following the April 2009 to the earthquake, which struck the city of L'Aquila, the activities of the experiment LASEX broke down and were fully incorporated in the second half of June 2010, after the necessary repairs of both structures of the equipment, with verification of their proper function.

The results of preliminary X-ray emission in the area between 70 eV and 1 keV were presented at the international conference "PPLA 4th Workshop Plasma Production by Laser Ablation", held in Messina 18 to 20 July 2009, subject also of an article submitted and accepted by the journal REDS entitled "X-ray emission from plasma produced by Nd: YAG / Glass on a Cu target: a preliminary analysis".

2 The X-ray source

In the figure 1, we provide an overview of the X-ray source located in the laboratory PLASMA-X of the Department of Physics, University of L'Aquila.

The X-ray source is, as we can see in figure 1, a laser Nd:Yag / Glass and two interaction chambers in which the laser beam is sent, in an alternative way, using a system of mirrors back (red and blue lines). To cover the entire range the source has two configurations, one for the X-ray emission between 70 eV and 1 keV (the interaction Chamber (Soft X-rays) in the bottom of the figure 1) and the other for X-rays between 1 keV and



Figure 1: The X-ray source, located in the Laboratory of the Department of X-PLASMA Physics, University of L'Aquila.

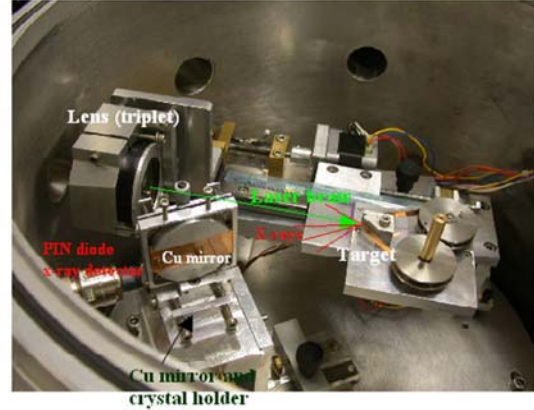


Figure 2: Chamber interaction (Soft X-rays) for the production of soft X-rays.

30 keV (the Chamber interaction HT (Hard X-rays) in the top left in photo 1) with the control circuit system of high voltage.

In both configurations, the mechanism of production of X is based on the generation of a plasma obtained by focusing a laser beam NdYag (5J per pulse, duration 6 ns, 0.3 mrad divergence, 536 nm wavelength) on a target metal or not.

The two interaction chambers are presented in detail in figures 2 and 3.

3 Soft X-ray source

The figure 2 shows the interaction chamber, where X-rays are produced directly from the plasma in the process of hydrodynamic expansion emitting soft X-rays with energy between 70 eV and 1 - 1.5 keV.

Plasma is obtained by irradiating the target (in figure is the copper) with a power density $I \sim 10^{11}$ to 10^{13} (W/cm^2) by using an aspheric lens (triplet) of 132 mm focal length ($f \# 3$). The mirror plane of copper is placed at an angle to 5 degrees grazing incidence analysis for a beam of X in the sub-keV region. The intensity of the radiation is measured using a solid state detector (125PIN100 Quantrad the system) with micro-filtered aluminum foil of a calibrated thickness between $0.8 \mu m$ and 7 microns.

In the table 1, we present the analysis of the measures obtained with the detector placed at 13.8 cm and 30 degree view-angle. The laser irradiance is about $10^{12} W/cm^2$. The fluence and the conversion efficiency are reported in two photon energy regions: 70 eV and > 700 eV. In these two regions the X-ray conversion efficiencies are $\eta_{sub-keV}$ (70 eV) = 30% and η_{keV} (> 700 eV) = 0.2 % respectively on 2π sr. Our conversion efficiencies, the most important parameter for a comparison in literature, are in accordance with Chaker et al. [1].

Using copper as target's material, for an efficient X-ray generation, in the sub-keV region, optimal laser intensities range between 10^{10} - $10^{12} W/cm^2$. Above this interval we have a small reduction in conversion efficiency as in Chaker et al.[1] shown, which can be

Energy regions	Fluence F_D	X-ray intensity E_x (J)	X-ray Instantaneous Brightness B (W/cm ² 2 π sr)	Conversion efficiency (in 2 π sr) h (%)
Sub-keV (70 eV)	0.102 \pm 0.002 (mJ/cm ²)	0.073 (in 2 π sr)	3.6×10^{11}	30 %
keV (> 700 eV)	0.65 \pm 0.17 (μ J/cm ²)	0.47×10^{-3} (in 2 π sr)	2.8×10^8	0.2 %

explained by the change in the plasma emitted spectrum for the emission shifts towards higher photon energies (Cu L-shell emission, at $h\nu \sim 1$ keV, begins to be predominant above 10^{12} W/cm²).

Other measurements were made with different laser power density and using for the target different types of material: mylar, yttrium, aluminum. The analysis of x-ray conversion efficiencies and the fluences of these measures are being developed.

4 Hard X-ray source and High-voltage circuit

The figure 3 shows the interaction chamber in which the X-ray emission in the range 1 keV to 30 keV.

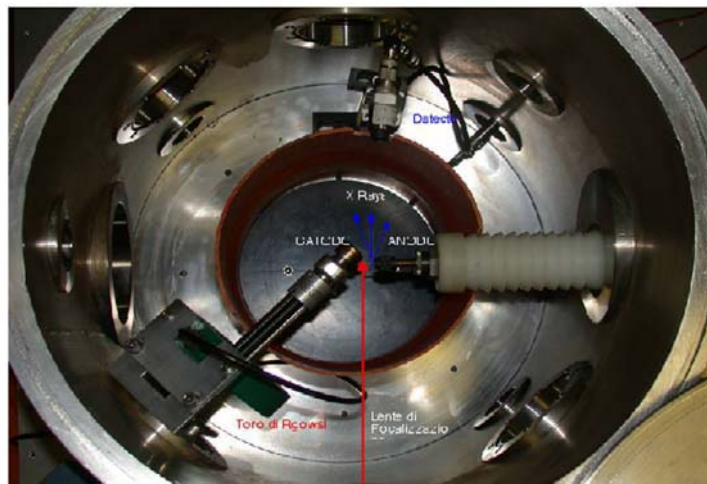


Figure 3: HT interaction chamber (Hard X-rays)

The X-rays are obtained, as in the case of a normal X-ray tubes, by the bremsstrahlung effect on the anode of the accelerated electrons of the plasma in an electric

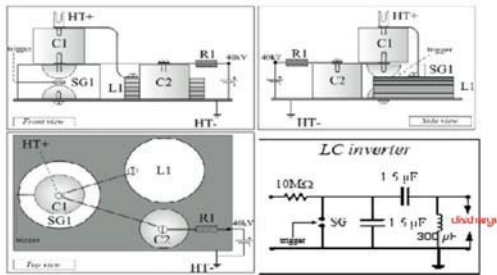


Figure 4: Schematic layout of the LC-inverter circuit. SG indicates the spark gap.

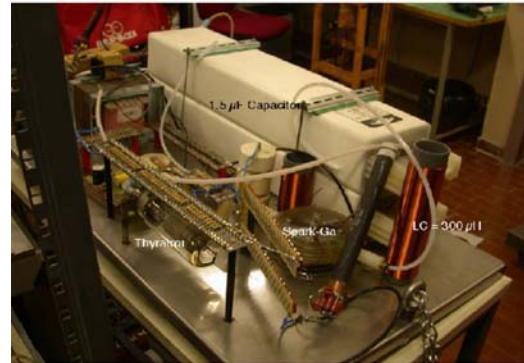


Figure 5: Implementation of the LC-inverter circuit with the major components indicated.

field. In this case, the focusing lens, with its handling, is placed outside the interaction chamber and the laser beam is focused onto a target (cathode) in continuous rotation.

These measures were taken in order to move out of the area of handling the high voltage discharge points and eliminate unwanted high voltage. The current is measured with a Rogowski coil.

The orange tube, that surrounds the production of X-rays, supports the safety shield of the X ray radiation. This consists of 3 mm of lead.

The circuit is based on a power supply that provides a maximum voltage of 40 kV and an LC-inverter circuit whose scheme is presented in figure 4, which shows the most important values of circuit elements, and its realization in figure 5.

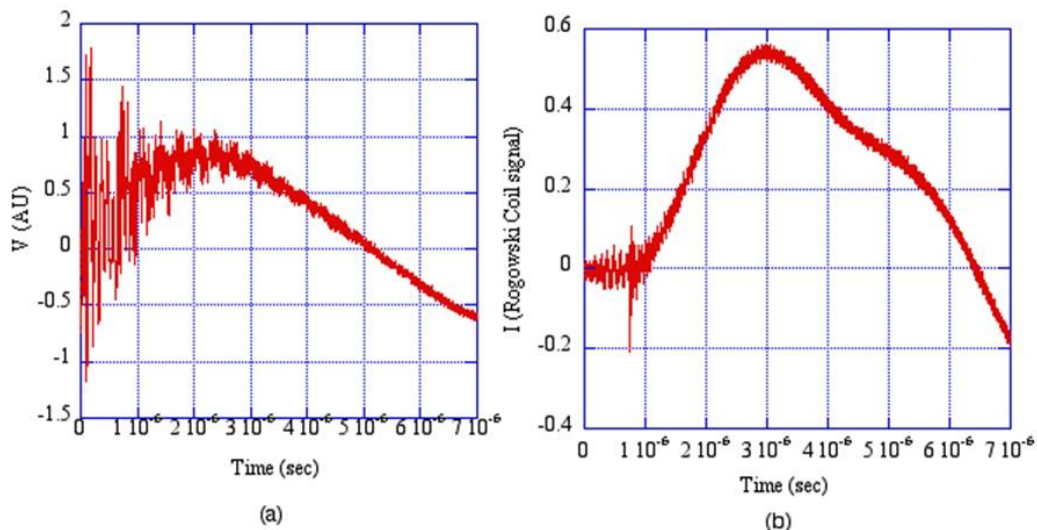


Figure 6: Evolution of voltage and current for a discharge in air with a supply voltage of 20 kV.

The first measures were performed in air and the results are shown in Figure 6a and 6b where the voltage applied to the discharge and its current are plotted. The signal characteristics of current and voltage are consistent with the characteristics of the circuit, as the oscillation period and damping of the signal.

The system is designed so that the charging circuit is equivalent to that released during a mammogram exposure to 18 keV.

5 Acknowledgments

We would like to thank Dott. L. Votano Director of Gran Sasso National Laboratory of INFN and Prof. S. Santucci Director of The Physics Department of LAquila University for supporting us. This work is financially supported by INFN, LASEX experiment.

References

- [1] M.Chaker, H.Pepin, V.Bareau, B.Lafontaine, I.Toubhans, R.Fabbro, B.Faral: J. Appl. Phys. 63 (3), 1 February 1988;

XILOPHON

L. Ottaviano^a, S. Prezioso^a, M. Donarelli^a, A. Gaudieri^a,
S. Penna^b, A. Reale^b

^a Dip. di Fisica, Univ. dell'Aquila, gc LNGS-INFN,
Via Vetoio, 67100, L'Aquila, Italy

^b Dip. di Ingegneria Elettronica, Univ. di Roma "Tor Vergata",
Viale Politecnico 1, 00133, Roma, Italy

1 Introduction

The goal of this project, as declared in the original proposal, is the fabrication of a miniaturized organic laser emitting in the infrared region for applications in the field of Telecommunications. In particular, scientists working in advanced laboratories like CERN or LNGS, where a big amount of data is produced for any single experiment, are interested in sharing higher and higher volumes of information at higher and higher speeds. Today, in some exceptional case, up to 10's of Peta-bytes per year are produced (the LHC experiment at CERN). After acquisition, all these data must be sent all around the world to be analyzed and interpreted by different research groups. The need of a network of all-optical platforms sending and receiving huge fluxes of data is, then, easy to understand. We believe our idea meets somehow this need.

Fabricating miniaturized organic-based lasers is, nowadays, trendy. Lasers emitting from UV to near-IR have been widely fabricated but no one has so far demonstrated laser emission from organic media in the the third band of Telecommunications, the so called c-band (1530 - 1560 nm). IR category is a very longed-for target due to the general request of better connections between optical fibers and computer processors for advanced optical communication technology. Here we propose a Distributed Feed-Back (DFB) approach for low-cost fabrication of small size laser cavities, easy to be integrated in all-optical platforms allowing on-chip fast connection with external optical networks. Our strategy is innovative because employing the prototypal lab-scale X-ray Interference Lithography (XIL) setup at the Physics Department of L'Aquila to fabricate DFB templates by large area ($\sim 8 \text{ mm}^2$) periodic patterning of photoresist films. DFB templates with opportune period are fabricated to match the IR light emission from Erbium-tris(8-hydroxyquinoline) (ErQ_3), the organic molecule used as active medium. On the whole, our approach is low-cost and, then, suitable for bulk device production.

2 Experimental results

An image of optimized DFB waveguide (492 nm period) is reported in Fig. 1 before (Fig. 1(a)) and after (Fig. 2(b)) deposition of 980 nm thick ErQ_3 film. The periodic lines are 13 nm high (~ 160 nm FWHM). Despite its thickness, ErQ_3 film keeps memory of the modulation of the template underneath, clear evidence of homogeneous deposition of the organic molecule by vacuum thermal evaporation. X-Ray Diffraction analysis proves the amorphous nature of the ErQ_3 film (inset of Fig. 1(b)). The $\sim 8 \text{ mm}^2$ half-moon shaped patterned area is reported in the inset of Fig. 1(a) (the half-moon shape derives from technical details reported in [1]).

The light emission from the DFB cavity is obtained by focalization of violet laser radiation ($\lambda = 406$ nm) on the device surface. Emitted light is collected in the perpendicular direction, as for second order DFB lasers, using a standard setup for telecommunications tests. IR device response is reported in Fig. 2 in two different optical pumping conditions: on (solid line) and outside the grating (dotted line). When exciting the active medium outside the half-moon shaped patterned area, a broad emission peaked at 1530 nm is observed (dotted line) that is the sum of the contributions of all the 4f - 4f transitions occurring between Er 4f multiplet levels. When exciting the active medium in correspondence of the area where the substrate has a 492 nm periodical modulation, a marked band narrowing effect is observed at 1530 nm (solid line) in consequence of the wavelength selection induced by the DFB grating. The same effect is not observed out of resonance, if the grating period is either too small (480 nm, corresponding to $\lambda \sim 1490$ nm) or too large (504 nm, corresponding to $\lambda \sim 1560$ nm), indicating the criticality of the period matching. In both the considered out-of-resonance cases the shape of the photoluminescence spectrum is alike to the dashed line of Fig. 2.

The evidence of wavelength selection in the proper range for telecommunication applications is an important result but laser emission has still not been demonstrated. An intrinsic problem is the compelled limitation in optical pumping power, each kind of organic molecule getting rapidly damaged by the heating effect due to the pumping laser focalization. This problem represents the main obstacle for fabrication of such devices but we think it can be overcome by the optimization of many other parameters. Our strategy is summarized in four points:

1. improved light collection
2. finer control over the template lines periodicity by optimization of XIL setup
3. better knowledge of the organic material
4. investigation of novel approaches for template patterning that preserve the use of XIL technique

1. The setup for light collection has been completely renewed introducing a photomultiplier tube for efficient light detection and disposing the optics in configuration for lateral pumping (first order DFB operation mode). The light collected by the old setup was most probably coming from light scattering inside the active layer. We hope, now, to observe a significant signal enhancement. What we can find without increasing the

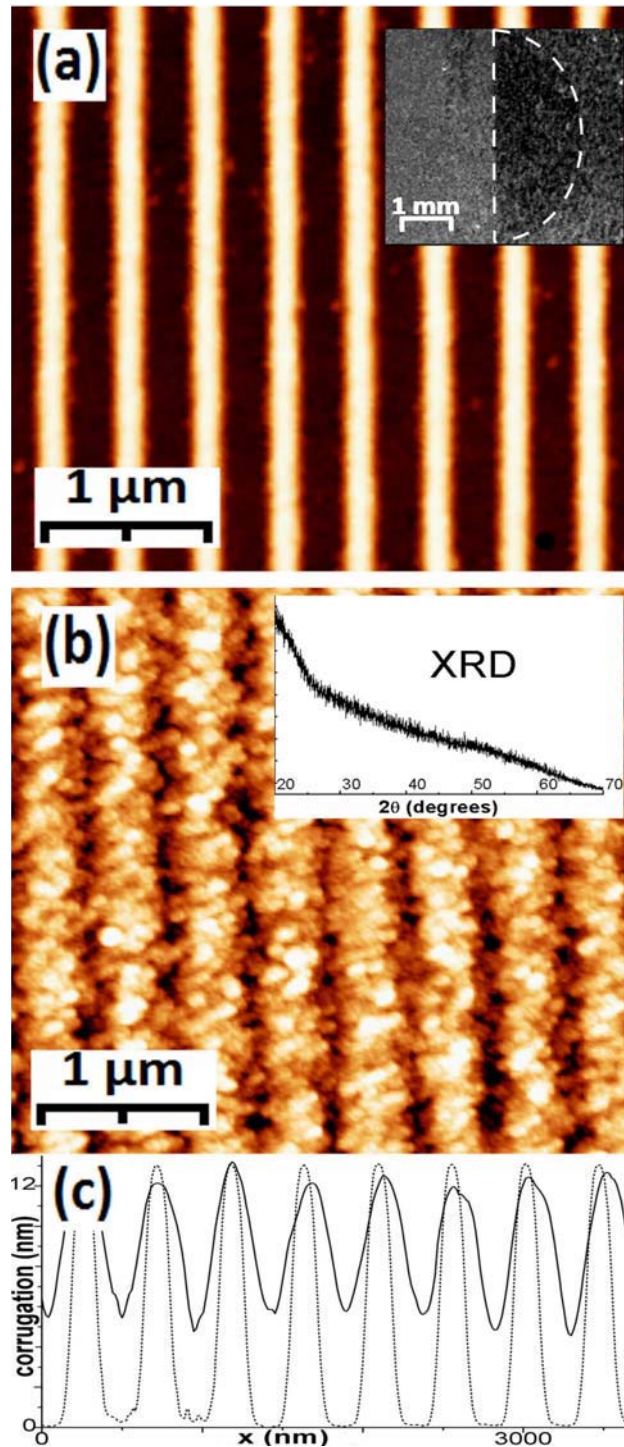


Figure 1: AFM images of a XIL patterned PMMA substrate (492 nm grating period) prior to (a) and after ErQ_3 deposition (980 nm) (b), and plot of the average of 256 horizontal line profiles (c), taken respectively from (a) (dashed line) and (b) (solid line). Inset of (a): large area photographic picture of the sample (the dashed line contours the XIL patterned area). Inset of (b): XRD spectrum of the deposited ErQ_3 film. [2]

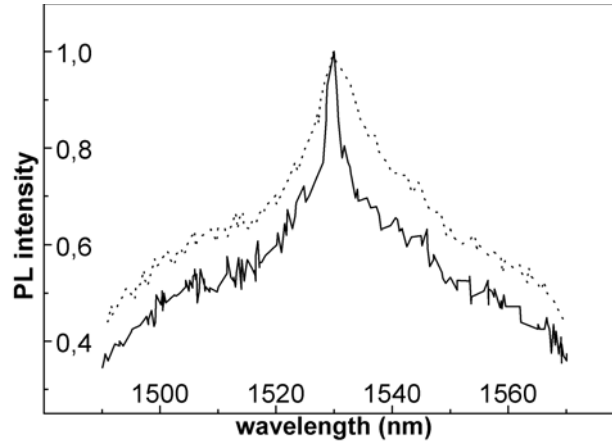


Figure 2: PL spectra of ErQ_3 on patterned (solid line) and smooth PMMA substrate (dotted line). The two spectra have been normalized to unit at their peak value. [2]

optical pumping power is, in the best case, that the device is lasing, i.e. that the peak reported in Fig. 2 was the first evidence of light emission beyond laser threshold. This setup will be readily tested.

2. An accurate study of vibrations affecting the XIL setup has been performed. Many causes of vibrations have been eliminated introducing shock absorber tools in all critical points and placing the entire XIL block over an anti-vibrating surface. The effects of attenuated vibrations have been studied by simulations of periodical template patterning as a function of the period (Fig. 3). Other details of this study are reported in [3].

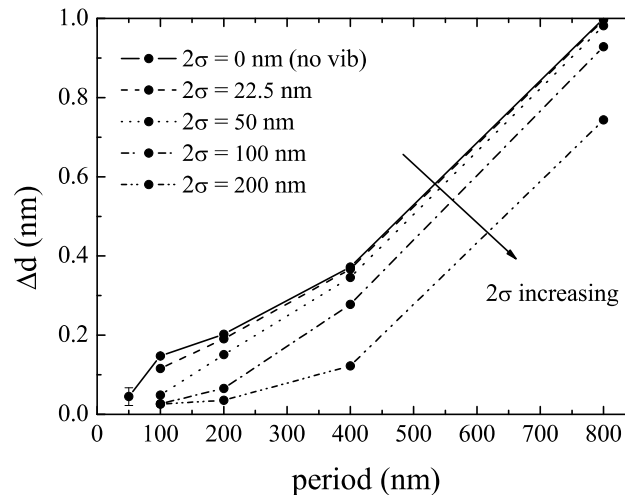


Figure 3: Template modulation amplitude vs. lines distance: experimental data, supposed to be unaffected by vibrations (solid line), and simulations with increasing vibrations.

The comparison between experimental points (solid line) and data obtained for a virtually vibrating setup indicates that vibrations actually affecting our system are negligible.

In fact, in the hypothesis of significant vibrations, simulations show that the peak-to-valley height should have rapidly reset when shrinking the period of periodic lines while, in the practice, the real modulation does not disappear. All the technical modifications carried out to improve the setup performance allow, at the present, to have a fine control over the template lines periodicity, with error margin smaller than 10 nm.

3. X-Ray and UV Photoemission Spectroscopy analyses have been performed to investigate the electronic structure of ErQ_3 . A preliminary study is reported in [2], where the purpose was to evaluate the purity of the deposited ErQ_3 film. Here we are interested in the complete identification of the energetic levels, a precious information that concerns the behavior at the interfaces and, for this reason, is of fundamental importance to finalize our efforts to the fabrication of an opto-electronic device. Data reported in Fig. 4 are a part of the experimental results that will be presented in an imminent publication, where they will be accurately discussed.

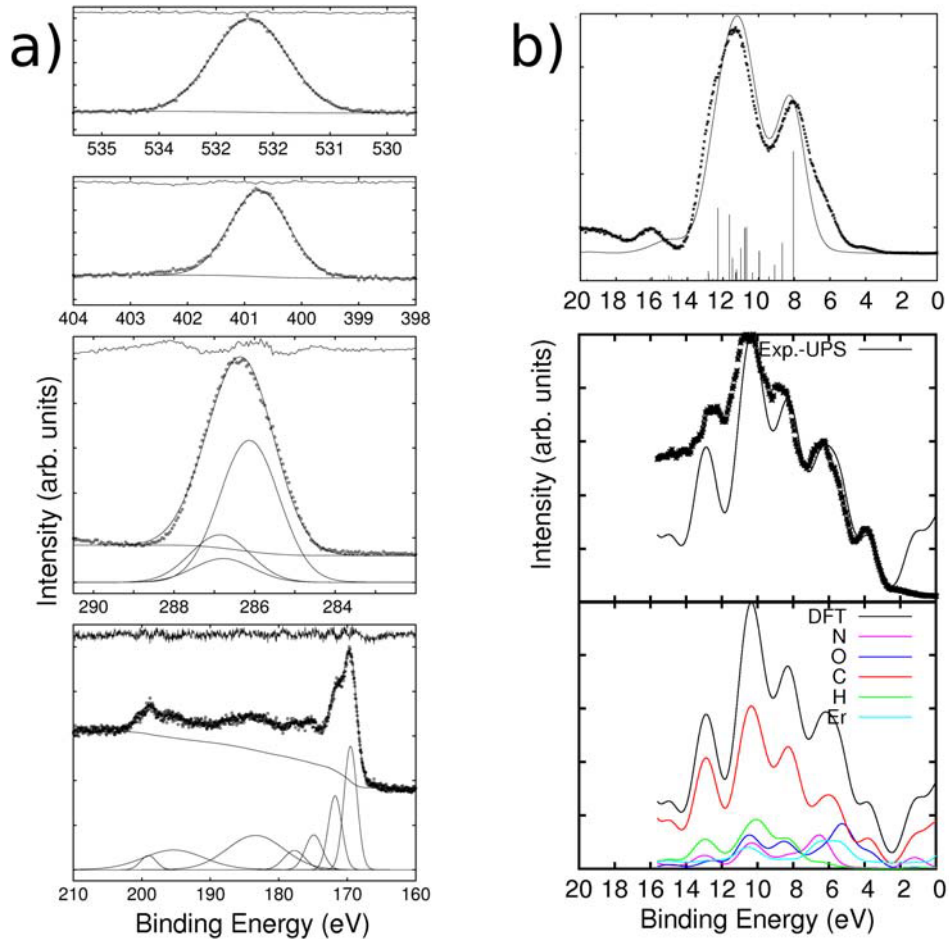


Figure 4: Core levels (a) and valence band (b) of ErQ_3 obtained respectively by X-Ray and UV Photoemission Spectroscopy. Experimental data are compared with Density Functional Theory calculations.

4. A novel resistless approach has been explored to engrave periodic patterns directly onto oxide films preserving the use of XIL technique but skipping the step of photoresist patterning. The direct exposure of the oxide films to the interfering X-Ray radiation is accompanied by complex phenomena. On the one hand, the sample surfaces are affected by a light-assisted carbon contamination due to the presence of residual hydrocarbons in the vacuum chamber (Fig. 5). On the other hand, a periodic pattern is still present after surface peeling (a thin layer of 10 nm is peeled by sputtering, eliminating any carbon residue). This technique is still almost entirely unexplored but the possibility of fabricating oxide-based templates without intermediate steps is a fascinating perspective, functional also for many other technological applications.

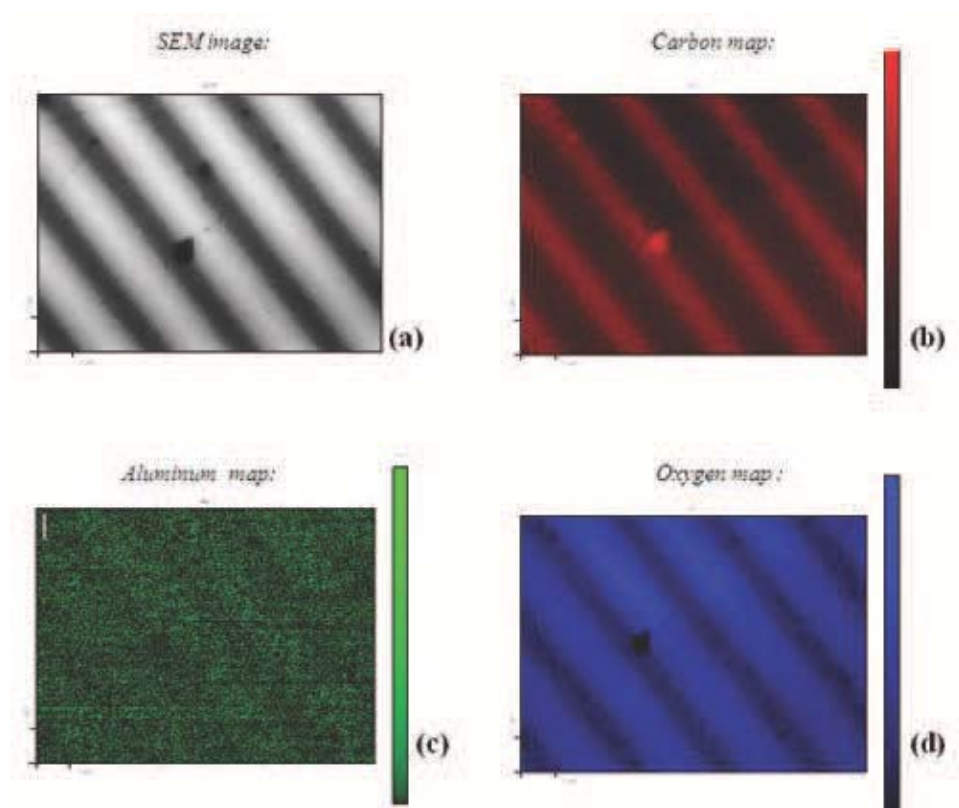


Figure 5: Surface study of a 72 nm thick Al_2O_3 film patterned by resistless XIL. Scanning Electron Microscopy image (a) and Scanning Auger Microscopy maps of Carbon (b), Aluminum (c), and Oxygen (d)

3 Conclusions

The experimental results presented in this report indicate that our approach is suitable for the fabrication of low-cost organic DFB waveguide cavities emitting in the range of interest for Telecommunications. The laser emission has still not been observed but

the conditions for succeeding in this challenge have been created. The XIL setup used to fabricate the DFB templates has been optimized. A renewed system for IR light collection has been assembled and is ready to be tested, and the organic molecule is almost completely known. This project has been also the occasion to touch topics of more general interest (like organic materials or EUV-assisted carbon contamination) and to search for innovative technological solutions (like the resistless lithography).

4 Acknowledgments

The work summarized in this LNGS Report has been funded by the National Institute of Nuclear Physics. The authors acknowledge Luigi Avaro, Ken Somerville, and Simona Spadoni (members of the R2 Technology Center - Physics and Materials Characterization) for the Scanning Auger Microscopy investigation, and Federico Bisti for the X-Ray and UV Photoemission Spectroscopy analyses.

5 Participation to, and organization of, national or international workshops or conferences

- L. Ottaviano (S. Prezioso and M. Donarelli in the Organizing Committed) launched the international workshop GraphITA to be held in May 2011 at the National Laboratories of Gran Sasso (INFN), with 200 attendees from 27 countries and 22 sponsors, and the participation of Prof. K. Novoselov, Nobel Prize in Physics 2010.
- 2010 International workshop on Extreme Ultraviolet Sources UCD Dublin (Ireland) L. Ottaviano (ORAL) *Interference lithography of graphene oxide with a table-top X-ray laser source*) L. Ottaviano, S. Prezioso, M. Donarelli, F. Bisti, F. Perrozzi, P. De Marco, S. Santucci.
- Nano2010 Rome (Italy) M. Donarelli (ORAL) *XPS and UPS analyses of a new organic molecule for DFB lasers fabrication: Erbium-tris(8-hydroxyquinoline)* M. Donarelli, F. Bisti, S. Prezioso, P. De Marco, L. Ottaviano.
- Nano2010 Rome (Italy) S. Prezioso (ORAL) *A novel approach to low-cost fabrication of organic-based lasers for optical communications using a versatile table-top X-ray Interference Nano-Lithography tool.* S. Prezioso, M. Donarelli, F. Bisti, P. De Marco, S. Santucci, L. Palladino, S. Penna, A. Reale, L. Ottaviano.
- Nanosea 2010 Cassis (France) S. Prezioso (ORAL) *Fabrication of an IR emitting ErQ₃-based distributed feedback laser by X-ray interference lithography* S. Prezioso, M. Donarelli, F. Bisti, S. Penna, A. Reale, L. Ottaviano.
- COST Action MP0601 (Short wavelength laboratory sources) Meeting in Krakow Poland (May 2010) (POSTER) *Table-to X-ray Interference Lithography as a tool to fabricate lasers emitting in the third window of optical communications.* S. Prezioso, M. Donarelli, F. Bisti, S. Santucci, L. Palladino, S. Penna, A. Reale, L. Ottaviano.

References

- [1] P. Zuppella, D. Luciani, P. Tucceri, P. De Marco, A. Gaudieri, J. Kaiser, L. Ottaviano, S. Santucci, A. Reale, *Large area interference lithography using a table-top extreme ultraviolet laser: a systematic study of the degree of mutual coherence*, Nanotechnology, **20** (2009) 115303.
- [2] S. Prezioso, L. Ottaviano, F. Bisti, M. Donarelli, S. Santucci, L. Palladino, S. Penna, A. Reale, *Infrared photoluminescence of erbium-tris(8-hydroxyquinoline) in a distributed feedback cavity*, J. Lumin., **131** (2011) 682
- [3] S. Prezioso, P. De Marco, P. Zuppella, S. Santucci, L. Ottaviano *A study of the mechanical vibrations of a table-top extreme ultraviolet interference nanolithography tool*, Rev. Sci. Instrum., **81** (2010) 045110